RATIONAL CONTROL
OF OPERABILITY OF THE MODEL UNIT
OF ELECTRIC FLYWHEEL MOTORS

2023

MINISTRY OF EDUCATION AND SCIENCE OF UKRAINE
National Aerospace University
«Kharkiv Aviation Institute»

RATIONAL CONTROL OF OPERABILITY OF THE MODEL UNIT OF ELECTRIC FLYWHEEL MOTORS

According to the general edition
of Anatoly Kulik

Kharkiv «KhAI» 2023

UDC 629.78.062.2.017
R27

Наведено результати теоретичних та експериментальних досліджень щодо раціонального управління працездатністю блока електродвигунів-маховиків, які застосовуються в системах орієнтації космічних апаратів. Описано моделі номінального і нештатного режимів функціонування електродвигунів-маховиків. Розглянуто інструментальні засоби глибокого діагностування та гнучкого відновлення працездатності електродвигунів-маховиків як об'єктів раціонального управління.

Описано експериментальну установку для дослідження макетного блока електродвигунів-маховиків і наведено результати раціонального управління працездатністю при дестабілізувальних впливах.

Для фахівців у галузі проєктування систем управління, а також докторантів, аспірантів, магістрів і студентів відповідних спеціальностей.

The author's team: V. Dzhulgakov, K. Dergachov, A. Kulik, M. Nechiporuk, S. Pasichnyk, V. Petrenko

Reviewers:

Oleg Zlatkin, General Director of SPE Hartron-Arcos LTD, candidate of technical science;

Petro Kachanov, professor of the «Automatics and control in technical systems» department of the National Technical University «Kharkiv Polytechnic Institute», laureate of the State Prize of Ukraine, doctor of technical sciences, professor

Approved as a monograph at a meeting of the Academic Council of the university (protocol No. 7 dated February 22, 2023)

Rational Control of Operability of the Model Unit of Electric
R27 Flywheel Motors [Text] : monograph / V. Dzhulgakov, K. Dergachov, A. Kulik and others; according to the general edition of A. Kulik. – Kharkiv: National Aerospace University «Kharkiv Aviation Institute», 2023. – 224 p.

ISBN 978-966-662-911-4

The results of theoretical and experimental research on the rational control of operability of the unit of electric motors-flywheels, which are used in the orientation systems of space vehicles, are presented. The models of the nominal and ubnormal modes of operation of electric motors-flywheels are described. Instrumental means of in-depth diagnosis and flexible restoration of the operability of electric flywheel motors as objects of rational control are considered.

An experimental stand for researching a model unit of electric flywheel motors is described and the results of rational control of operability under destabilizing influences are given.

For specialists in the field of design of control systems, as well as doctoral students, postgraduates, masters and students of relevant specialties.

Figures 134. Tables 7. References: 34 points

UDC 629.78.062.2.017

ISBN 978-966-662-911-4

Study, read,
And learn from someone else,
And don't shy away from yours.
Taras Shevchenko (1814-1861) – Ukrainian poet, novelist, thinker, painter, public figure. National hero and symbol of Ukraine

PREFACE

The trend of increasing the duration of space missions has led to the emergence of a new scientific and technical problem: ensuring the long-term operability of equipment and, in particular, the spacecraft orientation systems. The way to increase the reliability of components, assemblies and blocks has known limits. The traditional way of increasing the redundancy of the hardware part to ensure the necessary duration of the operational state of orientation systems leads to a significant increase in weight, size, energy and cost characteristics. The modern way is a way of finding a compromise between the use of components of ultimate reliability and the multiple use of their redundancy.

The modern level of development of on-board computing devices allows the implementation of many functions of controlling the operability of on-board navigation systems. During the execution of a space mission, these systems are affected by both external disturbing influences: aerodynamic, magnetic and gravitational forces, and internal influences: malfunctions and failures of equipment. These effects lead to malfunction of orientation systems, and sometimes to abnormal situations in space flight. In order to implement a rational control of the operability of orientation systems, it is necessary, firstly, to identify the cause of destabilization of the performance, and secondly, to counter it with available redundant means.

Identifying the causes of destabilization of performance is related to the process of deep diagnosis, which refers to the intellectual types of human activity. The process of parrying is a process of flexible restoration of operability based on the results of the diagnosis, associated with a real-time intellectual decision of multivariate tasks regarding a number of conflicting criteria.

Actiators are the key functional element of orientation systems, which have a greater influence on the effectiveness of the spacecraft's functioning. Electric flywheel motors are used as actuators for long-term and responsible

space missions. The idea of using electric flywheel motors belongs to the founder of theoretical cosmonautics K. Tsiolkovsky. The practical use of electric flywheel motors began in 1963 in space vehicles «Cosmos-14», «Cosmos -23» (USSR) and «Nimbus» (USA).

Electric flywheel motors belong to the class of inertial actuators that ensure the redistribution of the kinetic moment between the rotating rotor and the body of the device. Several redundant structures for the placement of electric flywheel motors are used. Two of the most common are known. The first one is the simplest redundant configuration, called the "NASA standard", where a cube is chosen as the reference body. In this configuration, four electric flywheel motors are used, three of which create control moments along the axes of the associated coordinate system, and the moment created by the fourth is directed along the inner diagonal of the cube. This configuration has a low level of fault tolerance, since failure of the diagonal electric flywheel motor results in a canonical, redundant configuration. According to the second configuration, a four-sided pyramid is chosen as a support body. This configuration was developed by General Electric. In this configuration, four electric flywheel motors are placed along the vertical edges of the pyramid. Such placement of electric flywheel motors in actuator units allows to significantly increase the resistance to failure due to the presence of significant redundancy, if the rational control of operability is applied.

The automatic control theory is a scientific basis for the design of spacecraft orientation systems. This theory is based on a number of provisions. Basic is the knowledge of the features of the operation of the control object, which is reflected in the corresponding mathematical models in the form of differential equations, transfer functions, descriptions in the space of states. These models usually describe the nominal mode of operation. In order to describe the abnormal, emergency modes, in accordance with the basic position of the automatic control theory, appropriate mathematical models are needed, which connect the signs of the causes of destabilization of operabity with the signs of disturbances that can be measured or estimated. Such models are called diagnostic, and they are used in the implementation of the principle of control by diagnosis for rational control of the operability of electric flywheel motors.

One of the modern trends in the development of the automatic control theory is related to the formation of the concept of adaptive control and the corresponding tools. The study of a new principle of control by diagnosis

leads to the formation of a new class of adaptive systems: systems of rational control. The monograph presents the results of research on the principle of control by diagnosis in relation to the control of operability of the electric flywheel motors unit.

The first section provides general information about spacecraft orientation systems. Typical flight modes of spacecraft, characteristic and disturbing effects are described. The classification of orientation systems is provided. Examples of the MS-2-8 remote sensing microsatellite orientation and stabilization control system, the “Spektr” spacecraft control system, and the “Monitor-E” spacecraft control system are given. The design of the DM20-250 series flywheel electric motor for the “Elektro” spacecraft is described. World-famous manufacturers of flywheel electric motors are presented.

The second section is devoted to the installation schemes of electric flywheel motors. The main provisions on the variety of possible installation schemes are considered. The provisions are based on the use of properties of regular convex polyhedra. The diagram of the cubic installation of three motors and the installation diagram of four electric flywheel motors is described. Examples of the practical use of the schematics of the cubic installation of electric flywheel motors on the “Meteor-M”, “Kupon”, “EgyptStat-1”, and “MS-2-8” spacecraft are given. Schemes of a pyramidal installation and examples of their use are considered. Prospective schemes for installing an excessive number of electric flywheel motors are described. The ball electric flywheel motor and examples of its use are presented.

The third chapter examines the electric motor-flywheel as an object of rational control. First, the main theses of rational control are outlined. The functional schemes of the rational control object and the rational control device are described. The areas of variation of the parameters of the transmission coefficient and the time constant are considered. The process of forming a functional scheme of rational control system of an electric flywheel motor for one channel of the actuator unit is described. The possibility of separate rational control of the operability of the power amplifier and the unit of the electric flywheel motor and the tachogenerator is considered. Corresponding functional diagrams are provided. A functional scheme of a two-loop system of rational control is proposed, which uses the principle of control by deviation and the principle of control by diagnosis. The possibility of separately using the principle of control by diagnosis to the functional elements of the control object and the principle of control by deviation to the

entire control object is considered. Models of the nominal functioning of the electric flywheel motor as an automatic control object, based on the Lagrangian approach, are presented. Models of abnormal functioning of the power amplifier and the unit of the electric flywheel motor and the tachogenerator are described. Models of abnormal functioning – diagnostic models – reflect the connection of indirect signs of destabilizing influences accessible to measurement, with direct signs of unmeasured destabilizing influences.

The tasks of diagnostic procedure for the rational control object and the methods of their solution are reflected in the fourth chapter of the monograph. Diagnosis is a technological process of identifying the reasons of the malfunctioning of the rational control object. A set of stages and means of diagnosis is diagnostic procedure. The formation of diagnostic supporting algorithms includes a number of interdependent tasks. The first of them is the detection of destabilization. A functional diagram of the destabilization detection process is presented and the necessary tools are described. The second considered task is the search for destabilizing functional elements. Instrumental means of forming indirect Boolean signs and search procedures are described. Variants of dichotomous destabilization search trees are presented. The third task is to determine the types of destabilizing influences. The essence of the task and methods of its solution are considered. Instrumental means of forming indirect Boolean signs are described in detail. The structure of the dichotomous tree for detecting types of destabilization is given. The fourth described task is determination of types of destabilization. The methods of its solution for specific types of destabilization are considered. A dichotomous tree of the complete diagnosis of the rational control object is given.

In the fifth chapter "Restoration procedure for the rational control object" the methods of restoring the operability based on the results of the diagnosis were reflected. Instrumental means and processes of power amplifier restoration under typical types of destabilizing influences are considered. The peculiarities of restoring the operability of the electric flywheel motor are described. Functional recovery schemes for individual types of destabilization and for all types of destabilization considered during diagnosis are provided. Algorithms for restoring the operability of the angular velocity sensor are described, and functional schemes of signal and parametric adjustment, reconfiguration of algorithms and equipment are given. The features of

restoration of current sensor are considered and the corresponding functional schemes are presented.

The sixth chapter is devoted to the description of the experimental stand for researching the model unit of the pyramidal installation of electric flywheel motors. The first version of the experimental stand was completed by O. Taran during his post-graduate studies. The second variant based on the newer microprocessor was performed by V. Petrenko, the leading engineer of the department. The composition of the experimental stand is presented in the section. Technical characteristics of electric flywheel motors and features of their pyramidal installation are given. Schematic solutions of the rational control device of the experimental stand and features of simulating destabilizing impacts are described. The static and transient characteristics of power amplifiers, electric flywheel motors and tachogenerators are given. Linearized mathematical models of functional elements for the nominal mode of their functioning are presented.

The seventh chapter presents the results of experimental studies of the model unit of electric flywheel motors. Specific algorithms and sofware of the destabilization detection procedure are described, as well as graphs of transient processes illustrating the features of detection of a malfunction of the rational control object for the example of one channel of the model unit. Algorithms, software and graphs of transient processes are described in detail when searching for destabilizing functional elements in a channel with a malfunction. The results of experiments on the identification of destabilizing impacts are also presented and described in detail in order to obtain a complete diagnosis of the causes of malfunctioning in the rational control object. The restoration of the operability of the model unit of electric flywheel motors is also presented by the results of experiments in the form of graphs of transient processes in response to a step setting action. Quantitative characteristics of the execution speed of the procedures for diagnosing and restoring the operability of the rational control object during the transitional process are given.

The results presented in the monograph were obtained over several years during the implementation of fundamental and applied state budget research on the subject of rational control of dynamic objects under conditions of destabilizing influences.

The authors thank to headship of the university for the opportunity to work fruitfully on the topic of the above research and publish the results.

The authors are grateful to Yu. Kuznetsov for professional consultations on the practical use of electric flywheel motors in space vehicles.

Department engineers Yu. Sytnyk and I. Mishina took an active part in preparing the manuscript for publication, deserving great gratitude from the author's team.

A great deal of constructive work on the final preparation of the manuscript for publication was performed by T. Kulik, and the authors are sincerely grateful to her for the impressive results of the fulfilled work.

The authors thank the reviewers O. Zlatkin and P. Kachanov for his friendly attitude towards the topic of research and the obtained results.

Chapter I SPACECRAFT ORIENTATION SYSTEMS

It can be said without exaggeration that the control of the spacecraft orientation is mostly the main mode of control of its movement

B. Raushenbah (1915-2001) – the developer of the first control and orientation systems for spacecrafts

When performing various space missions, spacecraft need to provide a certain orientation relative to its center of mass for different flight modes. Such tasks are performed by the orientation systems of spacecraft. Reasons that disrupt orientation. Principles and types of orientation. Classification of orientation systems. Examples of spacecraft control systems. Spacecraft control systems of "Spectr" and "Monitor-E". Electric flywheel motors. Structure and principle of operation. Types of electric flywheel motors. Specifications.

1.1 General information about spacecraft orientation systems

Spacecraft is a class of fluing vehicles that includes artificial satellites of the Earth and other planets, orbital and interplanetary stations, spaceships, and supply transport ships. During the execution of the flight program of the spacecraft, it is necessary to control its orientation. Control of the spacecraft orientation is the implementation of a specified angular movement of the trihedron of axes rigidly connected to the body of the spacecraft relative to some given system of axes of the same name located in space (the origins of both trihedra are located at the same point of the body of the spacecraft), in which movement around the center of mass does not affect the movement of the center of mass itself [1].

Orientation control is required in the following typical flight modes:

1) when changing the movement of the center of mass of the spacecraft, it is necessary to ensure the desired direction of the thrust vector before each inclusion of thrust rocket engines;

2) during the landing of the spacecraft before its entry into the atmosphere, an appropriate orientation with respect to the trajectory of movement is required;

3) when docking a spacecraft with other one, it is necessary to ensure the appropriate orientation with respect to the docking node;

4) to ensure high-quality communication sessions with the flight control center, a certain directionality of the spacecraft antenna is required;

5) ensuring the efficient functioning of the solar batteries of the power supply system is related to the orientation of the working surfaces of the batteries normally to the direction of the sun's rays;

6) in the case of using solar energy for the necessary organization of biological processes in a spaceship with a crew;

7) when performing the current tasks of the space mission, during scientific experiments, astronomical research, meteorology and other functional tasks, the appropriate orientation of the spacecraft is needed;

8) to parry the consequences of a violation of the necessary orientation of the spacecraft caused by the disturbing effects of the space environment;

9) when diagnosing and restoring the functionality of functional elements of the control system in the event of failures and malfunctions.

To understand the necessary composition of equipment and the structure of orientation systems, let’s consider the external conditions of the functioning of space vehicles. Space in which the apparatus moves has a low density of matter. Therefore, even at significant, compared to terrestrial, speeds of movement, there are no significant forces and moments of interaction with the environment. This circumstance leads to the possibility of separate consideration of the movements of the center of mass and movements relative to the center of mass.

In space, aircraft are subject to turbulent moments created by gravitational, magnetic, and electric fields, atmospheric resistance, solar and cosmic rays, and meteorite impacts. Knowledge of the values of the disturbing moments is necessary for a properly justified choice of the type and parameters of actuators of the orientation system. Thus, the nature of gravitational disturbances is determined by the law of universal gravitation. Gravitational moments are calculated according to the appropriate formulas [2]. For example, for a spacecraft moving in a circular orbit with moments of inertia $J_x = 5200\ \text{kg}\cdot\text{m}^2$, $J_y = 11100\ \text{kg}\cdot\text{m}^2$, $J_z = 6900\ \text{kg}\cdot\text{m}^2$, $J_{yz} = 210\ \text{kg}\cdot\text{m}^2$ with angular deviations of the orbit –2°, at the altitude $H = 800$ km turbulent moments will follow: $M_x = 10{,}7\cdot10^{-4}\,\text{N}\cdot\text{m}$; $M_y = 1{,}8\cdot10^{-4}\,\text{N}\cdot\text{m}$; $M_z = -0{,}22\cdot10^{-4}\,\text{N}\cdot\text{m}$ [3].

The high rarefaction of the upper layers of the atmosphere at high speeds of the space vehicle leads to the appearance of noticeable aerodynamic moments. Thus, the level of aerodynamic moments acting on the “Meteor” satellite at an altitude of 850 km was within $2 \cdot 10^{-4}$ N·m [3]. The moment from the pressure of the sun's rays does not exceed the value 10^{-2} N·m. The moment from the impacts of meteorites is not higher than 10^{-8} N·m [2]. The total moment of acting disturbances is defined as the sum of all moments acting on the spacecraft.

The estimated values of the perturbing moments give only a superficial idea of the total moment. Depending on the specific design of the spacecraft and the conditions of its flight, each of the considered moments may be dominant in the sum that determines the total moment. Thus, at a low altitude (200–300 km), the aerodynamic moment is more pronounced, and with an increase in the height of the orbit, it decreases sharply. At altitudes above 400 km, the gravitational moment is more pronounced. The magnetic moment can be compared to the gravitational moment, and its magnitude depends significantly on the electrical equipment of the spacecraft. In orbits near the Earth, the moment from the pressure of the sun's rays is significantly less than the gravitational, aerodynamic and magnetic moments. In high geostationary orbits, the moment from the pressure of the sun's rays is greater than the gravitational moment. In orbits with an altitude of 300–400 km, the gravitational, aerodynamic, and magnetic moments are approximately the same. The above comparison of moments is purely conditional in nature, since the specific choice of actuators requires the numerical values of the disturbing moments that act on a specific spacecraft under the conditions of flight in a specific orbit [1–3].

To parry the described turbulent moments and a number of others that change the required orientation of the spacecraft, as well as to perform both typical and other specific flight modes, on-board devices that create the necessary forces and moments are needed. Such forces and moments are created by the relevant actuators. Jet engines, electric flywheel motors, power gyroscopes, and magnetowires are widely used as actuators [1–4].

Jet engines create the necessary control moments due to the change in the thrust force, which is determined by the consumption of jet fuel, and the corresponding placement on the body of the device relative to its center of mass [1].

The use of electric flywheel motor as actuator is determined by the law of conservation of momentum of the system of bodies. According to the momentum theorem

$$\frac{dH}{dt} + \frac{dH_f}{dt} = M_e, \qquad (1.1)$$

where H and H_f – vectors of kinetic moments of the apparatus and the flywheel;

M_e – vector of moment of external forces.

An electric flywheel motor is an electric motor of a special design, in which a change in the angular speed of rotation of an inertial load – a flywheel ensures a corresponding change in the kinetic moment H_f, which leads both to parrying the moment of external forces M_e and when $M_з = 0$ to changing in the angular position of the spacecraft relative to the center of mass, i.e. to its necessary orientation [3, 4].

Power gyroscopes as actuators have a longer history of use and development, which originated in shipbuilding to stabilize the position of ships during pitching [4]. Electric flywheel motors are, in fact, a single-stage gyroscope that has one degree of freedom associated with the rotation of an inertial flywheel around the axis of symmetry, stationary relative to the spacecraft body. Two-stage power gyroscopes have two degrees of freedom relative to the spacecraft body. Three-degree force gyroscopes are gyroscopes with three degrees of freedom in the spacecraft body. In power gyroscopes, the control moments are formed by changing the magnitude and sign of the angular velocity of the rotor [1].

The principle of operation of the magnetic circuit as an actuator is based on the interaction of the magnetic field of the power coils or permanent magnets installed on the spacecraft with the Earth's magnetic field [2].

Information about the consequences of their influence on the angular positions of the spacecraft, i.e. on its orientation relative to the basic reference system, is necessary to parry the perturbing moments. Various measuring devices based on different physical principles are used as orientation sensors. When using external sources of information, such as magnetic and gravitational fields, streams of radiant energy emitted or reflected by celestial bodies, measuring devices corresponding to the source are also used. So, when using radiant energy, sensors of the Sun or star sensors (for example, sensors of the North Star and Canopus) are used,

which are based on the principle of optical-electronic conversion of radiant energy into an electrical signal.

A representative class of orientation sensors are inertial sensors. These sensors use the properties of the absolute angular movement of orientation axes and axes rigidly connected to the apparatus body. Gyroscopic devices, angular velocity sensors and accelerometers are used as sensitive elements in these sensors [1, 3].

The processing of measuring information about the angular position of the spacecraft and the formation of control signals to the actuators is carried out with the help of on-board computres. To ensure the high-quality functioning of sensor units and units of actuators, built-in microcontrollers are used, which are located in the network structure with the central control center of the spacecraft main computer.

The spacecraft's attitude control systems, and even their subsystems, are designed, manufactured, and operated using the classic principle of control by deviation. The positive experience of many years of using this principle in various automatic control systems of space vehicles testifies to the possibility of satisfactorily parrying the disturbing forces and moments of outer space. At the same time, in addition to external disturbing forces and moments in relation to the spacecraft, there are also internal causes, internal disturbing actions, which lead to a violation of the required angular position, within the orientation systems. These internal causes are caused by malfunctions, breakdowns, failures of sensor units, actuator units, and spacecraft bodies. In total, the subsystem which includes the actuator unit, the spacecraft body and the sensor unit is an orientation control object (OCO), and the subsystem of the on-board computre with the corresponding interfaces is an orientation control device (OCD). These two subsystems OCO and OCD, combined according to the principle of control by deviation, form the spacecraft orientation control system. Thus, if external disturbances affect the body of the spacecraft, then internal disturbances destabilize the operation of the subsystem OCD. All disturbing influences, both external and internal, disrupt the normal mode of orientation and are, in fact, destabilizing influences for the spacecraft orientation systems.

Orientation systems based on the principle of control by deviation can parry internal disturbances only in very rare situations when their magnitudes

are small. Traditionally, for parrying in this case, the principle of majorization is used, which consists in the excessive use of units with a selection of output signals that mostly coincide. The majority principle is not inherently a control principle, as it is not related to a purposeful change in the nature of the unit's output signal. The principle of reconfiguration is based on disconnecting the unit that failed and connecting the backup one by a failure detection signal, is also not a control principle in the classical sense. The use of the principle of majoritization and the principle of reconfiguration leads, firstly, to a significant increase in the mass-dimensional characteristics of orientation systems, secondly, to a significant increase in energy consumption, and thirdly, to inefficient use of excess on-board resources of the spacecraft.

It is possible to improve the situation with parrying destabilizing influences by jointly using the principle of in-depth diagnosis of the causes of destabilization and the principle of flexible management of excess resources. The use of these principles expands the functionality of orientation systems for parrying both normal and abnormal operation modes caused by destabilizing influences, and also increases the quality indicators of the process of controlling the angular position of the spacecraft.

1.2 Classification of orientation systems

Existing spacecraft (SC) orientation systems represent a large variety of different types. In order to make this set available for viewing from certain points of view, a method of classification is used, which consists in dividing the set into classes. The division is carried out according to the characteristics that reflect different points of view, that is, goals. Traditionally, the types of orientation axes, the level of human participation in control, the points used for orientation, and a number of other features determined by research tasks are used as features for the classification of orientation systems [1, 2, 5]. In accordance with the subject of the book, let’s consider a hierarchical classification based on a number of features characterizing the controlling moments for the implementation of orientation. Scheme on Figure 1.1 gives such a classification.

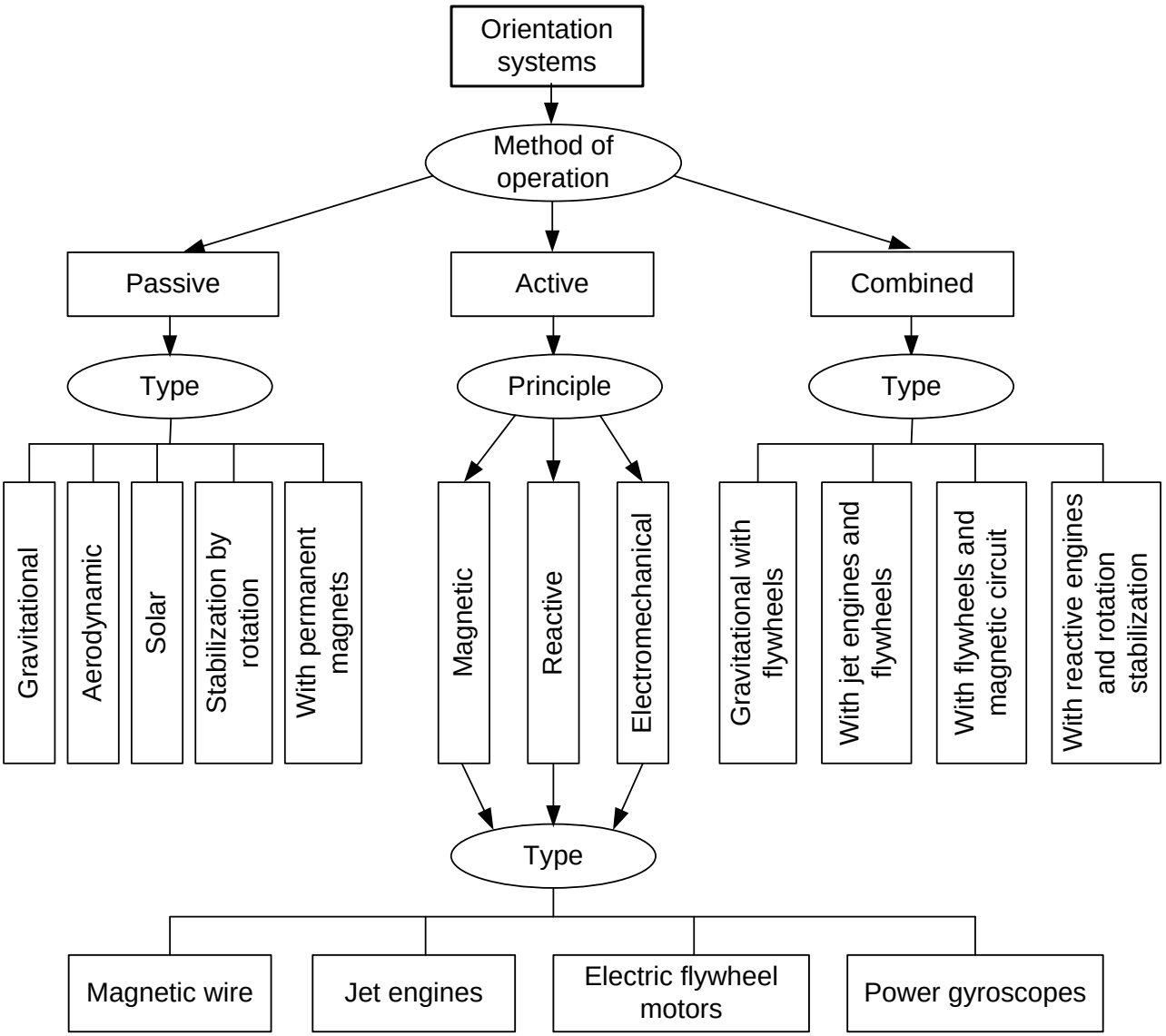

Figure 1.1 – Classification of orientation systems

The first feature of the classification – method of operation – is a method of creating control moments for spacecrafts. According to this feature, many known orientation systems can be divided into three classes. The first class is represented by passive orientation systems. The steering moment in such systems is created by the interaction of the spacecraft with the environment, in particular, as a result of interaction with gravitational or magnetic fields, or due to solar pressure, or aerodynamic resistance, or rotation relative to the longitudinal axis of the spacecraft. When maintaining the orientation of the spacecraft in passive systems, on-board energy sources that produce mass ejection are not used, and therefore are ideally economical. According to the type of external control moments used, gravity rod orientation systems, aerodynamic spherical and solar sails are distinguished. Gravitational

systems have become the most widespread. The analysis of the angular movements of spacecraft when using external control moments indicates the presence of oscillating undamped movements. Thus, the complete absence of damping is characteristic of the angular movements of the spacecraft when using passive orientation devices. Therefore, it is necessary to provide artificial damping using an automatic orientation system that responds to the angular velocity of the spacecraft [2].

In active orientation systems representing the second class, control torques are created due to the use of jet fuel or on-board power sources to rotate the flywheels. According to the principles of formation of control moments used in active systems, magnetic, reactive and electromechanical orientation systems are distinguished. In magnetic orientation systems, the control moment is created with the help of electromagnets interacting with the Earth's magnetic field. Jet engines of various types are used in jet orientation systems. Combustion products, compressed gas or ion-plasma flow, passing through special nozzles installed in a certain way, create reactive forces applied to the spacecraft relative to the center of mass. The electromechanical principle of creating control moments consists in the use of rotating inertial masses placed inside the spacecraft [3]. According to the type of implementation of the principles of creating active control moments, actuators such as magnetowire, jet engines, electric flywheel motors (EFM) and power gyroscopes are distinguished. Combined systems are active management systems that use combinations of different types of executive bodies.

The given classification is quite conditional, but at the same time, it definitely reflects the place of electric flywheel motors in the variety of known orientation systems.

1.3 Examples of spacecraft control systems

Examples of control systems of specific spacecrafts allow to understand the necessary composition of hardware for solving orientation tasks and the role of EFM when solving these tasks.

First, consider the generalized functional diagram of the spacecraft control system, which gives an idea of the tasks that the spacecraft control system solves [6] (Figure 1.2).

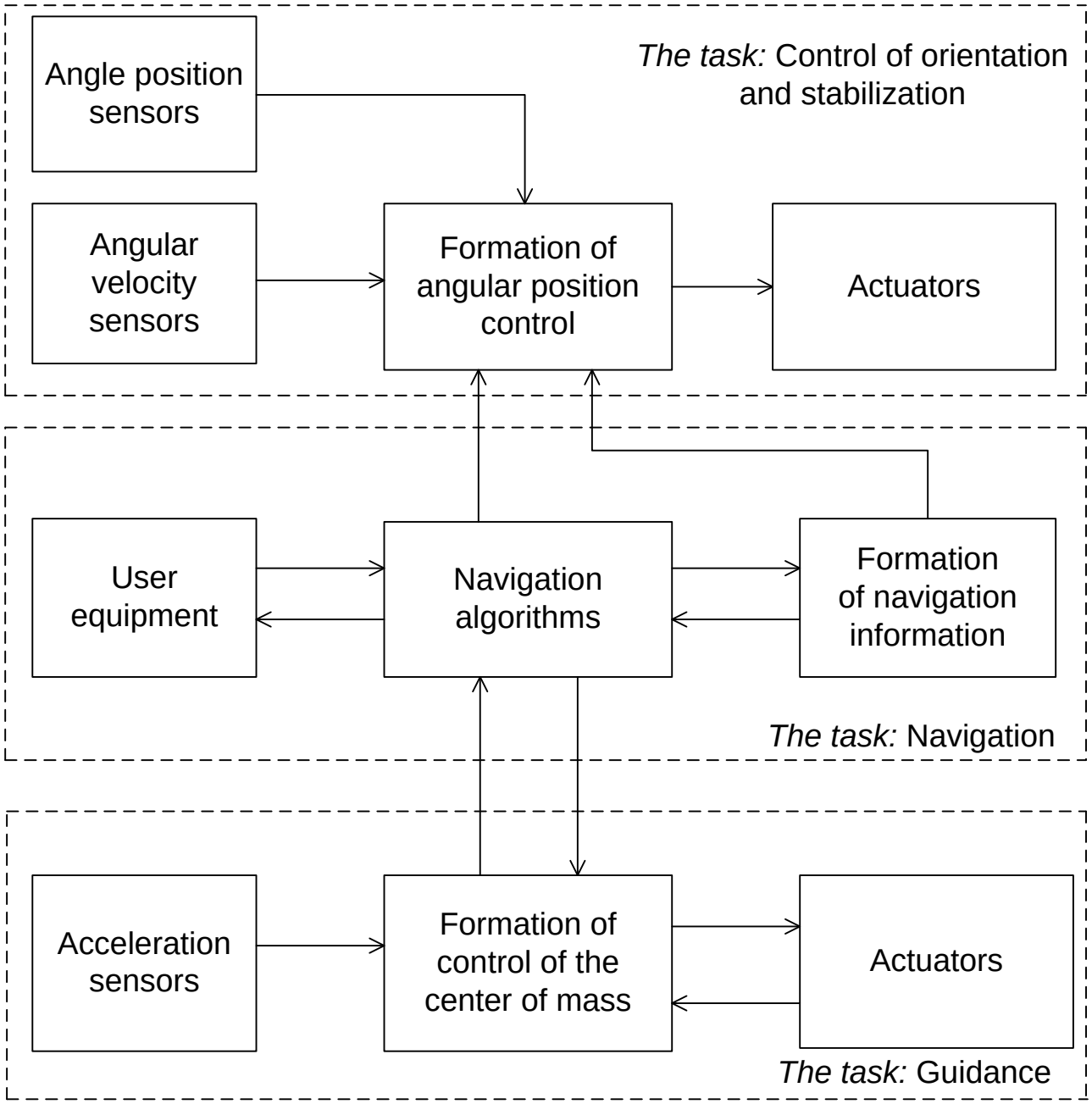

Figure 1.2 – Generalized functional scheme
of spacecraft control system

Three interrelated tasks are solved on a maneuverable autonomous spacecraft:

1) control of orientation and stabilization of angular positions relative to the center of mass;

2) spacecraft navigation in space;

3) guidance of the spacecraft on the target.

To solve these tasks, each control subsystem uses task-specific instrumentation, algorithms and software.

Let's consider in more detail the solution to the first task of orientation and stabilization control using the MS-2-8 Earth remote sensing microsatellite as an example [6]. A functional diagram of the orientation and stabilization control system is shown in Figure 1.3.

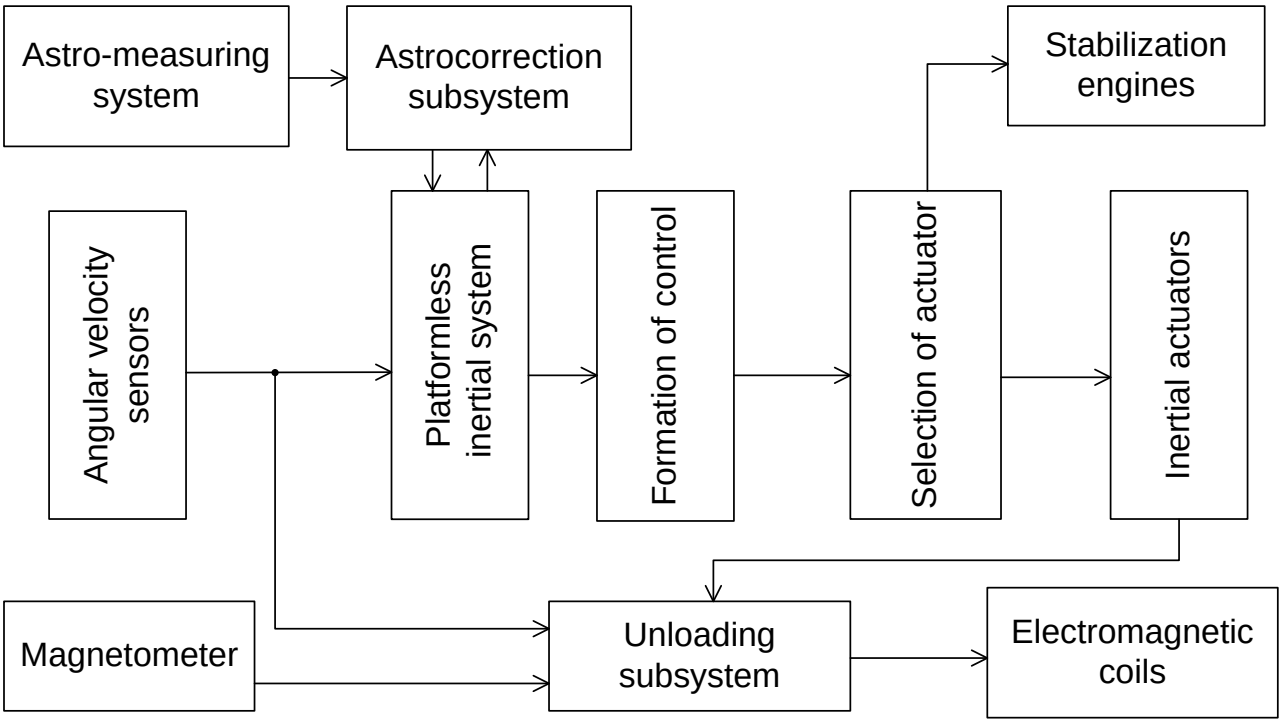

Figure 1.3 – Functional scheme of the orientation and stabilization control system of the MS-2-8 satellite

In the presented system, EFM and force gyroscopes are used as inertial actuators, the unloading of which is carried out with the help of magnetic coils. Jet engines are used as stabilization engines.

As an example, let's present a structural diagram of the control system of the “Spektr” scientific spacecraft, the development of the SME “Hartron-Arcos” [6]. Spasecraft was designed to study the magnetic radiation of the Galaxy and stars. Orbits of the device at apogee from 170,000 km to 350,000 km, at perigee from 300 km to 5,000 km; orientation accuracy 0,2″...3′; angular stabilization accuracy 0,1″...2,5′; by angular velocity $< 0{,}0001^{\circ}/_{\text{c}}$. The composition of the control system is described in the structural diagram shown in Figure 1.4.

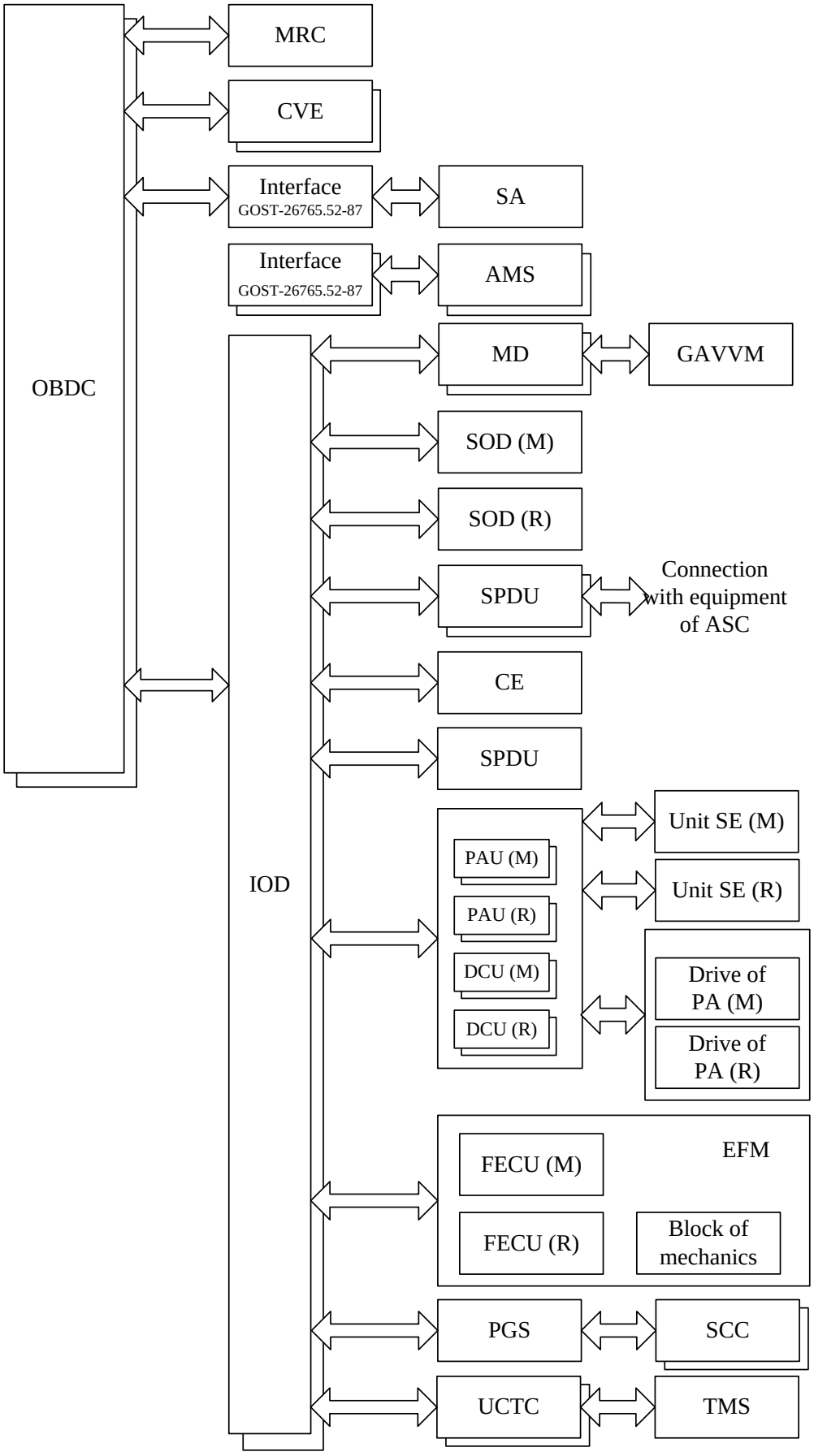

Figure 1.4 – Structural diagram of the “Spektr” spacecraft control system

In Figure 1.4 the following abbreviations are used: OBDC – on-board computer; MRC – module of relay commands; CVE – control and verification equipment; SA – scientific equipment; AMS – astro-metric system; IOD – input-output device; GAVVM – gyroscopic angular velocity vector meter; MD – matching device of GAVVM; SOD – sun orientation device; M – main; R – reserve; SPDU – switching and power distribution unit; ASC – automatic spacecraft; CE – correction engine; PAU – power amplifier unit; DCU – drive control unit; SE – stabilization engines; PA – pointed antenna; EFM – електродвигуни-маховики; FECU – flywheel engine control unit; PGS – power gyroscopic complex; UCTC – unit of coordination of telemetry control; SCC – static current converter; TMS – telemetry station.

From the given structural diagram, the hardware composition of the control system of the scientific spacecraft "Spectr" is obvious, and even the connection of the equipment with the OBC, which controls the process of its use. Along with SE(M) and SE(R), EDMs are also used for spacecraft orientation.

Let's consider the approach to the design of on-board control systems of the Moscow Research and Design Bureau "Mars" [7]. In the development of the bureau, on-board control systems (OBCS) perform the following basic functions:

1) control of the spacecraft movement around the center of mass using electromechanical actuators;

2) ensuring the given orientation of the spacecraft in the basic coordinate system;

3) implementation of angular stabilization of the spacecraft in the specified orientation system with the required accuracy;

4) determination of the current parameters of the angular and trajectory movement of the spacecraft;

5) damping of the residual angular velocity of the spacecraft after separation from the carrier;

6) rotation of the spacecraft to the desired orientation after damping;

7) unloading of EFM to reduce the accumulated kinetic moment;

8) correction of the spacecraft's orbit by turning on and off the engines;

9) control of the functioning of engines;

10) control of the orientation of solar panels;

11) control of the pyrotechnic equipment of the spacecraft;

12) management of target equipment and power supply system;

13) management of the telemetry measurement system (TMS);

14) management of the work of means that ensure the thermal regime;

15) real-time checking of the on-board control system and parrying the consequences of failures;

16) maintaining the on-board time scale with the specified accuracy.

The OBCS includes (Figure 1.5):

1) on-board digital computer system (OBDCS), in which control influences on actuator equipment are produced and information interaction with other spacecraft systems is carried out;

2) power automation units (PAU), which carry out power supply switching for actuator equipment;

3) an information and measurement system (IMS) that ensures the implementation of spacecraft control processes with the specified accuracy;

4) actuators (A) for working out the control influences in order to change or stabilize the position of the spacecraft in space.

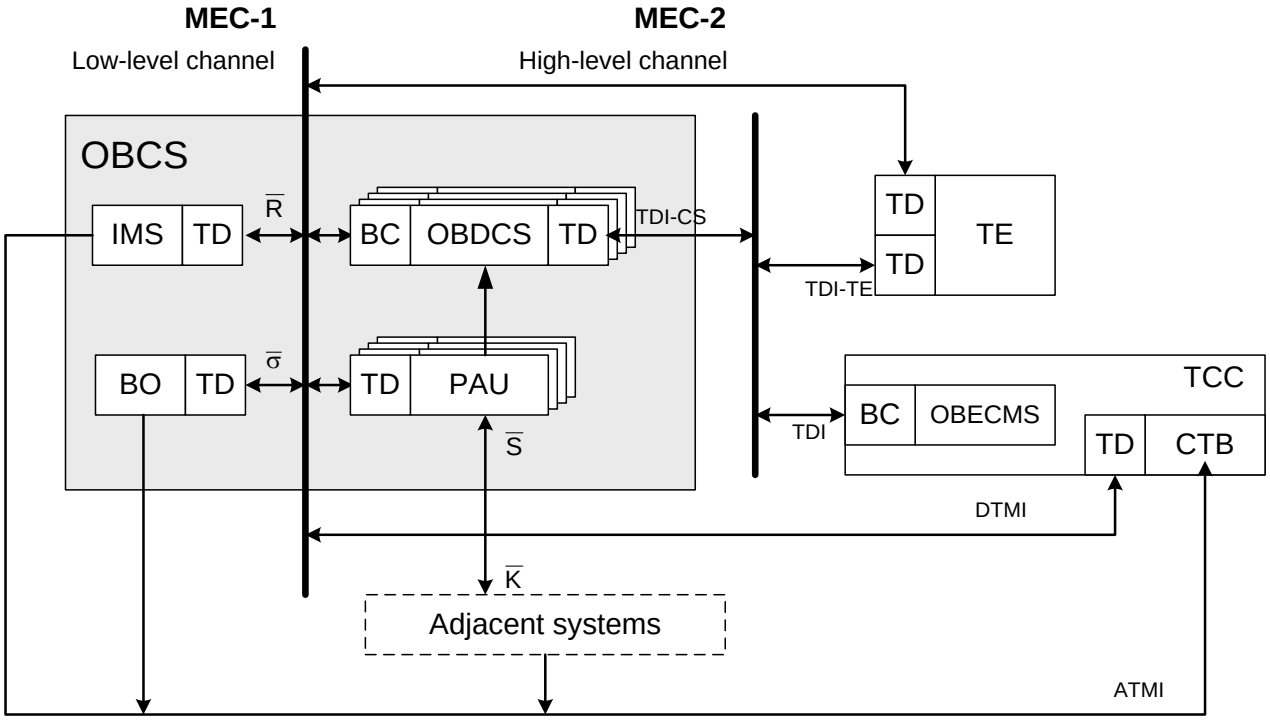

Figure 1.5 – Structural diagram of the on-board control system

OBDCS communication with units and systems, as well as with target equipment (TE) and STV is carried out via a multiplex exchange channel (MEC-1).

On-board equipment of the command and measurement system (OBECMS) is connected with OBDCS and TE via the second exchange

channel (MEC-2). The OBDCS is the bus controller (BCO) to all devices except OBECMS, to which it is the terminal device (TD).

In IMS, a vector of spacecraft state parameters is formed, which is sent to OBDCS, where it is used in computational algorithms. As a result of the calculations, a control vector $\bar{\sigma}$ is formed, which is sent to VO. PAUs receive a vector of signals from adjacent systems and transmit a vector of commands $\bar{K}$ to them. Command and program information (CPI) comes from the ground control complex through the TCC to the PAU, and analog (ATMI) and digital (DTMI) telemetry information - in the reverse order.

The structural diagram of OBCS "Monitor-E" is presented in Figure 1.6. This is the first development of the "Mars" bureau, which became the basis for further developments for the "KazSat", "Express-MD1", "Electro-L", "Spektr-R" spacecraft.

The following abbreviations are used in the scheme: TDSOS – thermodynamic satellite orientation system; AS – astrosensor; GAVVM – gyroscopic angular velocity vector meter; CFCE – a complex of flywheel control engines; FM – двигуни-маховики; ED – electronic device; PMC – power magnetic complex; SCD – switching and converting device; PFE – panchromatic film equipment; CU of ISTS – the control unit of the information storage and transformation system; DAFE – distributed access filming equipment; OBECMS – on-board equipment of the command and measurement system; TCS – telecommand system; SNE – satellite navigation equipment; OB – overclocking block; CECE – conversion and engine control equipment; SAOE – solar array orientation equipment; SETR – a system for ensuring a thermal regime; ERC of PSS– equipment for regulation and control of the power supply system; PCREE – pyro cartridges revealing external elements.

To solve the tasks of orientation and stabilization in the "Monitor-E" spacecraft, 4 flywheel engines were used. In subsequent technologies, CFCE was also implemented.

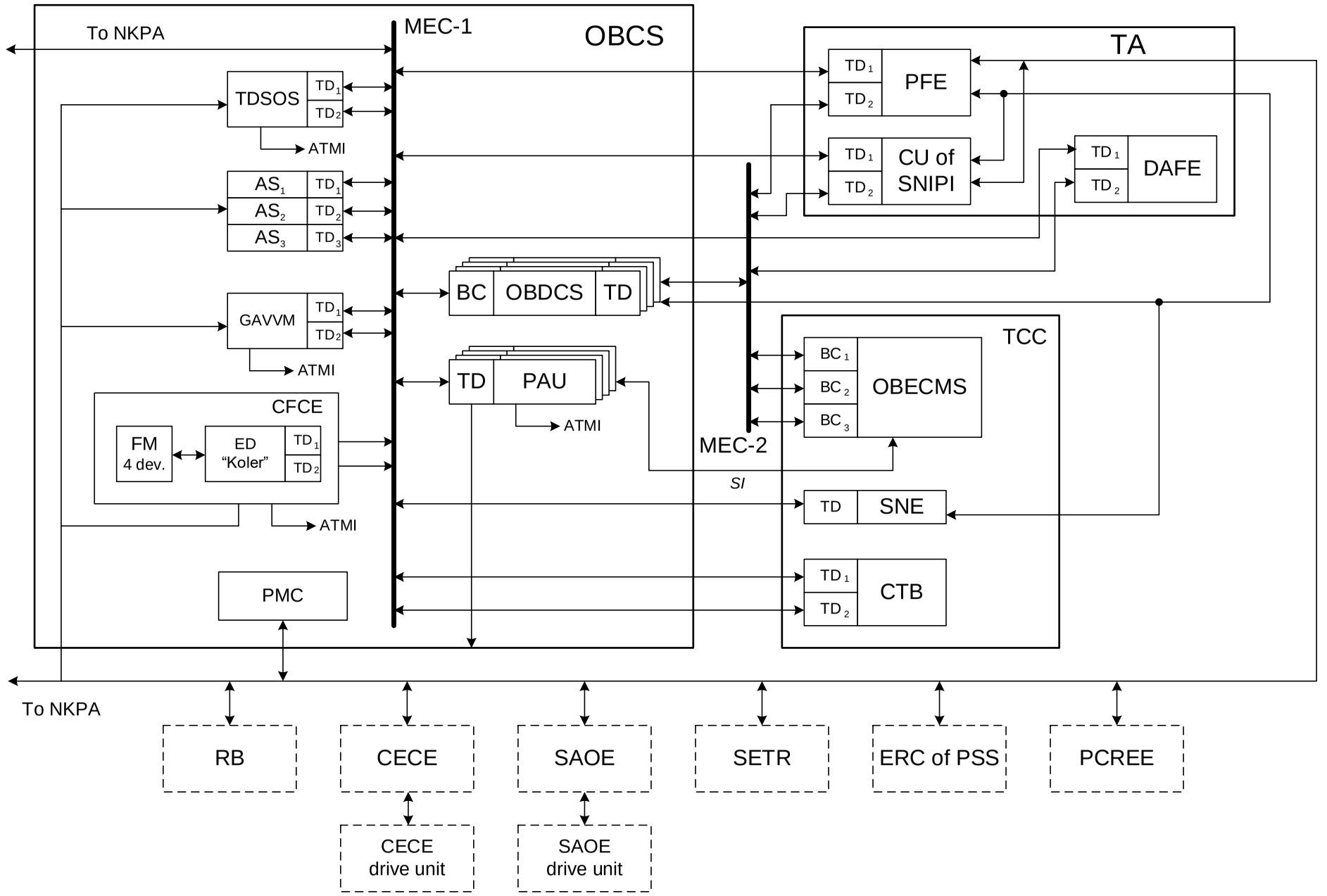

Figure 1.6 – Structural diagram of the on-board control system of "Monitor-E" spacecraft

1.4 Electric flywheel motors

The application of EFM as actuators located along the three axes of the spacecraft-related coordinate system was proposed by K. Tsiolkovskyi in 1902 [8].

In the first electromechanical orientation systems of the "Meteor" and "Resurs" spacecraft (1963), asynchronous electric flywheels motors with electronic converters were used, developed by " SME VNDIEM" [3]. According to the principle of action, they were relay. Later, a series of actuators based on controlled brushless DC motors with permanent magnets was developed. In these electric motors, torque control was carried out by changing the current in the armature winding. The current value is controlled by a regulator with pulse width modulation according to an external control signal, with which the current in the armature winding is compared. Application of the new EFM made it possible to implement linear control algorithms in flywheel orientation systems.

The design of the EFM of DM20-250 series for the spacecraft "Electro" is shown in Figure 1.7.

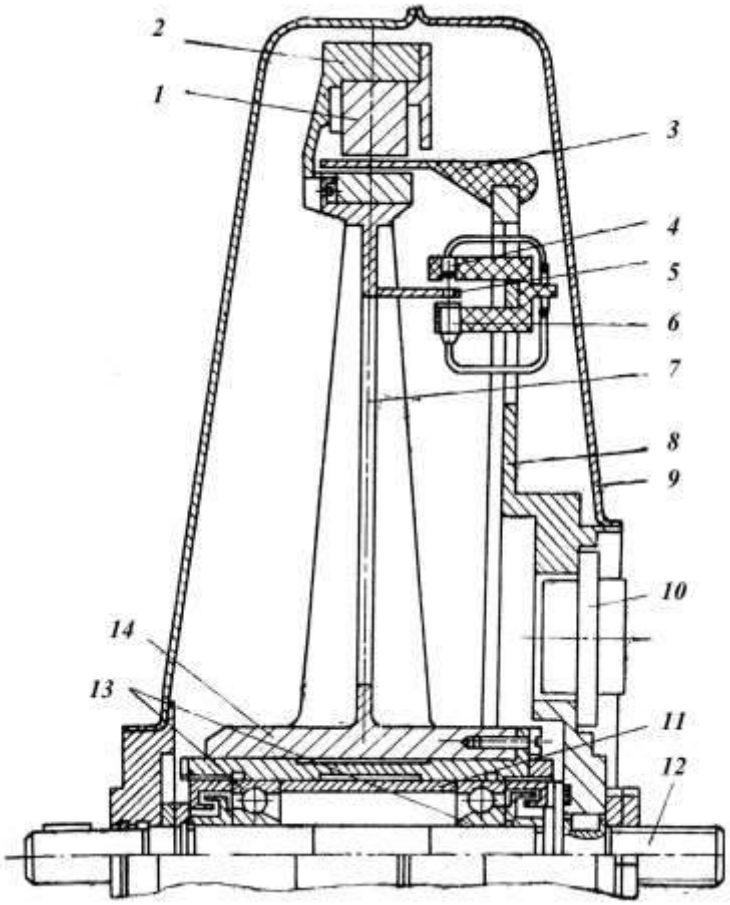

Figure 1.7 – The design of typical electric flywheel motor

In this design, the flywheel rotor, which is installed on two bearings 13, is expanded inside of the hermetic case 9. The inner rings of the bearing are mounted on a fixed axix 12. Through the narrowing of the end of the axis are brought outside the casing and serve to attach the EFM to the spacecraft. The distance between the bearings is maintained with the help of a bushing11.

The shape of the flywheel rotor 2 is a rim. The rim consists of external and internal magnetic conductors fixed on spokes 7 and hub 14. Permanent magnets 1 magnetized in the radial direction are located in the bore of the external magnetic conductor. The external and internal magnetic conductors are connected by a shielding jumper and form a single part. Magnetic shields localize magnetic fields in a given area, eliminating stray fields that could cause braking moments acting on the rotor from the side of the structural elements.

Stator 3 is located in the gap between the magnets and the internal magnetic conductor. It is made in the form of a thin-walled frameless cylinder formed by the conductors of the armature winding and filled with compound. The stator is fixed on the flange 8, welded to the casing 9. This design allows not only the rim to be used as an inertial mass, but also the active parts - magnets, which helps to minimize the specific mass characteristics of the EFM.

The switching of the windings is carried out by a commutator controlled by Hall sensors, which are located on the motor armature in the working gap.

On the flange there is a connector for connecting EFM electrical circuits with the control circuit, as well as valve 10 for maintaining a given pressure difference inside the casing in relation to the surrounding space.

To determine the kinetic moment, a block of emitting diodes 4 and a photodiode 6 are used. They are separated by a thin-walled screen cylinder 5 with 240 holes installed on the rotor. The block contains two optical pairs shifted by 90º. When the flywheel rotates, the photodiodes periodically light up through the screen holes. They generate an alternating voltage with a frequency that is proportional to the frequency of rotation of the rotor. As a result of processing the signals of two optical pairs, the frequency and direction of rotation of the flywheel is calculated.

EFM of the DM20-250 series with a diameter of about 0.4 m and a mass of 10 kg develops a maximum kinetic moment of 20 N·m·s (Figure 1.8). The maximum frequency of rotation of the rotor is 1100 min^{-1}. The control torque

varies in the range from 0.002 N·m (starting torque) to 0.25 N·m (maximum torque).

Figure 1.8 – View of electric flywheel motor DM20-250

Control of EFM is carried out using the principle of control by deviation. Scheme in Figure 1.9 presents the functional diagram of the electric flywheel actuator.

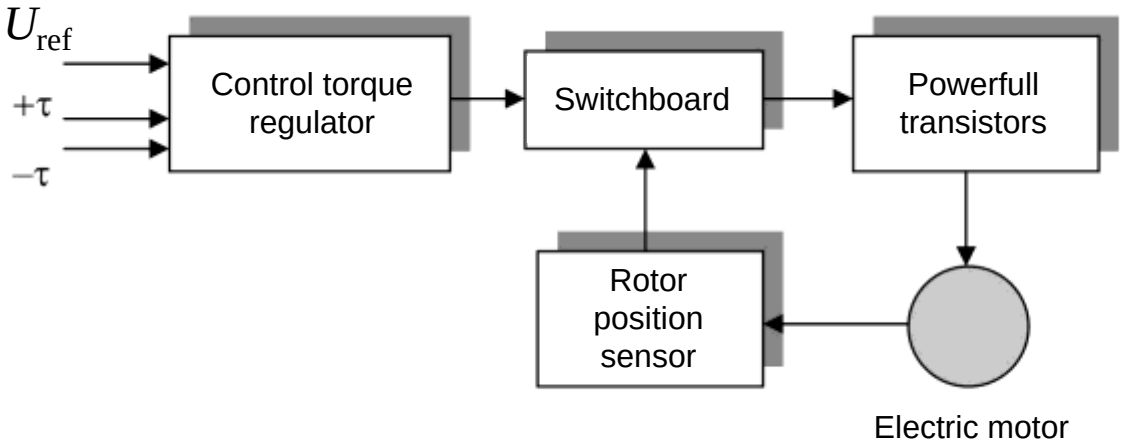

Figure 1.9 – Functional diagram of electric flywheel actuator

Control of EFM kinetic moment is carried out by means of PWM signals coming to the commutator and powerfull transistors. PWM signals are generated by setting time intervals $+\tau$ and $-\tau$. The commutator ensures the activation and deactivation of the sections of the electric motor winding according to the signals of the angular position sensor in accordance with the sign of the control signal $+\tau$ or $-\tau$.

Among the variety of EFM designs, we highlight the promising spherical EFM with a magnetic suspension of the rotor [3] (Figure 1.10). The flywheel

rotor is made in the form of an empty steel ball, which is held inside the case with the help of six electromagnets.

Figure 1.10 – Spherical electric flywheel motor

One spherical EFM replaces three uniaxial EFMs and thereby provides a gain in mass. A spherical EFM with a rotor diameter of 0.64 m and a total mass of 230 kg was used for three-axis stabilization and slow turns of the “Salyut” and “Diamant” orbital stations. It develops a control moment up to 3 N•m and a kinetic moment up to 200 N·m·s.

The production of EDM is carried out using high-tech equipment and with a high technological culture, therefore only a few companies that product high-quality EDM are known. The most famous EFM manufacturers are presented in Table 1.1 [9].

All EFMs are designed for the operation of electromechanical units outside the hermetic container of various spacecraft. For example, VNDIEM’s EFM is used as part of GLONASS-type satellite orientation and stabilization systems. The orientation and stabilization system provides damping of satellite oscillations after separation from the means of extraction, initial orientation of the solar panels to the Sun and the longitudinal axis of the satellite to the Earth, as well as stabilization of the satellite in the process of orbit correction. EFM unloading is carried out with the help of a magnetic circuit.

Therefore, promising EFMs are used in spacecraft orientation systems as actuators for long flights.

Table 1.1

Parameter name, dimension	Country, manufacturer, model of FM							
	Canada, Dynacon, MW1000	Canada, Dynacon, MW4000	Germany, Teldix, RSI 4-75/60	Germany, Teldix, RSI30-280/30	USA, Honeywell, HR16	Russia, VNDIEM, ДМ1-20	Russia, VNDIEM, ДМ5-50	Russia, VNDIEM, ДМ20-250
Kinetic moment, N·m·s	1,1	4	4,0	30,0	50	1,0	5,0	20,0
Control moment, mN·m	30	50 - 150	75	280	200	20	50	250
Rotation speed, rot/min.	10000	10000	7000	7300	6000	65000	63500	61470
Interface	RS-422/485	RS-422/485	-	-	-	-	-	-
Steady-state power, W	5	7,5	-	-	22	-	-	-
Maximum power, W	41	75	20	-	105	15	31	70
Supply voltage, V	28	28	-	-	14	-	-	-
Mass, kg	14,5	5,2	-	-	12	1,4	3,8	11,5
Dimensions, mm	130×130×90	250×250×110	-	-	Ø 351, height – 159	Ø 150, height – 95	Ø 225, height – 114	Ø 360, height – 160
Term of service, years	5	5	15	15	15	13	13	13

Chapter II PLACEMENT SCHEMES OF ELECTRIC FLYWHEEL MOTORS

Those who correctly find the general can also correctly consider partial things.

Pythagoras (VI century BC) – philosopher and scientist, founder of the Pythagorean school, whose achievements became fundamental for the development of ancient civilization

A number of practical schemes for placeing electric flywheel motors on spacecraft are known. What is the reason for such diversity? Is this diversity limited or not? What are the theoretical prerequisites for researching other possible placement schemes? What are the properties of known schemes for installing electric flywheel motors? These and other questions of practical installation are answered in the following chapter.

2.1 Basic provisions on the variety of possible placement schemes

Performance of long-term space missions requires the operability of spacecraft orientation systems and, in particular, EFM. The resource capabilities of EFM are limited and do not always coincide with the required resource of the spacecraft mission. Moreover, the passport service life of EFM is not always confirmed in practice due to malfunctions and failures inevitable in space flight. Therefore, the developers of electromechanical units are forced to use an excessive amount of EFM in order to ensure the trouble-free functioning of the actuators during the entire long-term mission.

Well-known practical EFM placement schemes are based on the use of such geometric figures as a cube and a pyramid. A cube and a pyramid belong to the class of convex polyhedra. It seems appropriate to consider the entire class of convex polyhedra, which will allow us to form a reasonable idea about the potentially possible variety of EFM placement.

A polyhedron in three-dimensional space is a collection of a finite number of planar polygons such that each side of any polygon is simultaneously a side of another [8]. A polyhedron is called convex if it lies on one side of the plane of any of its faces. The interior of the polyhedron is a convex body.

One of the main theorems of the general theory of convex polyhedra is Euler's theorem (1758): the number of vertices minus the number of edges

plus the number of faces equals two. It is symbolic that this is the Euler characteristic of polyhedra.

$$V - E + F = 2. \qquad (2.1)$$

The most important for this consideration is the canonical class of regular polyhedra.

Regular polyhedra are convex polyhedra whose faces are all regular polygons. A polygon is called regular if it has equal sides and angles. Polyhedral angles at all vertices of a regular polyhedron are equal to each other, since their plane and dihedral angles are equal. This means that each vertex has the same number of faces *q*. If we denote the number of angles of a polygon as *p*, then the following inequality is valid:

$$(p-2)(q-2) < 4. \qquad (2.2)$$

Considering now that *p* and *q* are integers at least 3, then all possible pairs (*p, q*) will be as follows: (3,3), (4,3), (3,4), (5,3), (3,5). Figure 2.1 gives regular polyhedras corresponding to inequality (2.2).

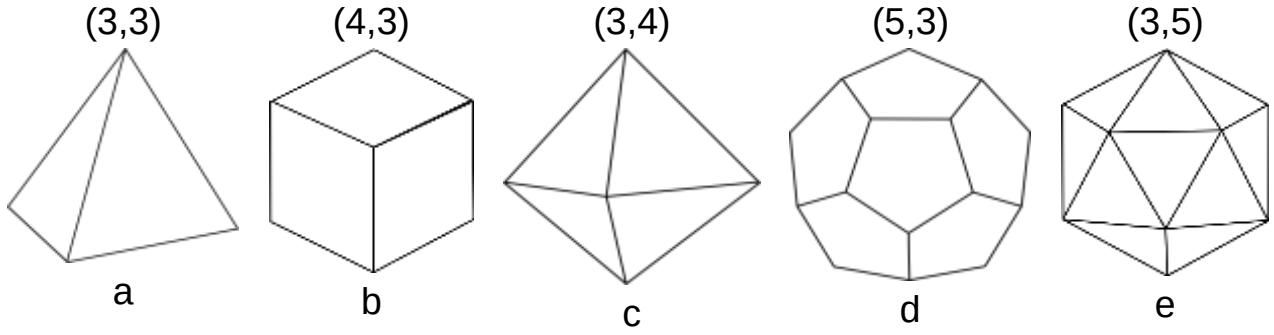

Figure 2.1 – Regular convex polyhedra

The presented polyhedra have a different number of faces and are named according to the number of faces. Thus, the polyhedron in Figure 2.1, a has four faces and therefore received the name tetrahedron (from the Greek "tetra" – four and "hedron" – face). The polyhedron in Figure 2.1, b is a hexahedron, it is better known as a cube. Eight faces of the polyhedron in Figure 2.1, c, so it is an octahedron. A polyhedron (Figure 2.1, d) with twelve faces is a dodecahedron, and a polyhedron (Figure 2.1, e) containing 20 faces is called an icosahedron.

The remaining four types of polyhedra can be built on the basis of the cube. Johann Kepler considered the cube to be the "father" of all regular

bodies. Thus, the ends of the intersecting diagonals of the opposite faces of the cube will be the vertices of a regular tetrahedron (Figure 2.2, a).

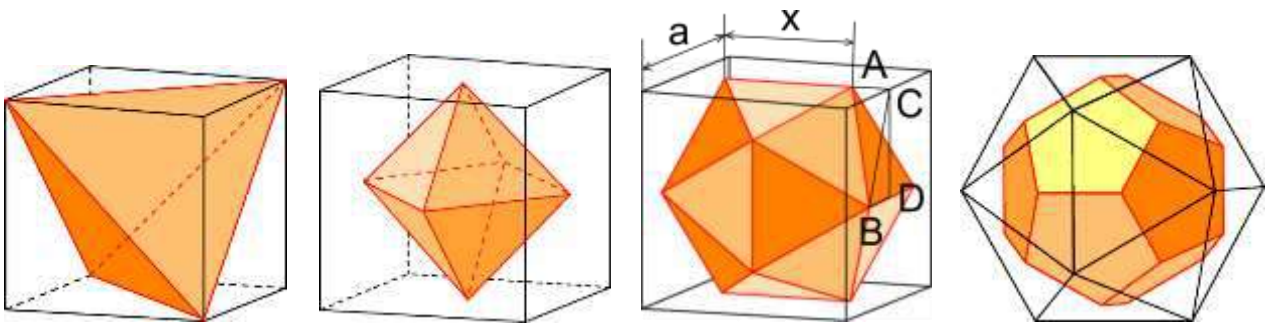

a b c d

Figure 2.2 – Regular polyhedra inscribed in a cube

If we connect the center of each face of the cube with the centers of the neighboring faces, we get 12 equal segments that form the edges of a regular octahedron (Figure 2.2, b). The icosahedron is more difficult to construct. On each face of the cube, parallel to its two sides, draw a segment of the same length x with the middle in the center of the face so that the segments on the adjacent faces are perpendicular. Let's connect the ends of these segments as shown in Figure 2.2, c. The result will be an icosahedron of type (3,5), that is, all its faces are triangles and there are five of them at each vertex. Let's choose x so that all edges are equal. Using the Pythagorean theorem, the length of the edge AB will be equal to

$$AB^2 = AC^2 + CB^2 = AC^2 + CD^2 + DB^2 = \frac{\left[x^2 + a^2 + (a-x)^2\right]}{4}, \qquad (2.3)$$

here a – the length of the edge of the cube.

The condition $AB^2 = x^2$ generates a quadratic equation $x^2 + ax - a^2 = 0$, which positive rott is equal $x = \frac{a\left(\sqrt{5}-1\right)}{2}$. Interestingly, the ratio $\frac{x}{a} = \frac{\sqrt{5}-1}{2}$ is the golden ratio. At a given value of x, all faces of the inscribed polyhedron are regular triangles. There is also a proof of the equality of dihedral angles.

The dodecahedron can be obtained from the icosahedron in the same way as the octahedron from the cube. If we connect the centers of adjacent faces of the icosahedron, we get pentagonal faces (Figure 2.2, d). In total, there will be twelve such pentagons. The proof of the equality of faces and dihedral angles leads to the conclusion that this is a regular dodecahedron [10, 11].

Kepler's cosmic mystery from his book "Mysterium Cosmographicum", published in 1596 [12] is presented in Figure 2.3.

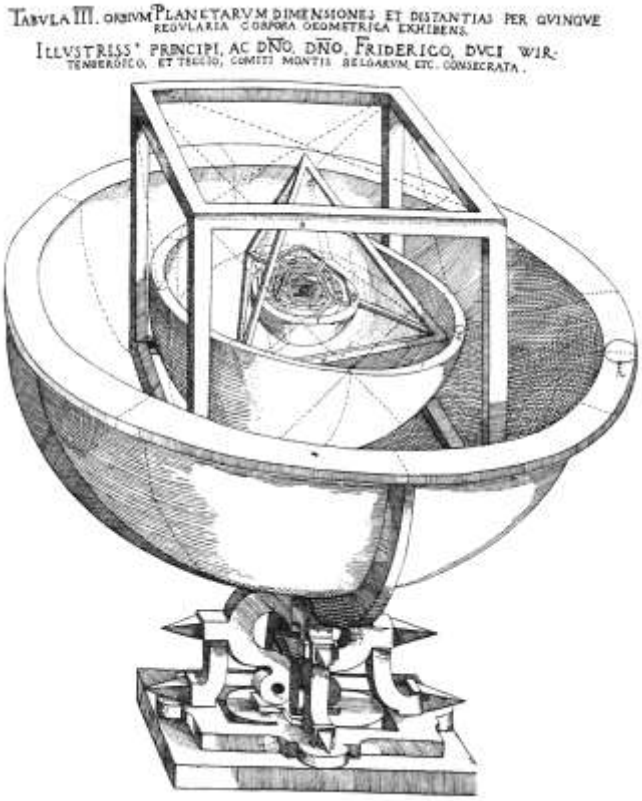

Figure 2.3 – Kepler's cosmic mystery

The spheres of the six planets known at the time, described around five regular Pythagorean (Platonic) solids, of which the outer one is a cube.

The most important property of regular polyhedra is their symmetry. Each regular polyhedron is associated with such a characteristic as a dihedral angle is the angle between adjacent faces. This angle is determined using the formula:

$$\sin\frac{\Theta}{2}=\frac{\cos\left(\pi/q\right)}{\sin\left(\pi/p\right)}. \qquad (2.4)$$

Regular polyhedra have long attracted the attention of scientists, builders, architects and philosophers. The beauty, perfection, harmony of these polyhedra was impressive. The Pythagoreans considered these polyhedra to be divine and used them in their philosophical teachings about the essence of the World. They believed that the elements of the primary basis of existence have the form of regular polyhedra.

The ancient Greek scientist Plato described the properties of regular polyhedra in detail, and that is why they are called Platonic solids. Book XIII of Euclid's famous rudiments [11] is devoted to regular polyhedra.

For the studies of Pythagoras, Kepler and their followers, the fact that there are only five regular bodies is of fundamental importance. Proof of this fact can be obtained from the relation discovered much later by Descartes and Euler, which connects the numbers of faces, edges and vertices in any polyhedron (2.1). Using this equation, we can prove that there are five regular polyhedra.

Therefore, each edge of a regular polyhedron is a common side of two adjacent faces. If all the faces of the polyhedron are *nF*, then the relationship with the edges will be as follows

$$nF = 2E. \tag{2.5}$$

We denote the number of edges that converge on one vertex as E'. Since each edge connects two vertices, then

$$E'V = 2E. \tag{2.6}$$

Substituting the expressions for F and V from the obtained ratios into equation (2.1), we obtain:

$$\frac{2E}{E'} - E + \frac{2E}{n} = 2.$$

Dividing both sides of this equation by 2E after appropriate transformations gives the following equation:

$$\frac{1}{n} + \frac{1}{E'} = \frac{1}{2} + \frac{1}{E}. \tag{2.7}$$

It is obvious that n cannot be less than 3, since a triangle is the simplest polygon, and also that at each vertex of a polyhedron at least three faces converge – $E' = 3$. If n and E' are greater than 3 at the same time, then taking into account the integrity of their values, the left side of the equation will be less than or equal to $\frac{1}{2}$, and for any value of E it will not turn into equality. Thus, the equation is valid when either $n = 3$ and $E' \geq 3$, or $E' = 3$ and $n \geq 3$.

If $n = 3$, equation (2.7) takes the following form:

$$\frac{1}{3} + \frac{1}{E'} = \frac{1}{2} + \frac{1}{E},$$

or

$$\frac{1}{E'} = \frac{1}{E} + \frac{1}{6}. \tag{2.8}$$

In this case, E' can only take the values 3, 4, and 5. When $E' \geq 6$, the equation has no solution. Values $n = 3$ and $E' = 3$ correspond to a polyhedron in which three triangles converge at each vertex. According to equation (2.8) it has 6 edges, then according to equation (2.6) it has 4 vertices, and according to equation (2.5) – 4 faces. It is obvious that it is a pyramid or a tetrahedron. When $n = 3$ and $E' = 4$, an octahedron is obtained, in which four triangular faces converge at each vertex.

If $E' = 3$, equation (2.7) turns into the form

$$\frac{1}{n} = \frac{1}{E} + \frac{1}{6}$$

and, repeating similar considerations, we will get that n can take only the values 3, 4 and 5. When again a tetrahedron is obtained. The value corresponds to a polyhedron of 6 squares – a cube, and the result will be a polyhedron consisting of pentagons – a dodecahedron.

Other combinations of integers are not suitable as solutions for equation (2.7), therefore, there are only five regular polyhedra [12].

This result significantly influenced the opinions and results of many researchers of natural laws.

So, a fundamental feature of the class of convex regular polyhedra is the use of polygons with equal sides and angles as faces. And that is why the class of convex regular polyhedra turned out to be limited and contains, as proved by Euclid, only five figures: tetrahedron, hexahedron or cube, octahedron and icosahedron, which received the generalized name of Plato's solids since ancient times.

In the initial practice of placement of EFMs and the formation of their layout scheme, the concept of "supporting bodies" began to be used – these are geometric figures, to the edges or faces of which the axes of rotation of EDMs were attached. Such geometric shapes were traditionally chosen as a cube or a pyramid. In the following years, they began to explore the possibilities of other support bodies for the formation of a rational layout scheme for the placement of EFM, which meets the tactical and technical requirements for the designed self-propelled missiles. This circumstance led to the fact that both fragments of regular convex polyhedra and their modifications began to be chosen as support bodies. This process is in transitory development, since the placement of EDM using regular convex polyhedra as support bodies often conflicts with the tactical and technical requirements of the spacecrafts being created. As a rule, this contradiction is resolved by a compromise associated with a departure from classical

geometrically correct polyhedral forms. Currently, many spacecraft in operation use placement schemes called "cube" and "pyramid". The search for other rational accommodation schemes continues. This search is due to the need to fulfill such contradictory requirements as increasing the time of active operation of orientation systems with EFM, reducing the weight, size, energy and cost characteristics of hardware equipment, improving the quality and efficiency of the spacecraft orientation and stabilization process.

2.2 The scheme of cubic placement

It is possible to control the orientation of the spacecraft by controlling its angular position around three axes. To obtain independent control moments along the three axes of the spacecraft, three EFMs with rotation axes parallel to the axes of the connected coordinate system are installed on its board. It should be noted that the moment created by the EFM does not depend on the location of its placement on the spacecraft. It is only necessary that the axis of rotation of the EFM is parallel to the corresponding axis of the connected coordinate system. A cube is used as a support body in such an installation. In Figure 2.4 presents the EFM installation scheme according to the cubic scheme.

In this installation diagram, EFM_1 creates a steering moment about the axis Ox:

$$M_x = -\dot{H}_1, \tag{2.9}$$

where $\dot{H}_1$ – the derivative of the kinetic moment EFM_1, equals to $J_1\dot{\omega}_1$, J_1 – moment of inertia of EFM_1 and $\dot{\omega}_1$ – derivative of its angular velocity.

Similarly, EFM_2 creates a steering moment about the axis Oy:

$$M_y = -J_2\dot{\omega}_2 = \dot{H}_2, \tag{2.10}$$

where J_2 and $\dot{\omega}_2$ – moment of inertia and acceleration of EFM_2, respectively, and $\dot{H}_2$ – derivative of its kinetic moment.

The control moment about the Oz axis is created by EFM_3 and is equal to

$$M_z = -J_3\dot{\omega}_3 = \dot{H}_3, \tag{2.11}$$

where J_3, $\dot{\omega}_3$ and $\dot{H}_3$ – respectively, the moment of inertia, the derivative of the angular velocity, and the derivative of the kinetic moment of EFM_3.

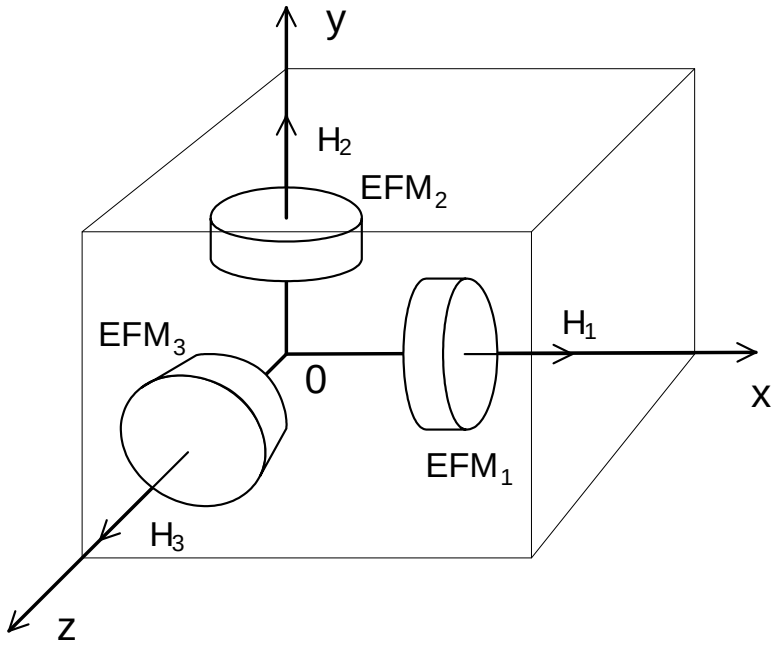

Figure 2.4 – Scheme of EFM placement on the faces of the cube

The given formulas do not take into account the gyroscopic components of the vector of control moments that appear during the rotation of the flywheel motor unit together with the spacecraft [3].

The independence of the control moment from the EFM location is due to the following. If we imagine the EFM moment as a moment created by a pair of forces, equal in magnitude and opposite in direction, then according to the provisions of theoretical mechanics, the moment of a pair of forces is a free vector that can be transferred to any point in space [13].

Also, according to the law of conservation of the momentum of the amount of motion [13] for any one channel of the spacecraft orientation, for example, for the first one, the following equation is valid:

$$\dot{H}_X + \dot{H}_1 = M_{EF}, \qquad (2.12)$$

where $\dot{H}_X$ – the derivative of the spacecraft kinetic moment;

M_{EF} – moment of external forces.

From the law of conservation of momentum of the amount of motion for the angular movements of spacecraft and EFM_1, it follows that the magnitude of the control moment is independent of the place of its generation, provided that the directions of the Ox_1 axis and the vector of kinetic moment H_1 coincide.

For the first time in world practice, EFM installed according to the "cube" scheme was used on the space object "Cosmos-14", launched on April 13, 1963 from the Kapustin Yar cosmodrome. The development of the

electromechanical system of spacecraft orientation was carried out by VNDIEM under the leadership of academician A. Yosypyan [3].

Increasing the requirements for the duration of the active operation of the spacecraft led to the appearance and modification of the considered scheme for installing three EFMs. The fundamental drawback of the traditional EFM placement scheme along the axes of the connected coordinate system was the impossibility of performing spacecraft orientation when one EFM fails, let alone two ones. In other words, the traditional placement showed a low level of resistance to failures in operation, and as a result, extraneous situations that lead to the termination of the space mission.

The need for long-term active functioning of spacecraft in various space missions led to a tendency to increase the level of resistance to failure of both orientation systems in general and hardware and software in particular. Increasing resistance to EFM failure, as the ability to function when individual components fail, in modern engineering practice is carried out by introducing additional EFM. Such a block, in which the number of EFMs is more than three, is called redundant.

The simplest solutions for ensuring redundancy are based on the using of redundant EFMs in a traditional placement scheme. The most common solution is to use two or three identical EFMs instead of one. Such a technical solution leads to a significant increase in the weight, size, energy and cost characteristics of the electromechanical unit

More advanced solutions consist in the use of four EFMs, three of which are placed according to the traditional scheme, and the fourth along the inner diagonal of the cube. Figure 2.5 shows the scheme of such a minimum-redundant EFM placement.

The position of the internal diagonal in this installation scheme or vector H_4 can be specified by two installation angles α and β. The angle α is determined on the condition that the projections of the vector H_4 on the axis of the connected coordinate system are identical $H_{4x} = H_{4y} = H_{4z}$, then $H_{4x} = \sin\alpha\cos\beta H_4$; $H_{4y} = \cos\alpha H_4$; $H_{4z} = \sin\alpha\sin\beta H_4$.

As a result of the transformation of these ratios, we get that $\beta = 45^\circ$, and $\mathrm{tg}\alpha = \dfrac{1}{\cos\beta} = \sqrt{2}$, so $\alpha = 54{,}74^\circ = 54^\circ 44' 8''$.

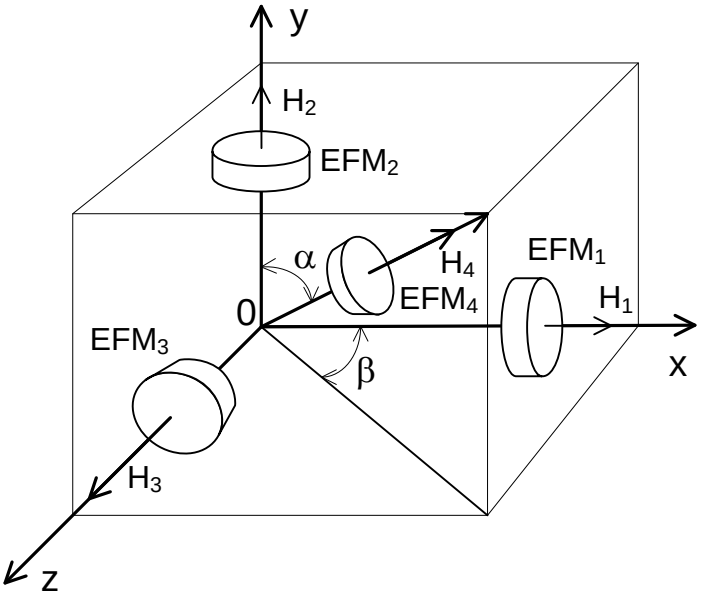

Fugure 2.5 – Placement scheme of minimum-redundant EDM

The presented scheme for placing four EFMs is approved by the NASA standard within the framework of the MMS multipurpose modular platform project. Additional, redundant EFM_4 is an unloaded reserve in case of failure of one of the main EFM_1, EFM_2, and EFM_3. Such an placement scheme provides independent channel-by-channel control of the spacecraft's orientation in case of failure of one of any EFM. The disadvantage of this scheme is that when one of the main EFMs fails, the control efficiency in this channel decreases by 1.73 times. When the backup EFM4 fails and any of the main EFM_i, $i = \overline{1,3}$ fails, orientation control becomes impossible.

The choice of the number and rational scheme of EFM placement depends on a number of factors. The first and main one is the functions and design of the spacecraft. Knowing the orbit and shape of the space vehicle allows you to form the area of action of disturbing moments in a connected coordinate system. Based on this, the area of EFM kinetic moments is formed, which are necessary for parrying disturbing moments. The tactical and technical requirements formulate requirements for solving control tasks, for example, such as extinguishing angular velocities on the final section, ensuring the necessary orientation with a given accuracy, angular maneuvers of the spacecraft to a given position, and a number of others. These requirements make it possible to expand the area of parrying kinetic moments to the area of necessary EFM kinetic moments, which are necessary for solving the problems of qualitative orientation of a specific spacecraft. The area formed in this way allows to proceed to the selection of specific types of

EFM and the search for their placement schemes, which ensure the fulfillment of the tactical and technical requirements for the spacecraft orientation system.

To illustrate, let's consider a fragment of the technology for the formation of requirements for EFM [12]. So, to solve the problem of damping the angular velocity of the spacecraft along one of the channels, the EFM control moment is required:

$$M_y = \frac{\kappa J \Delta\omega}{\Delta t}, \tag{2.13}$$

where κ – the margin factor for the control moment;
J – the moment of inertia of the spacecraft along the axis;
$\Delta\omega$ – range of angular velocity change during damping;
Δt – angular velocity damping time interval.

Then kinetic moment of EFM is needed

$$H = \kappa J \Delta\omega. \tag{2.14}$$

The requirement of high maneuverability of the spacecraft will be essential in the choice of EFM. From the EDM dynamics equation

$$J\omega = M_y \tag{2.15}$$

provided that the turnaround time is minimized, we get:

$$\frac{\gamma}{2} = \frac{M_y \Delta t^2}{8J}, \tag{2.16}$$

where γ – turning angle. Then a control moment is necessary

$$M_y = \frac{4J\gamma}{\Delta t^2}. \tag{2.17}$$

At the same time, the maximum angular speed is required

$$\omega = \frac{M_y}{J}\frac{\Delta t}{2}. \tag{2.18}$$

In a similar way, the requirements for EFM and for solving other tasks of the spacecraft are formed. Then the maximum calculated values of the parameters are selected and the area of the necessary kinetic moments is formed, from which the EFM is selected and the schemes for their placement on the spacecraft are formed.

In the minimum-redudant EDM placement scheme (see Figure 2.5), the kinetic moments H_1, H_2 and H_3 are determined under the condition that the region of the required kinetic moments is a parallelepiped with faces $2H_1$, $2H_2$ and $2H_3$.

The setting angles α and β for EDM_4 are determined under the condition of equal efficiency of action along the axes of the connected coordinate system. A different decision regarding the set angles is also possible, if we proceed from the ratio of equality of the proportionality factor:

$$\frac{H_{4x}}{H_1} = \frac{H_{4y}}{H_2} = \frac{H_{4z}}{H_3}. \qquad (2.19)$$

Other conditions are possible, which can be formed in the tactical and technical requirements for the spacecraft orientation system, regarding the distribution of the kinetic moment of the reserve EFM_4. Taking into account these conditions will make it possible to form the appropriate values of the set angles α and β.

Installation schemes of three EFMs (see Figure 2.4) were used in a number of spacecrafts. Thus, the orientation control of “Meteor-M No. 1” spacecraft (Figure 2.6) was carried out by three EFM DM20-250 with rotation axes parallel to the axes of the associated coordinate system. This is a meteorological type of spacecraft launched on September 17, 2009 from the Baikonur Cosmodrome, developed by VNDIEM under the leadership of A.Yosypyan [15].

Figure 2.6 – General view of “Meteor-M No. 1” spacecraft

"Meteor-M No. 1" is intended for prompt obtaining of information for weather forecasting, control of the ozone layer and the radiation situation in near-Earth space, as well as for monitoring the sea surface, including the ice situation. The weight of the spacecraft is 2630 kg; the average height of the orbit is 832 km; rotation period is 101 min; the diameter of the spacecraft body is 2.5 m; width with deployed solar panels is 14 m [3].

On the "Kupon" spacecraft (Figure 2.7), launched on November 12, 1997 from the Baikonur Cosmodrome, three EFMs of the traditional placement

scheme were used in the orientation system developed by SME "Hartron-Arcos Ltd".

Figure 2.7 – General view of the "Kupon" spacrcraft

Spacecraft "Kupon" is a small geostationary communication satellite intended for use in the "Bankir" system. The weight of the spacecraft is 2650 kg; the average height of the orbit is 36,000 km; rotation period is 24 hours 3 minutes 49 seconds; the accuracy of the North Star orientation is no worse than 7 degrees. min. [15].

In the prospective development of a satellite for Mars, fulfilled by the Institute of Mathematics named after M.V. Keldysh's, orientation system uses three EFMs in the traditional scheme of an orthogonal placement [16]. This design does not use flywheel unloading, as the kinetic torque is calculated to be sufficient to compensate for the perturbing torques that may occur in Mars orbit.

EgyptStat-1 is the first Egyptian satellite for remote sensing of the Earth. It was launched on April 17, 2007 from the Baikonur Cosmodrome using the “Dnipro” launch vehicle. The weight of the satellite is 165 kg. The satellite manufacturer is SDB "Pivdenne" (Figure 2.8).

The orbit of the satellite with an inclination of 97.8º is 666.9 km at apogee and 659.6 km at perigee; rotation period is 97.9 min; the estimated period of active operation is 5 years [17].

The development and production of the satellite orientation system was carried out by the SME “Hartron-Arkos Ltd”.

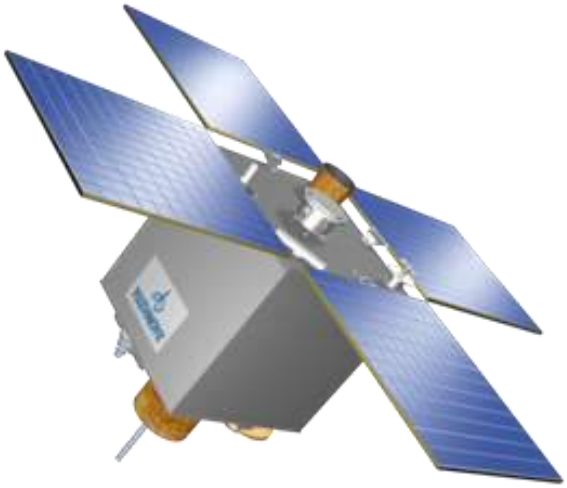

Figure 2.8 – General view of the EgyptStat-1 satellite

Four EFMs were used on the satellite, three of which were placed along the edges of the cube according to an orthogonal scheme, and the fourth backup EFM was installed in the pitch channel. The actual duration of the flight was 14 years, 3 months and 20 days.

Ukrainian satellite "MS-2-8" (Figure 2.9) for remote sensing of the Earth with optical-electronic high-resolution multi-zone observation devices was developed by the SDB "Pivdenne". Its weight was 135 kg; an orbital height was equal to 668 km; an inclination of orbit was 98.074º [18].

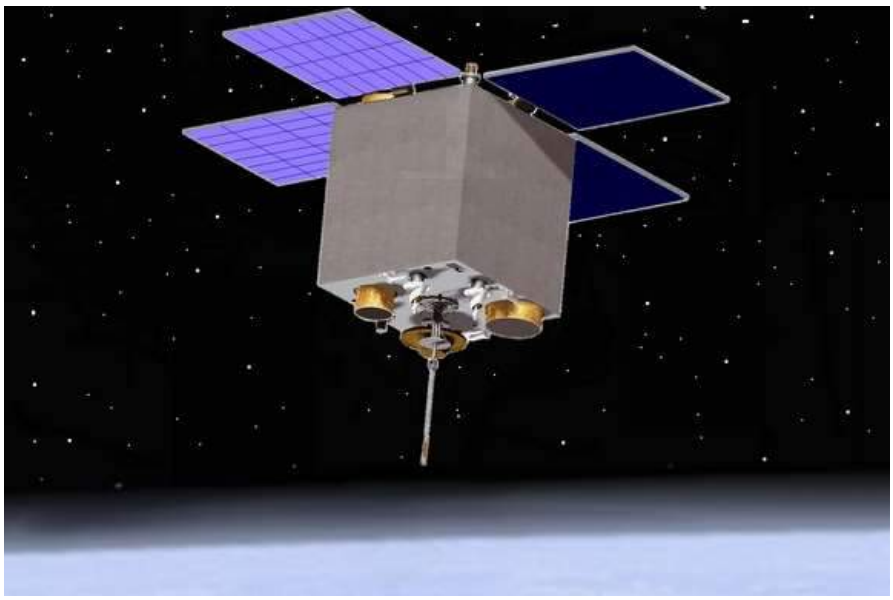

Figure 2.9 – General view of the “MC-2-8” satellite

Four EFMs were used in the satellite orientation system of the development of the SME “Hartron-Arcos Ltd”: three according to the "cube" scheme, and the fourth reserve EFM was places in the pitch channel.

Therefore, the EFM placement scheme using the "cube" reference body is used in the orientation systems of small-sized spacecraft with a relatively short period of active operation compared to long space missions of tens of years.

2.3 Schemes of pyramidal placement

To carry out long space missions due to the limited EDM resources, it is necessary to use redundant placement schemes. The existing restrictions on mass, size, energy and cost characteristics lead to the search for minimum-redundant schemes of the placement that satisfy both the restrictions and the tactical and technical requirements for the development of the spacecraft. The most satisfactory EFM placement scheme for long space missions, based on the known experience of development and operation, is the pyramidal placement scheme (Figure 2.10).

In this placement scheme, the kinetic moments $H_i, i = \overline{1,4}$ have directions that coincide with the edges of the pyramid. Scheme in Figure 2.10 presents the directions of positive kinetic moments directed to the top of the pyramid.

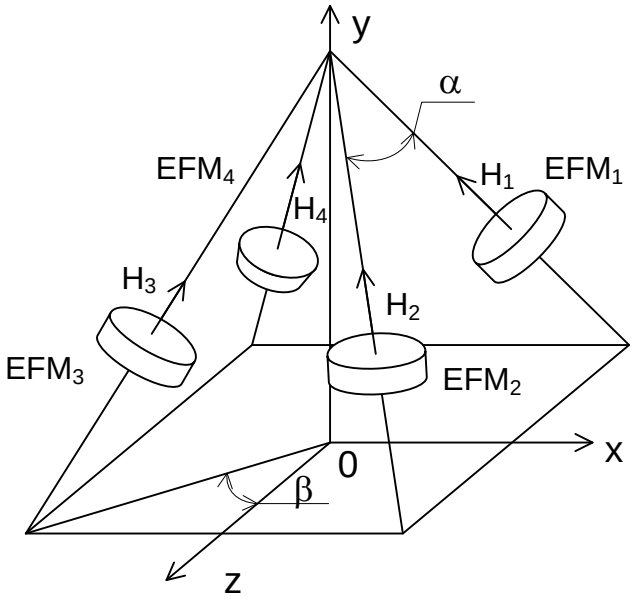

Figure 2.10 – Scheme of placement of EFM on the edges of the pyramid

To determine the control moments created by EFM_i around the corresponding axes of the Oxyz coordinate system associated to the spacecraft, such characteristics of the pyramid as the set angles α and β are necessary, if the base of the pyramid is a square. The angles α and β are

usually chosen from the condition of equal EFM efficiency for all control channels. Then

$$\frac{4\dot{H}\sin\alpha\sin\beta}{J_{xx}} = \frac{4\dot{H}\cos\alpha}{J_{yy}} = \frac{4\dot{H}\sin\alpha\cos\beta}{J_{zz}}, \qquad (2.19)$$

where J_{xx}, J_{yy} i J_{zz} – moments of inertia of the spacecraft relative to the corresponding axes of the associated coordinate system. As a result of the transformation, we get that

$$\mathrm{tg}\beta = \frac{J_x}{J_z}, \qquad (2.20)$$

and

$$\mathrm{tg}\alpha = \frac{J_x}{J_y \sin\beta}. \qquad (2.21)$$

The considered scheme of placement is the simplest configuration option developed by General Electric to ensure fault tolerance.

In the diagram in Figure 2.10, a pyramid is chosen as a reference body for EFM placement. Scheme in Figure 2.11 shows the transformation of a cube into a pyramid, following I. Kepler, if you connect the center of the upper face of the cube with the vertices of its base.

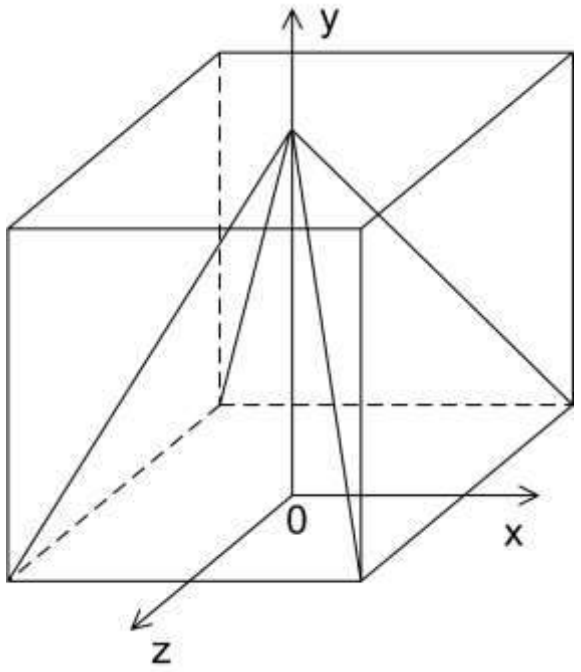

Figure 2.11 – Scheme of transformation of a cube into a pyramid

The most common and used in practice is the placement scheme of the General Electric company, in which a parallelepiped is chosen as the reference body and the vectors of kinetic moments are located on the edges

of the pyramid connecting the center of the upper face with the vertices of its base. In such placement scheme, the possibilities of a more effective redistribution of the total control torque of the EFM along the axes of the coordinate system associated with the spacecraft are expanded, taking into account its inertia tensor and the necessary control efficiency in the orientation channels. Scheme in Figure 2.12 shows a diagram of such pyramidal EFM placement.

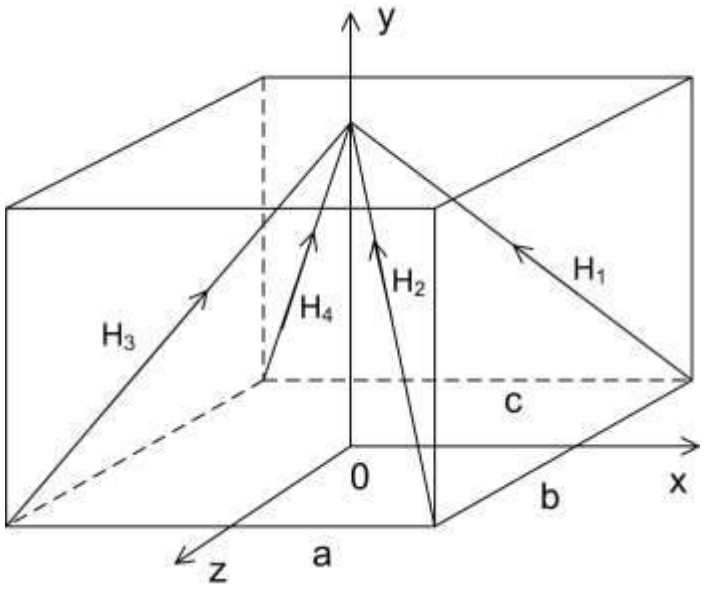

Figure 2.12 – EDM placement scheme using a parallelepiped

A parallelepiped is characterized by the following parameters: a – length; b – width; c – height. In the scheme, EFM_i, $i=\overline{1,4}$, are represented by the corresponding vectors of positive kinetic moments H_i, $i=\overline{1,4}$, tied to the lower corners of the pyramid and directed along the edges of the pyramid to its top. The axis of symmetry of the EFM_i placement is the Oy axis of the associated coordinate system. It should be noted that any axis of the associated coordinate system can be chosen as the axis of symmetry.

To obtain equal efficiency of EFM_i for three control channels, it is necessary that the parameters of the pyramid are proportional to the axial moments of inertia of the spacecraft [19]. Formally:

$$a=\kappa J_{xx};\ b=\kappa J_{zz};\ c=\kappa J_{yy}, \qquad (2.20)$$

where κ – proportionality factor.

If it is necessary to control the rapid movements of the spacecraft by means of different channels, the values of the modules of the angular accelerations ε_x, ε_y, ε_z of the spacecraft must be taken into account. Then the parameters of the pyramid will be determined from the following ratios:

$$a = \kappa J_{xx} |\varepsilon_x|;\ b = \kappa J_{zz} |\varepsilon_z|;\ c = \kappa J_{yy} |\varepsilon_y|. \qquad (2.21)$$

In order to obtain different efficiency of control for three channels, appropriate coefficients are introduced, which allow to redistribute the total moment from four EFMs taking into account the tactical and technical requirements of a specific space mission.

The company "SME VNDIEM" has developed a whole series of flywheel systems for orientation based on pyramidal structures, which were used in "Meteor", "Resurs" and "Electro" spacecrafts. Figure 2.13 presents a system of four EFMs of a pyramidal placement [3].

Figure 2.13 – Implementation of the EFM pyramidal placement

In this system, EFMs are installed on a stand which is a truncated quadrangular pyramid. Two EDFMs are located outside, the other two are inside the stand. The axes of rotation of the EFM are perpendicular to the side faces of the pyramid. The design of the stand ensures accurate mounting angles of the EFM. To the right of the stand is a peripheral adapter for connecting the flywheel system to the computer network of the spacecraft.

On the "Monitor-E" spacecraft, the control system of the Design Bureau "Mars" company was used. The orientation system includes four EFMs placed according to the "pyramid" scheme with the axis of symmetry along the Oz axis of the associated coordinate system and with setting angles $\alpha = 60^\circ$ and $\beta = 45^\circ$ [3] (Figure 2.14).

The relationship between the projections of the vector of kinetic moments of the "pyramid" and the vector of kinetic moments H_i, $i = \overline{1,4}$ of the EFMs is described by the following vector-matrix equation:

$$\begin{bmatrix} H_x \\ H_y \\ H_z \end{bmatrix} = A \begin{bmatrix} H_1 \\ H_2 \\ H_3 \\ H_4 \end{bmatrix} = \begin{bmatrix} a_{11} & a_{12} & a_{13} & a_{14} \\ a_{21} & a_{22} & a_{23} & a_{24} \\ a_{31} & a_{32} & a_{33} & a_{34} \\ a_{41} & a_{42} & a_{43} & a_{44} \end{bmatrix} \begin{bmatrix} H_1 \\ H_2 \\ H_3 \\ H_4 \end{bmatrix}, \quad (2.22)$$

where A – the matrix of cosines of set angles;

a_{ij} – matrix elements;

H_x, H_y and H_z – projections of the total vector of kinetic moments on the axis of the associated coordinate system.

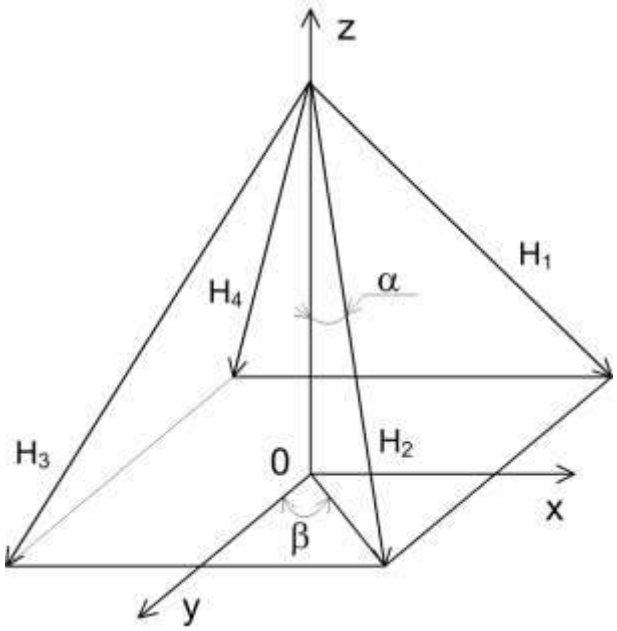

Fugure 2.14 – Scheme of orientation of EFM kinetic moment vectors

For setting angles $\alpha = 60^\circ$ and $\beta = 45^\circ$, the matrix A has the form:

$$A = \begin{bmatrix} 0,6124 & 0,6124 & -0,6124 & -0,6124 \\ -0,6124 & 0,6124 & 0,6124 & -0,6124 \\ -0,5 & -0,5 & -0,5 & -0,5 \end{bmatrix}. \quad (2.23)$$

For geostationary communications satellites and Earth remote sensing satellites, the company adopts the following main EDM characteristics:

1) maximum kinetic moment;
2) maximum control moment;
3) the weight of the low grade (accuracy) is 0.001 Nm;
4) the frequency of changing the control code is no more than 10 Hz;
5) time constant is no more than 0.1 s.

The "Monitor-E" spacecraft was launched on August 26, 2005 from the Plesetsk Cosmodrome using a Rokot launch vehicle and launched into a sun-

synchronous orbit at an altitude of 550 km. The mass of the spacecraft is 750 kg, the mass of the payload is 210 kg (Figure 2.15).

"Monitor-E" is an experimental satellite designed for information provision of solving problems of nature management, territory mapping, control of environmental pollution and emergency situations of natural and man-made nature. The main developer was the Central Complex of the M. Khrunichev National Center for Scientific Research [20].

Figure 2.15 – General view of «Monitor-E» spacecraft

A similar pyramidal EDM placement was used by the company Design Bureau "Mars" in the orientation systems of the "KazSat", "Express-MD1", "Electro-L", "Spektr-R" spacecrafts [3].

SME "Hartron-Arcos Ltd" has used four EDMs, placed according to the "pyramid" scheme, in the orientation system of the prospective development of the Ukrainian Earth remote sensing spacecraft "Sich-perspectiva".

The practice of using EDM in the "pyramid" scheme shows that such a minimal-redundant structure is the most effective for long-term space missions of spacecraft of various purposes.

2.4 Prospective schemes of placement

With any number of EFMs and different schemes of their placement on the spacecraft, as a result of the change of all vectors of kinetic moments $H_i, i = \overline{1,n}$, $-H_i^* \le H_i \le H_i^*$, in the three-dimensional space of the connected coordinate system Oxyz, an area S is formed, which is the geometric place of possible positions of the total vector

$$H = \sum_{i=1}^{n} H_i . \qquad (2.24)$$

It is obvious that the shape of the region S depends on the vectors of kinetic energy H_i, and its dimensions are proportional to the total kinetic momentum H [3]. So, for three EFM installed on the faces of the cube (see Figure 2.3), the region S will be in the shape of a cube (Figure 2.16).

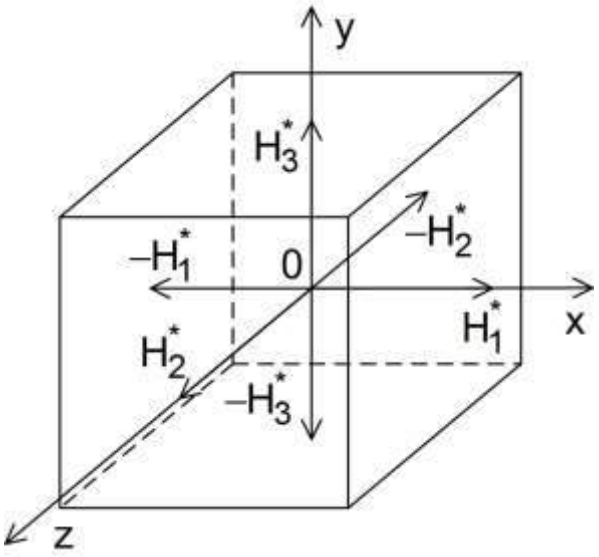

Figure 2.16 – The range of changes in the kinetic moment H for an orthogonal scheme

If the moments are equal $H_1 = H_2 = H_3 = H_0$, the faces of the cube will be of length $2H_0$.

The shape and dimensions of the necessary area S_n of changes in kinetic moment in general depend on the design of the spacecraft, disturbing influences and are determined by the tactical and technical requirements for the dynamics of orientation and stabilization. Thus, the selection of the installation scheme and the maximum kinetic moments of the EFM should satisfy the condition $S_n \subset S$ [3].

The area S of the minimum-excess pyramid scheme of the EFM installation is a rhombodecahedron – a 12-hedron with 14 vertices and 24 edges. Its faces are rhombuses with side lengths $2H_0$ (Figure 2.17).

The intersection of the area S with the coordinate planes are squares with side lengths $4\sqrt{\frac{2}{3}}H_0$, while the vertices of the squares are located on the coordinate axes.

Figure 2.17 – The range of changes in the vector of the kinetic moment H for a minimum-excess pyramid scheme

The radius of the circumscribed sphere is $R = \frac{4\sqrt{3}}{3} H_0 \approx 2{,}31 H_0$, and the radius of the inscribed sphere is equal to $r = 2\sqrt{\frac{2}{3}} H_0 \approx 1{,}63 H_0$.

The surface of the region S characterizes the saturation state of the EFM. The faces of the region are formed by the saturation of two, the edges – three, and the vertices – four EFMs.

The volume $V = \frac{64}{3}(H_0)^3$ of the region S consists of the volumes of 12 regular pyramids with a common vertex O. The rhombodecahedron-shaped region S has the maximum volume among all the regions S corresponding to the arbitrary patterns of the four EFMs on the spacecraft.

The domain S of five identical EFMs is a convex 20-hedron. Its faces will be rhombuses with corners at the vertices $\gamma_1 \approx 57{,}36^\circ$ and $\gamma_2 \approx 101{,}9^\circ$. The volume of the region consists of the volumes of 10 pyramids $V \approx 57{,}86 {H_0}^3$, and the radii of the circumscribed and inscribed spheres are $R \approx 2{,}89 H_0$, $r \approx 2{,}17 H_0$.

A domain S of six identical EFMs is a convex 30-hedron. Its faces will be rhombuses with corners at the vertices $\gamma_1 \approx 48{,}2^\circ$, $\gamma_2 \approx 90^\circ$ and $\gamma_3 \approx 109{,}5^\circ$. Polyhedron volume is $V = 96 {H_0}^3$, the radii of the circumscribed and inscribed spheres are equal $R \approx 3{,}46 H_0$, $r \approx 2{,}67 H_0$.

When one, two, or three EFMs fail, the region S degenerates into a 20-hedron, a 12-hedron, and a parallelepiped, respectively.

Let's compare the regions S for two traditional EFM setup schemes. The region S_3 for the scheme of three identical EFMs of an orthogonal structure has the shape of a cube with length $2H_0$ (see Figure 2.16). The radius of the

circumscribed $R = \sqrt{3}H_0 = 1{,}73H_0$, the radius of the inscribed sphere $r = H_0$. The minimum size of the area S_4 of the minimum-redundant pyramid scheme of the EFM placement is 1.63 times larger than the minimum size of the area S_3. By the volume $S_4 = 2{,}67S_3$.

To characterize the efficiency of electric flywheel actuators, the coefficient of use of the directed total kinetic moment in an arbitrary direction given by the h-unit vector was proposed [21]:

$$\chi_h = \frac{H_h}{H}, \tag{2.25}$$

where H_h – the maximum total kinetic moment produced by the EFM in the direction h;

H – the total kinetic moment of all EFMs used in the placement scheme.

If the direction h is arbitrary, then we can enter the coefficients [3]:

$$\chi_{min} = \frac{H_{min}}{H}, \chi_{max} = \frac{H_{max}}{H}. \tag{2.26}$$

Yes, for three EFMs in an orthogonal placement scheme

$$\chi_{min} = \frac{H_0}{3H_0} \approx 0{,}33, \chi_{max} = \sqrt{3}\frac{H_0}{3H_0} \approx 0{,}58. \tag{2.27}$$

For four EFMs in a pyramid scheme of the placement

$$\chi_{min} = 2\sqrt{\frac{2}{3}}\frac{H_0}{4H_0} \approx 0{,}41, \chi_{max} = \frac{4\sqrt{3}}{3}\frac{H_0}{4H_0} \approx 0{,}58. \tag{2.28}$$

The ratio of radii is used to characterize the non-sphericity of the region S $\frac{(R-r)}{r}$. For S_3, this value is 0,73, and for S_4 – 0,41.

Let's consider the placement scheme of six EDMs. Figure 2.18 presents a diagram of the location of positive vectors of kinetic moments of six EFMs in the accociated coordinate system Oxyz.

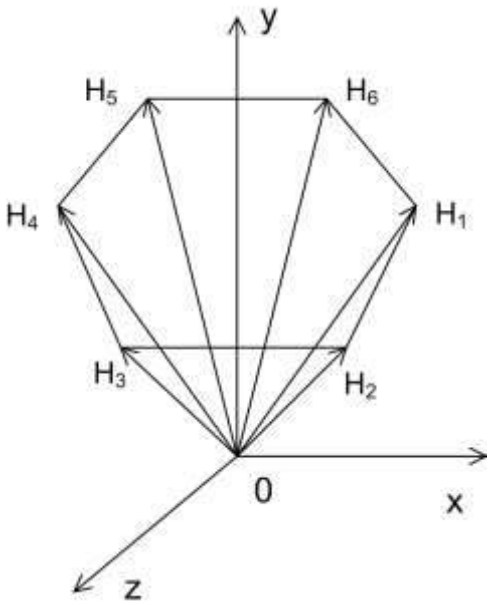

Figure 2.18 – Scheme of location of kinetic moment vectors of six EFM

A hexagonal pyramid is used as a support body in this scheme. EDMs are placed along the edges of this pyramid. By choosing the angle at the top of the pyramid, it is possible to vary the area S_6 of change of the total kinetic moment H, satisfying the tactical and technical requirements for the spacecraft [3].

For example, if program rotations of the spacecraft around one of the axes are required, then by reducing the angle at the top of the pyramid, you can extend the area of change H along this axis. In the image, the symmetry axis of the cone coincides with the Oy axis - the axis of the program rotation. In Figure 2.19 presents the construction scheme of placing six EFMs on the measuring platform [3].

Figure 2.19 – Placement scheme of six EFMs

In this scheme, the EFMs are located on two stands, since the EFMs can be placed in different places on the spacecraft if the conditions of the placement angles are met. The measuring platform was designed to measure the control moments created by EFM with respect to three mutually perpendicular axes.

Let's consider the possible EFM placement schemes using the positive directions of the vectors of kinetic moments H_i. These placement schemes have not been studied both theoretically and in applied terms. Such studies are necessary to identify the functional capabilities of schemes, obtain their quantitative characteristics, form a comparative analysis with known schemes and determine the tasks of their practical use.

The main disadvantage of the minimum-redundant four EFM installation scheme (see Figure 2.5) is the vulnerability to EFM_4 malfunctions. To eliminate this shortcoming, it is possible to use one more EFM_5 placed along the inner diagonal of the cube. The placement of the positive vectors of the kinetic moments of the five EFMs is presented in Figure 2.20.

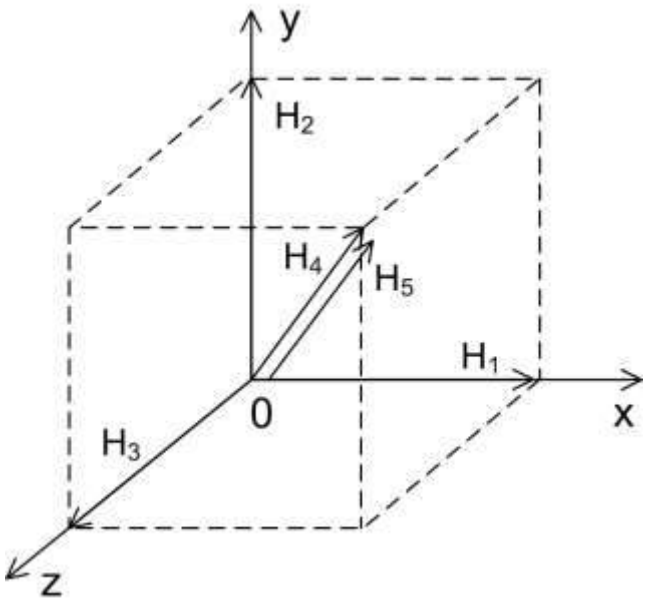

Figure 2.20 – The placement of five vectors of kinetic moments

In such an arrangement, the failure of any EFM does not lead to a malfunction of the electric flywheel actuator. Moreover, even with the simultaneous failure of two EFM_i, it will be possible to maintain the

functionality of the spacecraft orientation system with prompt diagnosis and flexible restoration of functionality.

The desire to reduce the redundancy of EFM_i and to ensure the necessary level of failure resistance of the electric flywheel executive body due to algorithmic and software tools of on-board digital computers lead to an installation scheme using a tetrahedron and its faces as a reference body (Figure 2.21).

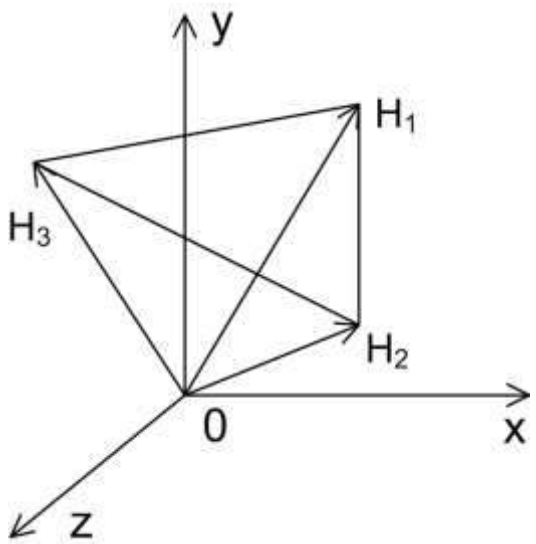

Figure 2.21 – The placement scheme of three kinetic moment vectors

It is obvious that in this scheme the vectors $H_i, i = \overline{1,3}$ are non-collinear to the axes of the connected coordinate system Oxyz and therefore each vector gives its projections on the axis. The attractiveness of this scheme lies in the minimum possible number of EFMs, but at the same time the inevitable complication of the spacecraft orientation control procedure, especially when one of the EFMs fails.

To increase the level of resistance to deviation of the electroflywheel executive body for long-term spacecraft missions, it is possible to complicate the EFM placement scheme using two referemce bodies: a cube and a tetrahedron. Scheme in Figure 2.22 presents the following diagram of the placement of six vectors of kinetic moments.

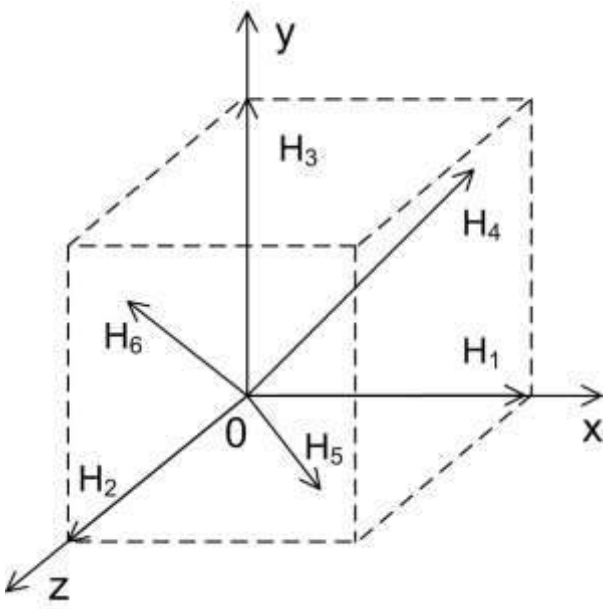

Figure 2.22 – Scheme of placement of six vectors of kinetic moments

In this scheme, the vectors H_1, H_2 and H_3 are located along the edges of the cube and coincide with the direction of the axes of the Oxyz coordinate system, and the redundant vectors H_4, H_5 and H_6 are located along the diagonals of the faces of the cube and give corresponding projections only on two axes of the coordinate system.

It it possible to increase the number of redundant vector projections H_4, H_5 and H_6 by reducing the angles at the top of the tetrahedron, placing them around the main diagonal of the cube. Then each excess vector will give projections on each axis of the connected coordinate system (Figure 2.23).

In this scheme, each redundant vector gives three projections on the axis of the associated coordinate system Oxyz, which increases the redundancy, and, accordingly, the level of fault tolerance of the scheme. Equations for the vector of kinetic moment created by EFM_4, EFM_5 and EFM_6 can be presented in vector-matrix form:

$$H_p = DH', \tag{2.29}$$

where $H_p = \left[H_{px}, H_{py}, H_{pz}\right]$ – the vector of the total reserve kinetic moment in projections on the axis of the associated coordinate system Oxyz;

D – matrix of guiding cosines;

$H' = \left[H_4, H_5, H_6\right]$ – vector of kinetic moments of EFM_i, $i = \overline{4,6}$.

The matrix D – $[\dim 3 \times 3]$ will have the following structure:

$$D = \begin{bmatrix} d_{11} & d_{12} & d_{13} \\ d_{21} & d_{22} & d_{23} \\ d_{31} & d_{32} & d_{33} \end{bmatrix}, \qquad (2.30)$$

where d_{ij} – values of the guiding cosines.

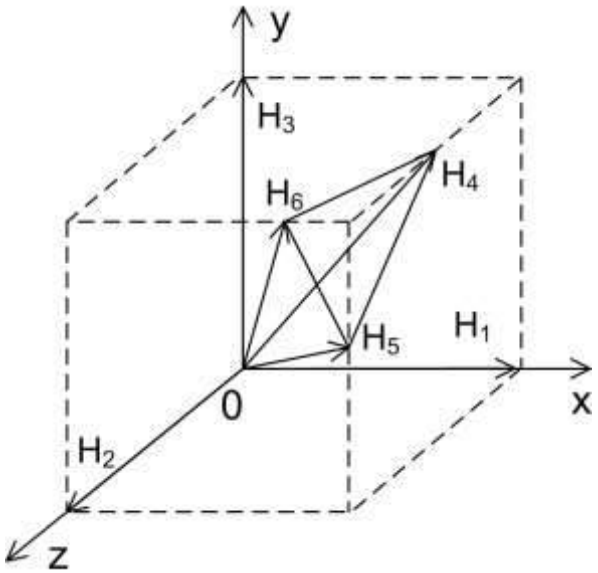

Figure 2.23 – Scheme of placement of vectors H_4, H_5 and H_6 around the main diagonal of the cube

For the scheme (see Figure 2.23), the matrix D will be as follows:

$$D = \begin{bmatrix} d_{11} & d_{12} & 0 \\ d_{21} & 0 & d_{23} \\ 0 & d_{32} & d_{33} \end{bmatrix}.$$

The matrix D is actually a matrix of the total excess vector of the kinetic moment, created in addition to the main vector of the kinetic moment of the electric flywheel actuator of the spacecraft.

The desire to reduce the weight, size, energy and cost characteristics of electric flywheel actuators led to the development of a ring EFM [3]. A prototype unit of such an EFM is shown in Figure 2.24.

In this design, a metal ring, which is a flywheel, rotates with the help of a drive electric motor on guide rollers. Such an EFM was used in the “Salyut” and “Almaz” orbital space stations. Ring EFM with a total weight of 140 kg develops control torques up to 200 Nm and kinetic torque up to 1000 Nms at a rotation frequency of up to 80 rpm.

Spherical EDM is more promising (Figure 2.25).

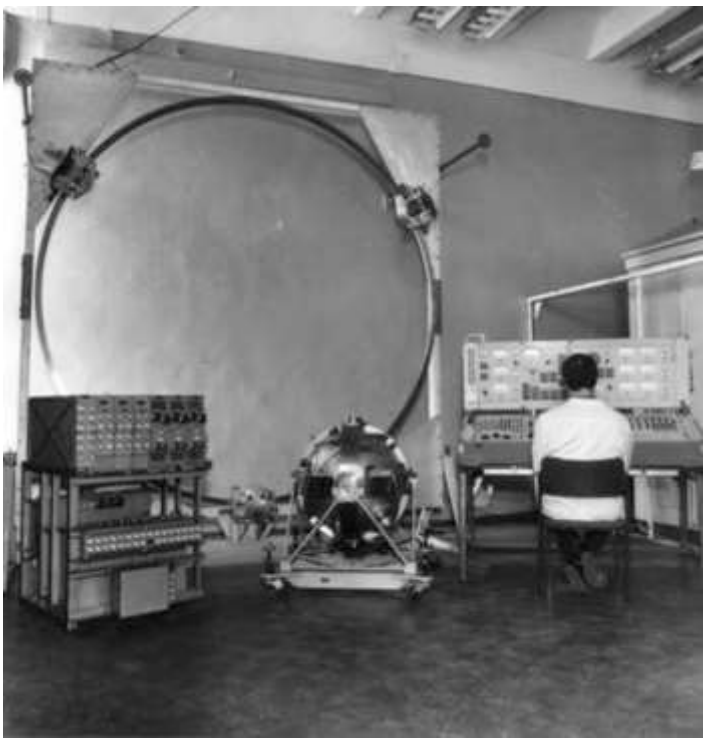

Figure 2.24 – A prototype unit of the ring EFM

Figure 2.25 – General view of a spherical EFM

The flywheel rotor is structurally made in the form of a hollow steel sphere, which is held inside the housing with the help of six electromagnets. According to the principle of operation, the ball EFM corresponds to an asynchronous electric motor. The spherical rotor is rotated by six arc stators

placed in three mutually perpendicular planes. The copper coating of the spherical layer serves as the rotor winding. With the help of the interaction of the magnetic field of the stators with the currents in the rotor, an electromagnetic moment arises, which causes it to rotate around any axis passing through the center of mass. Speed and direction of rotation are measured by tachogenerators. One spherical EFM replaces three uniaxial EFMs. With the same moments of inertia and diameters, a spherical EFM is twice as light as three ring EFMs. A spherical EFM with a rotor diameter of 0.64 m and a total mass of 230 kg was used for three-axis stabilization and slow turns of the “Salyut” and “Diamant” space orbital stations. Spherical EFM develops a control moment up to 3 Nm and a kinetic moment up to 200 Nms.

"Salyut" was the name of a series of piloted Soviet orbital scientific stations, which are heavy artificial satellites of the Earth with a long period of operation (Figure 2.26).

For example, the “Salyut-4” station was launched into orbit on December 26, 1984 and operated for 770 days. The mass of the station is 18,500 kg, the period of orbit around the Earth is 89.1 minutes.

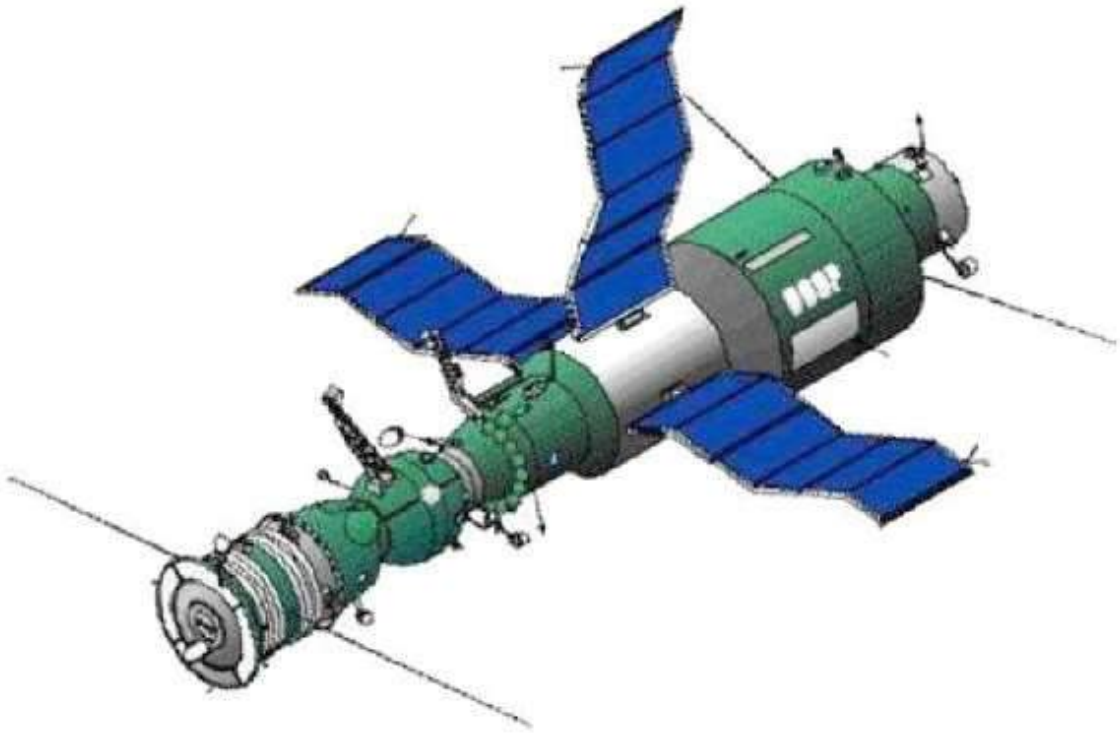

Figure 2.26 – General view of the station "Salyut-4"
with the “Soyuz” spacecraft docked to it

"Almaz" is a series of Soviet intelligence stations (Figure 2.27).

Figure 2.27 – General view of “Almaz” space station

A total of seven such stations were launched under different names. The station was developed at OKB-52 under the leadership of Volodymyr Chelomey.

Station "Almaz" had the following indicators. The maximum length is 14.6 m, the largest diameter is 4.2 m. The space of the residence reached 100 m^3. The total weight of the station is 17.8 tons, the payload is 5 tons. The station was powered by solar panels with an area of 52 m^2, which provided a power of 3.12 kW.

The search for new effective EFMs and their placement schemes continues in the direction of improving not only designs, but also the development of productive algorithms and software processes of such electromechanical drives for the tasks of orientation and stabilization of long-term spacecraft in various space missions.

Chapter III ELECTRIC FLYWHEEL MOTOR AS AN OBJECT OF RATIONAL CONTROL

Despite the obvious inconsistency of the opinion about the "waywardness" of inanimate objects, we are forced to state that various devices, processes and phenomena have a tendency to deviate from their intended mode of action.

R. Bellman (1920–1984) – American mathematician, "father of dynamic programming".

The functioning of the electric flywheel motor as part of the actuator unit of the orientation system in a long space flight is subject to the action of a number of destabilizing factors. What are these factors? How do they affect the performance of the actuator? Rational control makes it possible to ensure efficiency under conditions of destabilization.

3.1 Basic provisions of rational control

An electromechanical actuator is an automatic control system consisting of an automatic control object (ACO) and an automatic control device (ACD). For each EFM inside the actuator unit, the automatic control object consists of a serial connection of the power amplifier (PA), EFM and tachogenerator (TG) (Figure 3.1).

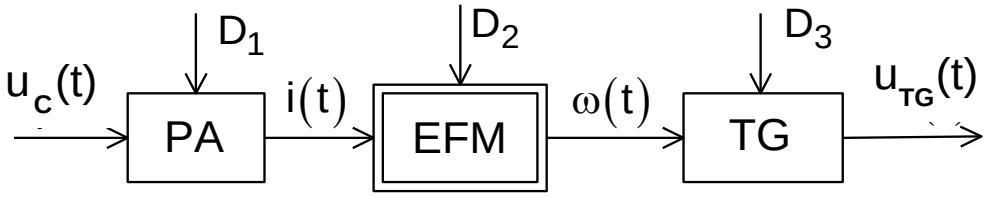

Figure 3.1 – Functional scheme of the automatic control object

Here $u_C(t)$ – control voltage; i(t) – value of current; $\omega(t)$ – angular velocity; $u_{TG}(t)$ – output tachogenerator voltage.

Functional elements are subject to destabilizing influences $D_i, i = \overline{1,3}$. Destabilizing influences are actions that disrupt the operability of functional elements and the automatic control object as a whole.

By the operability of a functional element, object, subsystem, and system, we understand their state in which the value of all parameters characterizing the ability to perform the given functions meets the tactical and technical requirements.

Destabilizing influences in spaceflight are various interferences, noises, disturbances, malfunctions and failures that lead to inoperability.

Traditionally, the construction of the EFM angular velocity automatic control system is based on the use of the principle of control by deviation. The closed-loop automatic control system allows to maintain efficiency under the influence of a number of obstacles, noises and disturbing influences, and in the event of malfunctions and failures, it enters the off-duty mode. To counter such abnormal modes, the automatic control object is supplemented with backup functional elements and means of reconfiguration, which ensure the disconnection of the failed element and the connection of the backup one. In this way, destabilizing influences are countered and workability is preserved. As a rule, detection of the failed functional element is carried out using the acceptance control procedure. When the controlled parameter of a functional element exceeds the tolerance limit, it is disconnected and a working, spare one is connected. In the tolerance control procedure, it is impossible to identify the reason for exceeding the tolerance limit, that is, the destabilizing influence that caused the abnormal situation, the failure of the functional element. In other words, there is no in-depth diagnosis of the causes of the malfunctioning state of the functional element. Shallow diagnosis leads to the fact that restoration of operability is carried out using cardinal means – replacement with reserve ones. This approach to ensuring the performance of automatic control systems is too expensive and ineffective. The most productive is an adaptive approach based on rational control of the operability of automatic control objects [22].

Let's consider the main provisions on which the rational control of the electromechanical actuator is based:

1) rational control system (RCS) consists of two subsystems: rational control object (RCO) and rational control device (RCD);

2) the RCO, in addition to the main functional elements (see Figure 3.1), contains a backup power amplifier (PA_R) and a tachogenerator (TG_R), and new connections (Figure 3.2).

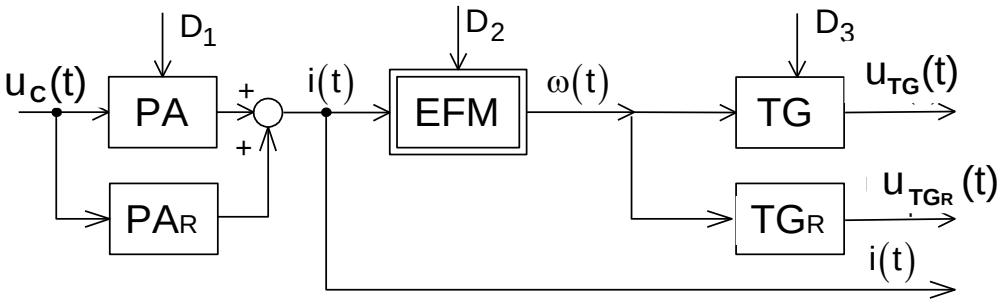

Figure 3.2 – Functional scheme of the rational control object

3) the RCD contains functional elements that implement deviation control procedures (DCP), diagnostic procedures (DP) and recovery procedures (RP) (Figure 3.3).

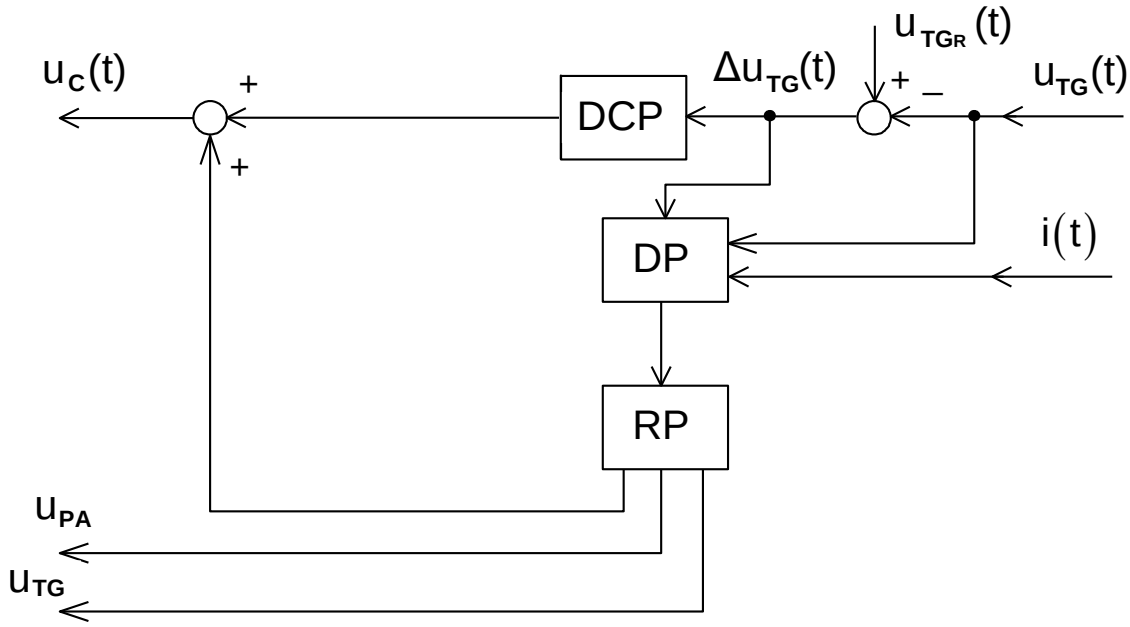

Figure 3.3 – Functional scheme of the rational control device

All optimal control procedures are implemented on microprocessor equipment. Output signals u_{PA} and u_{TG} – these are signals for disconnecting the main functional elements of the RCO and connecting the backup ones. Signal $\Delta u_{TG}(t)$ is a deviation signal: $\Delta u_{TG}(t) = u_{TG}(t) - u_{TGS}(t)$, $u_{TGS}(t)$ – given function of changing the output voltage of TG;

4) it is assumed that the RCD has higher level of reliability, fault tolerance and survivability compared to the RCO;

5) destabilizing influences D_1, D_2 and D_3 are uncertain events and generate in the RCO many of its destabilized states that do not correspond to the operational ones;

6) detection of the causes of destabilized states of RCO is carried out using diagnostic procedures that allow to detect the occurrence of destabilizations, find the functional element in which the destabilizing influence appeared, then detect the type of destabilizing influence and determine its magnitude; in other words, get a full diagnosis;

7) based on the results of a complete diagnosis, the selection of means of recovery from the available base is carried out and compensation or elimination of the cause that caused destabilization in the RCO, so as to restore operability within the regulated time and with the required accuracy.

Therefore, the formation of rational control procedures requires knowledge of the nominal mode of operation of the RCO. This knowledge in the form of mathematical models is obtained as a result of processing physical experiments. Traditionally, a mathematical model describing the relationship between the output signal $u_{TG}(t)$ and the input signal $u_C(t)$ is presented in the form of a transfer function of the following form:

$$W(s) = \frac{u_{TG}(s)}{u_C(s)} = \frac{k}{Ts+1}, \qquad (3.1)$$

where k – transfer factor of RCO; T – a time constant.

In the transfer function, the parameters are represented by point values. In the case of operation, the value of the parameters varies for various reasons, both external and internal. The range of variation can be shown in the Cartesian plane of these parameters (Figure 3.4).

The variation of the parameters occurs with respect to the nominal values of the parameters k and T and within the limits of the upper and lower values of the parameters. As a result, the region of possible values of the parameters turns out to be in the shape of a rectangle ABCD.

The range of possible ABCD values can be reduced using the deviation control principle. So, if the DCP is given by the coefficient - k_{CP}, then the transfer function of the closed EFM angular velocity control system will be as follows:

$$\Phi(s) = \frac{u_{TG}(s)}{u_C(s)} = \frac{k}{Ts+1+kk_{CP}}. \qquad (3.2)$$

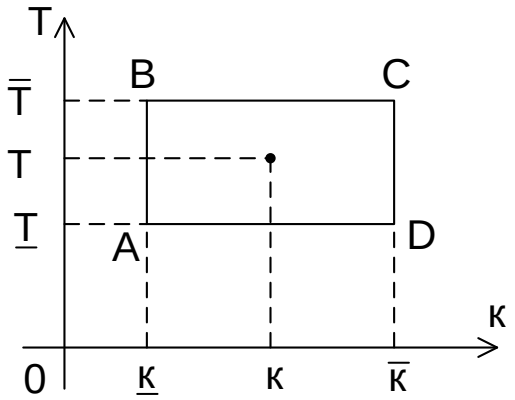

Figure 3.4 – Range of variation of parameters k and T

Let us transform the transfer function of the closed-loop system to a structure identical to the transfer function of the open-loop system (3.1). Then, will get:

$$\Phi(s) = \frac{u_{TG}(s)}{u_C(s)} = \frac{\dfrac{k}{1+kk_{CP}}}{\dfrac{T}{1+kk_{CP}}s+1} = \frac{k_1}{T_1 s+1}. \qquad (3.3)$$

Analyzing the new parameters of the closed control system, we came to the conclusion that they proportionally decreased by the amount of $\frac{k}{1+kk_{CP}}$. Therefore, the area of possible values of the parameters of the closed system will be smaller than the area of ABCD of the open system. Thus, the use of the deviation control principle allows to reduce the initial variation of parameters and significantly improve performance indicators of the electromechanical executive body. In Figure 3.5 this new area $A_1B_1C_1D_1$ is presented in the coordinate system $O\kappa_1T_1$.

Destabilizing influences, which are malfunctions, breakdowns, degradation, failures, in general, failures in the automatic control object, lead to a significant change of κ_1 and T_1, and, therefore, to the appearance of a new area of change of parameters $A_2B_2C_2D_2$ (Figure 3.5).

In terms of these areas, the tasks of rational control are: to identify the moment of appearance of parameter κ_1 and T_1 deviations, to identify the functional element of the automatic control object where the failure occurred, then to identify it, and then to counter the failure, so to move from the $A_2B_2C_2D_2$ area to the $A_1B_1C_1D_1$ operational area, i.e. to restore operability.

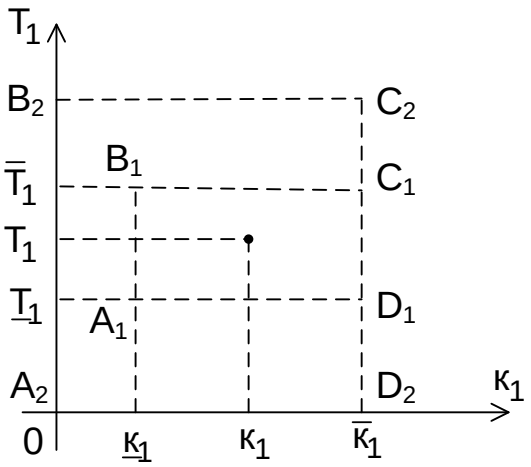

Figure 3.5 – Range of variation of parameters κ_1 and T_1

The field of operability of the electromechanical actuator can be formed in the space of quality indicators, which is more logical. The tactical and technical requirements for electromechanical actuators, as a rule, contain limitations on accuracy, transition time, and readjustment. In these terms, it is possible to form areas of variation of quality indicators. These regions will be parallelepipeds. The task of rational control remains the same as previously described.

Let's consider in more detail what is the difference between an automatic control object and a rational control object? The automatic control object displays the transformation properties in the nominal mode. In other words, the transformation of input controlling and disturbing influences into the initial state when the object is in good condition. The rational control object reflects transformative properties both in regular and non-regular modes of operation. Abnormal modes of functioning are caused by destabilizing influences that change both the technical and functional state of the object. The rational control object (see Figure 3.2) differs from the automatic control object (see Figure 3.1) in its structure. This difference is due to the need to ensure the ability to determine performance and is achieved by introducing additional functional elements, connections and modes of test operation.

Traditional EFM automatic control systems use the principle of control by deviation. In rational control systems, a new principle of control is applied – control by diagnosis. The use of this principle allows to expand the functionality of traditional control systems to effective control of operability in abnormal situations. Such a new property of rational EFM control systems can significantly increase the duration of active high-quality functioning at lower hardware, energy and cost, which is relevant for long-term space

missions. In addition, rational control systems during ground work will allow to reduce the time of adjustment and maintenance costs, since all this will take place in an automated mode.

3.2 Formation of a functional scheme of rational control of an electric flywheel motor

For the implementation of classic automatic EFM control for one channel of any placement scheme, an object of automatic control should be formed, which includes the following functional elements connected in series: power amplifier (PA), EFM and tachogenerator (TG) (Figure 3.6).

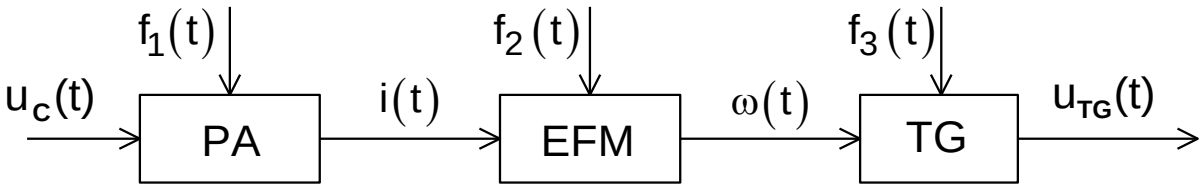

Figure 3.6 – Functional scheme of an automatic control object

Here $f_1(t)$, $f_2(t)$ and $f_3(t)$ – uncontrolled disturbing effects on the appropriate functional elements.

The rational control object is significantly different from the automatic control object both in the composition of functional elements and in the connections of these elements. The main reason for the difference lies in the expansion of the multitude of uncontrolled influences by including in it, in addition to disturbing influences, also potential malfunctions, breakdowns, and failures of functional elements. Thus, many destabilizing influences are formed for each functional element. These are D_1 for PA, D_2 for EFM and D_3 for TG. Further, as a result of deep diagnostic procedures, destabilizing influences $\hat{d}_{ij} \in D_i$, $i = \overline{1,3}$, $j = \overline{1,m}$ are revealed, that disrupted the functionality of the automatic control object. After obtaining a complete diagnosis, functional elements are restored. Restoring the functionality of functional elements is carried out using additional redundant means.

As additional redundant means, signal and parametric adjustment, additional algorithms and additional backup equipment are used. Such additional redundant means as signal and parametric tuning, additional algorithms are software modules and are implemented in RCD. Backup equipment is additional elements for the automatic control object, which are used when the main ones are decommissioned. So, in the case of a complete

failure of the PA, it can be replaced by an additional backup PAR that will take over the functions of the main one. If the TG is not working, it can be replaced by a backup TG_R.

Additional signals from the object of automatic control and modification of its structure are required for a greater possibility of obtaining reliable estimates $\hat{d}_{ij}$ of destabilizing influences based on the results of available measurements, i.e. a complete diagnosis. Thus, in the general case, the functional scheme of rational control can be presented in the following form (Figure 3.7).

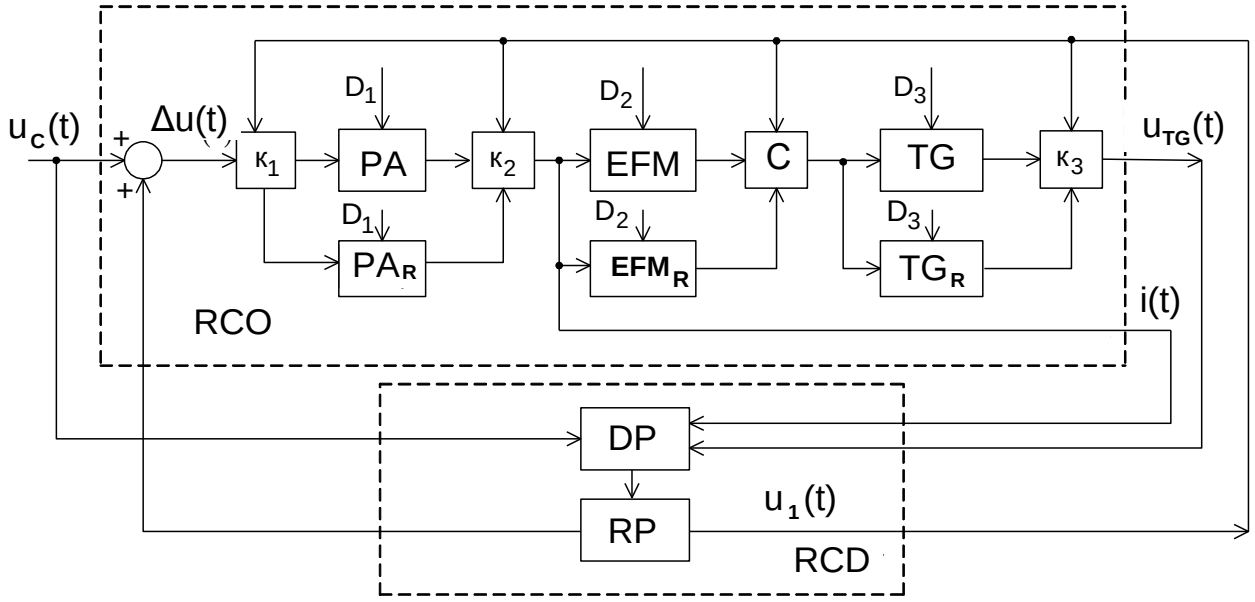

Figure 3.7 – Functional scheme of rational control of subsystem which includes PA, EFM and TG

Let's consider in more detail the composition and purpose of functional elements and connections in RCO. The first functional element is PA. It has a reserve as an extra PA_R. This additional backup PA_R is included in the control circuit with the help of switches k_1 and k_2 that, according to the switching signals $u_1(t)$ from the RCD, disconnect the signals from the faulty PA and connect it to the backup one. Another scheme of this block is also possible. This is when both amplifiers on one EFM work at the same time. In this case, in case of complete failure of one of the amplifiers, the switches k_1 and k_2 disconnect it from the control circuit, and the working amplifier is brought to a new working area for restoring the operability of the amplifier unit with the help of an additional signal $\Delta u(t)$.

When using this scheme, it is necessary to check additional output signals from each amplifier to diagnose their operation. With high

requirements for the reliability of the power amplifier unit, its fault tolerance or durability, the number of reserve or additional amplifiers can be increased with an increase in the number of switching elements and control outputs from additional amplifiers.

The second functional element is EFM with backup EFM_R. The reserve functional element EFM_R is included in the circuit of the rational control in the event of a complete failure of the main EFM by means of the switch k_2 and clutch C according to the signals from the RCD. It is also possible to operate the EFM_R in hot reserve with other cycle diagrams of the operation of the switch k_2 and clutch C according to signals from the control device RCD.

The power amplifier can be considered as an object of diagnosis, as it is prone to destabilizing influence D_1, both input $u_C(t)$ and output $i(t)$ are available to measurement. Following the principle of decentralization of rational control [23, 24], it is possible to form a block of amplifiers as an autonomous subsystem of rational management of its efficiency. For example, when using an additional PA_R in a cold reserve, the diagram of such a block can be summarized in the following form (Figure 3.8).

DP and RP diagnostic and recovery procedures are implemented in RCD using microprocessor tools for processing signals $u_3(t)$ and $i(t)$.

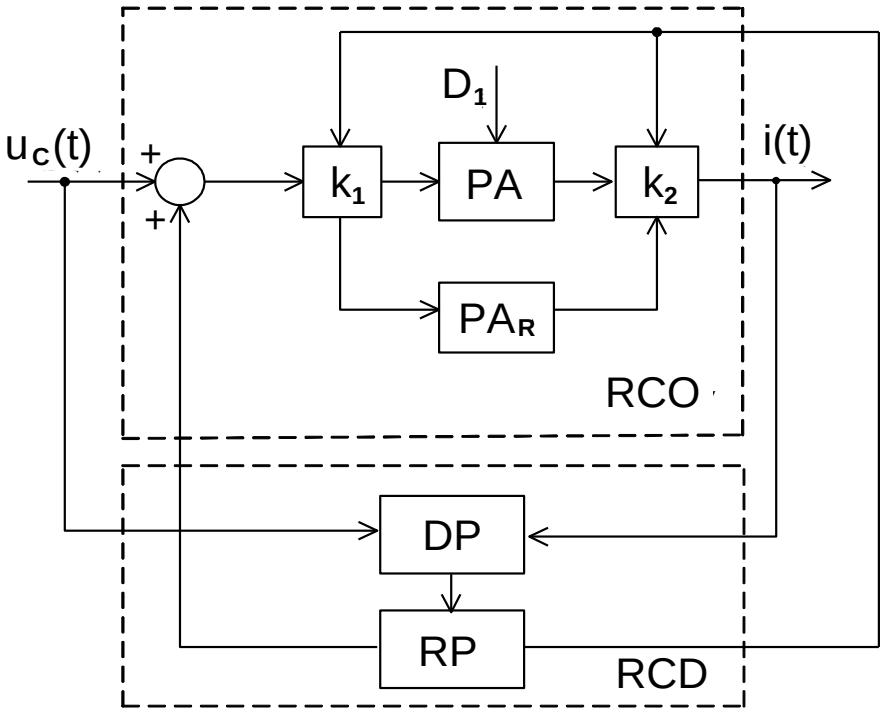

Figure 3.8 – Functional scheme of the power amplifier unit with rational control of its operability

Following the principle of decentralization of rational management, EFM does not meet the requirements for the object of diagnosis. One of the requirements for the object of diagnostics is the need for electrical control input and control output signals. Since the output signal of EFM is angular velocity $\omega(t)$, its values cannot be used during digital signal processing.

Therefore, in order for the EFM to be used as a diagnostic object, it must be supplemented with an angular velocity sensor. For example, a tachogenerator that produces an electrical signal $u_{TG}(t)$.

The EFM with TG serial connection has an electrical input – $i(t)$, and an electrical output – $u_{TG}(t)$; in other words the signals are available for digital processing to obtain a complete diagnosis. This complication of the object of diagnosis causes its further structural complication to ensure the possibility of rational management of the efficiency of the serial connection of EFM and TG. In Figure 3.9 one of the possible functional schemes of rational control of connection EFM+TG is presented.

In the presented functional scheme, a backup EFM_2 is used, which is activated by the switch k_2 and the clutch C according to signals from the RCD. TG2 is a second, identical to the first, angular velocity sensor, the signal from which is sent to the RCD to the signal processing unit to obtain a complete diagnosis. The second output from the RCD is a result of signal adjustment that is summed with the signal $i(t)$.

It is possible to increase the performance of optimal EFM control by using the principle of control ин deviation. Closed-loop automatic control systems, formed using this principle, compensate small deviations of the parameters of the automatic control object.

This property of closed control systems allows you to partially "unload" the RCD, which will increase both the accuracy of the operation of the electromechanical actuator and the efficiency of compensation for destabilizing influences.

Thus, in relation to the functional scheme of rational control (see Figure 3.7), a control loop of the output signal $u_{TG}(t)$ is introduced based on its deviation from the setting signal – $u_S(t)$ (Figure 3.10).

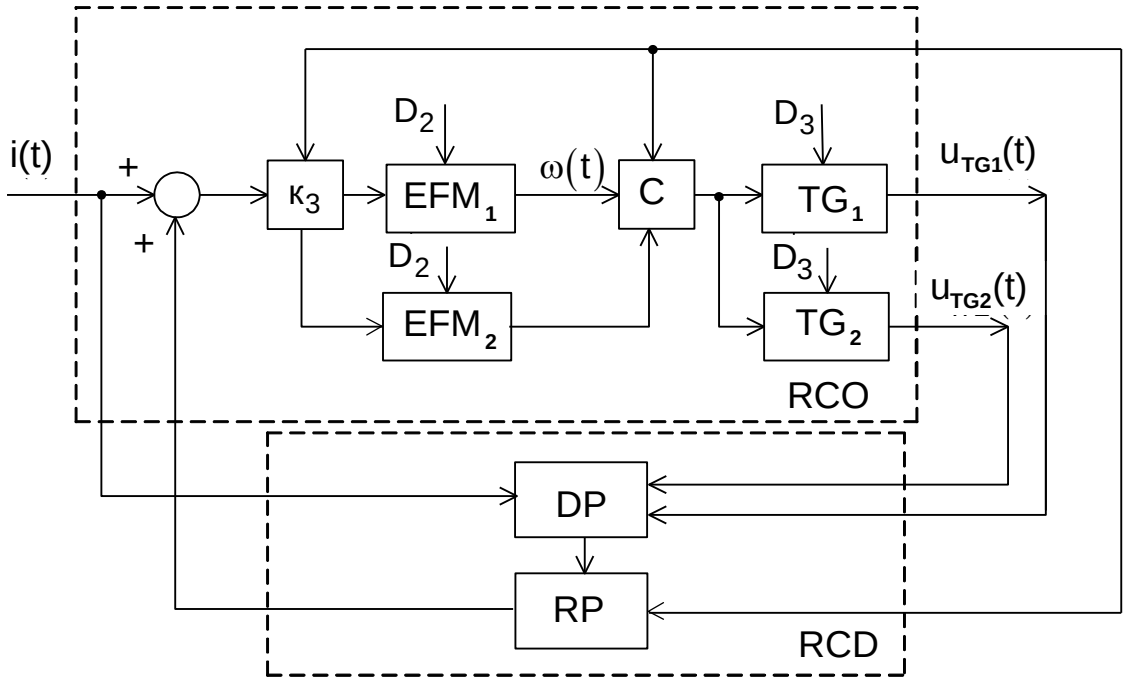

Figure 3.9 – Functional scheme of rational control of connection (EFM+TG)

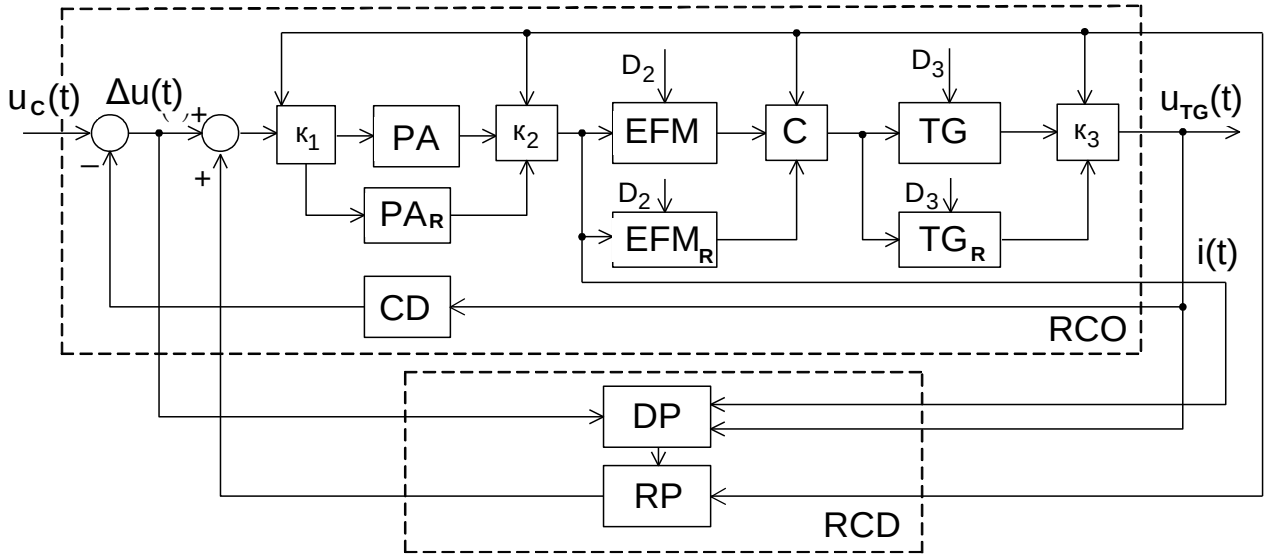

Figure 3.10 – Functional scheme of the two-circuit rational control system

The presented functional scheme contains two control loops. The first control circuit by the signal $u_{TG}(t)$ using the control device generates a signal on the negative input of the adder, which is compared with the setting signal $u_S(t)$ and a deviation signal is generated – $\Delta u(t)$.

The second control circuit based on the diagnosis is formed using signals $u_{TG}(t)$, $i(t)$ and $\Delta u(t)$, and also procedures DP and RP. Signals from RP are sent to the RCO to restore its operability.

Regarding the functional schemes of Figures 3.8 and 3.9, the use of the principle of control by deviation leads to a three-loop rational control system (Figure 3.11).

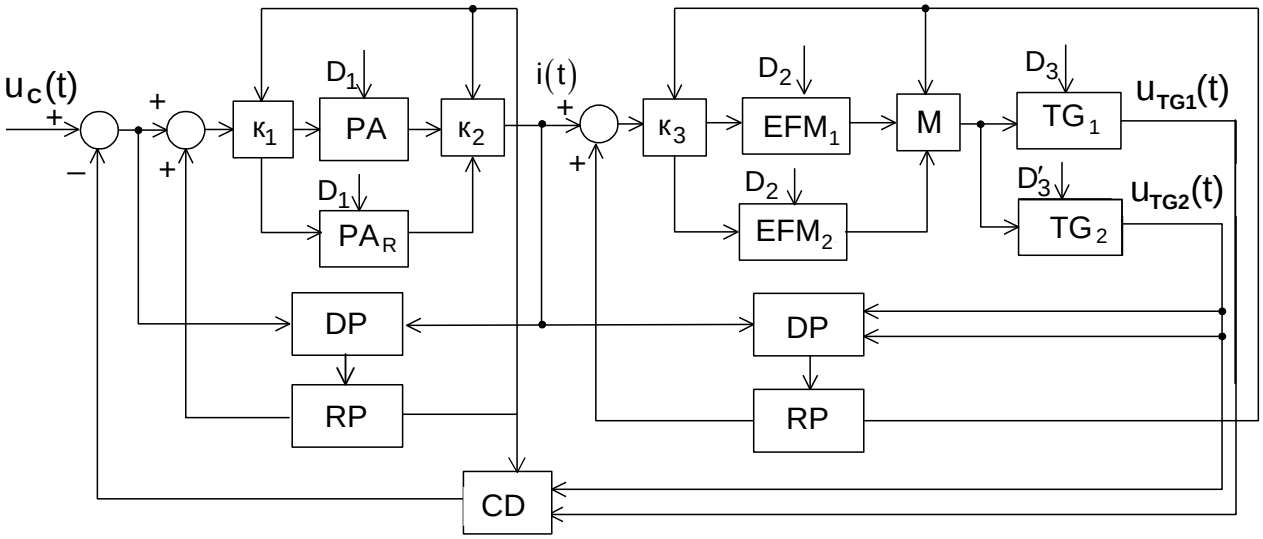

Figure 3.11 – Functional scheme of the three-loop rational control system

In the presented functional scheme, two internal control loops based on the PA and EFM serviceability diagnosis are implemented, and an external control loop based on deviation is formed using signals $u_{TG1}(t)$, $u_{TG2}(t)$, control device (CB) and adder.

The given functional schemes do not exhaust the entire variety of possible EFM rational cntrol schemes, but they are key. On the example of these key schemes, the instrumental means of deep diagnostics and flexible restoration of the operability of electromechanical actuators based on EFM will be considered.

3.3 Models of the nominal functioning of the electric flywheel motor as an automatic control object

The automatic control object of the electromechanical actuator consists of a power amplifier, an electric flywheel motor and a tachogenerator (see Figure 3.6). The central functional element of this unit is the EFM, which is a brushless DC electric motor that converts electrical energy into kinetic energy. Consider EFM from the point of view of energy conversion. In Figure 3.12 presents a graphical physical model of EFM.

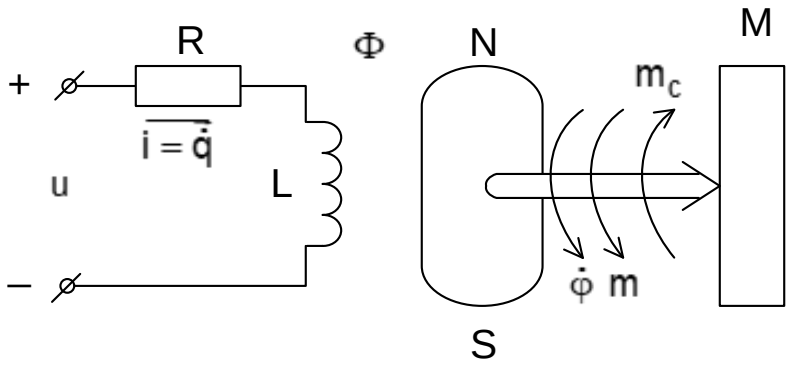

Figure 3.12 – Physical model of an electric flywheel motor

The following designations are used in the model: u – control voltage; $i = \dot{q}$ – excitation winding current; R – resistance of the excitation winding; L – inductance of the excitation winding; Φ – a stream of excitement; $\dot{\varphi}$ – angular speed of rotation of the rotor; m – rotation torque; m_c – resistance moment; M – flywheel; N and S – poles of the permanent magnet of the armature.

To formalize the processes of energy conversion in EFM, let's use the Lagrangian approach [25] in the following form:

$$\frac{d}{dt}\left(\frac{\partial T}{\partial \dot{\lambda}_i}\right) - \frac{\partial T}{\partial \lambda_i} = Q_i^u + Q_i^f;\ i = \overline{1,n}, \tag{3.4}$$

where T – kinetic energy of the modeling object;

λ_i – узагальнена координата;

Q_i^u – generalized force corresponding to controlling influences;

Q_i^f – the generalized force corresponding to the perturbing influences.

The process of converting energy into EFM has two degrees of freedom and is characterized by the following generalized coordinates: the angle of rotation of the rotor – φ; the amount of charge – q.

The kinetic energy of EFM is described by the following expression:

$$T = \frac{1}{2} I \dot{\varphi}^2 + \frac{1}{2} L \dot{q}^2, \tag{3.5}$$

where I – moment of inertia of the flywheel.

The generalized forces of each generalized coordinate are described as follows:

$$\begin{aligned} &Q_1^u = m;\ Q_1^f = m_c; \\ &Q_2^u = u;\ \ Q_2^f = -R\dot{q}. \end{aligned} \tag{3.6}$$

After performing the transformation according to equation (3.4), we obtain the following system of equations:

$$\begin{cases} I\ddot{\varphi} = m - m_c; \\ L\ddot{q} = u - R\dot{q}. \end{cases} \tag{3.7}$$

The moments and forces in the right-hand sides of the equations depend on the generalized coordinates.

Let's consider the qualitative type of nonlinear dependence of forces and moments of equation (3.7). The torque $m = f(u)$ depends nonlinearly on the control voltage u. In Figure 3.13 the graph of this non-linear dependence is shown.

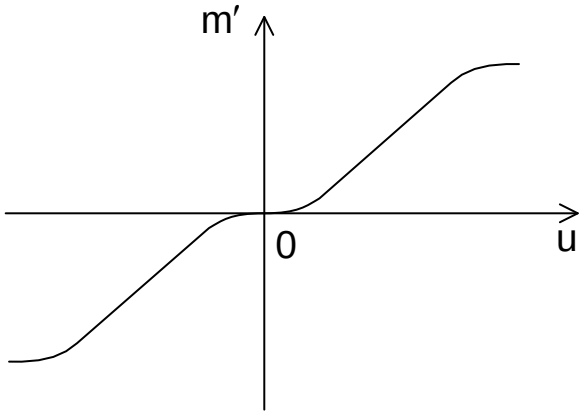

Figure 3.13 – Static characteristic EFM

There are three sections on the presented nonlinear characteristic: the first is the zone of insensitivity; the second is the average section, close to the linear dependence, and the third is the saturation section.

The torque depends nonlinearly on the angular velocity of the EFM (Figure 3.14).

It follows from the nature of the mechanical characteristics that while $\omega << \omega_{max}$, the control moment decreases and at $\omega = \omega_{max}$ the saturation speed of the EFM loses its ability to create a control moment.

The moment of resistance m_o on the EFM shaft is created by the forces of dry and viscous friction. The moment of dry friction m_o' depends significantly on the angular velocity of the EDM in a non-linear manner (Figure 3.15).

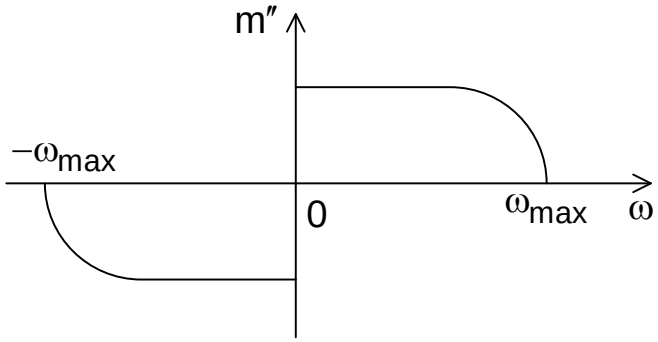

Figure 3.14 – Mechanical characteristics of EFM

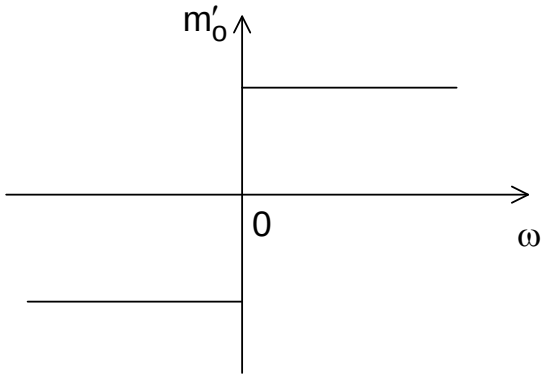

Figure 3.15 – Static characteristic of dry friction

The moment of viscous friction m_o'' depends on the angular velocity has a linear character with the transmission coefficient k_B.

EDM of direct current is characterized by a positional moment m_P which characterizes the dependence of the torque on the angular speed of rotation and takes into account the saturation of the kinetic moment.

The positional moment has a complex graphical dependence. As a result of the approximation of this dependence, an analytical description was obtained [3]. The analytical dependence of this moment is described by the following expression:

$$m_P = (1 - a\sin(n\varphi))m''m', \qquad (3.8)$$

where a – coefficient characterizing the amplitude of the positional moment;

φ – rotation angle of the EFM rotor;

n – the number of pole pairs of the magnetic system.

The nonlinear EFM model can be presented using Laplace transforms in the form of a structural diagram (Figure 3.16).

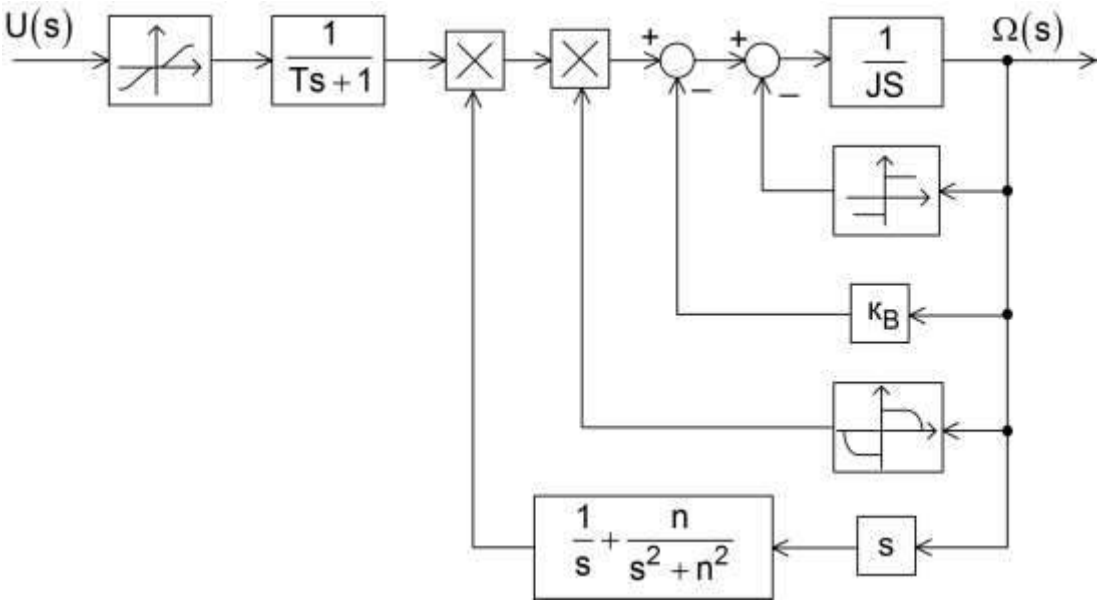

Figure 3.16 – Structural diagram of a nonlinear EFM

The presented nonlinear model can be used for research in the Simulink environment. For analytical studies, this model should be linearized and simplified so as to obtain the dependence in a linear approximation in the form of linear differential equations with constant coefficients and in the form of the corresponding transfer functions.

With the help of linear approximation of nonlinear characteristics, neglecting such secondary small effects as hysteresis, dry friction, focusing on the transforming properties of EFM near the operating point, we will obtain the corresponding linear dependences. These dependencies can be described analytically. So, EFM torque:

$$m = c_m \Phi \dot{q} = \kappa_m \dot{q}, \tag{3.9}$$

where c_m – constructive constant of electric motor;

κ_m – EFM transfer coefficient.

After performing certain actions in accordance with equation (3.4), we obtain the following equation for the generalized coordinate φ:

$$I\ddot{\varphi} = \kappa_м \dot{q} - \kappa_в \dot{\varphi}; \tag{3.10}$$

and the following equation for the generalized coordinate q:

$$L\ddot{q} = u - R\dot{q}. \tag{3.11}$$

The system of simplified and linearized equations (3.7), solved with respect to higher derivatives, has the following form:

$$\begin{cases} \ddot{\varphi} = \frac{\kappa_M}{I}\dot{q} - \frac{\kappa_B}{I}\dot{\varphi}; \\ \ddot{q} = \frac{u}{L} - \frac{R}{L}\dot{q}. \end{cases} \tag{3.12}$$

Let's change the obtained system of equations using EDM state space variables. Therefore, using the state space method [26, 27], we will define the following state variables: $x_1(t) = \dot{\varphi}; x_2(t) = \dot{q}$. У as a result of the corresponding transformations, we obtain a system of equations in vector-matrix form:

$$\begin{bmatrix} \dot{x}_1(t) \\ \dot{x}_2(t) \end{bmatrix} = \begin{bmatrix} -\frac{\kappa_B}{I} & \frac{\kappa_M}{I} \\ 0 & -\frac{R}{L} \end{bmatrix} \begin{bmatrix} x_1(t) \\ x_2(t) \end{bmatrix} + \begin{bmatrix} 0 \\ \frac{1}{L} \end{bmatrix} u(t); \begin{bmatrix} x_1(t_0) \\ x_2(t_0) \end{bmatrix} = \begin{bmatrix} 0 \\ 0 \end{bmatrix}. \tag{3.13}$$

For automatic control of EDM rotation, sensors of its angular velocity $\dot{\varphi}(t)$ and current $\dot{q}(t)$ changes are necessary. Then the output signals of the sensors $u_{S1}(t)$ and $u_{S2}(t)$ are related through the corresponding transfer coefficients $k_{S1}(t)$ and $k_{S2}(t)$ to the state vector as follows:

$$\begin{bmatrix} u_{S1}(t) \\ u_{S2}(t) \end{bmatrix} = \begin{bmatrix} k_{S1} & 0 \\ 0 & k_{S2} \end{bmatrix} \begin{bmatrix} x_1(t) \\ x_2(t) \end{bmatrix}. \tag{3.14}$$

If only one sensor is used – the angular velocity sensor, then the connection of the sensor's output signal with the state vector will be described as follows: $u_D(t)$

$$u_S(t) = \begin{bmatrix} k_S & 0 \end{bmatrix} \begin{bmatrix} x_1(t) \\ x_2(t) \end{bmatrix}. \tag{3.15}$$

In a more compact form, the system of equations (3.13) and (3.14) can be written as follows:

$$\dot{x}(t) = Ax(t) + bu(t);\ x_1(t_0) = 0;\ u_D(t) = Cx(t), \tag{3.16}$$

where $x(t) = \begin{bmatrix} x_1(t) \\ x_2(t) \end{bmatrix};\ A = \begin{bmatrix} -\frac{\kappa_B}{I} & \frac{\kappa_M}{I} \\ 0 & -\frac{R}{L} \end{bmatrix} = \begin{bmatrix} a_{11} & a_{12} \\ 0 & a_{22} \end{bmatrix}; b = \begin{bmatrix} 0 \\ \frac{1}{L} \end{bmatrix} = \begin{bmatrix} 0 \\ b_2 \end{bmatrix};$

(3.17)

$$u_S(t) = \begin{bmatrix} u_{S1}(t) \\ u_{S2}(t) \end{bmatrix};\quad C = \begin{bmatrix} k_{S1} & 0 \\ 0 & k_{S2} \end{bmatrix} = \begin{bmatrix} c_{11} & 0 \\ 0 & c_{22} \end{bmatrix};\ x(t_0) = \begin{bmatrix} x_1(t_0) \\ x_2(t_0) \end{bmatrix} = \begin{bmatrix} 0 \\ 0 \end{bmatrix}.$$

For systems of equations (3.13) and (3.15), the compact form will have the view:

$$\dot{x}(t) = Ax(t) + bu(t);\ x_1(t_0) = 0;\ u_D(t) = c^T x(t), \qquad (3.18)$$

where

$$c^T = \begin{bmatrix} c_1 & 0 \end{bmatrix} = \begin{bmatrix} k_S & 0 \end{bmatrix}. \qquad (3.19)$$

Graphic representation of mathematical descriptions in the space of states allows to visualize the structures of transformation processes for visual assessment of their properties.

A structural diagram showing the transformation processes in EFM as an automatic control object is presented in Figure 3.17.

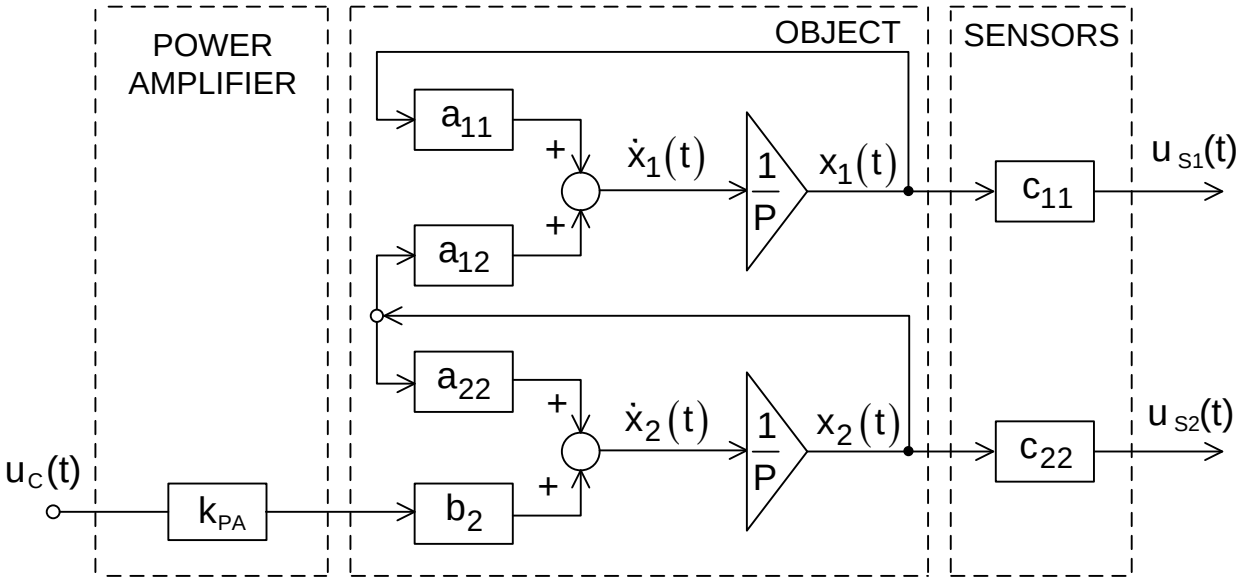

Figure 3.17 – Structural diagram of the automatic control object in the time domain

The given structural diagram reflects both the composition of the converting elements of the mathematical description and the connections between the elements and the characteristics of the signals.

The structural diagram of the automatic control object with an angular velocity sensor is shown in Figure 3.18.

To obtain a mathematical description of the EFM as an automatic control object in the frequency domain, let's use the Laplace transform for equations (3.13) and (3.14), and as a result we obtain the following operator equations:

$$sX(s) = AX(s) + bU(s); \quad U_S(s) = cX(s), \tag{3.20}$$

where s – variable of Laplace transform;

$X(s)$ – state vector image $x(t)$;

$U(s)$ – image of controlling influence (control signal);

$U_S(s)$ – vector image of sensor signals.

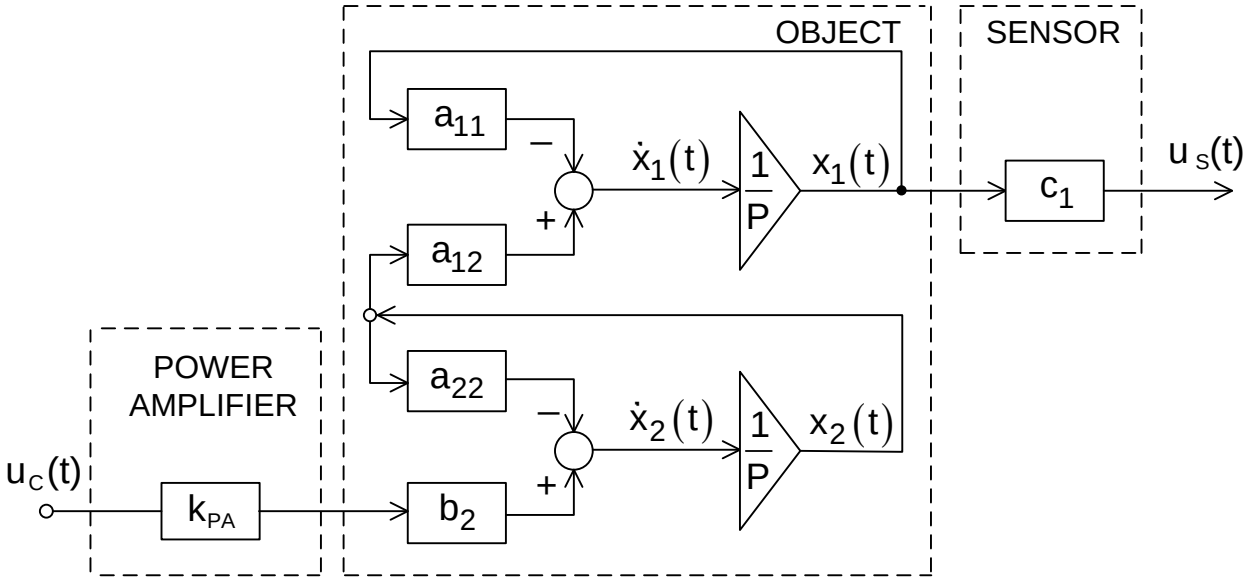

Figure 3.18 – Structural diagram of the automatic control object with one sensor

The operator equation for the image will be as follows:

$$U_S(s) = C\left[sI - A\right]^{-1} bU(s), \tag{3.21}$$

where $I - (2 \times 2)$ – unit matrix.

This operator equation allows to obtain two transfer functions that reflect the relationships of the output and input images of EFM signals as an automatic control object.

$$W_1(s) = \frac{U_{S1}(s)}{U(s)} = \frac{c_{11}a_{22}b_2k_{PA}}{(s - a_{11})(s + a_{22})} = \frac{k_{S1}k_Mk_{PA}}{k_BR\left(\frac{I}{k_B}s + 1\right)\left(\frac{L}{R}s + 1\right)}, \tag{3.22}$$

$$W_2(s) = \frac{U_{S2}(s)}{U(s)} = \frac{c_{22}(s - a_{11})b_2 k_{PA}}{(s - a_{11})(s + a_{22})} = \frac{k_{S2}\left(\frac{I}{k_B}s + 1\right)k_{PA}}{k_B R\left(\frac{I}{k_B}s + 1\right)\left(\frac{L}{R}s + 1\right)}. \quad (3.23)$$

Let's define $\frac{L}{R} = T_E$ – electrical constant of EFM, and $\frac{I}{\kappa_в} = T_{EM}$ – electromechanical constant of EFM. As usual, $T_E << T_{EM}$ and such as transfer function $W_1(s)$ may be represented by an aperiodic term

$$W_1(s) = \frac{U_{S1}(s)}{U(s)} = \frac{k_1}{(T_{EM}s + 1)}, \quad (3.24)$$

where $k_1 = \frac{k_{S1}k_M k_{PA}}{k_B R}$ – transfer coefficient of the automatic control object;

$T_{EM} = \frac{I}{\kappa_в}$ – electromechanical constant of the automatic control object.

The second transfer function $W_2(s)$ given that $T_E << T_{EM}$, as well as the sameness of the coefficient $\left(\frac{I}{\kappa_в}s + 1\right)$ in the numerator and denominator can be represented by an inertialess link

$$W_2(s) = \frac{U_{S2}(s)}{U(s)} = \frac{k_{S2}k_{PA}}{R} = k_2. \quad (3.25)$$

When using one tachogenerator as angular velocity sensor in the automatic control object, the transfer function will be as follows:

$$W_3(s) = \frac{U_S(s)}{U(s)} = \frac{c_1 a_{22} b_2 k_{PA}}{(s - a_{11})(s + a_{22})} = \frac{k_S k_M k_{PA}}{k_B R\left(\frac{I}{k_B}s + 1\right)\left(\frac{L}{R}s + 1\right)}. \quad (3.26)$$

Taking into account the condition $T_E << T_{EM}$, the expression of the transfer function will be simplified to the transfer function of the aperiodic link (3.24).

The obtained mathematical descriptions and graphical representations of the transforming properties of the EFM as an automatic control object reflect only the nominal, regular state without taking into account the influence of destabilizing factors on the performance.

3.4 Models of abnormal functioning of the automatic control object

A variety of destabilizing actions lead to abnormal functioning of EFM as an automatic control object. In case of abnormal functioning, the operable state of the automatic control object is violated. To identify the causes of abnormal behavior, models reflecting the impact of destabilizing factors on the output, available measurement signals characterizing the performance of the automatic control object are required. Such models are called diagnostic models [28].

As destabilizing influences, consider disturbing actions such as dry and viscous friction, voltage fluctuations of the power supply network, as well as defects, breakdowns, malfunctions, failures in the automatic control object. Under the action of destabilizing influences, a disturbed motion occurs in the object of mathematical control, which is described by the following equation of disturbed motion:

$$\begin{cases} \dot{\tilde{x}}(t) = \tilde{A}\tilde{x}(t) + \tilde{b}u(t) + \ell f(t);\ \tilde{x}(t_0) = 0; \\ \tilde{u}_S(t) = \tilde{C}\tilde{x}(t), \end{cases} \tag{3.27}$$

where $\dot{\tilde{x}}(t)$ – two-dimensional state vector of disturbed motion;

$\tilde{A}, \tilde{b}, \ell, \tilde{C}$ – matrices of appropriate dimensions characterizing destabilization;

$\tilde{u}_S(t)$ – the output signal of model of the object's disturbed motion.

For small deviations of destabilizing influences, the system of equations (3.27) can be presented in the following form:

$$\begin{cases} \dot{\tilde{x}}(t) = (A + \Delta A)\tilde{x}(t) + (b + \Delta b)u(t) + \ell f(t);\ \tilde{x}(t_0) = 0; \\ \tilde{u}_S(t) = (C + \Delta C)\tilde{x}(t). \end{cases} \tag{3.28}$$

To solve the problem of detecting destabilization, a reference model is needed. We will choose the system of equations (3.16) as the simplest reference model. Let's subtract the equations of the reference model from the system of equations (3.28). As a result, we get:

$$\begin{cases} \Delta\dot{x}(t) = A\Delta x(t) + \Delta A\Delta x(t) + \Delta b u(t) + \ell f(t);\ \Delta x(t_0) = 0; \\ \tilde{u}_S(t) = C\Delta x(t) + \Delta C\Delta x(t), \end{cases} \tag{3.29}$$

where $\Delta x(t) = \tilde{x}(t) - x(t);\ \Delta u_S(t) = \tilde{u}_S(t) - u_S(t)$.

The system of equations obtained in the deviations is the equation of the diagnostic model, which connects the measurable indirect diagnostic sign $\Delta u_D(t)$ with the inaccessible diagnostic sign of destabilization $\Delta A, \Delta b, l, \Delta C$.

The accuracy of determining an indirect sign of destabilization of an automatic control object can be increased by using a reference model in the form of an Luyenberger observer

$$\begin{cases} \dot{x}(t) = Gx(t) + K\tilde{u}_S(t) + bu(t); \quad x(t_0) = 0; \\ u_S(t) = Cx(t), \end{cases} \tag{3.30}$$

matrix $G = A - KC$.

Static reference models described by a system of equations (3.31) are used when solving the tasks of identifying control objects

$$\begin{cases} \dot{x}(t) = A\tilde{x}(t) + bu(t); \quad \tilde{x}(t_0) = \tilde{x}_0; \\ u_S(t) = Cx(t). \end{cases} \tag{3.31}$$

Of the above three forms of reference models, the Luenberger observer can be used as a general form of reference models. Indeed, if the matrix $K = 0$, and matrix $G = 0$ and the state vector can be recovered $\tilde{x}(t)$, that is, there is an inverse matrix C^{-1}, then a static reference model is obtained (3.31).

A diagnostic model for detecting destabilization using a Lueberger observer will look like this:

$$\begin{cases} \Delta\dot{x}(t) = G\Delta x(t) + \Delta A\Delta x(t) + bu(t); \quad \tilde{x}(t_0) = 0; \\ \Delta u_S(t) = C\Delta x(t) + \Delta C\Delta x(t). \end{cases} \tag{3.32}$$

Therefore, the influence of all destabilizing factors will be manifested in the vector of measurements $\tilde{u}_S(t)$, which are the output signals of the sensors.

After solving the task of detecting destabilization, it is necessary to find the place of destabilization – the structurally finished part of the EFM automatic control object. There are three such parts. This is a power amplifier, the EFM itself and sensors. Appropriate diagnostic models are used to find the place of destabilization. Yes, to detect destabilization in the power amplifier when

$$\tilde{u}_{PA}(t) = \tilde{k}_{PA}u(t) + u_0, \tag{3.33}$$

where $\tilde{k}_{PA}$ – the value of the amplification factor during destabilization;

u_0 – drift value of zero, reference model reflecting the nominal mode of operation

$$u_{PA}(t) = k_{PA}u(t), \tag{3.34}$$

then the diagnostic model reflecting the destabilization in the power amplifier will be as follows

$$\Delta u_{PA}(t) = \Delta k_{PA} u(t) + u_0 . \qquad (3.35)$$

In this model, the information about the destabilization of the power amplifier is given in a measurable deviation $\Delta u_{PA}(t)$.

The disturbed motion of EFM and sensors caused by destabilizing influences is described by the following system of equations:

$$\begin{cases} \dot{\tilde{x}}(t) = \tilde{A}\tilde{x}(t) + \tilde{b}' u_{PA}(t) + \ell f(t); \ \tilde{x}(t_0) = 0; \\ \tilde{u}_S(t) = \tilde{C}\tilde{x}(t), \end{cases} \qquad (3.36)$$

where b′ – a column vector representing the relationship $u_{PA}(t)$ to the state vector.

For small deviations of destabilizing influences, the diagnostic model describing the destabilization in this part of the automatic control object will be as follows:

$$\begin{cases} \Delta\dot{x}(t) = G\Delta x(t) + \Delta A\Delta x(t) + \Delta b' u(t) + \ell f(t); \ \ \Delta x(t_0) = 0; \\ \Delta u_S(t) = C\Delta x(t) + \Delta C\Delta x(t). \end{cases} \qquad (3.37)$$

With the help of this model, a measurable vector of signals $\Delta u_D(t)$ is formed, which reflects the influence of destabilizing effects on the functioning of the “EFM+sensors” subsystem.

Deeper diagnostic models are needed to find the specific functional element in which destabilization has occurred. So, if destabilization occurred in EFM, then the disturbed motion will be described by a system of equations

$$\begin{cases} \dot{\tilde{x}}(t) = \Delta A\tilde{x}(t) + \tilde{b}' u(t) + \ell' f(t); \ \tilde{x}(t_0) = 0; \\ \tilde{u}_S(t) = C\tilde{x}(t), \end{cases} \qquad (3.38)$$

here ℓ' – a line vector reflecting the effect of the disturbing action on EFM.

When using the reference model in Luyenberger observer form we will get a diagnostic model

$$\begin{cases} \Delta\dot{x}(t) = G\Delta x(t) + \Delta A\Delta x(t) + \Delta b' u_{PA}(t) + \ell' f(t); \ \ \Delta x(t_0) = 0; \\ \Delta u_S(t) = C\Delta x(t), \end{cases} \qquad (3.39)$$

the output signal of which contains information about destabilization of EFM functioning.

Malfunction of the angular velocity sensor k_{S1} is described using a diagnostic model of such view:

$$\begin{cases} \dot{x}(t) = Ax(t) + b'u_{PA}(t); \;\; x(t_0) = 0; \\ \Delta u_{S1}(t) = \Delta k_{S1} x_1(t) + u_{01}, \end{cases} \tag{3.40}$$

where $\Delta u_{S1}(t)$ – deviation of the angular velocity sensor signal from the reference signal;

Δk_{S1} – deviation of the sensor conversion factor caused by destabilization;

u_{01} – the value of the zero drift of the sensor;

$x_1(t)$ – the first component of the state vector.

Disturbances in the functioning of the current sensor Δk_{S2} can be represented with the help of a diagnostic model of this type:

$$\begin{cases} \dot{x}(t) = Ax(t) + b'u_{PA}(t); \;\; x(t_0) = 0; \\ \Delta u_{S2}(t) = \Delta k_{S2} x_2(t) + u_{02}, \end{cases} \tag{3.41}$$

where $\Delta u_{S2}(t)$ – deviation of the current sensor signal from the reference value;

Δk_{S2} – deviation of the conversion factor of the sensor during destabilization;

$x_2(t)$ – the second component of the state vector $x(t)$;

u_{02} – the size of the measurement error.

The use of diagnostic models (3.40) and (3.41) allows to find in which of the sensors a malfunction occurred, caused by destabilizing effects on these functional elements of the automatic control object.

When using two angular velocity sensors TG_1 and TG_2 (see Figure 3.9), disturbed motion caused by disturbances in their functioning is generally described by a system of equations:

$$\begin{cases} \dot{x}(t) = Ax(t) + b'u_{PA}(t); \;\; x(t_0) = 0; \\ \tilde{u}_S(t) = C\Delta x(t) + \Delta C x(t) + u_0, \end{cases} \tag{3.42}$$

where u_0 – two-dimensional vector of sensor zero drifts.

The diagnostic model of TG_1 dysfunction will look like this:

$$\begin{cases} \dot{x}(t) = Ax(t) + b'u(t); \;\; x(t_0) = 0; \\ \Delta u_{D1}(t) = \Delta k_1 x_1(t) + u_{01}, \end{cases} \tag{3.43}$$

where $\Delta u_{S1}(t)$ – deviation of the TG_1 voltage from the reference voltage;

Δk_1 – deviation of the TG_1 conversion factor during destabilization;

$x_1(t)$ – the first component of the state vector $x(t)$;

u_{01} – value of zero drift of TG1.

If TG_2 malfunctions, the diagnostic model will look like this:

$$\begin{cases} \dot{x}(t) = Ax(t) + b'u(t); \quad x(t_0) = 0; \\ \Delta u_{S2}(t) = \Delta k_2 x_2(t) + u_{02}, \end{cases} \tag{3.44}$$

where $\Delta u_{S2}(t)$ – deviation of the TG_2 voltage from the reference voltage;

Δk_2 – deviation of the TG_2 conversion factor during destabilization;

$x_2(t)$ – the second component of the state vector $x(t)$;

u_{02} – value of zero drift of TG_2.

Therefore, in case of destabilization of the performance of sensors TG_1 and TG_2, it is possible to identify an inoperable sensor using the presented diagnostic models (3.43) and (3.44), which reflect cause-and-effect relationships between direct and indirect diagnostic signs.

To establish the type of destabilization, appropriate diagnostic models are required that connect indirect diagnostic features with direct diagnostic features of the class. Types of destabilization for a power amplifier are formed from a set D_1 of types of destabilizing influences. For a power amplifier, let's consider the following types of destabilizing influences: d_{11} – recoverable reduction of transfer factor; d_{12} – irreversible reduction of transfer factor; d_{13} – recoverable zero drift; d_{14} – non-recoverable zero drift; d_{15} – unknown type of destabilization. So, the set D_1 contains five types of destabilization:

$$D_1 = \{d_{11}, d_{12}, d_{13}, d_{14}, d_{15}\}. \tag{3.45}$$

The current gain value $\tilde{k}_{PA}$ will be a direct diagnostic sign of types of destabilization d_{11} and d_{12}. Thus, the type of reduction of k_{PA} will consist of two types of recoverable and non-recoverable destabilization. And the feature that characterizes this class will be the current value $\tilde{k}_{PA}$. The second type of drift contains species d_{13} and d_{14}, and the offset value of the static current characteristic of the power amplifier u_0 will be the class feature. The third type includes a type of destabilization, and the diagnostic feature of this type will be the absence of signs of the first and second types. The diagnostic model for these two types is described by the same model as for detection of destabilization in a power amplifier (3.35).

When forming diagnostic models for types of destabilization for EFM, it is necessary to first form a set D_2 of types of destabilizing influences. Let the set D_2 include such destabilizing influences: d_{21} – disturbances in the functioning of EFM, which lead to a recoverable reduction of the coefficient k_M, d_{22} – irreversible reduction of the conversion factor; d_{23} – recoverable increase in transition time; d_{24} – irreversible increase in the time of the transition process; d_{25} – unknown type of destabilization. Thus, the set D_2 will consist of five types of destabilizing influences

$$D_2 = \{d_{21}, d_{22}, d_{23}, d_{24}, d_{25}\}. \quad (3.46)$$

Types of destabilization d_{21} and d_{22} can be combined into one type, which will be characterized by a parameter $\tilde{k}_M$ (3.1). Types of destabilization d_{23} and d_{24} depend on the parameter $\tilde{k}_B$ (3.10), therefore, they will form the second type of destabilization. The third type is type d_{25}, the diagnostic feature of which will be the absence of diagnostic features of the first and second types.

A diagnostic model describing these types of destabilization in expanded form would look like:

$$\begin{bmatrix}\Delta\dot{x}_1(t)\\ \Delta\dot{x}_2(t)\end{bmatrix} = \begin{bmatrix}-\sigma_1 & 0\\ 0 & -\sigma_2\end{bmatrix}\begin{bmatrix}\Delta x_1(t)\\ \Delta x_2(t)\end{bmatrix} + \begin{bmatrix}-\frac{\Delta k_B}{I} & \frac{\Delta k_B}{I}\\ 0 & 0\end{bmatrix}\begin{bmatrix}\Delta x_1(t)\\ \Delta x_2(t)\end{bmatrix} + \begin{bmatrix}0\\ \frac{1}{L}\end{bmatrix}u_{PA}(t);$$
$$\begin{bmatrix}\Delta x_1(t_0)\\ \Delta x_2(t_0)\end{bmatrix} = \begin{bmatrix}0\\ 0\end{bmatrix};\quad \begin{bmatrix}\Delta u_{S1}(t)\\ \Delta u_{S2}(t)\end{bmatrix} = \begin{bmatrix}\Delta k_{S1} & 0\\ 0 & \Delta k_{S2}\end{bmatrix}\begin{bmatrix}\Delta x_1(t)\\ \Delta x_2(t)\end{bmatrix}. \quad (3.46)$$

Here $-\sigma_1$ and $-\sigma_2$ are coefficients of the matrix of the Luenberger observer.

The performance of sensors of the automatic control object is affected by destabilizing actions from the set D_3. To specify the types of destabilization, consider the following: d_{31} – recoverable reduction of the conversion factor of the first sensor; d_{32} – irrecoverable reduction of the conversion factor of the first sensor; d_{33} – recoverable zero drift value of the first sensor; d_{34} – irrecoverable zero drift value of the first sensor, d_{35} – recoverable reduction of the conversion factor of the second sensor; d_{36} – irrecoverable reduction

of the conversion factor of the second sensor; d_{37} – recoverable zero drift value of the second sensor; d_{38} – irrecoverable zero drift value of the second sensor; d_{39} – unknown type of destabilization. With such types of destabilization, the set D_3 will consist of nine elements:

$$D_3 = \{d_{31}, d_{32}, d_{33}, d_{34}, d_{35}, d_{36}, d_{37}, d_{38}, d_{39}\}. \quad (3.47)$$

Types of destabilization d_{31} and d_{32} constitute the first type with a diagnostic feature $\tilde{k}_{D1}$. The type of drifts of zero will include species d_{33} and d_{34} with a sign u_{01}. Similarly, the third type is species d_{35} and d_{36} with a feature $\tilde{k}_{D2}$. The fourth type includes species d_{37} and d_{38} with a feature u_{02}. The fifth type is a type of destabilization from the previous classes.

The diagnostic model reflecting the types of sensor destabilization will have the following structure:

$$\begin{bmatrix} \Delta u_{S1}(t) \\ \Delta u_{S2}(t) \end{bmatrix} = \begin{bmatrix} \Delta k_{S1} & 0 \\ 0 & \Delta k_{S2} \end{bmatrix} \begin{bmatrix} x_1(t) \\ x_2(t) \end{bmatrix} + \begin{bmatrix} u_{01} \\ u_{02} \end{bmatrix}. \quad (3.48)$$

The given forms of diagnostic models are the models of abnormal functioning of EFM as an automatic control object. These models are necessary for the implementation according the principle of control by diagnosis, which consists in identifying the causes of malfunctioning of functional elements, i.e. in establishing a complete diagnosis of an inoperable automatic control object.

Chapter IV DIAGNOSTIC SUPPORT OF THE RATIONAL CONTROL OBJECT

Nothing happens without a reason. If something happened, you can be sure that there was a reason for it.

Hippocrates (460-370 BC) – a famous ancient Greek physician, the "father of medicine".

Diagnosis is a technological process of identifying the reasons for the malfunctioning of the rational control object. In order to form a diagnostic process, it is necessary to solve a number of consecutive and interrelated tasks: detecting destabilization, finding the place of its occurrence, detecting the class of destabilization and identifying their type. Diagnostic support includes a set of tools and the sequence of its use to form a machine diagnosis of a rational control object, prone to destabilizing influences.

4.1 Detection of destabilization

In the rational control object, destabilization of operability may occur at any moment of time, since the types of destabilization are uncertain events from the set

$$D = D_1 \cup D_2 \cup D_3, \tag{4.1}$$

where $\cup$ – disjunction symbol.

Because of implementation of rational control algorithms on microprocessor tools of digital signal processing, it is advisable to move from differential equations (3.16) to mathematical equations of discrete state space using the Kotelnikov-Shannon theorem. Then

$$\begin{cases} x\left[(k+1)T_0\right] = Ax(kT_0) + bu(kT_0);\ x(kT_0) = x_0; \\ u_S(kT_0) = Cx(kT_0), \end{cases} \tag{4.2}$$

where T_0 – quantization period;

$k = 0,1, 2, ...;$

A, b and C – coefficient matrices of the discrete representation of the system (3.16), differing in structure and coefficients.

In the following statement, to simplify the writing of variables T_0, we will omit them.

The essence of the process of detecting destabilization in the rational control object is represented by a functional scheme (Figure 4.1).

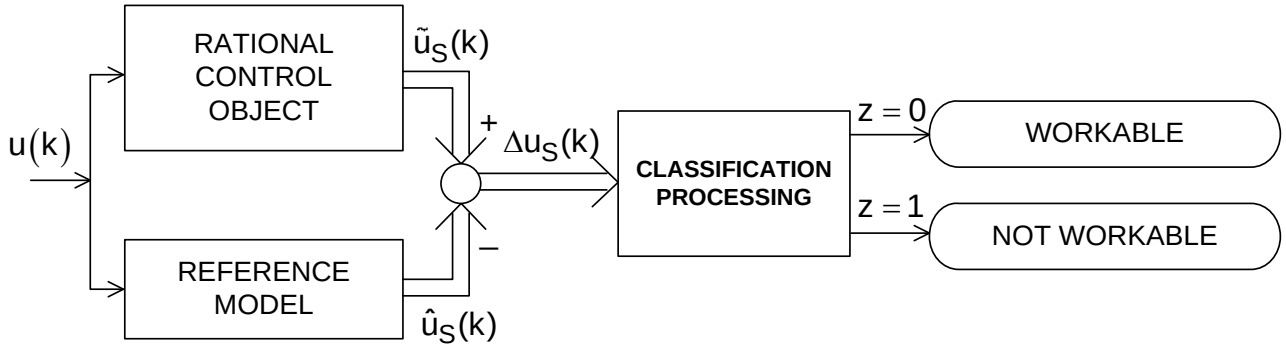

Figure 4.1 – Functional diagram of the destabilization detection process

Having chosen as a reference model a system of finite-difference equations of the form:

$$\begin{cases} \hat{x}(k+1) = A\hat{x}(k) + bu(k);\ \hat{x}(k_0) = 0; \\ \hat{u}_S(k) = C\hat{x}(k), \end{cases} \tag{4.4}$$

here the symbol $\wedge$ – symbol of the estimated values of the variables.

From the equation (4.4) we will get a difference signal $\Delta u_S(k)$, that will contain information about the current functional state of the rational control object.

The expanded form of the reference model (4.3) can be represented as follows:

$$\begin{bmatrix} \hat{x}_1(k+1) \\ \hat{x}_2(k+1) \end{bmatrix} = \begin{bmatrix} 1 - \frac{k_в T_0}{I} & \frac{k_м T_0}{I} \\ 0 & \frac{RT_0}{L} \end{bmatrix} \begin{bmatrix} \hat{x}_1(k) \\ \hat{x}_2(k) \end{bmatrix} + \begin{bmatrix} 0 \\ \frac{T_0}{L} \end{bmatrix} u(k);\ \begin{bmatrix} \hat{x}_1(k_0) \\ \hat{x}_2(k_0) \end{bmatrix} = \begin{bmatrix} 0 \\ 0 \end{bmatrix};$$
$$\begin{bmatrix} u_{S1}(k) \\ u_{S2}(k) \end{bmatrix} = \begin{bmatrix} k_{S1} & 0 \\ 0 & k_{S1} \end{bmatrix} \begin{bmatrix} \hat{x}_1(k) \\ \hat{x}_2(k) \end{bmatrix}. \tag{4.6}$$

If we use a static reference model

$$\begin{aligned} &\hat{x}(k+1) = A\tilde{x}(k) + bu(k);\ \hat{x}(k_0) = \tilde{x}_0; \\ &\hat{u}_S(k) = C\hat{x}(k), \end{aligned} \tag{4.7}$$

then the expanded form of this model will be described as follows:

$$\begin{bmatrix}\hat{x}_1(k+1)\\ \hat{x}_2(k+1)\end{bmatrix}=\begin{bmatrix}\frac{I-k_в T_0}{Ik_{D1}} & \frac{\kappa_м T_0}{Ik_{D2}}\\ 0 & \frac{RT_0}{Lk_{D2}}\end{bmatrix}\begin{bmatrix}\tilde{u}_{S1}(k)\\ \tilde{u}_{S2}(k)\end{bmatrix}+\begin{bmatrix}0\\ \frac{T_0}{L}\end{bmatrix}u(k);\begin{bmatrix}\hat{x}_1(k_0)\\ \hat{x}_2(k_0)\end{bmatrix}=\begin{bmatrix}\tilde{x}_{10}(k_0)\\ \tilde{x}_{20}(k_0)\end{bmatrix};$$
$$\begin{bmatrix}\hat{u}_{S1}(k)\\ \hat{u}_{S2}(k)\end{bmatrix}=\begin{bmatrix}k_{S1} & 0\\ 0 & k_{S2}\end{bmatrix}\begin{bmatrix}\hat{x}_1(k)\\ \hat{x}_2(k)\end{bmatrix}. \quad (4.8)$$

The use of any of the considered reference models allows, according to the functional scheme (see Figure 4.1), to obtain a difference signal $\Delta u_S(k)$. This difference signal is a discrete function of time, which contains information about the current functional state of the rational control object, which is subject to the influence of destabilizing actions from the set D. The classification of the difference signal $\Delta u_S(k)$ requires appropriate digital processing in real time. Thus, classification processing is related to the formalization of knowledge about destabilizing actions.

There are several ways of formalizing knowledge in the theory of artificial intelligence [29, 30]. The most productive for diagnostic tasks, as evidenced by the experience of using expert systems, is the method of formalization using products or modeling. This method is based on rules that allow to present knowledge in the form of a proposition of the type "if ..., then ...". To form a set of products, we will use two-valued predicate equations of the general form [31]:

$$z = S_2(x) = \begin{cases}1, \text{ if } x \in \Omega;\\ 0, \text{ if } x \notin \Omega,\end{cases} \quad (4.9)$$

where Ω – numerical set.

More detailed two-valued predicate equations have the following form:

$$z_1 = S_2(x-a) = \begin{cases}1, \text{ if } x \ge a;\\ 0, \text{ if } x < a;\end{cases}$$
$$z_2 = S_2(b-x) = \begin{cases}1, \text{ if } x \le b;\\ 0, \text{ if } x > b;\end{cases} \quad (4.10)$$
$$z_3 = z_1 \Lambda z_2 = \begin{cases}1, \text{ if } a \le x \le b;\\ 0, \text{ if } x < a \text{ and } x > b,\end{cases}$$

where *a* and *b* – постійні числа, and $b > a$.

When forming a priori and a posteriori knowledge about destabilizing influences, we will proceed from the following:

1) destabilizing effects are uncertain events in terms of time of appearance, location, class and type of manifestation;

2) knowledge about a specific species can be obtained on the basis of information about the presence of destabilization in the object, the place of localization and the class of destabilizing influence;

3) destabilizing actions are actions that change the conditions of normal functioning of the diagnostic object. Therefore, any deviations from the nominal static and dynamic characteristics of the diagnostic object are types of destabilization;

4) a priori knowledge of signs of destabilizing influence will be incomplete. Therefore, during the entire life cycle of rational control systems, when new destabilizing influences appear, it is necessary to form new a posteriori knowledge about them that clarifies or supplements a priori;

5) for the computer implementation of both a priori and a posteriori knowledge, two-valued predicate equations are the most productive form of their formalization.

Knowledge about direct signs of destabilizing influences $d_i \in D$, $i = \overline{1,q}$ is presented in the form of Boolean variables z_j, $j = \overline{1,\tau}$. It is advisable to use this knowledge to obtain a diagnosis using dichotomous trees [32].

The task of forming a dichotomous tree consists in the systematization of predicate knowledge in accordance with the principle of sequential removal of the uncertainty of abnormal situations caused by destabilizing influences.

The Boolean form of representation of knowledge about direct signs of destabilization allows you to form a tree-like dichotomous structure for a quick search for the type of destabilizing influence.

A dichotomous structure is a hierarchical knowledge structure where each node has a value and links to left and right descendants. The node at the very top is called the root. Nodes that have no descendants are leaves.

For operational search, dichotomous trees are balanced according to various criteria, which makes it possible to form a tree structure that meets the requirements for the speed of diagnosis processes.

With the help of knowledge of direct signs of destabilizing influences obtained at the stage of designing predicate equations, a support tree for searching for a diagnosis is formed. At the next stages of the life cycle of a rational control system, the supporting tree is supplemented with new branches from the leaves of the uncertainty of situations that arose during

localization, class determination and the detecting of a specific type of destabilizing influence.

When forming two-valued predicate equations, the assumption of quasi-stationarity of direct signs of destabilizing influences on the intervals of diagnosis and recovery is used.

Information about the destabilization of the object of rational management (see Figure 4.1) is contained in the difference signal $\Delta u_S(k)$. The difference signal is a vector discrete function of time. To convert this time function into a Boolean function, we need to form a two-valued predicate equation with a domain of definition $\forall k \in [k_0, k_1]$. The components of the vector $\Delta u_S(k)$: $\Delta u_{S1}(k)$ and $\Delta u_{S2}(k)$ contain related destabilization information, so they must be used as arguments in a binary predicate equation. These components may be as greater as less than zero. Therefore, the predicate equation can have the following structure:

$$z_0 = S_2\left\{\left[\left|\Delta u_{S1}(k)\right| + \left|\Delta u_{S2}(k)\right| \geq \delta_0\right]\right\}, \qquad (4.11)$$

where δ_0 – tolerance for the total change of sensor signal deviations from reference values.

The predicate is calculated for $\forall k \in [k_0, k_1]$. After the k_1 comparisons have been made, a final "detection" is made if a given number of matches are made $k_т \geq k_1\rho_0$, here ρ_0 is a confidence factor that allows to discard false measurements, zero points, ignore errors, random effects and other factorsи.

Therefore, in order to detect the fact of destabilization of the object's operability, it is necessary to rationally control it:

1) form an array of differences $\Delta u_S(k), k = \overline{k_0, k_1}$ for the nominal operating mode of the object and calculate δ_0 and ρ_0;

2) record the obtained values of the tolerance and the confidence factor in the database file and further use to detect destabilization;

3) form an array of current differences $\Delta u_S(k), k = \overline{k_0, k_1}$;

4) calculate the predicate (4.11) for $\forall k \in [k_0, k_1]$ by counting the number of units using a counter k_T;

5) compare the content of the counter $k_т$ with the product of the total number of measurements k_1 on the confidence factor ρ_0 and report one of the possible diagnoses:

a) is workable;

б) is unworkable.

When using one sensor in the rational control object – the angular velocity sensor (Fig. 3.18), it is possible to detect the destabilization that caused the malfunction using a two-digit predicate of the form:

$$z_0 = S_0\left\{\left[\left|\Delta u_{S1}(k)\right| \geq \delta_0\right]\right\};\ \ k = \overline{k_0,k_1};\ \ \rho_0 . \qquad (4.12)$$

When using an excessive angular velocity sensor with a transmission factor k'_{D1}, classification processing of differential digital data from the sensors is possible using a two-digit predicate

$$z_0 = S_2\left\{\left[\left|\Delta u_{S1}(k)\right| + \left|\Delta u'_{S1}(k)\right|\right] \geq \delta_0\right\};\ \ k = \overline{k_0,k_1};\ \ \rho_0 , \qquad (4.13)$$

where $\Delta u'_D(k)$ – deviation of the signal from the redundant angular velocity sensor relative to the discrete signal of the reference model.

Therefore, in order to solve the problem of diagnostic support for the process of detecting destabilization in the rational control object, it is necessary to form the structure at the first stage, and then select the parameters of the reference model that meets the tactical and technical requirements for speed and adequacy of the dynamics of sensor signals. At the second stage, a two-valued predicate equation and its attributes are formed, which provide the necessary classification of difference signals $\Delta u_D(k)$ into the operational and non-operational functional state of the rational control object. The third stage is related to the development and adjustment of destabilization detection programs.

4.2 Search for destabilizing functional elements

When destabilization is detected in the rational control object, the next logical step from the point of view of diagnostics should be taken – to find a functional element that brings destabilization into operability of the object.

The rational control object consists of four functionally necessary elements (Figure 4.2).

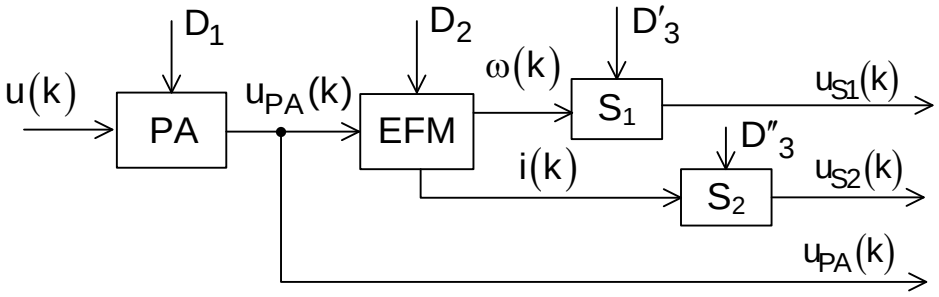

Figure 4.2 – Functional scheme of the rational control object

Each of these functional elements is affected by a corresponding set of destabilizing influences D_1, D_2, D_3' and D_3'' that disrupt the functionality of both the elements and the object as a whole. In the rational control object, it is assumed that destabilization of only one functional element is possible during the diagnostic interval. To search for a destabilizing functional element, it is necessary to form appropriate signs of destabilization of functional elements using available signal measurements $u(k), u_{PA}(k), u_{S1}(k)$ and $u_{S2}(k)$. Appropriate diagnostic models are used to form signs. Thus, for PA it will be diagnostic model (3.39), for D_1 – diagnostic model (3.40), and for D_2 – diagnostic model (3.41). As a result of processing difference signals using predicates:

1) for PA:

$$z_1 = S_2\left\{\left|\Delta u_{PA}(k)\right| \geq \delta_1\right\}; k = \overline{k_1,k_2};\ \rho_1; \tag{4.14}$$

2) for D_1:

$$z_2 = S_2\left\{\left|\Delta u_{S1}(k)\right| \geq \delta_3\right\}; k = \overline{k_1,k_2};\ \rho_3; \tag{4.15}$$

3) for D_2:

$$z_3 = S_2\left\{\left|\Delta u_{S2}(k)\right| \geq \delta_4\right\}; k = \overline{k_1,k_2};\ \rho_4; \tag{4.16}$$

4) for EFM:

$$z_4 = z_2 \wedge z_3 \tag{4.17}$$

we get ambiguous signs of destabilization. The formation of Boolean signs $z_1 \ldots z_4$ is carried out on the interval of discrete values $k \in (k_1, k_2]$. This is not a mandatory condition. Predicate equations can be applied to the array of destabilization detection data, i.e. $\forall k \in (k_0, k_1]$, as well as to other data arrays as long as Boolean signs are used to search for a destabilizing functional element.

Let's compile a table of the effect of destabilization of functional elements (FE) on Boolean signs (Table 4.1).

Table 4.1

FE	Destabilization signs			
	z_1	z_2	z_3	z_4
PA	1	0	0	0
EFM	0	1	1	1
D_1	0	1	0	0
D_2	0	0	1	0

The small size of the table allows to do a visual analysis without using formal tools for analyzing the visibility of rows. So, as a result of the analysis of the Table 4.1, it is possible to determine an obvious structural difference between the lines, which means the possibility of unambiguously detecting the destabilizing functional element using Boolean signs $z_1...z_4$.

The functional scheme of the formation of Boolean signs for the search for a destabilizing functional element in the rational control object is presented in Figure 4.3.

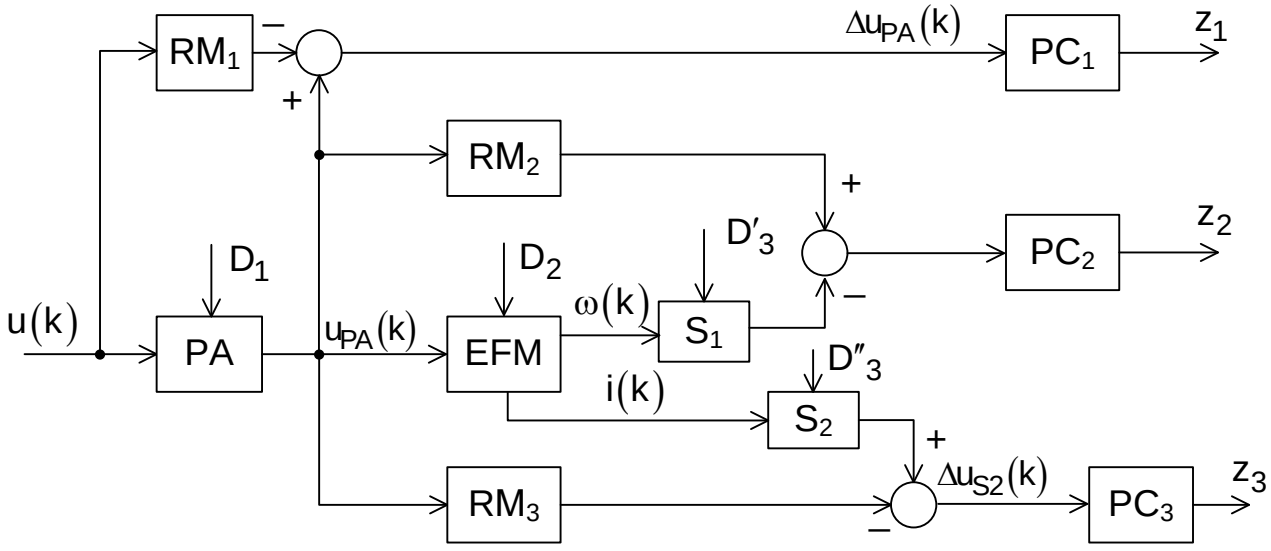

Figure 4.3 – Functional diagram of the formation of Boolean signs

Reference models RM_1, RM_2, RM_3 are used in the diagram. The difference signals are transformed with the help of predicate converters PC1, PC2 and PC3 into signs of destabilization.

With the help of signs of destabilization of functional elements, it is possible to form element search rules (ESR). The simplest rule is to use the principle of direct selection of all signs and comparison with the Table 4.1.

The time-consuming and costly nature of such rules is obvious. The second approach to the formation of ESR is based on the principle of parallel search, which allows obtaining unconditional ESR.

Table 4.1 is used to form unconditional ESR. Each row of this table corresponds to its own set of Boolean variables (binary code), which is different from the others. Therefore, for each functional element, a Boolean function can be written as a conjunction of features containing "1" in a given line, and their negations, if the feature is equal to "0". The set of such Boolean functions will be the structure of an unconditional ESR. If the rational control object is impaired, the i-th Boolean function $\rho_i = 1$ is impaired, this means that destabilization has occurred in the i-th functional element. Let's write the unconditional ESR based on the Table 4.1:

$$\Phi_1[z_i] = \begin{cases} \rho_1 = z_1 \wedge \overline{z_2} \wedge \overline{z_3} \wedge \overline{z_4}; \\ \rho_2 = \overline{z_1} \wedge z_2 \wedge z_3 \wedge z_4; \\ \rho_3 = \overline{z_1} \wedge z_2 \wedge \overline{z_3} \wedge z_4; \\ \rho_4 = \overline{z_1} \wedge \overline{z_2} \wedge z_3 \wedge z_4. \end{cases} \quad (4.18)$$

Since the feature z_4 is a conjunction of the features z_2 and z_3, the structure of the unconditional ESR can be simplified, then

$$\Phi_2[z_i] = \begin{cases} \rho_1 = z_1 \wedge \overline{z_2} \wedge \overline{z_3}; \\ \rho_2 = \overline{z_1} \wedge z_2 \wedge z_3; \\ \rho_3 = \overline{z_1} \wedge z_2 \wedge \overline{z_3}; \\ \rho_4 = \overline{z_1} \wedge \overline{z_2} \wedge z_3. \end{cases} \quad (4.19)$$

Moreover, taking into account that the attribute z_1 takes the value "1" only for the function ρ_1, it is possible to simplify the structure of the ESR to the form

$$\Phi_3[z_i] = \begin{cases} \rho_1 = z_1; \\ \rho_2 = \overline{z_1} \wedge z_2 \wedge z_3; \\ \rho_3 = \overline{z_1} \wedge z_2 \wedge \overline{z_3}; \\ \rho_4 = \overline{z_1} \wedge \overline{z_2} \wedge z_3. \end{cases} \quad (4.20)$$

In the given unconditional ESRs, all signs z_1 , z_2 , z_3 are used, and therefore the principle of parallel search is a variant of the principle of direct enumeration.

The third approach of forming ESR is based on the principle of sequential search [28]. The use of this principle leads to obtaining conditional

ESR. Let's consider the essence of the method in relation to the table. 4.1. Each line of the table reflects the qualitative connection of a specific FE with Boolean signs. Any Boolean attribute z_i divides the entire set of attributes into two subsets. The first includes FEs for which $z_i = 1$, the second includes residual FEs with a sign $z_i = 0$. The use of this circumstance allows to convert the Table 4.1 in the form of graph tree-shaped schemes – dichotomous trees. Dichotomous trees will differ in the lengths of the search paths for the destabilizing FE. It is desirable to choose such a dichotomous tree from all possible ones, so that the lengths of the paths, which depend on the number of Boolean signs $z_i = 1$ used, are approximately the same. In other words, the dichotomous tree was balanced across signs.

The structure of the dichotomous tree depends on the choice of the basic sign z_i. Consider dichotomous trees, choosing as basic signs z_1, z_2 and z_3. A dichotomous tree for the basic PC – z_1 is presented in Figure 4.4.

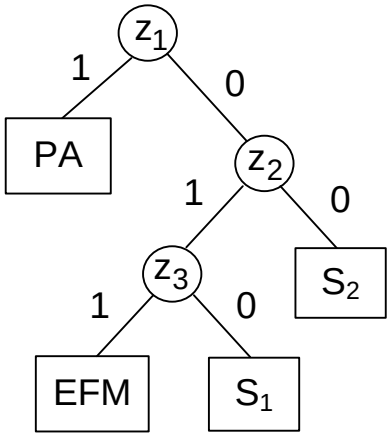

Figure 4.4 – A dichotomous tree for the base sign z_1

So, when computing the sign z_1 according to the predicate (4.14), if a value $z_1 = 1$ is obtained, it means that the destabilizing functional element is PA. If the value of the sign $z_1 = 0$ is zero, the sign z_2 is calculated according to the formula (4.15) and by its value $z_2 = 0$ we find a destabilizing functional element S_2. If $z_2 = 1$, it is necessary to calculate the sign z_3 using the expression (4.16) and if $z_3 = 1$ – it is EFM, but when $z = 0$ – it's S_1. The length of the paths in this dichotomous tree to find the destabilizing functional element are different. Average path length ℓ_a = 2,25. Thus, with the help of this dichotomous tree, the search for a destabilizing functional element in the rational control object is carried out.

Let's choose z_2 as a basic sign. The corresponding dichotomous tree is presented in Figure 4.5.

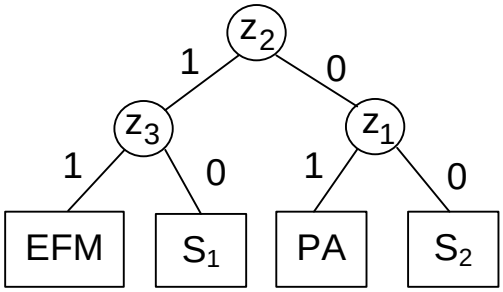

Figure 4.5 – A dichotomous tree for the base sign z_2

The sign z_2 divides the entire set of features into two equal subsets. In the first subset, destabilizing functional elements EFM or S_1 are determined using the sign z_3. In the second subset, the sign z_1 allows to detect inoperable elements PA or S_2. The paths in this dichotomous tree have the same length $\ell = 2$.

A sign z_3 as a base generates such a dichotomous tree (Figure 4.6).

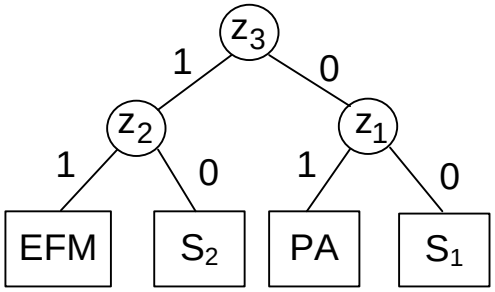

Figure 4.6 – A dichotomous tree for the base sign z_3

The sign z_3, as in the previous dichotomous tree, generates two equal subsets. In the first subset, the sign z_2 allows you to establish which of the two functional elements is inoperable EFM or S_2. In the second subset, the inoperability of functional elements PA or S_1 is determined using the sign z_1. The length of the search paths for an inoperable functional element in this dichotomous tree is the same and $\ell = 2$.

Two of the considered dichotomous trees turned out to be balanced: for basic signs z_2 and z_3. In the presented dichotomous trees, it is possible to reduce computational resources and, accordingly, the time to search for a faulty functional element in the form of feature exclusion z_1. The use of signs z_2 and z_3 allows to unambiguously find any inoperable functional element in

the rational control object. Consider a minimized dichotomous tree for the basic sign z_2 (Figure 4.7).

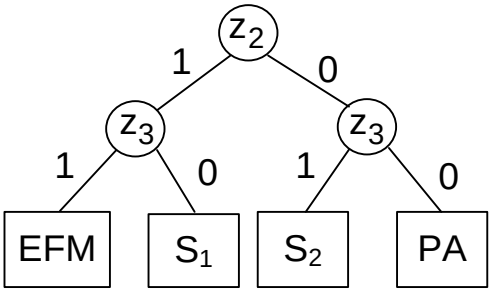

Figure 4.7 – A minimized dichotomous tree

So, by calculating the values of two signs z_2 and z_3, it is possible to unambiguously find an inoperable functional element in the rational control object. A similar minimized dichotomous tree can be formed for a trait z_3.

The search for a destabilizing functional element is carried out after the inoperability of the rational control object is detected. Let's present a dichotomous tree for detecting object inoperability and searching for destabilizing functional elements (Figure 4.8).

Therefore, three Boolean signs z_0, z_2 and z_3 were used to detect and search for destabilization in the rational control object. These signs are calculated using the corresponding two-digit predicate equations on certain samples of discrete values of the corresponding difference signals of the rational control object.

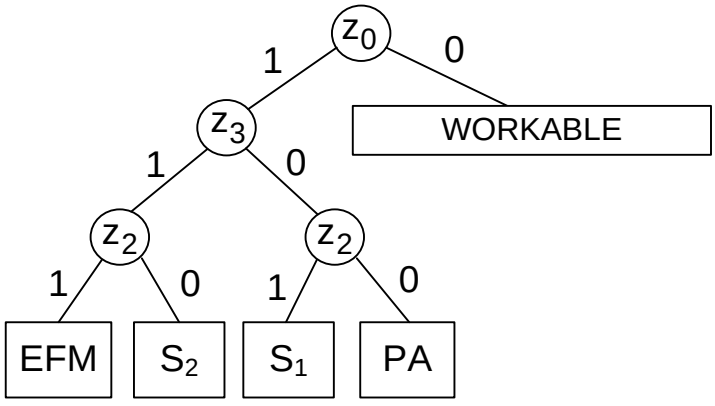

Figure 4.8 – Dichotomous destabilization detection and search tree

After finding a destabilizing functional element, for a full diagnosis it is necessary to detect the reason that caused its malfunction.

4.3 Determination of types of destabilizing influences

Various sets of destabilizing influences act on the functional elements of the rational control object. Among these influences are those of the same type, which lead to a change in one parameter of the functional diagnostic model. Yes, there are actions on PA from the set D_1. Let us consider the specific composition of the types of destabilization of the set D_1:

$$D_1 = \{d_{11}, d_{12}, d_{13}, d_{14}, d_{15}, d_{16}, d_{17}\}, \quad (4.21)$$

where d_{11} – compensated gain reduction;

d_{12} – uncompensated gain reduction;

d_{13} – positive compensated zero drift;

d_{14} – positive uncompensated zero drift;

d_{15} – negative compensated zero drift;

d_{16} – negative uncompensated zero drift;

d_{17} – breaks in signal and power wires.

The types of destabilizing influences d_{11}, d_{12} and d_{17} are characterized by a change in the PA amplification factor and therefore belong to the same type of destabilizing influences. Параметр k_{PA} характеризує цей тип дестабілізуючих впливів.

Types of destabilizing influences d_{13}, d_{14}, d_{15} and d_{16} lead to the drift of the PA zero. The parameter u_0 corresponds to this type of influence. Therefore, the entire set of seven types of destabilizing influences can be represented by two types described by the parameters k_{PA} and u_0. The diagnostic functional model of PA will be described by the following algebraic equation:

$$\Delta u_{PA}(k) = \Delta к_{PA} u(k) + u_0, \quad (4.22)$$

where $\Delta к_{PA} = \Delta \tilde{к}_{PA} - к_{PA}$.

To determine the types, it is necessary to formulate two-valued features with the help of corresponding two-valued predicate equations. Using the assumption about the one-time occurrence of types of destabilization, and it also extends to types, as well as the assumption about the quasi-stationarity of diagnostic signs during diagnosis and restoration of work capacity, we will consider possible constructions of predicate equations.

For the first type of types of destabilizing influences, the diagnostic functional model will be as follows:

$$\Delta u_{PA}(k) = \Delta \kappa_{PA} u(k). \tag{4.23}$$

A direct diagnostic sign $\Delta \kappa_{PA}$ of the type can be defined as

$$\Delta \kappa_{PA} = \frac{\Delta u_{PA}(k)}{u(k)}. \tag{4.24}$$

As follows from the expression (4.24), to determine the estimated value of the direct sign $\Delta \kappa_{PA}$, the operation of division into discrete values of the control signal is used $u(k)$. This signal can take both zero values and small values close to zero. To exclude such situations, we use the assumption of quasi-stationarity of the direct diagnostic sign and obtain the following relation

$$\frac{\Delta u_{PA}(k)}{u(k)} \approx \frac{\Delta u_{PA}(k+1)}{u(k+1)}, \tag{4.25}$$

from which it follows that

$$\Delta u_{PA}(k) u(k+1) \approx \Delta u_{PA}(k+1) u(k). \tag{4.26}$$

Then the two-valued predicate equation for the Boolean sign of the first type will have the following form

$$\begin{aligned} &z_{11} = S_2\left\{\delta_{11} - \left|\Delta u_{PA}(k) u(k+1) - \left|\Delta u_{PA}(k+1) u(k)\right\}\right\}; \\ &k = \overline{k_2, k_3};\ \rho_{11}, \end{aligned} \tag{4.27}$$

where δ_{11} – the tolerance value for the sign of the first type.

For the second type of types of destabilizing influences, the diagnostic functional model will take the following form:

$$\Delta u_{PA}(k) = u_0. \tag{4.28}$$

The condition of quasi-stationarity of the direct sign u_0 allows to form such an argument for the predicate equation:

$$\delta_{12} = \left|\Delta u_{PA}(k+1) - \Delta u_{PA}(k)\right|. \tag{4.29}$$

Then the two-digit sign of the drifts will be determined using the equation:

$$\begin{aligned} &z_{12} = S_2\left\{\delta_{12} - \left|\Delta u_{PA}(k+1) - \Delta u_{PA} u(k)\right|\right\}; \\ &k = \overline{k_2, k_3};\ \rho_{12}, \end{aligned} \tag{4.30}$$

where δ_{12} – the tolerance value for the sign of the second type.

Therefore, z_{11} and z_{12} serve as signs of two types of destabilizing influences from the set D_1. If $z_{11} = 0$ and $z_{12} = 0$, then this is a sign of the presence of a type of destabilization z_{17}.

Five types of destabilizing influences from the set D_2 disrupt the performance of EFM (3.45), The types of destabilizing influences d_{21} and d_{22} associated with a change in the transfer coefficient are of the same type and are characterized by a parameter $k_м$. Types of destabilizing influences d_{23} and d_{24} lead to an increase in the time of the transition process and belong to the second type of EDM destabilization with the corresponding coefficient $k_в$. The third type includes a type of destabilization d_{25} and is characterized by the absence of signs of the first and second types.

A diagnostic functional model in digital form reflecting these types of destabilizing influences is obtained from the general description (3.46), assuming that the matrix $G = A$, then

$$\begin{bmatrix}\Delta x_1(k+1)\\ \Delta x_2(k+1)\end{bmatrix}=\begin{bmatrix}1-\dfrac{k_в T_0}{l} & \dfrac{k_м T_0}{l}\\ 0 & \dfrac{RT_0}{L}\end{bmatrix}\begin{bmatrix}\Delta x_1(k)\\ \Delta x_2(k)\end{bmatrix}+\begin{bmatrix}-\dfrac{\Delta k_в T_0}{l} & \dfrac{\Delta k_м T_0}{l}\\ 0 & 0\end{bmatrix}\begin{bmatrix}\hat{x}_1(k)\\ \hat{x}_2(k)\end{bmatrix};$$
$$\begin{bmatrix}\Delta\hat{x}_1(k_0)\\ \Delta\hat{x}_2(k_0)\end{bmatrix}=\begin{bmatrix}0\\ 0\end{bmatrix}\begin{bmatrix}\Delta u_{S1}(k)\\ \Delta u_{S2}(k)\end{bmatrix}=\begin{bmatrix}k_{S1} & 0\\ 0 & k_{S2}\end{bmatrix}\begin{bmatrix}\Delta x_1(k)\\ \Delta x_2(k)\end{bmatrix}. \quad (4.31)$$

A diagnostic functional model in digital form reflecting these types of destabilizing influences is obtained from the general description (3.46), assuming that the matrix:

$$\begin{bmatrix}\Delta x_1(k+1)\\ \Delta x_2(k+1)\end{bmatrix}=\begin{bmatrix}1-\dfrac{k_в T_0}{l} & \dfrac{k_м T_0}{l}\\ 0 & \dfrac{RT_0}{L}\end{bmatrix}\begin{bmatrix}\Delta x_1(k)\\ \Delta x_2(k)\end{bmatrix}+\begin{bmatrix}-\dfrac{\Delta k_в T_0}{l} & 0\\ 0 & 0\end{bmatrix}\begin{bmatrix}\hat{x}_1(k)\\ \hat{x}_2(k)\end{bmatrix};$$
$$\begin{bmatrix}\Delta\hat{x}_1(k)\\ \Delta\hat{x}_2(k)\end{bmatrix}=\begin{bmatrix}0\\ 0\end{bmatrix}\begin{bmatrix}\Delta u_{S1}(k)\\ \Delta u_{S2}(k)\end{bmatrix}=\begin{bmatrix}\kappa_{S1} & 0\\ 0 & \kappa_{S2}\end{bmatrix}\begin{bmatrix}\Delta x_1(k)\\ \Delta x_2(k)\end{bmatrix}. \quad (4.32)$$

Destabilizing types of influences of the first type do not affect the state variable $x_2(k)$ and, under zero initial conditions $x_2(k_0)=0$, the second component of the state of the diagnostic functional model $\Delta x_2(k)=0$, thus

$$\Delta u_{S1}(k+1)=\left(1-\frac{k_в T_0}{l}\right)\Delta u_{S1}(k)-\frac{k_{S1}\Delta k_в T_0}{l}\hat{x}_1(k). \quad (4.33)$$

To form an argument of a two-valued predicate, let's solve the resulting equation with respect to Δk_B.

$$\Delta k_B = -\frac{\left[\Delta u_{S1}(k+1) - \left(1 - \frac{k_B T_0}{l}\right)\Delta u_{S1}(k)\right]}{k_{S1}\Delta k_B T_0}. \quad (4.34)$$

From the conditions of quasi-stationarity of the diagnostic sign Δk_B, we obtain the following ratio:

$$\Delta k_B = \frac{\left[\Delta u_{S1}(k+2) - \left(1 - \frac{k_B T_0}{l}\right)\Delta u_{S1}(k+1)\right]}{\hat{x}_1(k+1)} \approx \approx \frac{\Delta u_{S1}(k+1) - \left(1 - \frac{k_B T_0}{l}\right)\Delta u_{S1}(k)}{\hat{x}_1(k)}, \quad (4.35)$$

with the help of which we will form such an argument

$$\delta_{21} - \left| \begin{array}{l} \left[\Delta u_{S1}(k+2) - \left(1 - \frac{k_B T_0}{l}\right)\Delta u_{S1}(k+1)\right]\hat{x}_1(k) - \\ -\left[\Delta u_{S1}(k+1) - \left(1 - \frac{k_B T_0}{l}\right)\Delta u_{S1}(k)\right]\hat{x}_1(k+1) \end{array} \right|. \quad (4.36)$$

The two-valued predicate equation for the first type will be as follows:

$$z_{21} = S_2\left\{\delta_{21} - \left| \begin{array}{l} \left[\Delta u_{S1}(k+2) - a\Delta u_{S1}(k+1)\right]\Delta\hat{x}_1(k) - \\ -\left[\Delta u_{S1}(k+1) - a\Delta u_{S1}(k)\right]\Delta\hat{x}_1(k+1) \end{array} \right|\right\}; \quad (4.37)$$

$$k = \overline{k_3, k_4};\ \rho_{21},$$

where $a = \left(1 - \frac{k_B T_0}{l}\right)$.

The diagnostic functional model for the second type of destabilizing influences will be as follows:

$$\Delta u_{S1}(k+1) = \left(1 - \frac{k_B T_0}{l}\right)\Delta u_{S1}(k) + \frac{k_{S1} k_M T_0}{l}\hat{x}_2(k) \frac{k_{S1}\Delta k_M T_0}{l}\hat{x}_2(k). \quad (4.38)$$

Solving this equation with respect to Δk_M, we will obtain

$$k_м = \frac{\left[\Delta u_{S1}(k+1) - \left(1 - \frac{k_B T_0}{I}\right)\Delta u_{S1}(k) - \frac{k_{S1} k_M T_0}{I \kappa_{S2}} \Delta u_{S2}(k)\right] I}{k_{S1} T_0 \hat{x}_2(k)}. \quad (4.39)$$

Then the two-valued predicate equation will be the following

$$z_{22} = S_2\left\{\delta_{22} - \left\|\left[\Delta u_{S1}(k+2) - a\Delta u_{S1}(k+1) - b\Delta u_{S2}(k+1)\right]\hat{x}_2(k) - \right.\right.$$
$$\left.\left. - \left[\Delta u_{S1}(k+1) - a\Delta u_{S1}(k) - b\Delta u_{S2}(k)\right]\Delta\hat{x}_2(k+1)\right\|\right\}; \quad (4.40)$$
$$k = \overline{k_3, k_4};\ \rho_{22},$$

where $b = \frac{k_{S1} k_M T_0}{J k_{D2}}$.

A sign of the third type will be a condition

$$z_{23} = \overline{z}_{21} \wedge \overline{z}_{22}. \quad (4.41)$$

Thus, the obtained Boolean signs z_{21} and z_{22} allow to unambiguously detect each of the three types of destabilization of EFM operability.

A subset D'_3 of types of destabilization acts on the angular velocity sensor S_1.

Let's form this subset from the set D_3 (3.47). Then

$$D'_3 = \{d_{31}, d_{32}, d_{33}, d_{34}, d_{39}\}. \quad (4.42)$$

As described earlier (section 3.4), types of destabilization d_{31} and d_{32} lead to a decrease in the transmission coefficient k_{S1}, and the types of destabilization d_{33} and d_{34} are of the same type, as they are related to zero drift u_{01}. The diagnostic functional model for the types of destabilization of the first sensor can be represented by the following equation:

$$\Delta u_{S1}(k) = \Delta k_{S1} \hat{x}_1(k) + u_{01}. \quad (4.43)$$

The assumption that types of destabilization are unique allows us to provide a diagnostic functional model of each type of destabilization. Thus, for the first type of destabilization

$$\Delta u_{S1}(k) = \Delta k_{S1} \hat{x}_1(k). \quad (4.44)$$

Transfer factor deviation

$$\Delta k_{S1} = \frac{\Delta u_{S1}(k)}{\hat{x}_1(k)}. \quad (4.45)$$

On the interval of diagnosis and recovery, by assumption, Δk_{S1} is quasi-stationary, therefore the following relation is valid:

$$\frac{\Delta u_{S1}(k+1)}{\hat{x}_1(k+1)} \approx \frac{\Delta u_{S1}(k)}{\hat{x}_1(k)}, \tag{4.46}$$

from which we can form an argument for a two-valued predicate equation in the following form:

$$\delta_{31} = \left|\Delta u_{S1}(k+1)\hat{x}_1(k) - \Delta u_{S1}(k)\hat{x}_1(k+1)\right|. \tag{4.47}$$

Then

$$\begin{aligned} z_{31} = S_2\left\{\delta_{31} - \left|\Delta u_{S1}(k+1)\hat{x}_1(k) - \Delta u_{S1}(k)\hat{x}_1(k+1)\right|\right\}; \\ k = \overline{k_3,k_4};\ \rho_{31}. \end{aligned} \tag{4.48}$$

When $z_{31} = 1$ we get a conclusion about the first type of destabilization, and for $z_{31} = 0$ – about its absence.

The diagnostic functional model for the second type of destabilization associated with sensor zero drift will take the following form:

$$\Delta u_{S1}(k) = u_{01}. \tag{4.49}$$

The quasispace of the sign u_{01} allows to form such a condition

$$\Delta u_{S1}(k+1) - \Delta u_{S1}(k) \approx 0, \tag{4.50}$$

with the help of which the structure of the two-valued predicate equation will be as follows:

$$z_{32} = S_2\left\{\delta_{32} - \left|\Delta u_{S1}(k+1) - \Delta u_{S1}(k)\right|\right\};\ k = \overline{k_3,k_4};\ \rho_{32}. \tag{4.51}$$

This equation makes it possible to unambiguously detect the sensor destabilization caused by zero drift.

At $z_{31} = 0$ and $z_{32} = 0$ in sensor S_1, the type of destabilizing effect is unknown.

Types of destabilization from a subset $D_3'' \subset D_3$ act on the current sensor S_2 (3.47). The subset D_3'' consists of five types of destabilizing influences, namely:

$$D_3'' = \{d_{35}, d_{36}, d_{37}, d_{38}, d_{39}\}. \tag{4.52}$$

The same types of influences d_{35} and d_{36} are characterized by a decrease in the transmission coefficient k_{S2}, types of destabilizing influences d_{37} and d_{38} are described by the drift parameter u_{02}, and the third type d_{39} is associated with the absence of the listed specific types of destabilization in the sensors S_1 and S_2.

The diagnostic functional model for two types of destabilization of the second sensor can be obtained (3.48) for discrete arguments in the following form:

$$\Delta u_{S2}(k) = \Delta k_{S2}\hat{x}_2(k) + u_{02}. \quad (4.53)$$

The first type of destabilization of the second sensor is described by the following equation:

$$\Delta u_{S2}(k) = \Delta k_{S2}\hat{x}_2(k), \quad (4.54)$$

from which

$$\Delta k_{S2} = \frac{\Delta u_{S2}(k)}{\hat{x}_2(k)}. \quad (4.55)$$

Due to the quasi-stationarity of the diagnostic sign Δk_{S2}, we have that

$$\frac{\Delta u_{S2}(k+1)}{\hat{x}_2(k+1)} = \frac{\Delta u_{S2}(k)}{\hat{x}_2(k)}, \quad (4.56)$$

then the two-digit predicate equation for detecting the presence of the first type of destabilization in sensor S_2 will be as follows:

$$z_{33} = S_2\left\{\delta_{33} - \left|\Delta u_{S2}(k+1)\hat{x}_2(k) - \Delta u_{S2}(k)\hat{x}_2(k+1)\right|\right\};\ k = \overline{k_3,k_4};\ \rho_{33}. \quad (4.57)$$

For the second type of destabilization, the diagnostic functional model will be described by the following equation:

$$\Delta u_{S2}(k) = u_{02}, \quad (4.58)$$

from which it follows that

$$\Delta u_{S2}(k+1) - \Delta u_{S2}(k) \approx 0. \quad (4.59)$$

Then, to detect the presence of the second type of destabilization in S_2, it is necessary to process the discrete difference signal $\Delta u_{S2}(k)$ according to the equation

$$z_{34} = S_2\left\{\delta_{34} - \left|\Delta u_{S2}(k+1) - \Delta u_{S2}(k)\right|\right\};\ k = \overline{k_3,k_4};\ \rho_{34}. \quad (4.60)$$

At $z_{34} = 1$, the presence of the second type of destabilization in S_2 is confirmed, and at $z_{34} = 0$, its absence.

The obtained Boolean signs of destabilization types allow to supplement the dichotomous tree (see Figure 4.8) with the process of diagnosing types of destabilization (Figure 4.9).

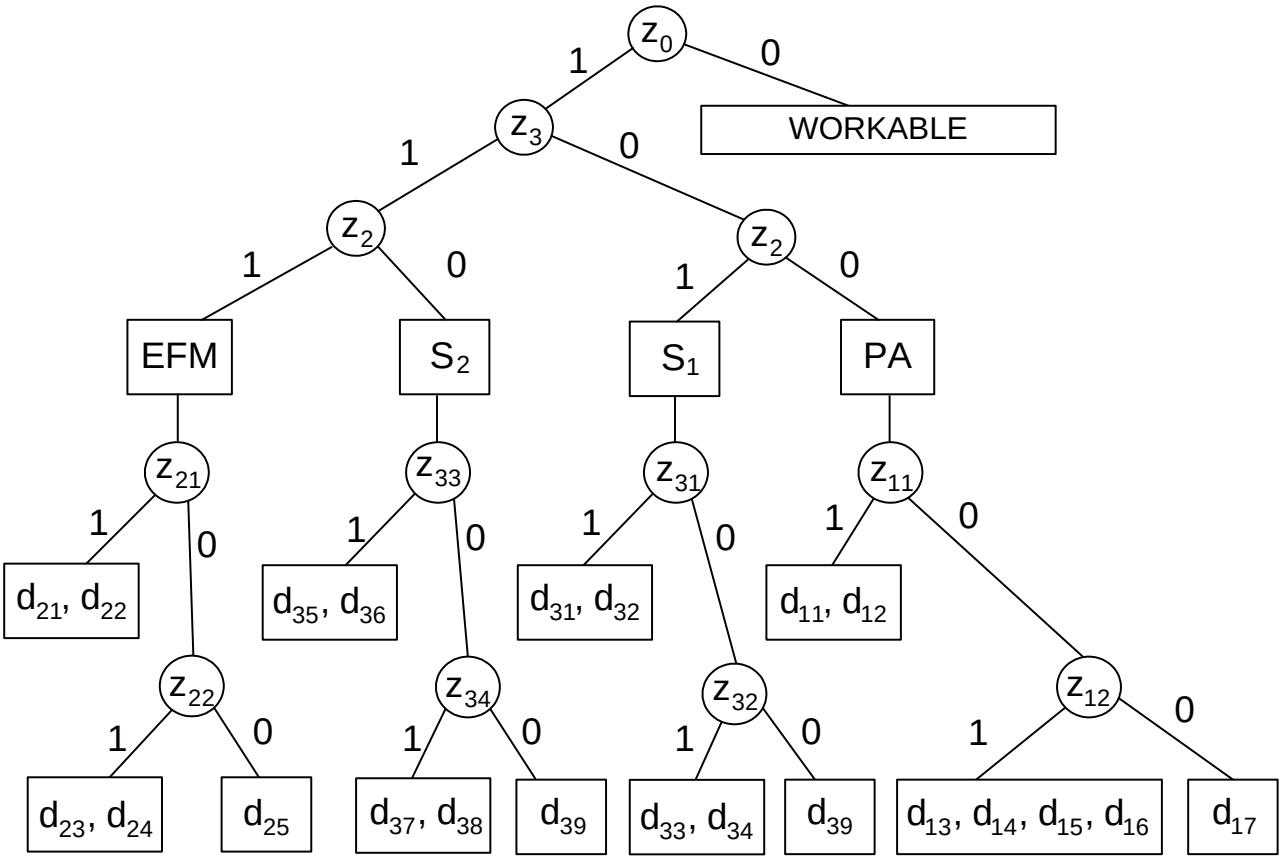

Figure 4.9 – Dichotomous tree of setting types of destabilization

The presented dichotomous tree makes it possible to diagnose the rational control object with depth to the types of destabilization. An obvious implementation in a tree of the hierarchical principle of sequential removal of uncertainty in an inoperable rational control object. The use of the Boolean attribute at the first level allows you to detect an inoperable state. With the help of signs z_3 and z_2 on the second level there is an inoperable functional element of the object. The use of Boolean signs of the third level makes it possible to detect the type of destabilization, which caused a malfunction of the functional element of the rational control object.

Determination of a specific type of destabilizing influence is carried out at the fourth level of diagnosis using appropriate Boolean signs.

4.4 Determination of kinds of destabilization

In each type of destabilization, there can usually be several kinds. For a complete diagnosis of a functional rational control object, it is necessary to

determine the specific cause – the kind of destabilization of the functional element. Let's consider for each of the functional elements the procedure for determining its kinds of destabilization.

In PA, kinds of destabilization d_{11} and d_{12} are characterized by a decrease in the amplification factor and a diagnostic functional model

$$\Delta u_{PA}(k) = \Delta k_{PA} u(k) \tag{4.61}$$

displays the connection of signals with the diagnostic parameter Δk_{PA}. In order to find out what kind of destabilization has currently occurred in the PA, it is necessary to obtain a numerical estimate of the parameter Δk_{PA}. Since measurement errors and interference are possible when measuring signals $\Delta u_{PA}(k)$ and $u(k)$, and the numerical value k_{PA} used in calculations is obtained as a result of linearization, we use known methods of identifying diagnostic parameters to obtain a numerical estimate Δk_{PA} [28]. As a result of measuring m+1 discrete signal values, we get the following vector equation:

$$\begin{bmatrix} \Delta u_{PA}(k) \\ \Delta u_{PA}(k+1) \\ . \\ . \\ . \\ \Delta u_{PA}(k+m) \end{bmatrix} = \Delta k_{PA} \begin{bmatrix} u(k) \\ u(k+1) \\ . \\ . \\ . \\ u(k+m) \end{bmatrix} \text{ або } v(k) = \Delta k_{PA} s(k). \tag{4.62}$$

According to the method of least squares, during batch processing of signal values, we will get the following algorithm for numerical evaluation of the sign Δk_{PA}:

$$\Delta \hat{k}_{PA} = \left[s^T(k) \right]^{-1} s^T(k) v(k), \tag{4.63}$$

where **т** – vector transpose symbol.

The estimate obtained with the help of the algorithm will be optimal according to the quadratic criterion of the discrepancy of the equation (4.61).

The recurrent least squares method allows you to obtain the current values of the numerical evaluation of the sign Δk_{PA} using the following algorithm:

$$\Delta \hat{k}_{PA}(k+1) = \Delta \hat{k}_{PA}(k) + \gamma(k) \left[\Delta u_{PA}(k+1) - \Delta \hat{k}_{PA}(k) u(k) \right], \tag{4.64}$$

where $\gamma(k)$ – algorithm convergence correction vector.

Simpler algorithms for obtaining numerical values of the estimate can be obtained using ratios

$$\frac{\Delta u_{PA}(k+1)}{u(k+1)} = \frac{\Delta u_{PA}(k)}{u(k)}, \tag{4.65}$$

from which it follows that

$$\Delta\hat{k}_{PA} = \frac{\Delta u_{PA}(k+1)u(k)}{u(k+1)\Delta u_{PA}(k)}. \tag{4.66}$$

This algorithm for pairwise processing of discrete measurements can be extended to the entire measurement interval.

Good grades can also be obtained using the arithmetic mean algorithm

$$\Delta\hat{k}_{PA} = \frac{1}{m}\sum_{k=1}^{m}\frac{\Delta u_{PA}(k)}{u(k)} \tag{4.67}$$

in the mode of batch processing of discrete values of signal measurements.

After obtaining a numerical evaluation of diagnostic sign $\Delta\hat{k}_{PA}$, an argument for a two-digit predicate equation is formed. Using the limit value of the diagnostic sign $\Delta\bar{k}_{PA}$, which separates the types of destabilization d_{11} and d_{12}, it is possible to form two expressions for the predicate equation

$$\Delta\bar{k}_{PA} - \Delta\hat{k}_{PA} \text{ and } \Delta\hat{k}_{PA} - \Delta\bar{k}_{PA}.$$

Then to determine the kind d_{11}

$$z_{111} = S_2\left\{\Delta\bar{k}_{PA} - \Delta\hat{k}_{PA}\right\}, \tag{4.68}$$

and to determine the kind d_{12}

$$z_{122} = S_2\left\{\Delta\hat{k}_{PA} - \Delta\bar{k}_{PA}\right\}. \tag{4.69}$$

Since there are two kinds of destabilization, one two-valued predicate equation can be used, which gives two values of the Boolean attribute, which is sufficient to determine d_{11} or d_{12}.

For kinds of destabilization d_{13}, d_{14}, d_{15} and d_{16}, the diagnostic functional model of PP will be as follows:

$$\Delta u_{PA}(k) = u_0. \tag{4.70}$$

It is possible to determine the types of destabilization only with the help of a numerical estimate of drift $\hat{u}_0$ and the limit value of drift $\bar{u}_0$, which separates two kinds of destabilization. The numerical value of the drift estimate can be obtained using the arithmetic mean algorithm

$$\hat{u}_0 = \frac{1}{m}\sum_{k=1}^{m}\Delta u_{PA}(k) \qquad (4.71)$$

in the mode of batch processing of discrete values of the difference signal $\Delta u_{PA}(k)$.

The obtained numerical value of the drift estimate $\hat{u}_0$ and the limiting value of the drift $\bar{u}_0$ make it possible to form the arguments of the corresponding two-valued predicate equations. Yes, for kinds of uncompensated zero drift d_{14} and d_{16}: $\bar{u}_0 - |\hat{u}_0|$, and for kinds of compensated drift d_{13} and d_{15}: $\hat{u}_0 > \delta_0$.

Then the two-digit predicate equations for the Boolean signs of kinds determination d_{14} and d_{16}

$$z_{121} = S_2\{\bar{u}_0 - |\hat{u}_0|\}, \qquad (4.72)$$

and for kinds d_{13} and d_{15}

$$z_{122} = S_2\{\hat{u}_0 > \delta_0\}, \qquad (4.73)$$

where δ_0 is the threshold value.

The kind of destabilizing influence d_{17} is determined under the condition that the Boolean sign $z_{12} = 0$.

Three types of destabilization are defined in EFM. To determine the kinds of destabilizing influences d_{23} and d_{24} of the first type, the numerical value of the diagnostic parameter Δk_B is required. The numerical value of the estimate $\Delta\hat{k}_B$ can be obtained using the discrete signal processing of equation

$$\Delta u_{S1}(k+1) - \left(1 - \frac{k_в T_0}{J}\right)\Delta u_{S1}(k) = -\Delta k_в \frac{\kappa_{S1} T_0}{J}\hat{x}_1(k). \qquad (4.74)$$

If we use *m* discrete signal values, then we will get *m* equations. Denoting the vector array on the left side of the equation with a symbol $p(k)$, and the array on the right side as $q(k)$, then

$$p(k) = -\Delta k_B q(k). \qquad (4.75)$$

For batch processing of the obtained arrays, the method of least squares may be applyed according to which

$$\Delta\hat{k}_B = \left[q^T(k)q(k)\right]^{-1} q^T(k)p(k). \qquad (4.76)$$

The current value of the numerical evaluation of the diagnostic sign $\Delta\hat{k}_B(k)$ can be obtained using a recurrent algorithm

$$\Delta\hat{k}_B(k+1) = \Delta\hat{k}_B(k) + \gamma(k)\left[p_1(k) + \Delta\hat{k}_B(k)q_1(k)\right], \quad (4.77)$$

where $p_1(k)$ i $q_1(k)$ are the first components of the vectors $p(k)$ and $q(k)$.

To obtain an arithmetic mean estimate of a diagnostic sign Δk_B, the formula for obtaining discrete estimates should be used

$$\Delta k_B(k+1) = \frac{\left[\Delta u_{S1}(k+1) - a\Delta u_{S1}(k)\right]J}{\hat{u}_{S1}(k)T_0}, \quad (4.78)$$

where $a = \left(1 - \frac{k_B T_0}{J}\right)$; $\hat{u}_{S1}(k) = k_{S1}\hat{x}(k)$.

Then the arithmetic mean score

$$\Delta\hat{k}_B = \frac{1}{m}\sum_{k=1}^{m}\Delta k_B(k+1). \quad (4.79)$$

Knowing the limit value $\Delta\bar{k}_B$, which separates the kinds of destabilization d_{23} and d_{24}, and the current assessment of the diagnostic feature $\Delta\hat{k}_B$ allows to form two-valued predicate equations for the corresponding Boolean features.

$$z_{223} = S_2\left\{\Delta\bar{k}_B - \Delta\hat{k}_B\right\};\ z_{224} = S_2\left\{\Delta\hat{k}_B - \Delta\bar{k}_B\right\}. \quad (4.80)$$

To determine the kinds of destabilization d_{21} and d_{22} of the first type, numerical estimates of the change in the transmission coefficient Δk_M are necessary. These estimates can be obtained using the following expression

$$\Delta u_{S1}(k+1) - a\Delta u_{S1}(k) - b\Delta u_{S2}(k) = c\Delta k_M\hat{u}_{S2}(k), \quad (4.81)$$

where $a = \left(1 - \frac{k_B T_0}{J}\right)$; $b = \frac{k_{S1}k_M T_0}{Jk_{S2}}$; $c = \frac{k_{S1}T_0}{k_{S2}J}$;

$\hat{u}_{S2}(k)$ is an output signal from sensor S_2 of the reference model.

When using m signal values, we get m equations. If we mark the vector array of the left part of the equation as $g(k)$, and the array of the right part as $h(k)$, then we get the vector equation

$$g(k) = \Delta k_M h(k). \quad (4.82)$$

The method of least squares allows to get an estimate of a diagnostic sign with the help of such an expression

$$\Delta\hat{k}_M = \left[h^T(k)h(k)\right]^{-1}h^T(k)g(k) \qquad (4.83)$$

or using a recursive algorithm

$$\Delta k_M(k+1) = \Delta k_M(k) + \gamma(k)\left[g_1(k) - \Delta k_M h_1(k)\right], \qquad (4.84)$$

where $g_k(k)$ and $h_k(k)$ – stepwise components of vectors $g(k)$ and $h(k)$.

In order to obtain an arithmetic mean estimate of the diagnostic sign Δk_M, its values $\Delta k_M(k+1)$ are calculated based on equation (4.74); then

$$\Delta\hat{k}_M = \frac{1}{m}\sum_{k=1}^{m}\Delta k_M(k+1). \qquad (4.85)$$

The threshold value of the diagnostic sign $\Delta\bar{k}_M$ divides the kinds of destabilization. The obtained evaluation of the sign $\Delta\hat{k}_M$ can be attributed to the kinds d_{21} or d_{22} using Boolean signs:

$$z_{211} = S_2\left\{\Delta\bar{k}_M - \Delta\hat{k}_M\right\}; \quad z_{212} = S_2\left\{\Delta\hat{k}_M - \Delta\bar{k}_M\right\}. \qquad (4.86)$$

An unknown kind of destabilization d_{25} is detected when $z_{211} = z_{212} = z_{223} = z_{224} = 0$.

The failure of the sensor S_1 is caused by a set of destabilizing influences D'_3 (4.42). The first type of these effects is related to the reduction of the transfer coefficient k_{S1} and is described by the equation

$$\Delta u_{S1}(k) = \Delta k_{S1}\hat{x}_1(k). \qquad (4.87)$$

To recognize the kinds of destabilization d_{31} and d_{32}, the numerical value of the diagnostic sign of this type is required, i.e Δk_{S1}. A sign estimate can be obtained by processing arrays of available digital signals using appropriate identification methods. Thus, as a result of obtaining *m+1* discrete signal values, the following equation can be written

$$\begin{bmatrix}\Delta u_{S1}(k)\\ \Delta u_{S1}(k+1)\\ .\\ .\\ .\\ \Delta u_{S1}(k+m)\end{bmatrix} = \Delta k_{S1}\begin{bmatrix}\hat{x}_1(k)\\ \hat{x}_1(k+1)\\ .\\ .\\ .\\ \hat{x}_1(k+m)\end{bmatrix} \quad \text{або} \quad a(k) = \Delta k_{S1}b(k). \qquad (4.88)$$

When processing these arrays using the method of least squares, we get

$$\Delta\hat{k}_{S1} = \left[b^T(k)b(k)\right]^{-1}b^T(k)a(k). \qquad (4.89)$$

The recurrent least squares method allows you to obtain step-by-step interconnected estimates with the help of such an algorithm

$$\Delta\hat{k}_{S1}(k+1) = \Delta\hat{k}_{S1}(k) + \gamma(k)\left[\Delta u_{S1}(k+1) - \Delta\hat{k}_{S1}(k)\hat{x}_1(k)\right]. \quad (4.90)$$

Stepwise unrelated estimates $\Delta k_{S1}(k)$ can be obtained by distribution $\Delta u_{S1}(k)$ to $\hat{x}_1(k)$, and then the arithmetic mean score will be calculated as follows:

$$\Delta\hat{k}_{S1} = \frac{1}{m}\sum_{k=1}^{m}\Delta k_{S1}(k). \quad (4.91)$$

Kinds of destabilization d_{31} and d_{32} can be recognized with the help of the following Boolean signs:

$$z_{311} = S_2\left\{\Delta\bar{k}_{S1} - \Delta\hat{k}_{S1}\right\}; \quad z_{312} = S_2\left\{\Delta\hat{k}_{S1} - \bar{k}_{S1}\right\}, \quad (4.92)$$

where $\bar{k}_{S1}$ – limit value.

The second type of destabilization includes kinds of destabilization d_{33} and d_{34} and is described by equation

$$\Delta u_{S1}(k) = u_{01}. \quad (4.93)$$

The simplest numerical assessment of a diagnostic sign u_{01} can be obtained as the arithmetic mean value of the difference signal

$$\hat{u}_{01} = \frac{1}{m}\sum_{k=1}^{m}\Delta u_{S1}(k). \quad (4.94)$$

To recognize the non-recoverable value of the drift of zero, i.e. kind d_{34}, one can use the Boolean sign

$$z_{321} = S_2\left\{\hat{u}_{01} - \bar{u}_{01}\right\}, \quad (4.95)$$

where $\bar{u}_{01}$ – limit value.

For the recoverable species d_{33}, knowledge of the sign of the drift using the Boolean sign is required

$$z_{322} = S_2\left\{\hat{u}_{01} > \delta_{01}\right\}, \quad (4.96)$$

where δ_{01} – limit value.

Destabilization kind d_{39} is detected when no destabilization types are set d_{31}, d_{32}, d_{33} and d_{34}.

Kinds of destabilization from the set (4.52) characterize the failure of the S_2 sensor. The first kind of destabilization is described by the equation

$$\Delta u_{S2}(k) = \Delta k_{S2}\hat{x}_2(k), \tag{4.97}$$

with the help of which you can get an estimate of the diagnostic sign Δk_{S2} by processing m+1 discrete values of the equation signals with a vector representation of data arrays

$$\begin{bmatrix} \Delta u_{S2}(k) \\ \Delta u_{S2}(k+1) \\ . \\ . \\ . \\ \Delta u_{S2}(k+m) \end{bmatrix} = \Delta\kappa_{S2} \begin{bmatrix} \hat{x}_2(k) \\ \hat{x}_2(k+1) \\ . \\ . \\ . \\ \hat{x}_2(k+m) \end{bmatrix} \quad \text{or} \quad c(k) = \Delta k_{S2} d(k). \tag{4.98}$$

During batch processing of arrays by the method of least squares

$$\Delta\hat{k}_{S2} = \left[d^T(k)d(k)\right]^{-1} d^T(k)c(k). \tag{4.99}$$

In step-by-step processing

$$\Delta\hat{k}_{S2}(k+1) = \Delta\hat{k}_{S2}(k) + \gamma(k)\left[\Delta u_{S2}(k+1) - \Delta\hat{k}_{S2}\hat{x}_2(k)\right]. \tag{4.100}$$

Arithmetic average score

$$\Delta\hat{k}_{S2} = \frac{1}{m}\sum_{k=1}^{m}\frac{\Delta u_{S2}(k)}{\hat{x}_2(k)}. \tag{4.101}$$

Types of destabilization d_{35} and d_{36} are recognized with the help of the following Boolean signs

$$z_{331} = S_2\left\{\Delta\bar{k}_{S2} - \Delta\hat{k}_{S2}\right\}; \quad z_{332} = S_2\left\{\Delta\hat{k}_{S2} - \Delta\bar{k}_{S2}\right\}. \tag{4.102}$$

Zero drift is included in the second type of destabilization and is described by equations

$$\Delta u_{S2}(k) = u_{02}, \tag{4.103}$$

from which the arithmetic average score of the diagnostic sign

$$\hat{u}_{02} = \frac{1}{m}\sum_{k=1}^{m}\Delta u_{S2}(k). \tag{4.104}$$

The Boolean feature z_{341} allows to determine the types of d_{37} and d_{38}.

$$z_{341} = S_2\left\{\hat{u}_{02} - \bar{u}_{02}\right\}. \tag{4.105}$$

The sign of the zero drift is set using a Boolean sign

$$z_{342} = S_2\left\{\hat{u}_{02} > \delta_{02}\right\}. \tag{4.106}$$

Kind of destabilization d_{39} is detected when $z_{34} = 0$.

The obtained Boolean signs of the types of destabilization of the functional elements of the rational control object make it possible to supplement the dichotomous tree (see Figure 4.9) and obtain a dichotomous tree of the complete diagnosis of the object (Figure 4.10).

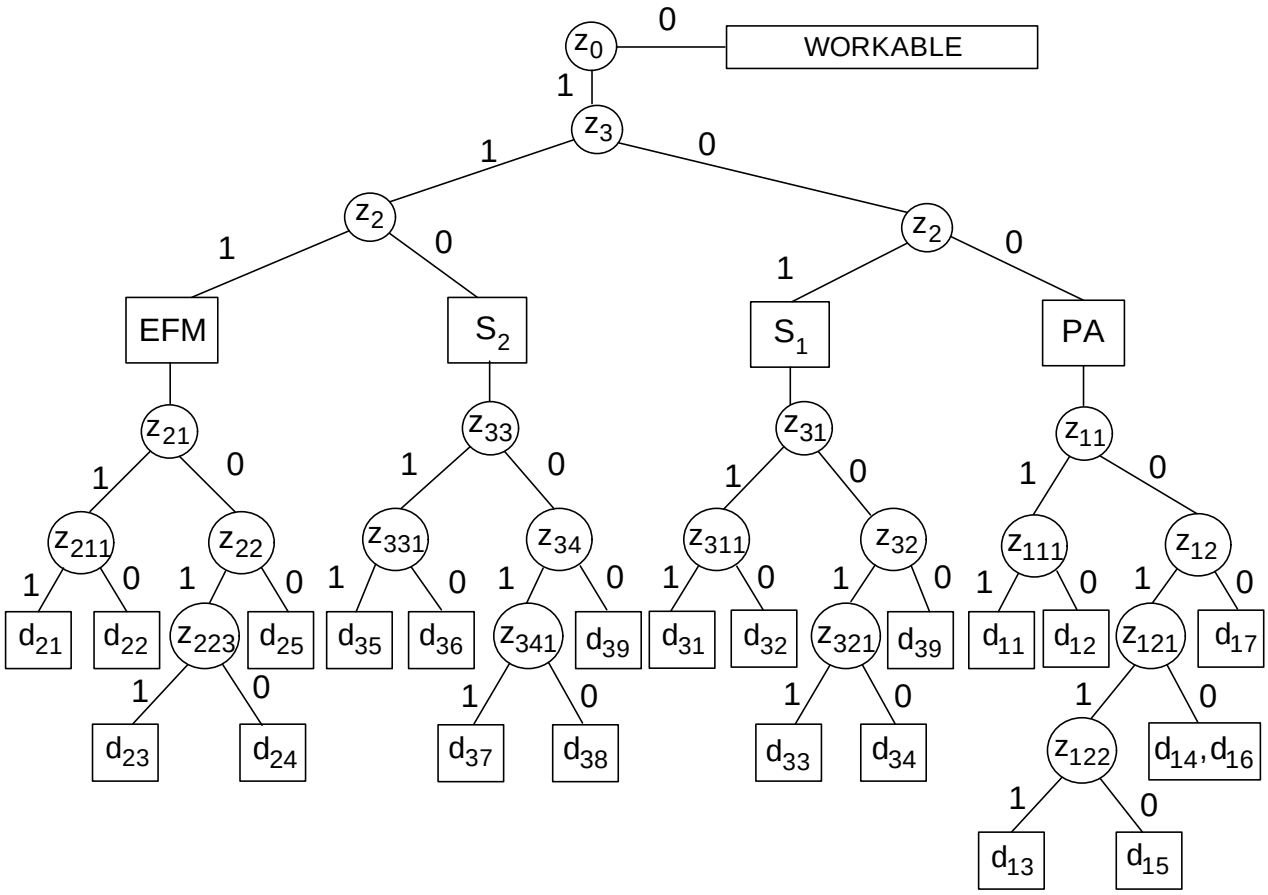

Figure 4.10 – Dichotomous tree of complete diagnosis of rational control object

The formed dichotomous tree makes it possible to determine each of the twenty one types of destabilizing influences in the rational control object in the form of conditional transitions along balanced branches with the help of twenty Boolean signs.

The knowledge of specific types of destabilizing influences obtained as a result of the diagnosis allows to proceed to the next procedure of rational control – restoration of the functionality of the rational control object.

Chapter V REHABILITATION SUPPORT OF THE RATIONAL CONTROL OBJECT

Bene dignoscitur, bene curatur. –
Well recognized, well treated
Winged Latin expression

The word *rehabilitation* comes from the late Latin *rehabilitatio*, which means restoration. Rehabilitation support includes instrumental means and procedures for countering types of destabilizing influences in order to restore the functionality of the rational control object.

5.1 Restoration of the operability of the power amplifier

The power amplifier is a part of the object of rational control and its destabilizing influences from the set D_1 cause malfunctions of both the PA itself and the rational control object. As a result of deep diagnostic procedures (see Figure 4.10), it is possible to diagnose all types of destabilizing influences. The task of restoring the operability of the PA consists in choosing such means and procedures that would allow neutralizing the causes of destabilization so as to quickly transition from an inoperable state to an operational state.

The following recovery tools can be used to restore the PA. The first is the use of an additional signal $u_A(k)$ to the input control sugnal $u(k)$. The value of the signal $u_A(k)$ depends on the value of the estimated value of the corresponding diagnostic feature. This method of restoration is called signal tuning. With the help of signal tuning, you can parry such types of PA destabilization as d_{11}, d_{13} and d_{15}, associated with a compensated change in diagnostic parameters Δk_{PA} and u_0.

The second means of recovery is associated with the use coefficient k_{PA} adjusted by a signal $u_P(k)$, which is formed based on the evaluation of the diagnostic sign $\Delta\hat{k}_{PA}$. This method of recovery is called parametric tuning. So, with the help of parametric tuning, it is possible to neutralize such kinds of destabilization as d_{11}, d_{13} and d_{15}.

The third means of recovery consists in the use of a backup PA based on the results of the diagnosis, when it is impossible to use both signal and

parametric adjustments to neutralize the types of destabilization. This means of recovery is called hardware reconfiguration. Reconfiguration of equipment is applicable for kinds of destabilization d_{12}, d_{14}, d_{16} and d_{17}.

The distribution of means of recovery by types of destabilization and a quantitative assessment of the recovery of PA can be presented using the following Table 5.1.

Table 5.1

d_{ij}	Recovery means			Level
	ν_1	ν_2	ν_3	
d_{11}	1	1		2
d_{12}			1	1
d_{13}	1	1		2
d_{14}			1	1
d_{15}	1	1		2
d_{16}			1	1
d_{17}			1	1
Rank	3	3	4	

In the table: ν_1 – means of signal tuning; ν_2 – means of parametric adjustment and ν_3 – reconfiguration of equipment. The symbol "1" means that the kind of destabilization can be parried by the tool ν_i, $i=\overline{1,3}$. The number of "1"s in the column characterizes the rank of recovery tools. The number of "1" in the row characterizes the level of recovery of PA when a kind of destabilization occurs d_{ij}. The higher the level, the more means can be used to neutralize the kind of destabilization d_{ij}.

The selection of the recovery tool for the current diagnosis is carried out by analyzing the ranks of the recovery tools in order to find the minimum one [33]. A recovery tool with a minimum rank and chosen to counter the current kind of destabilization d_{ij}. Kinds of destabilization d_{11}, d_{13} and d_{15} can be parried by a tool ν_1 – signal tuning, as by a tool ν_2 – parametric adjustment. Let us consider in more detail the features of signal tuning.

Therefore, when receiving a diagnosis that the performance of the PA is impaired due to a kind of destabilization d_{11}, it is necessary to generate an additional signal $u_A(k)$. An additional signal is formed on the basis of the assessment $\Delta\hat{k}_{PA}$ obtained as a result of diagnostics using the equation

$$u_A(k)=\Delta\hat{k}_{PA}\,u_C(k)=\Delta u_{PA}(k). \qquad (5.1)$$

Figure 5.1 presents the functional scheme of signal compensation of the destabilization kind d_{11}.

An additional signal $u_A(k)=-\hat{u}_0$ is generated when the PA malfunctions caused by the kind of destabilization d_{13}. This signal is numerically equal to

the difference signal $-\Delta u_{PA}(k)$.

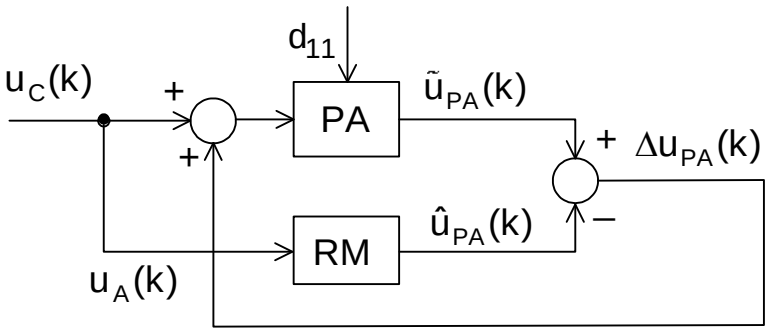

Figure 5.1 – Functional scheme of signal compensation of the kind of destabilization d_{11}

The functional scheme of signal adjustment of PA with a positive zero drift is shown in Figure 5.2.

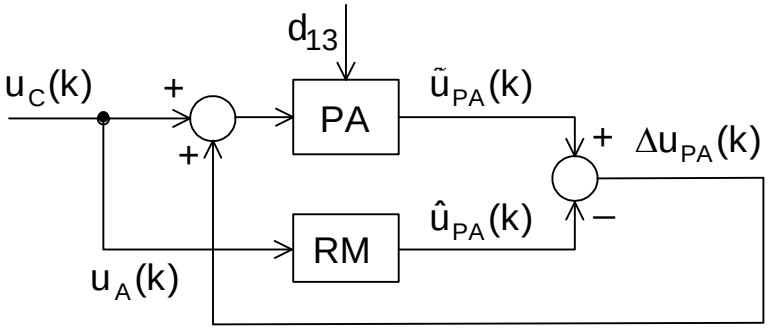

Figure 5.2 – Functional scheme of the signal adjustment of PA during destabilization d_{13}

If the kind d_{15} caused a malfunction, then its impact can be compensated with the help of an additional signal $u_A(k) = \Delta u_{PA}(k)$ according to the functional scheme in Figure 5.3.

The kind of destabilization d_{11} can be compensated also by means of parametric tuning. To implement such a scheme, it is necessary that the PA has the ability to adjust the coefficient k_{PA}.

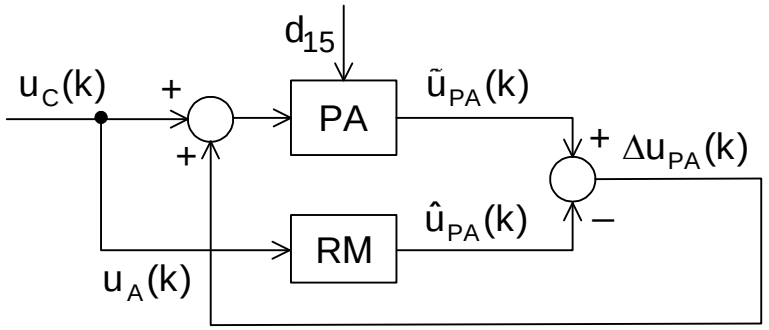

Figure 5.3 – Functional diagram of signal compensation of destabilization d_{15}

Then a difference signal $\Delta u_{PA}(k)$ is applied to the tuning circuit, which will provide such an increase in k_{PA} that will lead to the restoration of the original signal $\tilde{u}_{PA}(k)$ up to the value $\hat{u}_{PA}(k)$ (Figure 5.4).

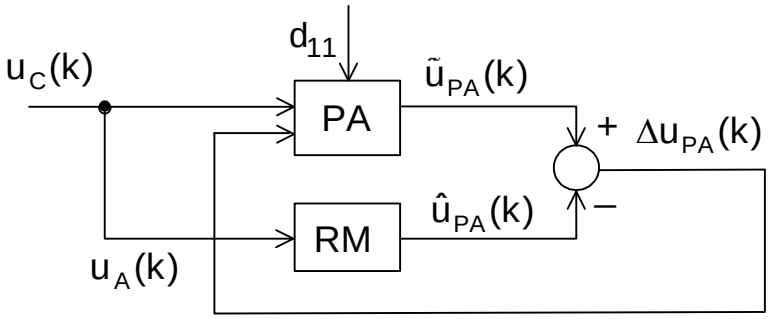

Figure 5.4 – Functional diagram of parametric compensation of d_{11}

The functional schemes of parametric compensation of kinds of destabilization d_{13} and d_{15} will look similar.

For kinds of destabilization d_{12}, d_{14}, d_{16} and d_{17}, the third means of restoring operability is used – reconfiguration of the equipment.

To ensure the restoreability of the rational control object in the case of a PA failure, the availability of backup PAs is provided, which can function both in "hot" and "cold" modes. When the main PA fails, its power is turned off, as well as input and output signals, that is, isolation from the control circuit is performed. After that, the standby PA_R power amplifier is connected. A possible functional diagram of such a reconfiguration is presented in Figure 5.5.

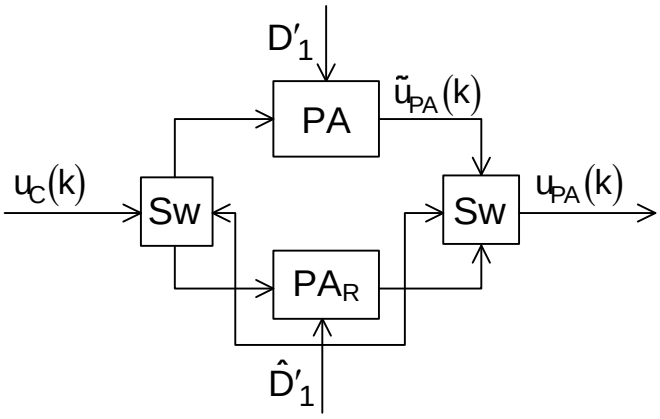

Figure 5.5 – Functional scheme of PA reconfiguration

In the presented scheme, there is a set $D'_1 = \{d_{12}, d_{14}, d_{16}, d_{17}\}$; Sw – switches. The input for Sw is the result of the diagnosis about the types of

destabilizing influences d_{12}, d_{14}, d_{16} and d_{17}, which indicates the non-renewable performance of the PA with the help of signal and parametric adjustments.

We will present a general functional scheme for restoring PA performance for all types of destabilization from the set D'_1 (Figure 5.6).

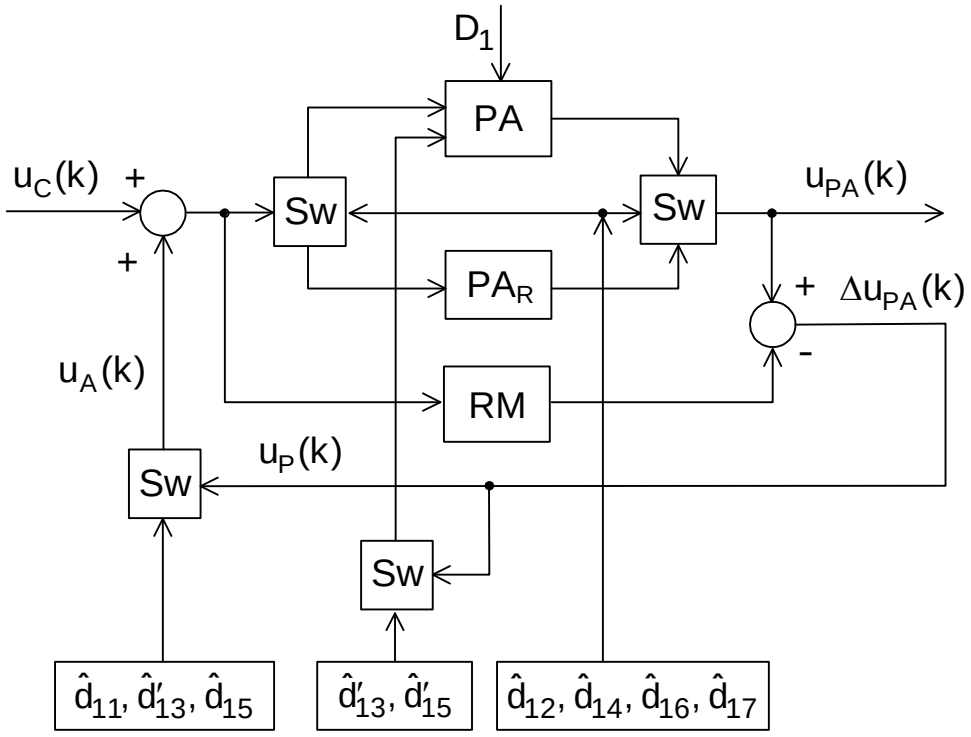

Figure 5.6 – Functional scheme of restoration of PA operability according to the results of the diagnosis

The switches Sw connect the appropriate signals to restore the operational efficiency of the PA based on the results of the diagnosis. So, when the kind of destabilization d_{11}, d_{13} or d_{15} is detected as a result of diagnostics, the difference signal $\Delta u_{PA}(k)$ is connected to the second input of the adder for signal adjustment $u_A(k)$ of the PA. At the same time, it is necessary to invert the difference signal for the kind d'_{13}.

When diagnosing kinds d_{13} and d_{15}, a difference signal $\Delta u_{PA}(k)$ is connected for parametric compensation of PA malfunction. In the case of uncompensated types of PA destabilization d_{12}, d_{14}, d_{16}, d_{17}, using switches Sw, the main PA is replaced with a backup PA_R, and in this way, the functionality of this functional element of the rational control object is restored.

After the procedures for restoring the operability of the PA, its in-depth diagnosis is carried out both to confirm the fact of full restoration of its

operability and to identify the reasons for incomplete parrying of kinds of destabilization. In other words, the recovery process can be iterative in nature.

5.2 Restoration of the operability of the electric flywheel motor

Violation of EFM performance is caused by kinds of destabilization from the set D_2. This reduction in the transfer factor is species d_{21} and d_{22}, increasing the time of the transition process – kinds d_{23} and d_{24}, as well as an unknown kind of destabilization d_{25}. The process of deep diagnostics allows to determine all kinds of destabilization from the set D_2. Restoring of EFM functionality consists in neutralizing the causes of kinds of destabilization with redundant means, and in cases of their non-compensation, turning off EFM.

Table 5.2

d_{ij}	Recovery means			Level
	ν_1	ν_2	ν_3	
d_{21}	1			1
d_{22}			1	1
d_{23}		1		1
d_{24}			1	1
d_{25}			1	1
Rank	1	1	3	

Let's consider the means and procedures for restoring the operational efficiency of EFM for each kind of destabilization using the table of recoverability (Table 5.2).

The following recovery means are presented in the table: ν_1 – signal adjustment of the coefficient k_M reduction; ν_2 – reconfiguration of the EFM control algorithm; ν_3 – reconfiguration of equipment.

The level of presented EFM recovery means is low and equal to 1. The highest rank is 3 and is associated with EFM shutdown. In order to ensure the conditions for the long-term functioning of the EFM, it is necessary to expand the number of means of recovery and increase their rank. Such possibilities exist in the pyramid scheme of EFM placement. In this presentation, only one control channel of the kinetic energy vector is considered.

There is no need to choose recovery tools in this situation, since the recovery means ν_1 and ν_2 have the same rank equal to 1.

Let's consider the possibility of restoring EFM operability in case of destabilization d_{21} detected during the diagnosis process. The reduction of the coefficient k_M can be compensated, if the range of the change of the

control signal allows, with the help of an additional signal. An additional control signal can be determined by using the transmission functions of the automatic control object (3.22), (3.23), (3.26). Therefore, the transfer function (3.22) under the condition that $\frac{L}{R} << \frac{J}{k_B}$, will be as follows:

$$W_1(s) = \frac{U_{S1}(s)}{U_C(s)} = \frac{k_{S1} k_M k_{PA}}{k_B R\left(\frac{J}{k_B} s + 1\right)}. \qquad (5.1)$$

In the time domain, the communication of signals is described by the following equation:

$$\dot{u}_{S1}(t) = -\frac{k_B}{J} u_{S1}(t) + \frac{k_{S1} k_M k_{PA}}{JR} u_C(t). \qquad (5.2)$$

When quantizing the signals, we get an equation of the form:

$$u_{S1}(k+1) = \left(1 - \frac{T_0 k_B}{J}\right) u_{S1}(k) + \frac{k_{S1} k_M k_{PA} T_0}{JR} u_C(k) \ . \qquad (5.3)$$

The control of disturbed motion at $\tilde{k}_M = k_M - \Delta k_M$ will be as follows

$$\Delta u_{S1}(k+1) = \left(1 - \frac{T_0 k_B}{J}\right) \Delta u_{S1}(k) - \frac{k_{S1} \Delta k_M k_{PA} T_0}{JR} u_C(k). \qquad (5.4)$$

To understand the possibility of restoring the operability of EFM in the case of destabilization d_{21} with the help of signal adjustment, let's consider fragments of the static characteristics of the rational control object in the interval of possible restoration (Figure 5.7).

In the Figure 5.7, graph 1 shows the normal nominal static characteristic of RCO, and gragh 2 shows the abnormal static characteristic. To restore the operating point $(u'_C, \hat{u}_{S1})$, it is necessary to provide an additional control value signal Δu_C. The additional control signal Δu_C is related to the available signal Δu_{S1} by such a ratio in the right-angled triangle ABC:

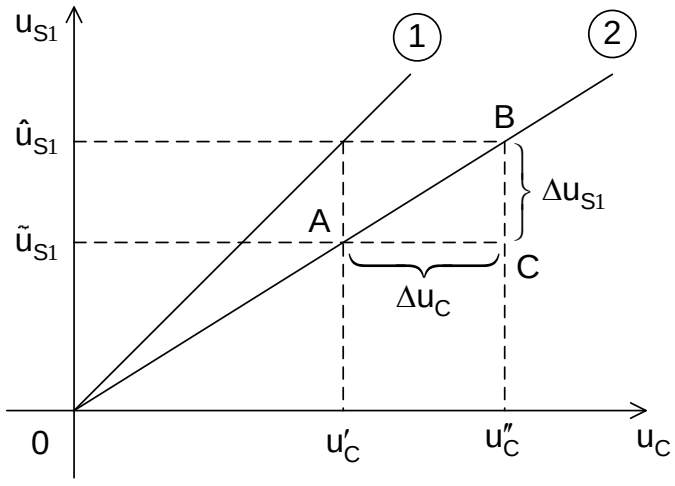

Figure 5.7 – Fragment of static characteristics of RCO

$$\Delta u_C = \frac{\Delta u_S}{\tilde{k}}, \qquad (5.5)$$

where $\tilde{k}$ – the transmission coefficient of the serial connection PA+EFM+S_1 in the abnormal mode caused by the type of destabilization d_{21}.

Based on the equation (5.4), the adjustment signal can be formed taking into account the relation (5.5) using the following equation:

$$u_A(k+1) = \frac{\left[\Delta u_{S1}(k+1) - \left(1 - \frac{T_0 k_B}{J}\right)\Delta u_{S1}(k)\right] JR}{k_{S1}\tilde{k}_M k_{PA} T_0}. \qquad (5.6)$$

The functional scheme of EFM signal adjustment at d_{21} can be presented as follows (Figure 5.8).

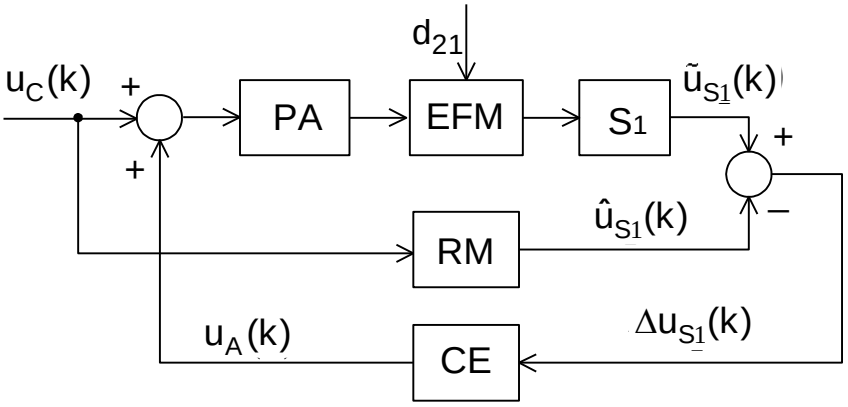

Figure 5.8 – Functional scheme of the signal adjustment of EFM at d_{21}

In the presented scheme, CE is a converting element that implements the equation (5.6).

The kind of EFM destabilization d_{23} leads to a change in the diagnostic parameter k_B. The transforming properties of the automatic control object are described in terms of transfer functions by the following expression:

$$W_1(s) = \frac{U_{S1}(s)}{U_C(s)} = \frac{k}{Ts+1}, \qquad (5.7)$$

where $k = \frac{k_{S1} k_M k_{PA}}{k_B R}$; $T = \frac{J}{k_B}$.

Changing the diagnostic parameter causes changes in the inertial properties of the control object. The time constant T nonlinearly depends on k_B. Let's expand this nonlinear function into a Taylor series:

$$\tilde{T} = T - \frac{J}{k_B^2}\Delta k_B + \frac{2J}{k_B^3}\Delta k_B^2 + \dots \ . \qquad (5.8)$$

Limiting ourselves to members of the first order of smallness, we get:

$$\Delta T = -\frac{J}{k_B^2}\Delta k_B \, . \qquad (5.9)$$

Then the disturbed motion of the control object can be described by the transfer function

$$\tilde{W}_1(s) = \frac{U_{S1}(s)}{U_C(s)} = \frac{k}{(T + \Delta T)s + 1}. \qquad (5.10)$$

If the polynomial of the denominator is imagined as the product of such binomial expressions

$$(Ts + 1)(\Delta Ts + 1), \qquad (5.11)$$

the product of which

$$T\Delta Ts^2 + (T + \Delta T)s + 1 \qquad (5.12)$$

can be simplified by taking into account that $T\Delta T << T + \Delta T$. At the same time, the transfer function of the disturbed motion of the control object can be represented as

$$\tilde{W}_1(s) = \frac{\tilde{U}_{S1}(s)}{U_C(s)} = \frac{k}{(Ts + 1)(\Delta Ts + 1)}. \qquad (5.13)$$

Based on the expression of this transfer function, it is obvious that in order to restore the functional properties of the rational control object, it is necessary to introduce a first-order forcing corrective element with a transfer function into the control circuit

$$W_{CE}(s) = \frac{U_1(s)}{U_C(s)} = \Delta Ts + 1. \qquad (5.14)$$

Product of transfer functions (5.13) and (5.14)

$$\tilde{W}_1(s)W_{CE}(s) = \frac{U_{S1}(s)}{U_C(s)} = \frac{\kappa\cancel{(\Delta Ts + 1)}}{(Ts + 1)\cancel{(\Delta Ts + 1)}} = \frac{\kappa}{(Ts + 1)} \qquad (5.15)$$

indicates the possibility of restoring the efficiency of the rational control object in case of destabilization d_{23}.

In the digital implementation of the forming corrective element of the first order, it is necessary to use a recurrent equation of the form

$$u_1(k + 2) = \frac{\Delta T}{T_0}u_C(k + 1) + \left(1 - \frac{\Delta T}{T_0}\right)u_C(k) \qquad (5.16)$$

or taking into account the value of the assessment of the diagnostic sign

$$u_1(k+2) = \frac{\Delta T}{T_0} u_C(k+1) + \left(1 - \frac{J\Delta\hat{k}_B}{T_0 k_B^2}\right) u_C(k). \qquad (5.17)$$

Estimated values of $\Delta\hat{k}_B$ are described by formulas (4.76), (4.77) and (4.79) and are determined at the diagnostic stage when determining types of destabilization.

Restoring the functionality of the rational control object, which is associated with a change in the control algorithm, is such a means of recovery as the reconfiguration of algorithms.

Let's show the features of such restoration of operability with the help of a functional scheme (Figure 5.9).

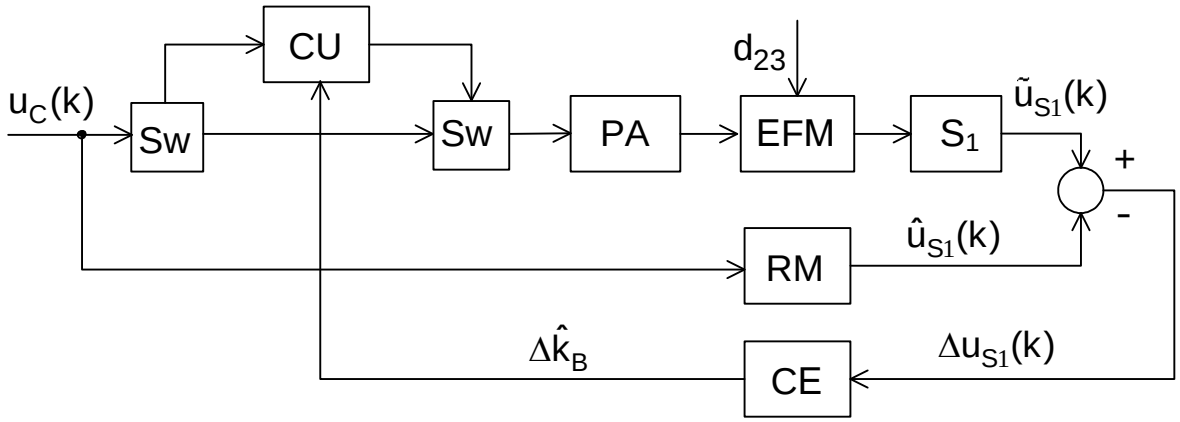

Figure 5.9 – Functional scheme of reconfiguration of EFM control algorithms at destabilization d_{23}

In the presented functional scheme, switches Sw are used to connect the corrective control algorithm. The formation of the estimate $\Delta\hat{k}_B$ is carried out using the converting element CE, which converts the difference signal $\Delta u_{S1}(k)$ into the estimated value of the diagnostic sign. After several iterations, in accordance with equation (5.17), full compensation of the consequences of the type of destabilization will occur d_{23}.

Kinds of destabilization d_{22}, d_{24} and d_{25} are associated with such a non-operating state of the EFM that cannot be recovered using recovery tools ν_1 – signal tuning and ν_2 – reconfiguration of algorithms. The presence of these kinds of destabilization in the rational control object leads to the need to remove it from the process of functioning in the EFM block. To decommission the rational control object, it is necessary to first of all turn off the control

signal $u_C(k)$ and the output signal $u_{S1}(k)$, and then turn off the power supply of the functional elements. The functional scheme of disconnection of the rational control object from the process of functioning in the EFM unit is summarized in Figure 5.10.

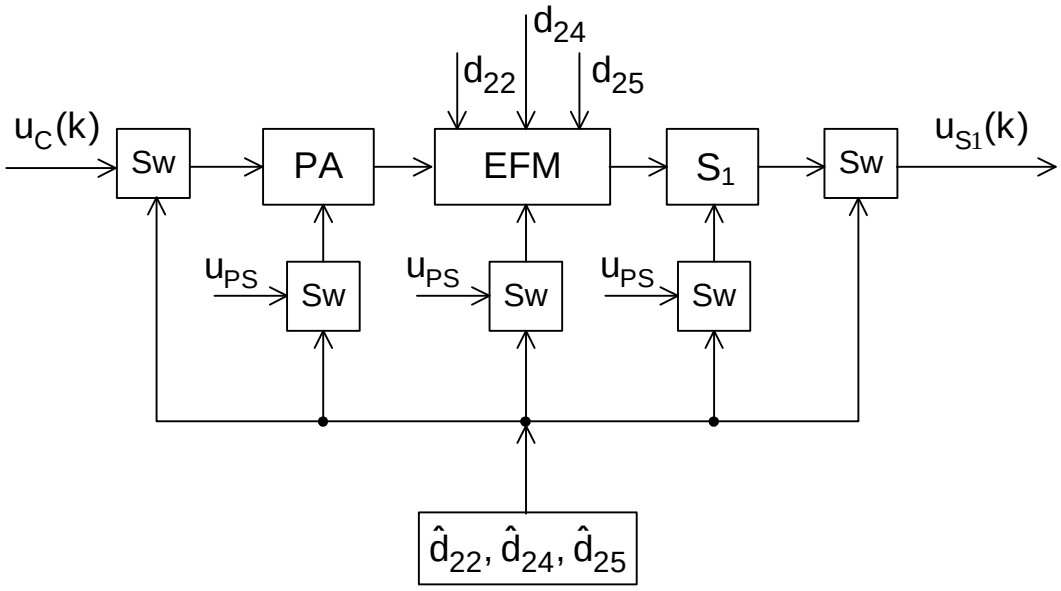

Figure 5.10 – Functional scheme of disconnection of the rational control object at destabilizations d_{22} and d_{24}

Additional information is required to make a different decision regarding the restoration of EFM operability in the case of a detected kind of destabilization $\hat{d}_{25}$. This information can be obtained during the magnitude analysis of. To determine the value of $\Delta\hat{u}_{S1}(k)$, you can use the average arithmetic estimate

$$\Delta\hat{u}_{S1}(k) = \frac{1}{m}\sum_{k=1}^{m}\Delta u_S(k). \qquad (5.18)$$

Based on the functionality of the signal adjustment, a threshold value $\Delta\bar{u}_{S1}$ is set at which, if $\Delta\hat{u}_{S1} \le \bar{u}_{S1}$, then an additional signal circuit is connected that compensates for the current difference $\Delta u_S(k)$.

If $\Delta\hat{u}_{S1} > \bar{u}_{S1}$, then the rational control object is decommissioned. Such a classification of an undefined kind of destabilization d_{25} can be carried out with the help of a two-valued predicate.

$$z_{251} = S_2\{\Delta\bar{u}_{S1} - \Delta\hat{u}_{S1}\}. \qquad (5.19)$$

At $z_{251} = 1$, recovery is carried out with the help of an additional signal

$$u_A(k) = \Delta\hat{u}_{S1} \qquad (5.20)$$

according to the functional scheme (Figure 5.11).

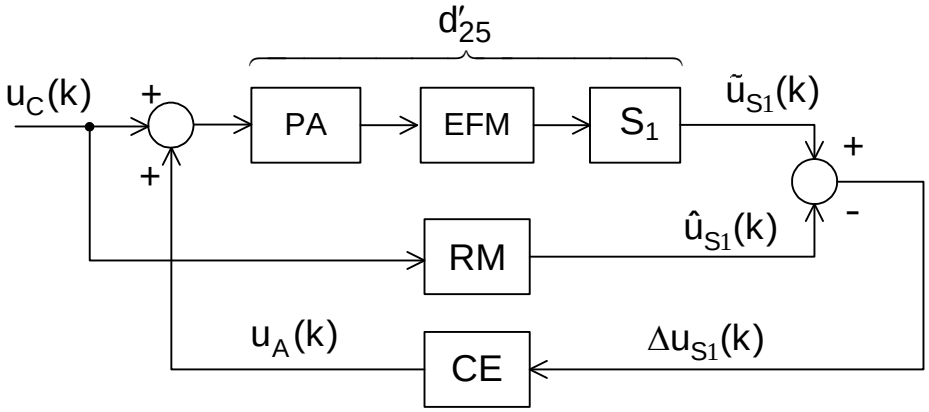

Figure 5.11 – Functional diagram of the signal adjustment of the rational control object at destabilization d'_{25}

The kind of destabilization d'_{25} is a compensated type of destabilization. CE – the converting element, in this case, performs the processing of the difference signal $\Delta u_{S1}(k)$ according to the expressions (5.18), (5.19) and (5.20).

At $z_{251} = 0$, the EFM is decommissioned by turning off the control signal $u_C(k)$ and the sensor output $\tilde{u}_{S1}(k)$, as well as turning off the power supply of all functional elements of the rational control object in accordance with the functional scheme (Figure 5.12).

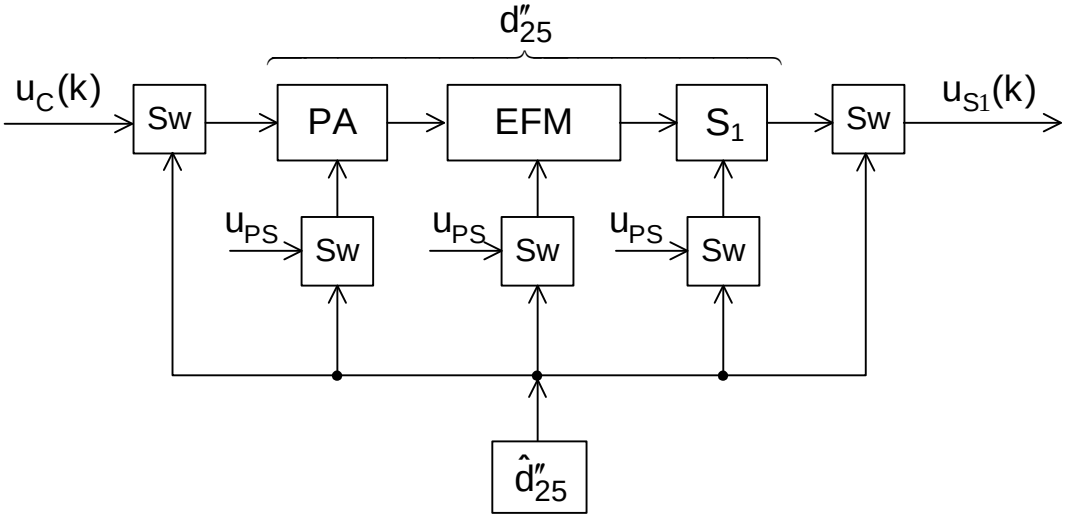

Figure 5.12 – Functional diagram of decommissioning of the rational control object at destabilization d''_{25}

In the presented scheme, d''_{25} is an uncompensated kind of destabilization.

With the help of partial functional schemes of restoration for certain kind of destabilization (see Figures 5.8–5.10), we will present a general functional scheme of restoration of EFM operability (Figure 5.13).

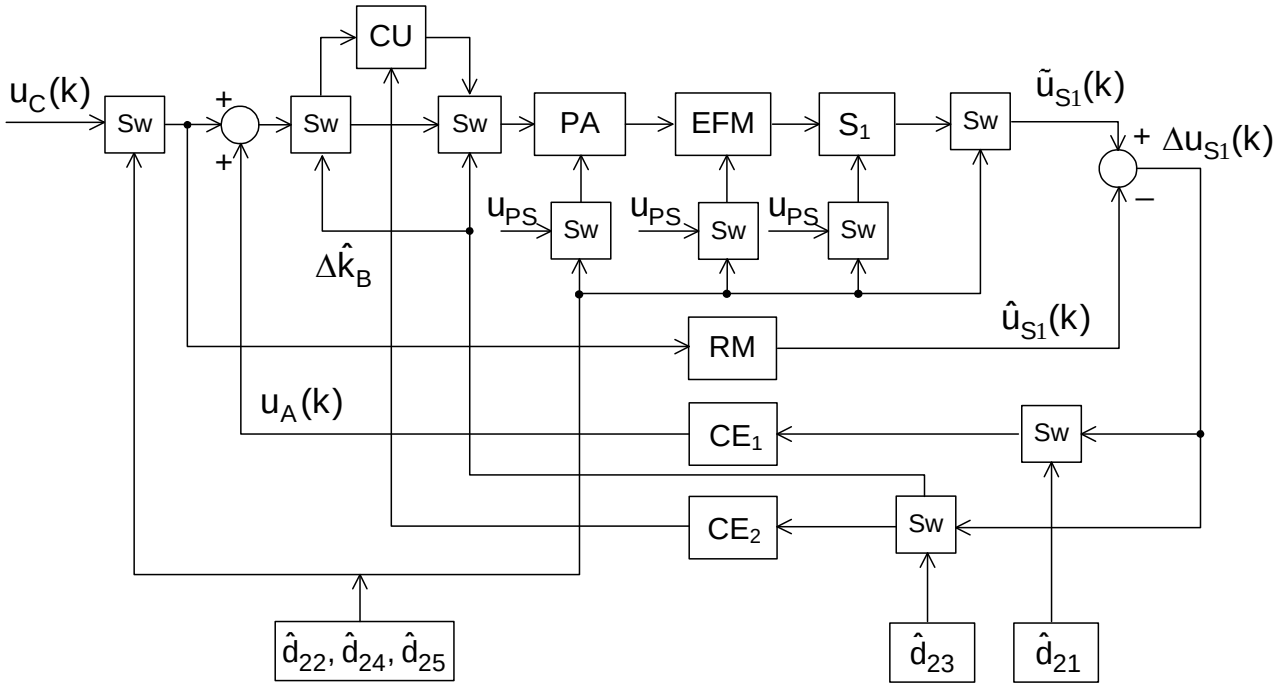

Figure 5.13 – Functional diagram of EFM recovery based on the results of the diagnosis

In the general functional scheme, the switches carry out switching of signals and supply voltage in accordance with the results of the diagnosis and procedures for restoring operability for each kind of destabilization.

After the restoration of EFM functionality by means of ν_1 and ν_2, a cycle of in-depth EFM diagnostics is carried out, during which the complete restoration of EFM functionality or the reason for incomplete restoration of its functions is confirmed in order to further work out the flexible recovery cycle.

5.3 Restoring the functionality of the angular velocity sensor

Five kinds of destabilization disrupt the functionality of the S_1 angular velocity sensor: d_{31} and d_{32} are associated with a reduction in the

transmission ratio; d_{33} and d_{34} lead to zero drift; d_{39} – unknown type of destabilization.

To restore the functionality of the S_1 sensor, you can use such recovery tools as ν_1 – signal tuning, ν_2 – parametric adjustment, ν_3 – reconfiguration of algorithms, ν_4 – reconfiguration of equipment. The distribution of recovery means by kinds of destabilization can be presented using the recovery table (Table 5.3).

Table 5.3

d_{ij}	Recovery means				Level
	ν_1	ν_2	ν_3	ν_4	
d_{31}	1	1			2
d_{32}			1	1	2
d_{33}	1	1			2
d_{34}			1	1	2
d_{39}			1	1	2
Rank	2	2	3	3	

As can be seen from the table, the level of the presented means of recovery is the same and is equal to 2. This indicates an even distribution of means. The ranks of recovery tools are different. The highest is 3 for means ν_3 and ν_4.

Let's consider the possibility of restoring the operability of S_1 when a kind of destabilization d_{31} appears. $\tilde{k}_{S1}$ The reduction in the sensor transfer factor can be compensated for by an additional trim signal to the sensor output signal $\tilde{u}_{S1}(k)$. The equation of the disturbed motion of the rational control object at $\tilde{k}_{S1} = k_{S1} - \Delta k_{S1}$ will be as follows:

$$\Delta u_{S1}(k+1) = \left(1 - \frac{T_0 k_B}{J}\right)\Delta u_{S1}(k) - \frac{\Delta k_{S1} k_M k_{PA} T_0}{JR} u_C(k). \qquad (5.21)$$

According to the formula (5.5), the adjustment signal of the sensor output is described by the equation

$$u_C(k+1) = \frac{\left[\Delta u_{S1}(k+1) - \left(1 - \frac{T_0 k_B}{J}\right)\Delta u_{S1}(k)\right] JR}{\tilde{k}_{S1} k_M k_{PA} T_0}. \qquad (5.22)$$

The functional scheme of S_1 signal tuning can be presented as follows (Figure 5.14).

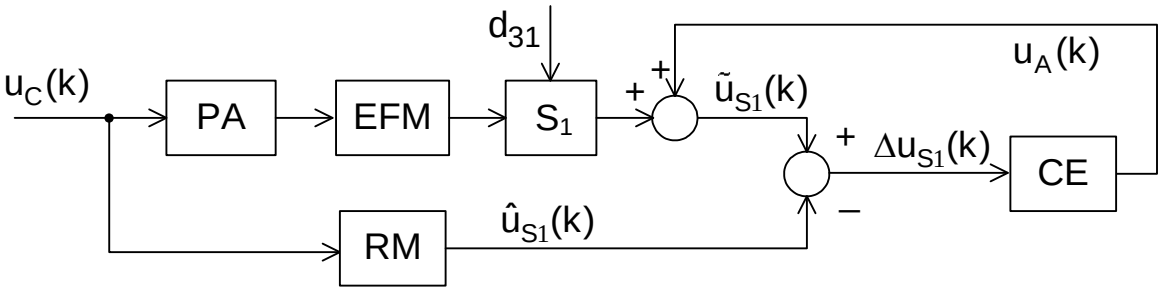

Figure 5.14 – Functional scheme of the signal adjusting of S_1 at destabilization d_{31}

The converting element PE in this scheme implements equation (5.22).

When using the parametric tuning of S_1 recovery, it is necessary to know the value of the deviation of the coefficient. Estimated values $\Delta\hat{k}_{S1}$ can be used from the diagnostic knowledge base on kinds of destabilization. These are formulas (4.89), (4.90) or (4.91). In the sensor S_1 for parametric adjustment, a circuit solution for adjusting the transmission coefficient should be provided. Then, when detecting the type d_{31}, the transfer factor is increased by an amount $\Delta\hat{k}_{S1}$. The estimated value Δk_{S1} can also be obtained from equation (5.21).

$$\Delta\kappa_{S1} = \frac{\left[\Delta u_{S1}(k+1) - \left(1 - \frac{T_0 k_B}{J}\right)\Delta u_{S1}(k)\right] JR}{k_M \kappa_{PA} T_0 u_y(k)} \qquad (5.23)$$

or use the recurrent equation to obtain the current value of the coefficient deviation $\Delta\kappa_{S1}(k+2)$ and apply it to parametric tuning according to the scheme (Figure 5.15).

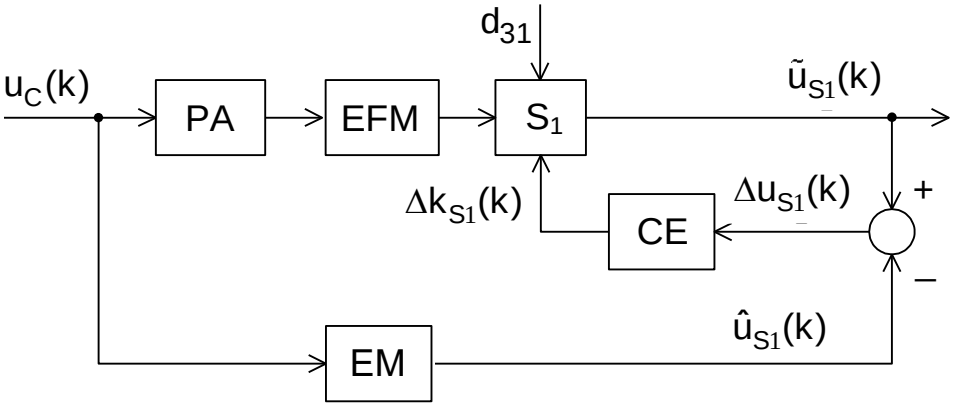

Figure 5.15 – Functional scheme of the parametric adjustment S_1 at destabilization d_{31}

In the conversion element CE, the current value $\Delta\kappa_{S1}(k)$ is formed using the equation (5.23).

When a compensated drift of zero appears in S_1, this is a kind of destabilization d_{33}, it is possible to restore operability both with the help of signal adjustment ν_1 and with the help of parametric adjustment ν_2. When using signal tuning, you need to use the equation of perturbed motion

$$\Delta u_{S1}(k+1) = \left(1 - \frac{T_0 k_B}{J}\right)\Delta u_{S1}(k) - \frac{u_{01} k_M k_{PA} T_0}{JR} u_C(k), \qquad (5.24)$$

from which the current value of zero drift is

$$u_{01}(k+2) = \frac{\left[\Delta u_{S1}(k+1) - \left(1 - \frac{T_0 k_B}{J}\right)\Delta u_{S1}(k)\right] JR}{k_M k_{PA} T_0 u_C(k)}. \qquad (5.25)$$

Signal adjustment of S_1 can be implemented according to the functional scheme shown in Figure 5.16.

In the conversion element CE, a correction signal is formed using the equation (5.25).

When using parametric tuning ν_2, we can apply the conversion element of the algorithm (5.24), adapted to the transfer factor $\tilde{k}_{S1}$ tuning scheme.

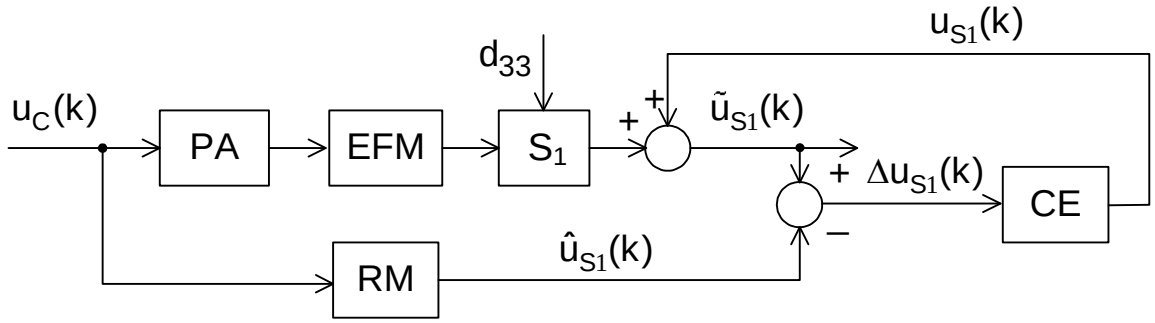

Figure 5.16 – Functional scheme of the signal tuning of the sensor S_1 at destabilization d_{33}

A possible functional scheme of parametric adjustment is shown in Figure 5.17.

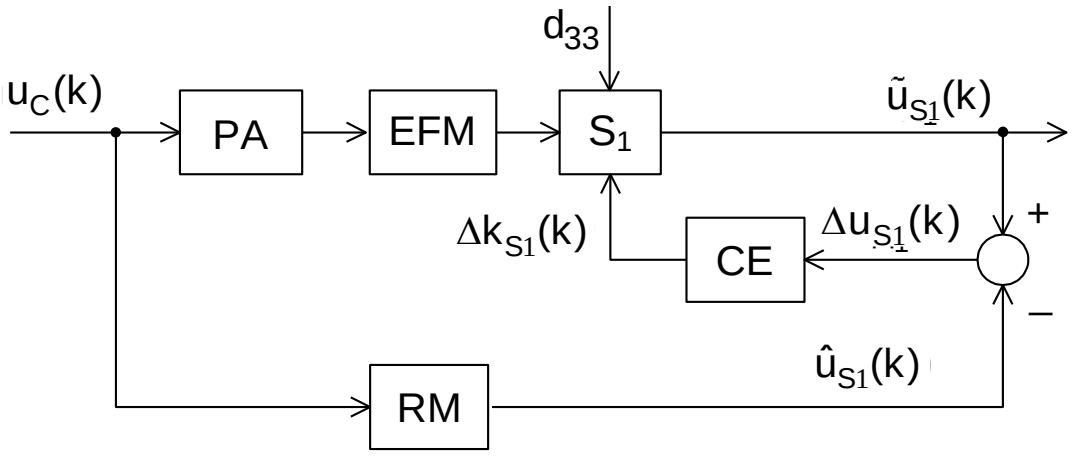

Figure 5.17 – Functional scheme of the parametric adjusting of the sensor S_1 at destabilization d_{33}

In the conversion element CE, a signal for adjusting $\Delta k_{S1}(k)$ the transfer factoe of the sensor is formed.

Now let's consider the kinds of destabilization d_{32}, d_{34} and d_{39} that cannot be neutralized by recovery means ν_1 and ν_2. A recovery mean ν_3 is suitable for neutralizing these kinds of destabilization, which allows for the reconfiguration of algorithms to restore the operability of the rational control object. Therefore, with uncompensated kinds of destabilization, we can use the evaluation of the reference model $\hat{u}_{S1}(k)$, which indirectly reflects the state of the (PA+EFM) subsystem and will be used in the process of forming management. The functional diagram of this recovery process is presented in Figure 5.18.

The switches Sw in this scheme remove the angular velocity sensor S_1 from operation and provide replacement of the output signal $\tilde{u}_{S1}(k)$ of the rational control object by the signal $\hat{u}_{S1}(k)$, which contributes to the recovery of measurement of the EFM angular velocity.

A possible mean of restoring operability of S_1, or rather restoration of measurements in cases of destabilization d_{32}, d_{34} and d_{39}, can be the mean ν_4 – reconfiguration of the equipment.

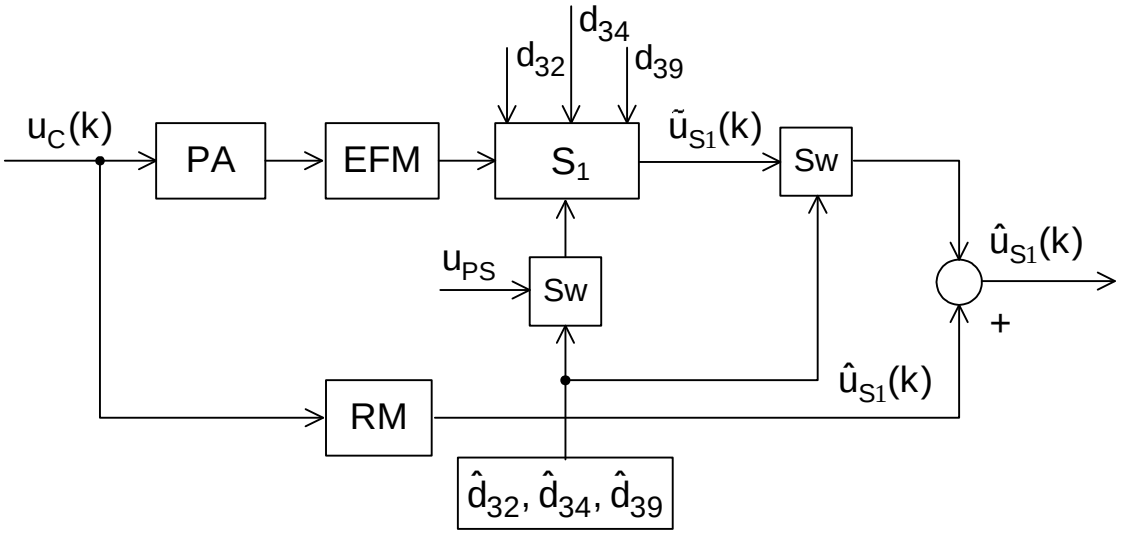

Figure 5.18 – Functional scheme of reconfiguration of algorithms

In this situation, the reconfiguration of the equipment is the connection of a backup sensor D_{1R} instead of the main sensor S_1. The reserve sensor can be both in the "hot" reserve and in the "cold". When the D_{1R} sensor is in the "hot" reserve, the process of restoring the EFM angular velocity measurements can be represented using a functional diagram (Figure 5.19).

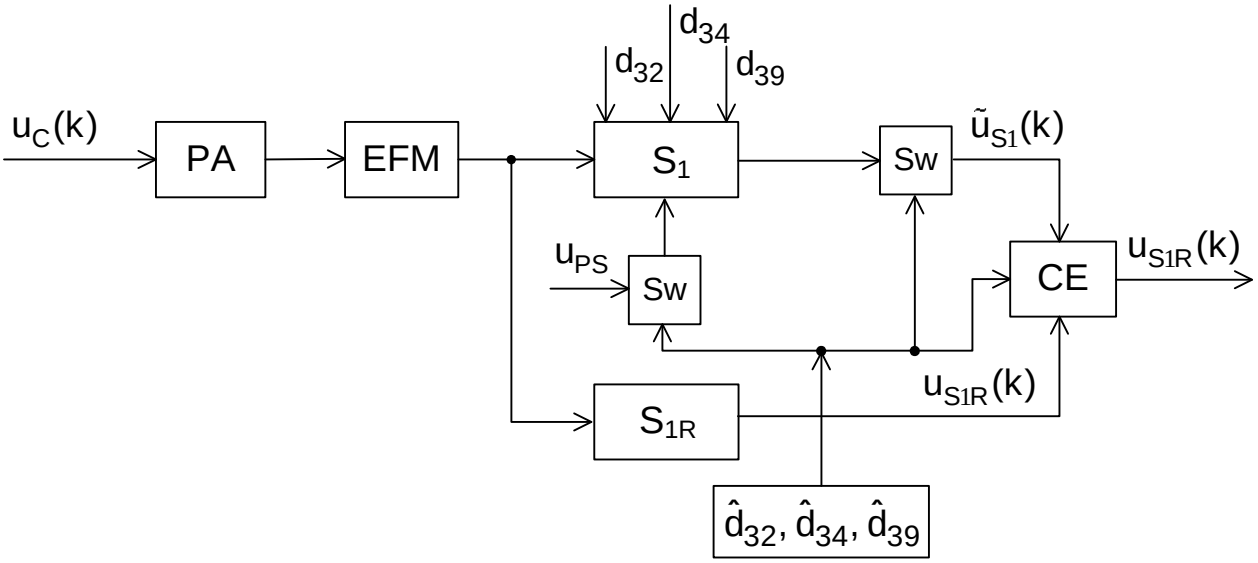

Figure 5.19 – Functional scheme of restoration of measurements with the help of a "hot" reserve

The results of measurements of EFM angular velocity are sent from two sensors to the converting element CE, in which, if the sensors are working, the arithmetic mean value of the measurement is formed.

When a diagnosis $\hat{d}_{32}$, $\hat{d}_{34}$ or $\hat{d}_{39}$ occurs, the main S_1 sensor is decommissioned by the switches and the CE transmits only the measurement $u_{S1R}(k)$.

When using S_{1R} as a "cold" reserve, when information about $\hat{d}_{32}$, $\hat{d}_{34}$ or $\hat{d}_{39}$ appears, it is necessary to disconnect the inoperable sensor S_1 and connect the reserve S_{1R} using circuit switching. The functional diagram in Figure 5.20 shows the main features of this process of restoring EFM angular velocity measurements.

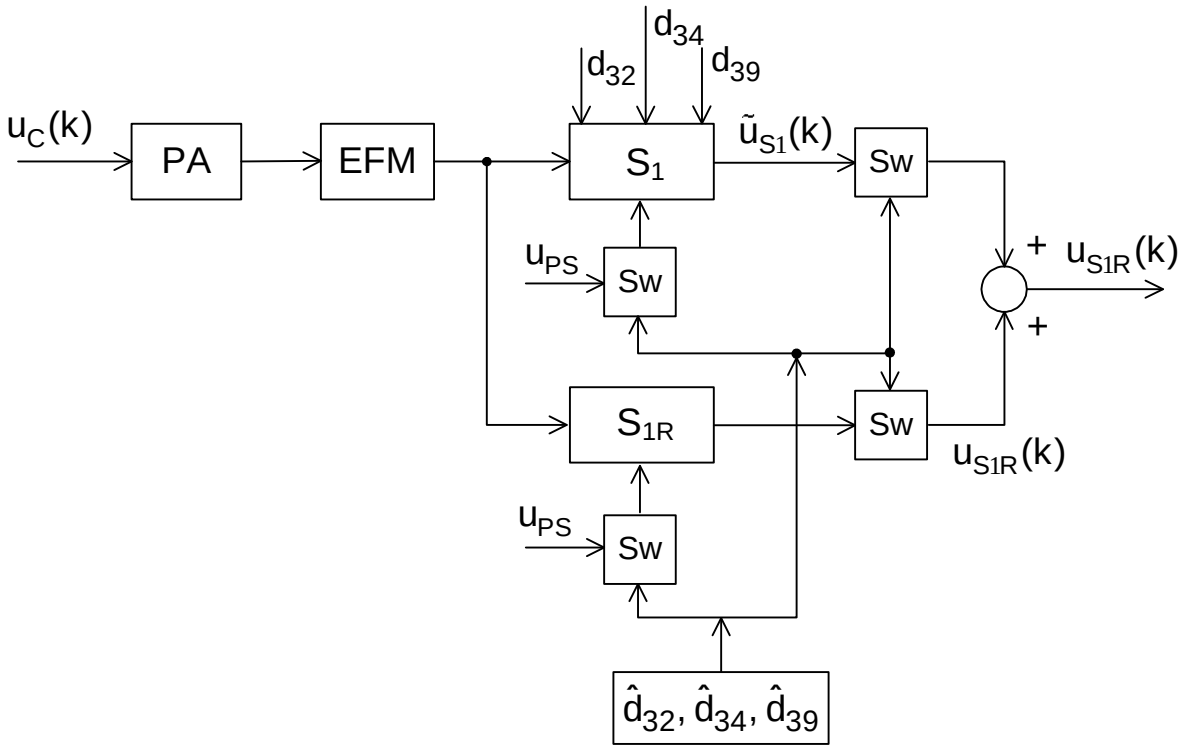

Figure 5.20 – Functional scheme of restoration of measurements with the help of a "cold" reserve

The scheme uses switches that commutate the sensors and switches that switch the measurement signals of EFM angular velocity.

With the help of partial functional schemes of signal adjustment and reconfiguration of algorithms, we will form a general functional scheme of restoring operability of sensor S_1 (Figure 5.21).

CE_1 and CE_2 are converting elements which implement the signal tuning algorithm and the parametric tuning algorithm, respectively.

After the procedure for restoring the functionality of S_1 – the EFM angular velocity sensor, a repeated diagnostic control procedure is performed. In the case of incomplete recovery of one or another kind of destabilization, a

repeated procedure is carried out to restore the EFM angular velocity sensor measurements to the required accuracy.

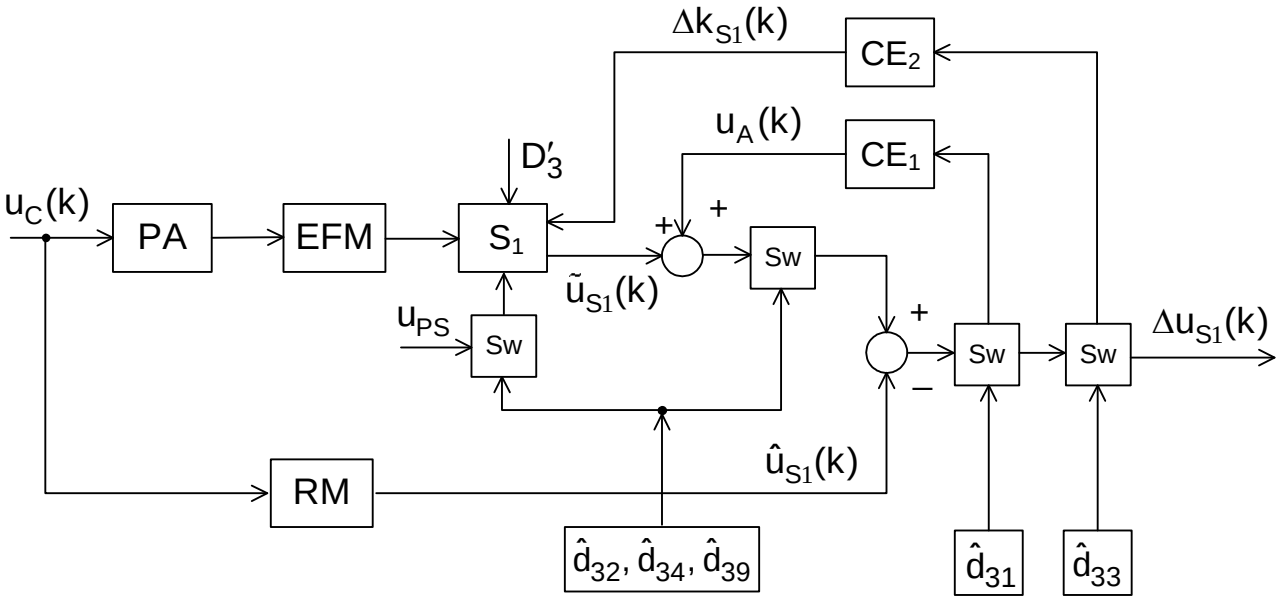

Figure 5.21 – Functional scheme of recovery
operability of sensor S_1 according to the results of the diagnosis

Other combinations of the previously considered functional schemes of restoration are possible, which ensure the necessary restoration of EFM angular velocity sensor measurements under specific conditions.

5.4 Restoring the functionality of the sensor of current

The object of rational control (see Figure 4.2) uses the second sensor S_2 – a sensor of current. Malfunction of the current sensor can be caused by kinds of destabilization from the set $D''_3 = \{d_{35}, d_{36}, d_{37}, d_{38}, d_{39}\}$. Kinds of destabilization d_{35} and d_{36} are caused by a decrease in the conversion factor of the sensor k_{S2}. Kinds of destabilization d_{37} and d_{38} are related to the zero drift of the sensor u_0. Kind d_{39} is an unspecified type of destabilization.

The following means can be used to neutralize the kinds of destabilization of the set D''_3: ν_1 – signal tuning, ν_2 – parametric adjustment, ν_3 – reconfiguration of algorithms and ν_4 – reconfiguration of equipment. The distribution of these means by kinds of destabilization is given in the table of recoverability (Table 5.4).

Table 5.4

d_{ij}	Recovery means				Level
	ν_1	ν_2	ν_3	ν_4	
d_{35}	1	1			2
d_{36}			1	1	2
d_{37}	1	1			2
d_{38}			1	1	2
d_{39}			1	1	2
Rank	2	2	3	3	

Means of recovery are distributed gradually according to the kinds of destabilization, which follows from the numerical values of the level. The rank of the recovery table is not uniform. The means ν_1 has low rank. Recovery means ν_3 and ν_4 have a higher rank.

Let's consider the possibilities and features of using recovery means $\nu_1 \div \nu_4$ in sequence. Therefore, when diagnosing in an inoperable sensor S_2, the kind of destabilization d_{35} can be used to restore its operability by signal adjustment, i.e. a mean ν_1.

To generate the tuning signal, we will use the structural diagram (see Figure 3.17). The connection of the output signal of sensor S_2 with the control signal $u_C(t)$ is described by the following differential equation:

$$\dot{u}_{S2}(t) = a_{22}\, u_{S2}(t) + c_{22}\, \kappa_{PA}\, b_2\, u_C(t) \qquad (5.26)$$

or in terms of specific parameters of the control object

$$\dot{u}_{S2}(t) = -\frac{R}{L} u_{S2}(t) + \frac{k_{S2} k_{PA}}{L} u_C(t). \qquad (5.27)$$

Multiplying both parts of the equation by $\frac{L}{R}$, we get

$$\frac{L}{R}\dot{u}_{S2}(t) = -u_{S2}(t) + \frac{k_{S2} k_{PA}}{R} u_C(t). \qquad (5.28)$$

The ratio $\frac{L}{R} = T_E$ characterizes the electrical time constant of the EFM based on the expression of the transfer function $W_2(s)$ (3.23). Since $T_E << T_{EM}$, therefore, it can be considered an infinitely small value and then equation (5.28) can be simplified to the following form:

$$u_{S2}(t) = \frac{k_{S2} k_{PA}}{R} u_C(t). \qquad (5.29)$$

The equation of the perturbed motion caused by the kind of destabilization d_{35} will be the following for discrete time values:

$$\tilde{u}_{S2}(k) = \frac{\tilde{k}_{S2} k_{PA}}{R} u_C(k). \quad (5.30)$$

The equation of the reference model of communication of these signals

$$\hat{u}_{S2}(k) = \frac{k_{S2} k_{PA}}{R} u_C(k). \quad (5.31)$$

Subtracting the equation of the reference model (5.31) from the equation of the disturbed motion (5.30), we obtain the equation for the deviation of the output signal of the sensor S_2:

$$\Delta u_{S2}(k) = \frac{\Delta k_{S2} k_{PA}}{R} u_C(k). \quad (5.32)$$

Therefore, the kind of destabilization d_{35} leads to a proportional decrease in the signal of the sensor of current S_2. To compensate for this destabilization, it is necessary to add an additional signal of magnitude $\Delta u_{S2}(k)$ to the output signal $\tilde{u}_{S2}(k)$ of the faulty sensor. Graphically, the principle of signal adjustment can be presented using a functional scheme (Figure 5.22).

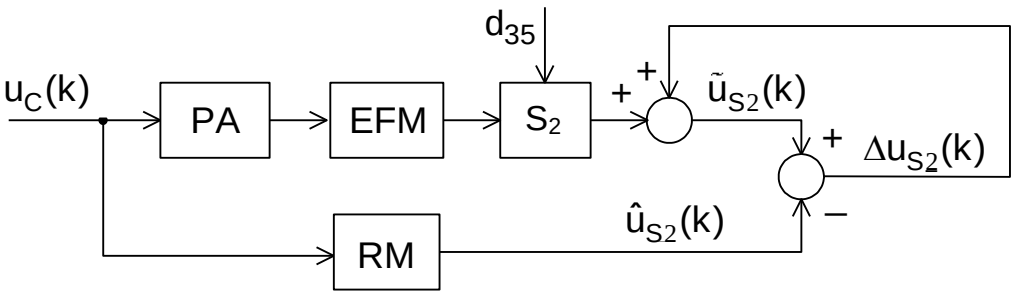

Figure 5.22 – Functional scheme of the signal adjusting of the sensor S_2 at destabilization d_{35}

The functional element RM – the reference model transforms the control signal according to equation (5.31). In the adder, the correction of the output signal S_2 is made, which ensures the neutralization of the effect of the kind of destabilization d_{35}.

When using the means of recovery ν_2 – parametric adjustment, it is necessary to form a parametric adjustment signal from the difference signal $\Delta u_{S2}(k)$ corresponding to the decrease in the conversion coefficient of the sensor (5.32). In the simplest case, this signal will be equal to Δk_{S2}:

$$\Delta\kappa_{S2}(k) = \frac{R\Delta u_{S2}(k)}{k_{PA} u_C(k)}. \quad (5.33)$$

Then the features of parametric compensation of the kind of destabilization d_{35} can be presented using a functional scheme (Figure 5.23).

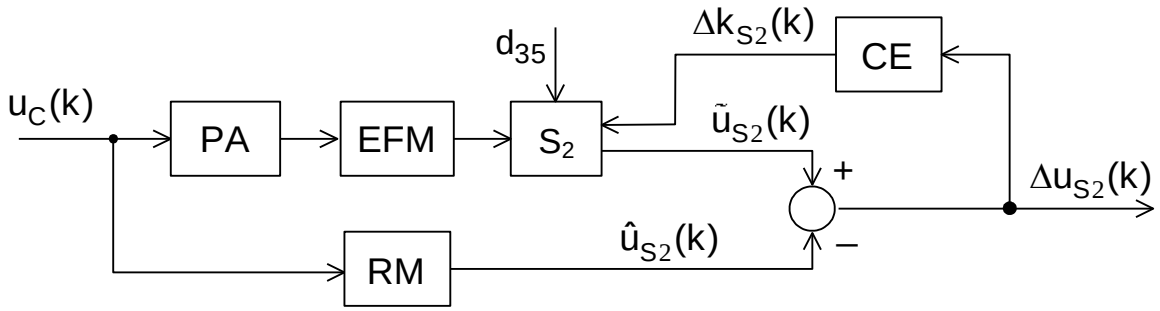

Figure 5.23 – Functional scheme of the parametric adjusting of the sensor S_2 at destabilization d_{35}

The kind of destabilization d_{37} characterizes the eliminated zero drift of the sensor of current, which can be countered by recovery means as ν_1, as ν_2. Let's consider the features of signal adjustment.

The difference signal in this case will be equal to the drift value u_{02}. If the drift value is positive $u_{02} > 0$, the difference signal $\Delta u_{S2}(k)$ should be subtracted from the output signal $\tilde{u}_{S2}(k)$ of the sensor; if the drift value is negative $u_{02} < 0$ the difference signal should be addded. The functional diagram of such signal tuning is shown in Figure 5.24.

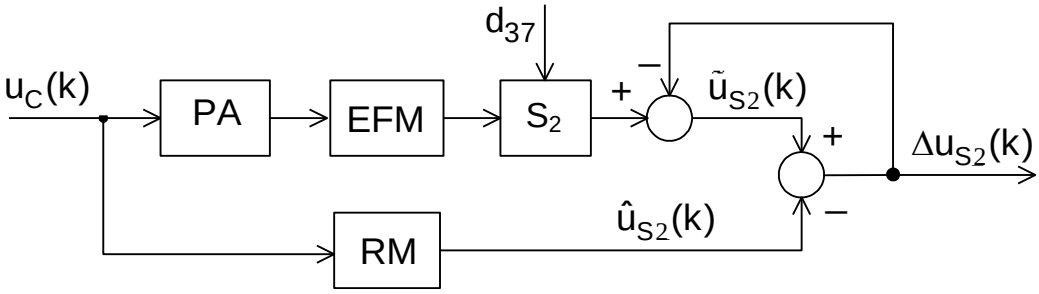

Figure 5.24 – Functional scheme of the signal tuning of sensor S_2 at destabilization d_{37}

When using parametric adjustment to restore measurements of the sensor of current when its zero drifts, the difference signal $\Delta u_{S2}(k)$ must be converted into a corresponding change in the conversion coefficient. The functional scheme (Figure 5.25) reflects the corresponding composition of functional elements and their connection.

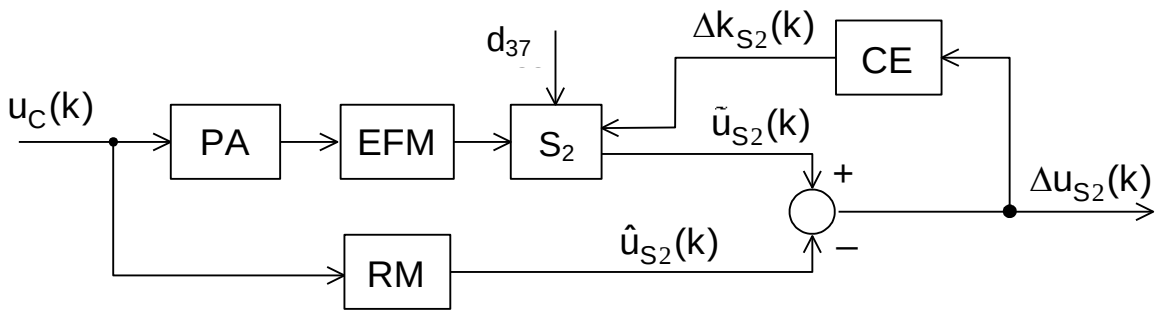

Figure 5.25 – Functional scheme of the parametric adjusting of sensor S_2 at destabilization d_{37}

Kinds of destabilization d_{36}, d_{38} and d_{39} can be neutralized according to Table 5.4 by two means ν_3 – reconfiguration of algorithms or by ν_4 – reconfiguration of equipment. Let's consider the peculiarities of the use of measurement recovery, and therefore the efficiency of S_2, by reconfiguration of algorithms.

A redundant resource in the object of rational control is the reference model, which generates the estimated value of the output signal $\hat{u}_{S2}(k)$ of the sensor. Since the destabilization of the sensor at kinds d_{36}, d_{38} i d_{39} is such that it is impossible to restore its operability by means ν_1 and ν_2, then it is necessary to remove it from operation by disconnecting the supply voltage u_{PS} and disconnecting the output signal $\tilde{u}_{S2}(k)$. And instead of the readings of the disconnected sensor, use the output of the reference model $\hat{u}_{S2}(k)$. The composition of functional elements and the corresponding connections for such a procedure are presented in Figure 5.26.

The switches, based on the results of the diagnosis, disconnect the faulty sensor and ensure that its output signal $\tilde{u}_{S2}(k)$ is replaced by the signal $\hat{u}_{S2}(k)$ of the reference model, which ensures the restoration of measurements.

We can restore the functionality of the sensor of current in the case of destabilizations d_{36}, d_{38} and d_{39} by replacing the faulty sensor with a working one, which is the essence of the mean ν_4 – reconfiguration of equipment. A working backup sensor of current can be used in two ways. The first, when the current sensor works simultaneously with the main one, is the so-called "hot" reserve. The second option is when a working sensor is connected to work instead of the main one. This is a variant of "cold" reserve.

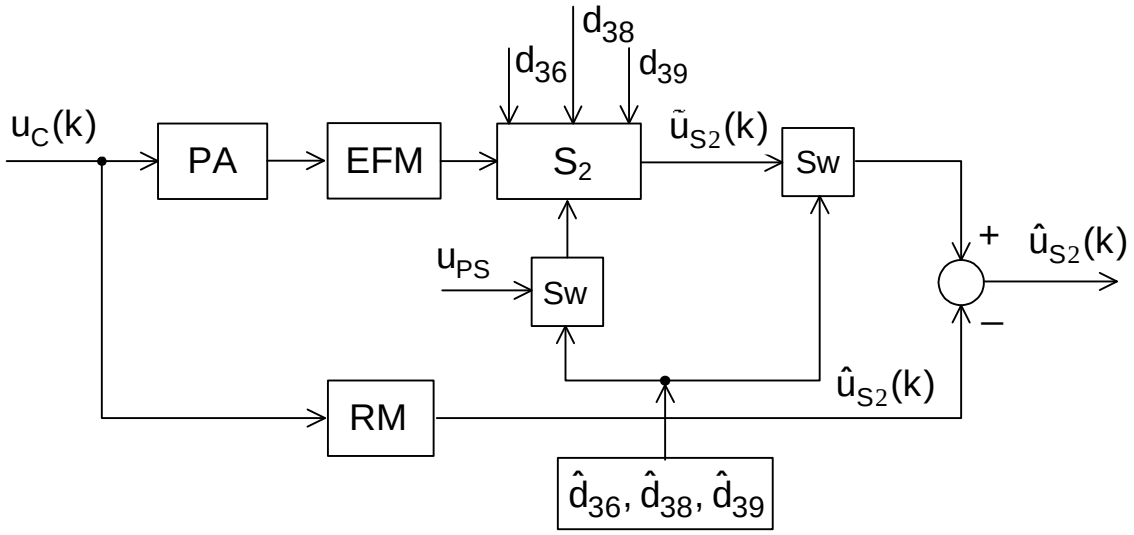

Figure 5.26 – Functional scheme of reconfiguration of algorithms

A functional diagram that reflects the composition of the necessary functional elements and their connection for the implementation of the process of restoring the operability of S_2 when using a "hot" reserve, is shown in Figure 5.27.

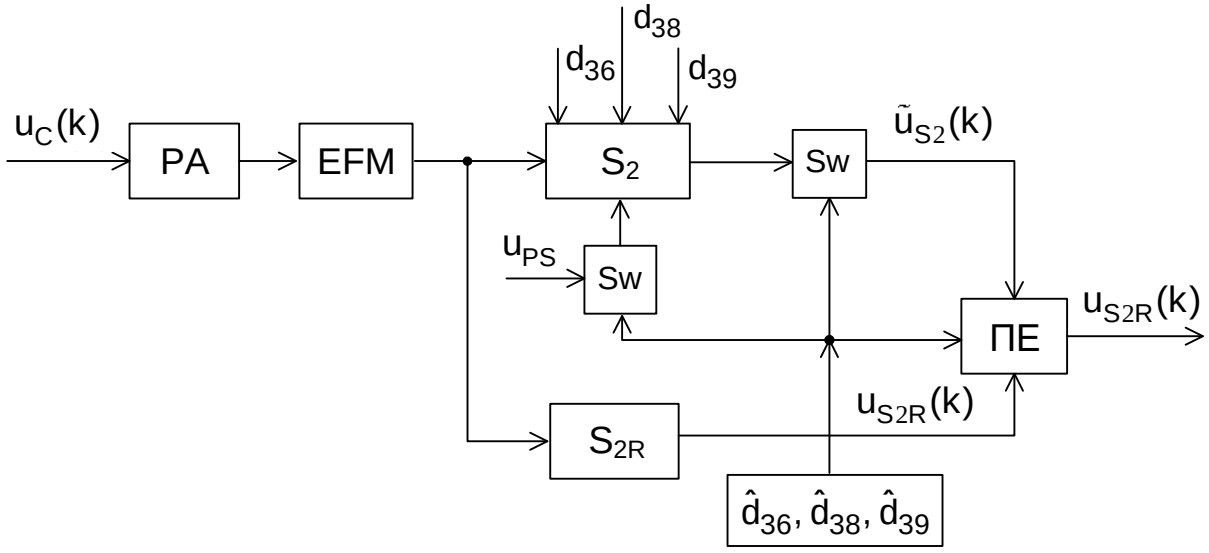

Figure 5.27 – Functional diagram of recovery
current sensor using a "hot" reserve

With the simultaneous operation of the serviceable S_2 and the backup S_{2R}, the conversion element CE forms the arithmetic mean value of the measurement of current. If a diagnosis of the kind of destabilization $\hat{d}_{36}$, $\hat{d}_{38}$ or $\hat{d}_{39}$ has appeared, the switch isolates the failed S_2 sensor by means of disconnection and disconnection of its output signal $\tilde{u}_{S2}(k)$ from CE. A signal

from the output of the backup current sensor $u_{S2R}(k)$ appears at the PE output and the recovery of measurements of current sensor is completed. $\hat{d}_{36}$ або $\hat{d}_{38}$ або $\hat{d}_{39}$

The procedure for restoring the measurements of the failed sensor S_2 with the backup sensor S_{2R} located in the "cold" reserve corresponds to the procedure described in clause 5.3 for the sensor S_1. To implement this procedure, switches are used, which, based on the results of diagnostics of the sensor S_2 ($\hat{d}_{36}$, $\hat{d}_{38}$ or $\hat{d}_{39}$), isolate it from the control process and connect the backup sensor S_{2R}. The functional diagram (Figure 5.28) shows the composition of functional elements with the corresponding connections necessary to restore measurements of the failed sensor S_2.

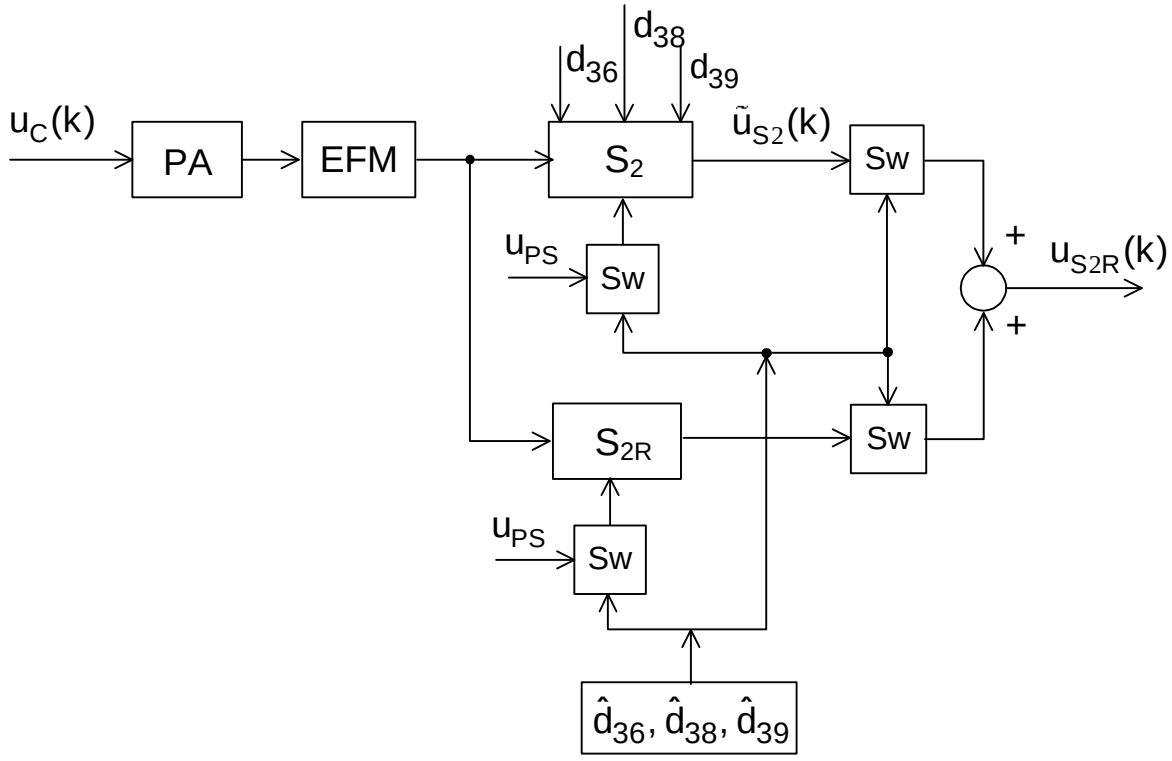

Figure 5.28 – Functional diagram of restoration of measurements of the current sensor with the help of a "cold" reserve

Let's consider one of the possible combinations of the described functional schemes for restoring measurements of the sensor S_2 (Figure 5.29).

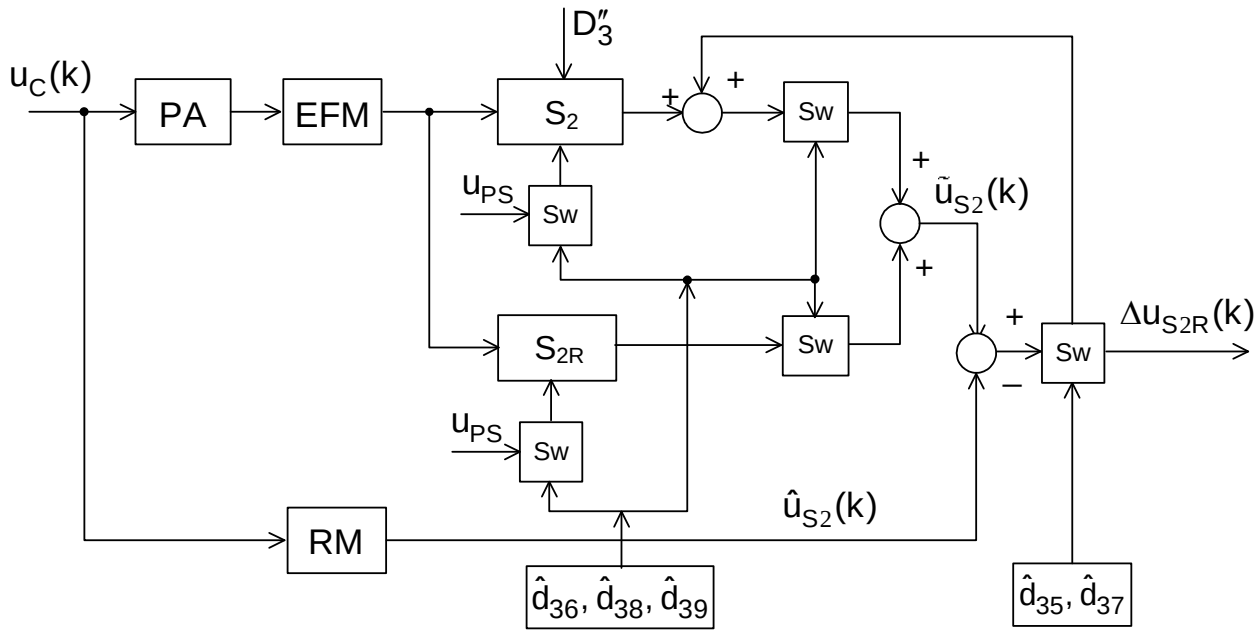

Figure 5.29 – Functional scheme of restoration of measurements S_2 according to the results of the diagnosis

In the presented functional scheme, two means of restoring measurements are used: ν_1 – signal tuning and ν_4 – reconfiguration of equipment using a "cold" reserve. Signal tuning is connected using the appropriate switches when kind of destabilization $\hat{d}_{35}$ and $\hat{d}_{37}$ are detected. The connection of the backup sensor D2 is carried out if the kinds of destabilization $\hat{d}_{36}$, $\hat{d}_{38}$ or $\hat{d}_{39}$ are detected as a result of diagnosis. At the same time, with the help of the appropriate switches, the main sensor S_2, which failed, is taken out of operation.

The procedure for restoring the measurement of the sensor of current ends when the repeated diagnostic procedure for the S_2 sensor confirms its operability. Otherwise, the procedure for resuming measurements is repeated until complete neutralization of destabilizing influences from the set D''_3 occurs.

So, all functional elements that are part of the rational control object, prone to specific kinds of destabilization, and the possibility of rehabilitating their functional properties with the help of restoration of operability have been considered. Summarizing the described procedures for restoring the functionality of functional elements, two obvious approaches can be distinguished. The first approach to recovery consists in parrying, neutralizing the consequences of destabilizing influences, rather than eliminating their

causes. This approach uses such means of recovery as signal and parametric adjustment, reconfiguration of equipment. The second approach to restoring operability is based on the principle of eliminating the causes of destabilization, that is, isolating an inoperable functional element by removing it from the process of controlling the kinetic moment vector of the spacecraft. In this whole approach, such means of recovery as reconfiguration of algorithms and reconfiguration of hardware are applicable.

The considered means of restoring the operability of functional elements do not exhaust the entire variety of possible means. Sources of diversity can be structural and functional features of functional elements, permissible levels of redundant software and hardware, goals of long-term spacecraft missions. The choice of recovery tools used in this section is due to the desire to show the fundamental possibility of autonomous and flexible real-time recovery with the help of algorithmic and hardware means of rational control of an electric flywheel motor.

Chapter VI EXPERIMENTAL STEND FOR THE RESEARCH OF THE MODEL UNIT OF ELECTRIC FLYWHEEL MOTORS

The properties of bodies are understood
in no other way than through tests.
Isaac Newton (1643-1727)
- English scientist, genius
physicist and mathematician

The experimental stend is a hardware and software complex designed for the study of models, methods and tools for the rational control of a model unit of electric flywheel motors. The experimental stend includes a model unit of electric flywheel motors, a rational control device and a laptop. The experimental stend allows to conduct research on a model block of electric flywheel motors in nominal operating modes, simulate types of destabilization from a given set, diagnose and restore performance based on the results of the diagnosis, using excess hardware and software resources.

6.1 Purpose and composition of the experimental stend

An experimental stend with a model unit of electric flywheel motors, designed at the Department of Aircraft Control Systems, provides such research:

1) simulation of unit movement in nominal and non-standard operating modes;
2) the setting of destabilizing influences to the functional elements of the unit;
3) diagnostics of the unit's operability with depth to the kind of destabilizing influence;
4) flexible restoration of unit performance using excess resources;
5) visualization of parameters and signals reflecting the state of the unit.

The experimental stend is a hardware and software complex consisting of the following structurally finished components:

1) unit of electric flywheel motors;
2) rational control device;
3) Dell inspiron 3582 laptop.

The general view of the stend is presented in Figure 6.1. To ensure angular movement in three degrees of freedom, the model unit of electric flywheel motors is placed in a cardan suspension, which is fixed on a platform that is adjustable in the horizontal plane.

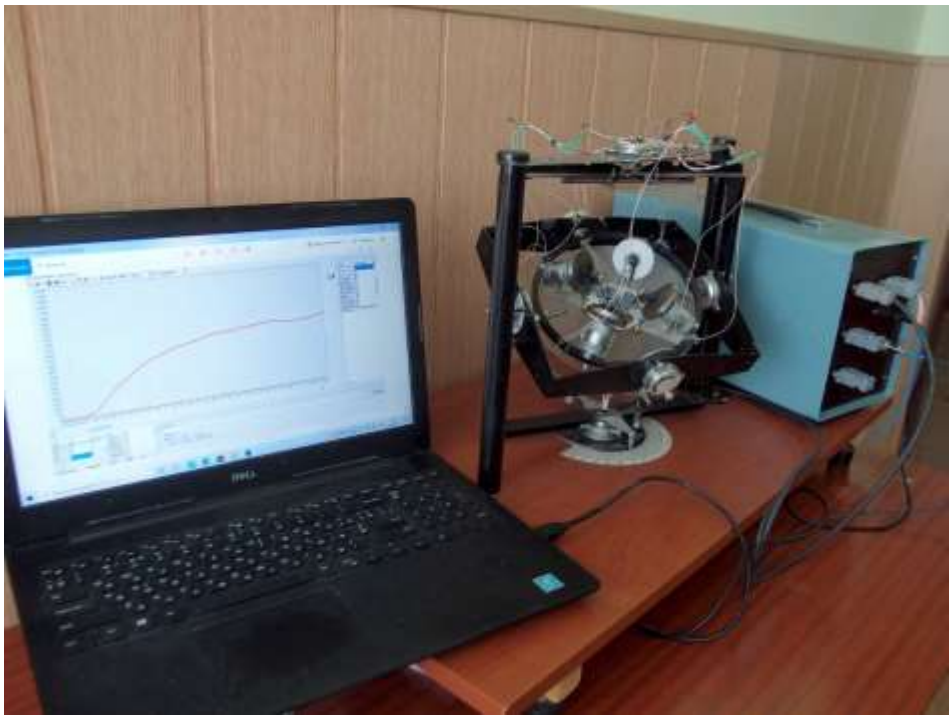

Figure 6.1 – General view of the experimental stend

Since the tensor of inertia of the model unit depends on the current angular position of the gimbal frames, to minimize this effect, the model is made in such a way that the axial moments of inertia of the gimbal frames are much less than the axial moments of inertia of the electric flywheel motor unit. This makes it possible to neglect the influence of changes in axial moments of inertia when considering movements characterized by slight angular deviations of the model unit from the zero position.

The total external moment applied to the model unit and gimbal suspension includes: moments of dry and viscous friction in the supports of the gimbal frames, gravitational moments caused by the inequality of the axial moments of inertia of the structure, as well as the displacement of the center of mass of the model relative to the point of intersection of the axes.

To reduce the influence of gravitational moments, the structure of the electric flywheel motors unit is designed in such a way that its axial moments of inertia are close to each other. In addition, mechanical means of its level adjustment in the horizontal plane are mounted in the platform. Preliminary balancing of the platform, on which the model unit of electric flywheel motors

is installed, allows to reduce the influence on the experiment of the displacement of the center of mass from the desired position.

A diagram with a pyramidal placement of electric flywheel actuators, consisting of four electric flywheel motors ($EFM_1 - EFM_4$), four tachometers of the angular speed of the flywheels ($TM_1 - TM_4$) and three sensors of the angular motion of the control object AS_x, AS_y, AS_z. is shown in Figure 6.2.

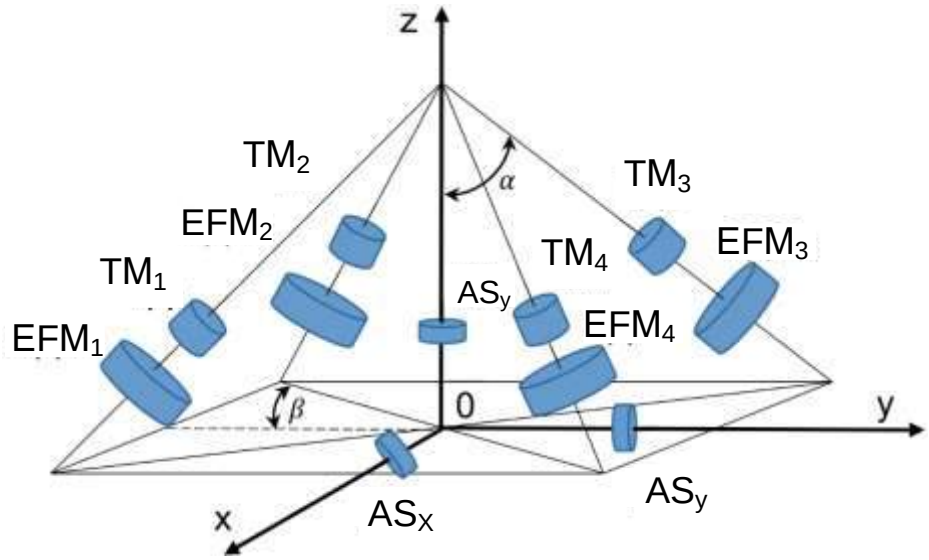

Figure 6.2 – Scheme of placement of electric motors-flywheels

Constructive placement of flywheel motors outside the regular pyramid at angles $\alpha = 60^\circ$ and $\beta = 45^\circ$, is such due to the fact that the intended spacecraft has the simplest spherical design for research purposes. The axis of symmetry of the installation diagram can be any axis of the related coordinate system. The angles α and β are chosen from the condition of equal efficiency of electric flywheel motors on all control channels of the spacecraft.

Кутові швидкості обертання електродвигунів-маховиків вимірюються за допомогою оптичних таходатчиків обертів ($TM_1 - TM_4$). The main elements of tachometers are an LED and a photodiode, between which discs with slots are installed. Disks are rigidly fixed on the shafts of electric flywheel motors. Each of the disks along the perimeter contains 50 through slots. This design of the tachometer makes it possible to generate 50 amplitude-normalized rectangular electric pulses for one revolution of the electric flywheel motor, which are further processed by the computational means of the rational control device. In addition, the tachometers additionally generate

potential signals at the logic "0" or logic "1" level, which identify the direction of rotation of the flywheels.

To control the angular position of the block with electric flywheel motors, potentiometric sensors are installed on the axes of the gimbal suspension frames AS_x, AS_y, AS_z.

In order to simulate operating conditions during experimental studies, hardware and software means of getting destabilizing influences are used. Due to the impossibility of physically simulating part of the operating conditions, most of them are implemented by software. At the same time, the measured and control signals of the unit of electric flywheel motors are distorted in such a way that the reaction to them is similar to the reaction to the receached types of destabilization.

The rational control device is based on a microcontroller (Figure 6.3).

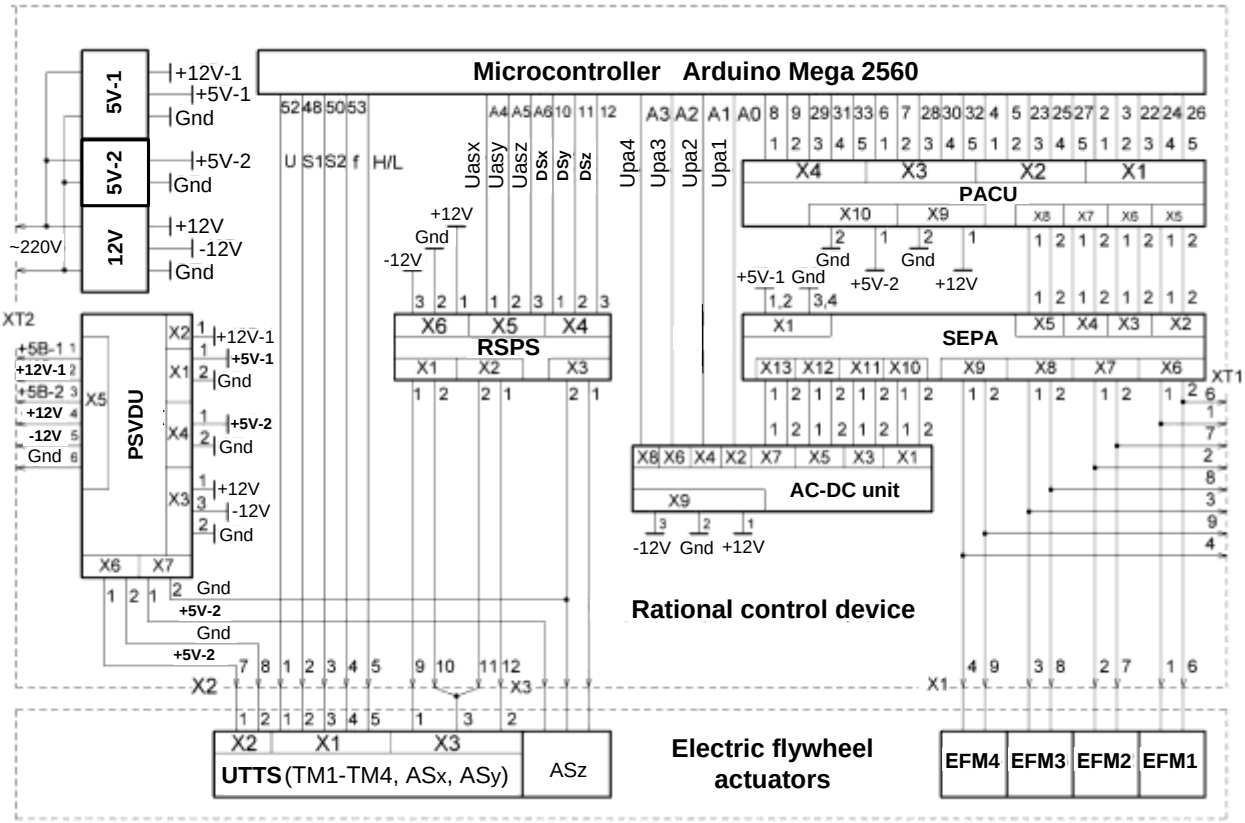

Figure 6.3 – General electrical scheme of the rational control device

RCD includes:

1) power amplifier control unit (PACU);

2) unit of switching elements of power amplifiers (SEPA);

3) unit for converting pulse of alternating voltage to direct one (AC-DC unit);

4) unit for receiving signals from potentiometric sensors (RSPS);

5) power supply unit (5V-1);

6) power supply unit (5V-2);

7) power supply unit (±12V);

8) power supply voltage distribution unit (PSVDU);

9) unit for pre-processing and transmission of tachometer signals (UTTS).

All electronic components (see Figure 6.3) included in the rational control device, except for UTTS, are placed in a single hardware module (Figure 6.4). The UTTS unit is placed in a cardan suspension at the bottom of the layout with electric flywheel motors.

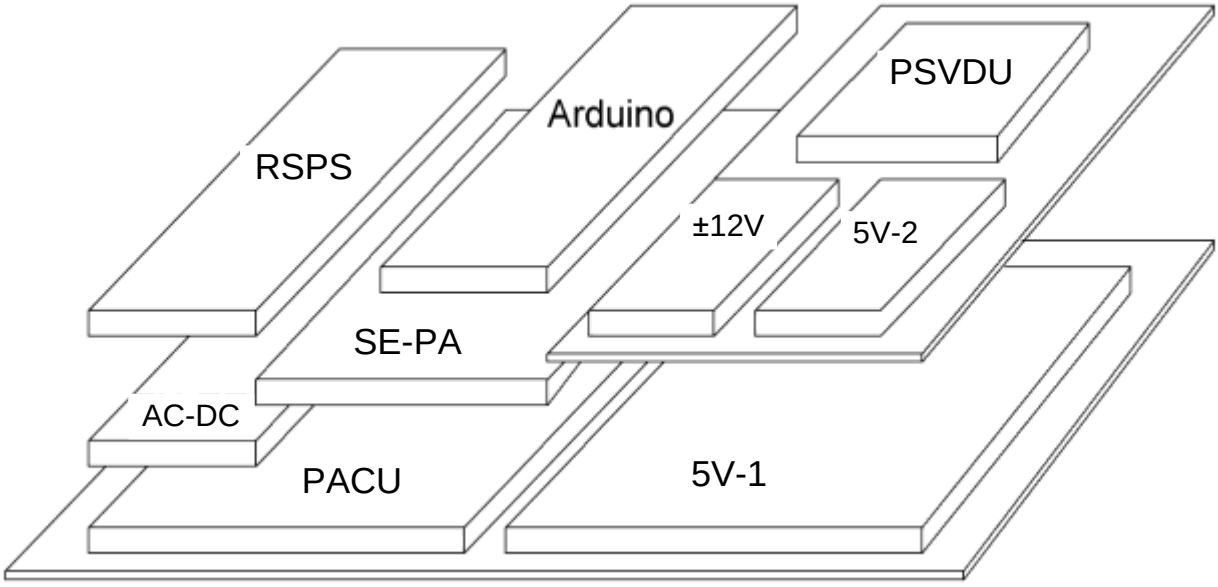

Figure 6.4 – Scheme of placing components in the rational control device

Two technological connectors XT1 and XT2 are provided in the rational control device to control the main electrical parameters of the block of electric flywheel motors by external standard measuring means. Control voltages for flywheel electric motors are controlled through the contacts of the XT1 connector ($EFM_1 - EFM_4$). The output voltages of secondary power sources "5V-1", "5V-2", "12V" are monitored through the contacts of the XT2 connector. Marker marks are placed on all flywheels to control the angular velocities of electric flywheel motors by external means of measurement (optical angular velocity meter of the DIGITAL TACHOMETER type).

The primary power supply of the automatic control device is the industrial network ~220V, 50Hz.

6.2 The model unit of electric flywheel motors

The appearance of the design of the model unit, its main dimensions and the dimensions of the component parts in two projections is shown in Figure 6.5.

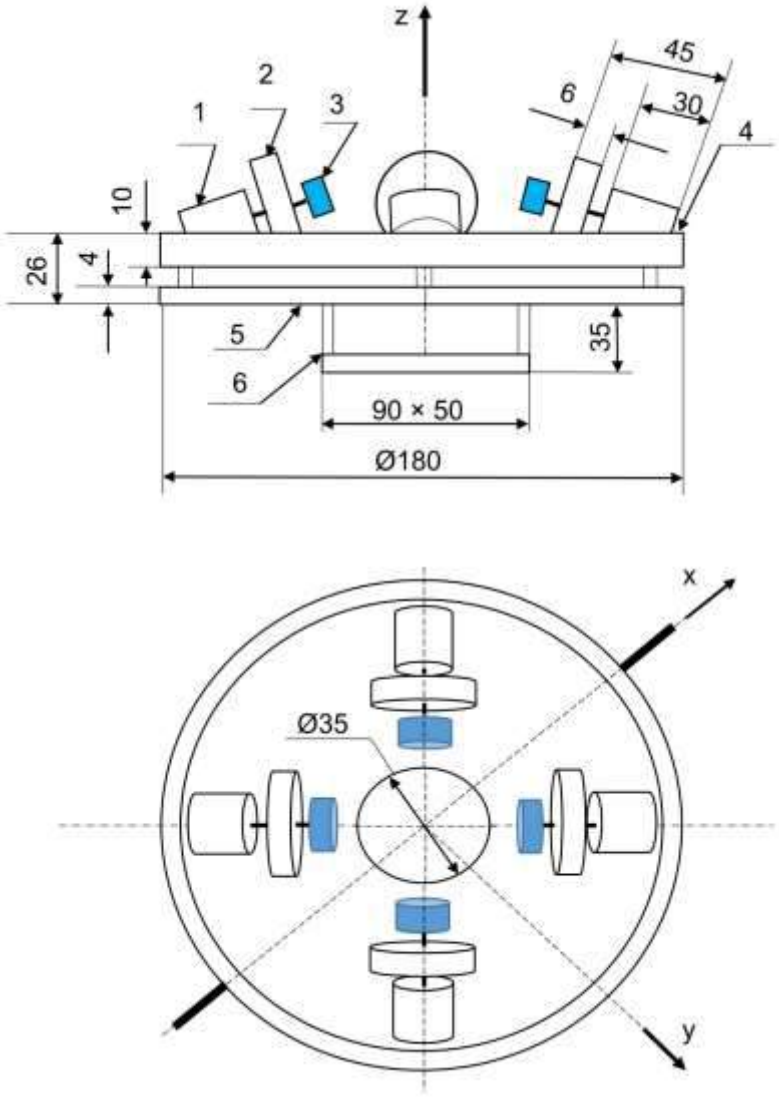

Figure 6.5 – View of the construction of the model unit of electric flywheel motors

The model unit includes: 1 – electric DC-motor; 2 – flywheel; 3 – tachometer; 4 – metal ring; 5 – flat disc; 6 – electronic unit for pre-processing and transmission of signals from tachometers (RSPS).

The ring (item 4) is made of a hollow rectangular aluminum alloy profile. The ring is the basic element of fastening of all structural parts and has supports for fastening the platform in the inner frame of the cardan suspension.

RS-280RA-2865 DC collector electric motors with an operating voltage (4.5–6.0) V and an angular speed of up to 1400 rad/s are used as executive elements (item 1) of the electric flywheel motor unit. The weight of one electric motor is 42 g.

Flywheels (item 2) are rigidly fixed on the shafts of electric motors, made of steel material with a diameter of 45 mm and a weight of 74 g each.

Tachometers (pos. 3) are also rigidly fixed on the shafts of electric motors. When evaluating the inertial characteristics of the model unit, the tachometers were not taken into account due to their insignificant mass and dimensions.

A flat disk (item 5) with an outer diameter of 180 mm and a hole in the center with a diameter of 5.5 mm, a thickness of 20 mm is made of plexiglass. In the related coordinate system of the model unit, the disk along the Oz axis is offset relative to the coordinate center by 20 mm. As part of the platform, the disk is the basis for fastening the block of electric motors-flywheels and the electronic block (item 5). The electronic unit (item 6) is a rectangular printed circuit board with installed radio elements, with overall dimensions: width 50 mm, length 90 mm, height 10 mm. The weight of the electronic unit is 34 g.

The outer frame of the rectangular-shaped gimbal has one degree of freedom and can perform angular movement only with respect to the Oz axis. The horizontal parts (upper and lower) of the outer frame are made of T-shaped aluminum alloy profile, and the vertical ones are made of U-shaped. Overall dimensions of horizontal parts 270 mm, vertical 280 mm. The total weight of the outer frame is 205 g.

The inner frame of a rectangular shape has two degrees of freedom and can perform angular movement with respect to the Oz and Oy axes. The frame is made of strips of sheet aluminum alloy with an average width of 40 mm and overall dimensions of 200 mm x 250 mm. The total weight of the inner frame is 194 g.

The moment of inertia relative to the axes of the associated coordinate system was estimated for each component part of the model unit individually, based on the geometric parameters of the component and the specific density of the material from which the component is made.

The moments of inertia of the model unit of electric flywheel motors with respect to each axis of the associated coordinate system consist of the sum of the moments of inertia of all component parts with respect to these axes.

The main technical characteristics of the model unit of electric flywheel motors:

1) mass of the unit, taking into account the frames of the cardan suspension:

$$m_x = 0{,}8\,\text{kg};\ m_y = 1{,}0\,\text{kg};\ m_z = 1{,}2\,\text{kg};$$

2) moments of inertia of the unit, taking into account the frames of the gimbal with respect to the axes of the gimbal:

$$I_x = 0.0017\ \text{kg}\cdot\text{m}^2;\ I_y = 0.003\ \text{kg}\cdot\text{m}^2;\ I_z = 0.009\ \text{kg}\cdot\text{m}^2;$$

3) axial moments of inertia of electric flywheel motors:

$$I_{M1} = I_{M2} = I_{M3} = I_{M4} = 0.000019\ \text{kg}\cdot\text{m}^2;$$

4) conversion factors of electric flywheel motors:

$$k_{FM} = [240; 260]\ \text{rad}/\text{V}\cdot\text{s};$$

5) time constants of electric flywheel motors:

$$T_{FM} = [1.5; 1.7]\ \text{s}.$$

A graphical representation of the experimentally obtained static and dynamic characteristics of the elements included to the unit of electric flywheel motors is shown in Figures 6.6–6.8.

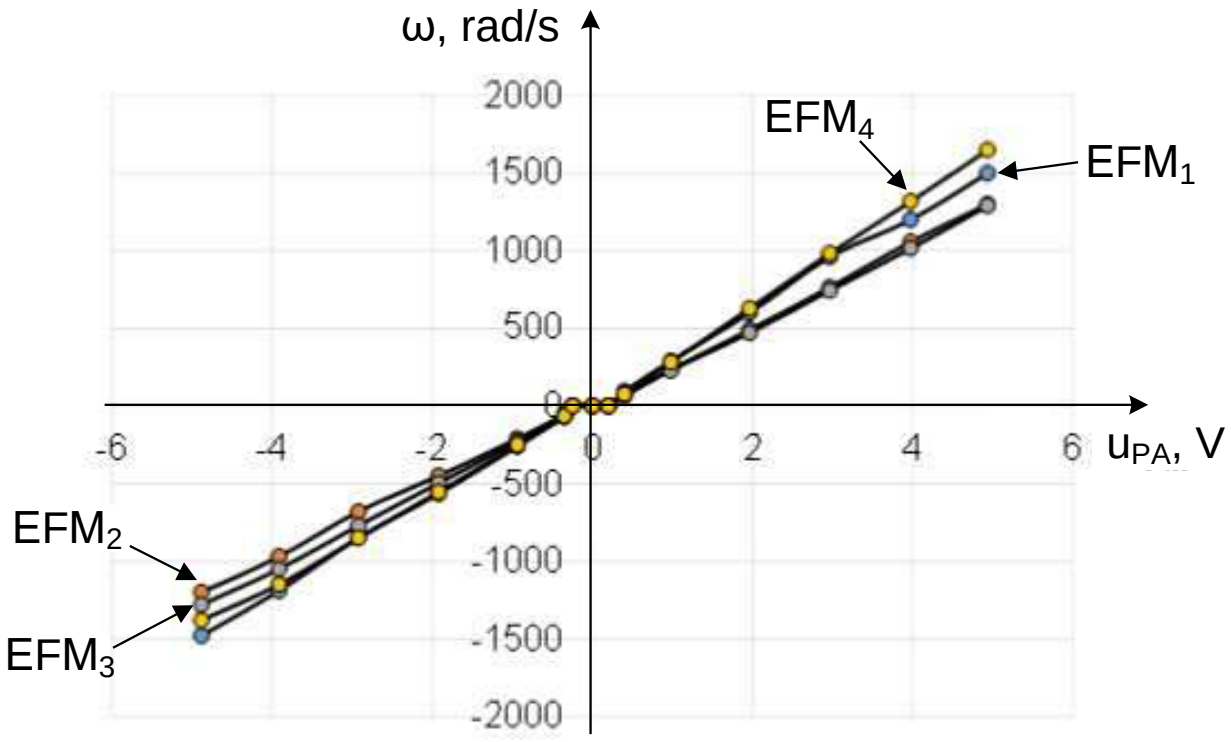

Figure 6.6 – Static characteristics of electric flywheel motors (EFM_1 – blue, EFM_2 – orange, EFM_3 – grey, EFM4 – yellow markers)

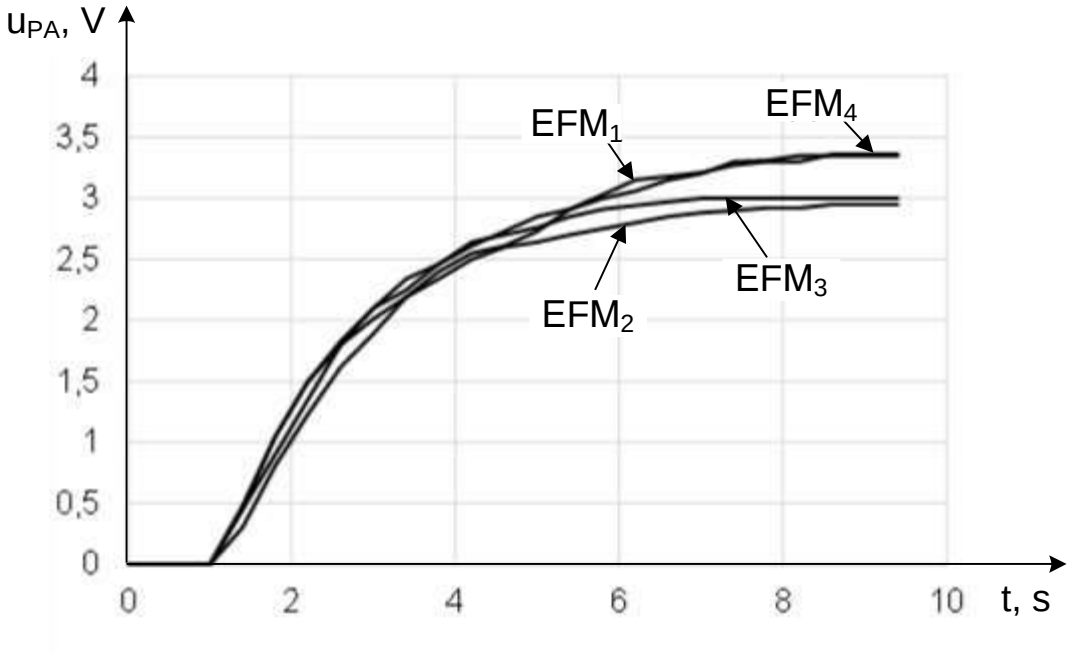

Figure 6.7 – Transient characteristics of electric flywheel motors

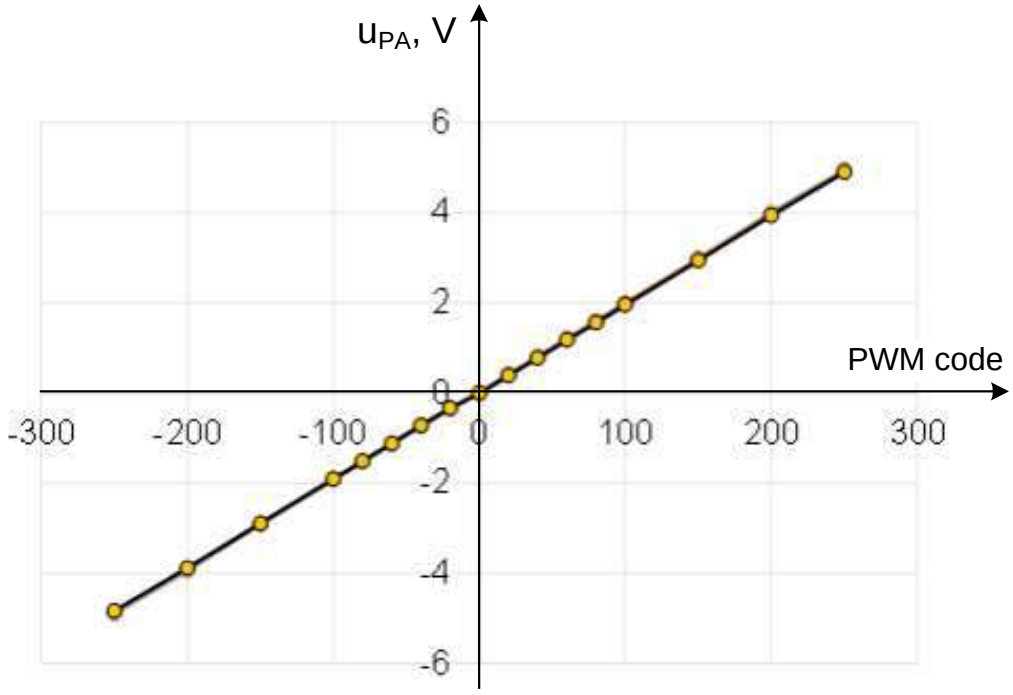

Figure 6.8 – Static characteristics of the power amplifier

Static characteristics of electric flywheel motors (see Figure 6.6) are obtained by two methods of measuring angular velocity:

1) using technical measurement tools built into the rational control device;

2) using a standard non-contact angular speed meter of the "DIGITAL TACHOMETR" type.

The static characteristics of electric flywheel motors, regardless of the measurement method, are practically linear. With positive and negative values of the control signal, the static characteristics are symmetrical with respect to the origin. The zone of insensitivity, within 0.2 V, of static characteristics on the abscissa axis is due to the presence of moments of dry and viscous friction on the shafts of electric motors, and corresponds to the magnitude of the contact voltage of electric motors-flywheels.

As a result of the processing of the obtained experimental data, it was possible to form linearized mathematical models of the functional elements of the model unit.

Attributes of the mathematical model of the EFM_1:

1) maximum linearization error

$$\delta_{max} = \frac{\Delta_{max}}{\Delta\omega_1} \cdot 100\% = 1.96\%;$$

2) coordinates of the working point (w.p.): {0;0};

3) range of linearization by voltage $u_1 \in \{-4.88; 4.93\}$; $\Delta u_1 = 9.81\,\text{B}$;

4) range of linearization by angular velocity

$$\omega_1 \in \{-1480; 1500\};\ \Delta\omega_1 = 2980\,\frac{\text{rad}}{\text{s}};$$

5) estimated parameter values

$$\hat{k}_{EFM1} = \frac{\Delta\omega_1}{\Delta u_1} = 304.6\,\frac{\text{rad}}{\text{V}\cdot\text{s}};\ \ \hat{T}_1 = 1.7\,\text{s};$$

6) transfer function $W_{EFM1}(s) = \dfrac{\Omega_1(s)}{U_1(s)} = \dfrac{\hat{k}_{EFM1}}{\hat{T}_1 s + 1}$;

7) time scale $m_t = 1$.

Attributes of the mathematical model of the EFM_2:

1) maximum linearization error

$$\delta_{max} = \frac{\Delta_{max}}{\Delta\omega_2} \cdot 100\% = 2.2\%;$$

2) coordinates of the working point (w. p.): {0; 0};

3) range of linearization by voltage

$$u_2 \in \{-4.62;\ 4.95\};\ \ \Delta u_2 = 9.57\,\text{V};$$

4) range of linearization by angular velocity

$$\omega_2 \in \{-1170;1300\};\ \ \Delta\omega_2 = 2470\,\frac{\text{rad}}{\text{s}};$$

5) estimated parameter values

$$\hat{k}_{EFM2} = \frac{\Delta\omega_2}{\Delta u_2} = 256.3\,\frac{\text{rad}}{\text{V}\cdot\text{s}};\ \ \hat{T}_2 = 1.6\,\text{s};$$

6) transfer function $W_{EFM2}(s) = \dfrac{\Omega_2(s)}{U_2(s)} = \dfrac{\hat{k}_{EFM2}}{\hat{T}_2 s + 1};$

7) time scale $m_t = 1$.

Attributes of the mathematical model of the EFM_3:

1) maximum linearization error

$$\delta_{max} = \frac{\Delta_{max}}{\Delta\omega_3}\cdot 100\% = 1.5\%;$$

2) coordinates of the working point (w.p.) {0; 0};
3) range of linearization by voltage

$$u_3 \in \{-4.88;4.95\};\ \ \Delta u_3 = 9.83\,\text{V};$$

4) range of linearization by angular velocity

$$\omega_3 \in \{-1287;1287\};\ \Delta\omega_3 = 257.4\,\frac{\text{rad}}{\text{s}};$$

5) estimated parameter values

$$\hat{k}_{EFM_3} = \frac{\Delta\omega_3}{\Delta u_3} = 259.2\,\frac{\text{rad}}{\text{V}\cdot\text{s}};\ \ \hat{T}_3 = 1.45\,\text{s};$$

6) transfer function $W_{EFM3}(s) = \dfrac{\Omega_3(s)}{U_3(s)} = \dfrac{\hat{k}_{EFM3}}{\hat{T}_3 s + 1};$

7) time scale $m_t = 1$.

Attributes of the mathematical model of the EFM_4:

1) maximum linearization error

$$\delta_{max} = \frac{\Delta_{max}}{\Delta\omega_4}\cdot 100\% = 4.1\%;$$

2) coordinates of the working point (w.p.): {0; 0};
3) range of linearization by voltage $u_4 \in \{-4.82;\ 4.9\};\ \Delta u_4 = 9.72\,\text{V};$
4) range of linearization by angular velocity

$$\omega_4 \in \{-1380;\ 1653\};\ \ \Delta\omega_4 = 303.3\,\frac{\text{rad}}{\text{s}};$$

5) estimated parameter values

$$\hat{k}_{\text{ЕДМ4}} = \frac{\Delta\omega_4}{\Delta u_4} = 311.7\,\frac{\text{rad}}{\text{V}\cdot\text{s}};\ \ \hat{T}_4 = 1.6\,\text{s};$$

6) transfer function $W_{EFM4}(s) = \dfrac{\Omega_4(s)}{U_4(s)} = \dfrac{\hat{k}_{EFM4}}{\hat{T}_4 s + 1}$;

7) time scale $m_t = 1$.

Attributes of the mathematical model of the PA_1:

1) maximum linearization error

$$\delta_{max} = \frac{\Delta_{max}}{\Delta u_1}\cdot 100\% = 0.48\%;$$

2) coordinates of the working point (w.p.): {0; 0};
3) range of linearization by voltage $u_1 \in \{-4.88; 4.93\}$; $\Delta u_1 = 9.81\,\text{V}$;
4) PWM linearization range: {-250; 250}; $\Delta = 500$;
5) estimated parameter value $\hat{k}_{PA1} = \dfrac{\Delta u_1}{\Delta} = 0.0196\,\text{V}$;
6) transfer function $W_{PA1}(s) = \dfrac{U_1(s)}{\Delta(s)} = \hat{k}_{PA1}$;
7) time scale $m_t = 1$.

Attributes of the mathematical model of the PA_2:

1) maximum linearization error

$$\delta_{max} = \frac{\Delta_{max}}{\Delta u_2}\cdot 100\% = 2.43\%;$$

2) coordinates of the working point (w.p.): {0; 0};
3) range of linearization by voltage $u_2 \in \{-4.62; 4.95\}$; $\Delta u_2 = 9.57\,\text{V}$;
4) PWM linearization range: {-250; 250}; $\Delta = 500$;
5) estimated parameter value $\hat{k}_{PA2} = \dfrac{\Delta u_2}{\Delta} = 0.0194\,\text{V}$;
6) transfer function

$$W_{PA2}(s) = \frac{U_2(s)}{\Delta(s)} = \hat{k}_{PA2};$$

7) time scale $m_t = 1$.

Attributes of the mathematical model of the PA_3:

1) maximum linearization error

$$\delta_{max} = \frac{\Delta_{max}}{\Delta u_3} \cdot 100\% = 0.63\%;$$

2) coordinates of the working point (w.p.): {0; 0};
3) range of linearization by voltage $u_3 \in \{-4.88; 4.95\}; \Delta u_3 = 9.83\,\text{B}$;
4) PWM linearization range: {-250;250}; $\Delta = 500$;
5) estimated parameter value $\hat{k}_{PA3} = \frac{\Delta u_3}{\Delta} = 0.0196\,\text{V}$;
6) transfer function

$$W_{PA3}(s) = \frac{U_3(s)}{\Delta(s)} = \hat{k}_{PA3};$$

7) time scale $m_t = 1$.

Attributes of the mathematical model of the PA_4:

1) maximum linearization error

$$\delta_{max} = \frac{\Delta_{max}}{\Delta u_4} \cdot 100\% = 0.0195\%;$$

2) coordinates of the working point (w.p.): {0; 0};
3) range of linearization by voltage $u_4 \in \{-4.82; 4.9\}$; $\Delta u_4 = 9.72\,\text{V}$;
4) PWM linearization range: {-250; 250} $\Delta = 500$;
5) estimated parameter value $\hat{k}_{PA4} = \frac{\Delta u_4}{\Delta} = 0.0195\,\text{V}$;
6) transfer function

$$W_{PA4}(s) = \frac{U_4(s)}{\Delta(s)} = \hat{k}_{PA4};$$

7) time scale $m_t = 1$.

6.3 A device for rational control of the model unit

The rational control device, which is part of the hardware and software complex, performs the functions of controlling the block's kinetic moment vector and maintaining the necessary operating mode of the electric flywheel motors unit in the presence of destabilizing influences. The functional composition of the device and built-in software tools allow to simulate various types of destabilization from a given set into the electric flywheel motors unit and investigate its behavior in the nominal and non-standard modes of

operation, form control influences, carry out flexible diagnostics and flexible restoration of the unit's operability.

The functional diagram of the hardware and software complex for experimental studies of the electric flywheel motor unit is shown in Figure 6.9.

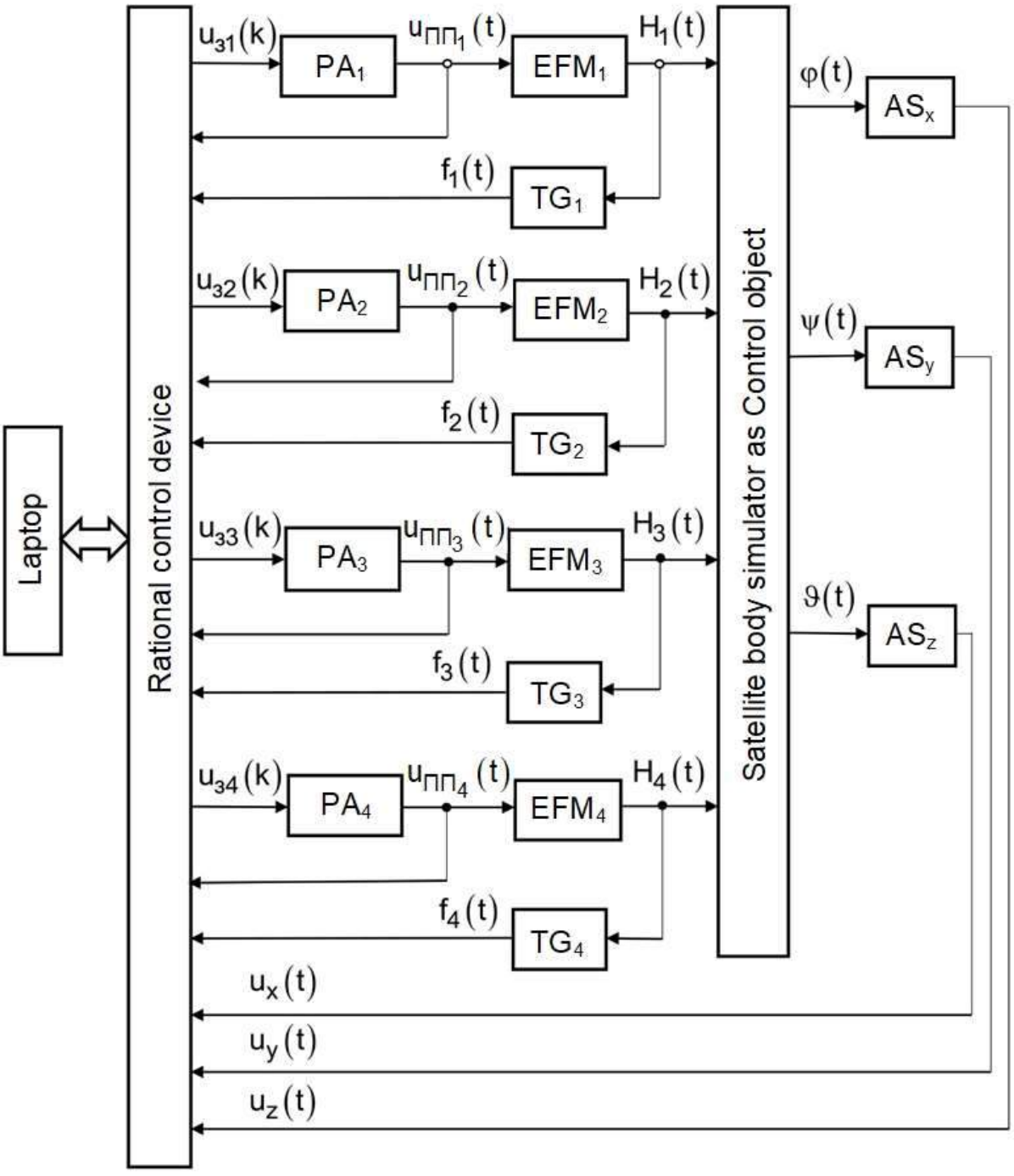

Figure 6.9 – Functional scheme of the hardware and software complex

EFM_1–EFM_4 – electric flywheel motors; TM_1–TM_4 – tachometers; AS_x, AS_y, AS_z, – sensors of the angular position of the control object relative to the

axes of the gimbal frames; $u_{з1}(k) - u_{з4}(k)$ – influences set at the inputs of power amplifiers ; $u_{PA1}(t) - u_{PA4}(t)$ – control voltages at the inputs of electric flywheel motors; $\omega_1(t) - \omega_4(t)$ – angular velocities of electric flywheel motors; $f_1(t) - f_4(t)$ – sequence of pulses at the outputs of tachometers; ϕ, ψ, ϑ – angular position of the gimbal frame; $u_x(t), u_y(t), u_z(t)$ – output voltages of angular position sensors.

The control object as part of the hardware and software complex is the structure shown in Figure 6.5, which is installed within the gimbal suspension and taking into account the moments of inertia of the gimbal suspension frames.

The laptop as part of the hardware and software complex performs dispatching functions: generation of output data for the operating modes of the electric flywheel motor unit, simulation of destabilization types, visualization and storage of the results of experimental studies.

The rational control device implements: control algorithms for the power amplifiers of the electric flywheel motor unit in nominal and non-standard modes of operation, the functions of converting analog signals into a digital code, generating control signals for executive mechanisms, and exchanging data with a personal computer. The rational control device is built on the base of single-chip microcontroller ATmega256 and implemented as Arduino Mega 2560 unit.

Information exchange between a personal computer and a smart control device is carried out via a USB channel.

The following microcontroller resources are used to implement control tasks and diagnose the current technical condition of the flywheel motor unit:

- 11 outputs of the formation of control signals with pulse width modulation;
- 16 inputs/outputs for receiving and issuing logical and digital signals;
- 7 ADC inputs for receiving analog signals with an amplitude from zero to 5 volts.

The distribution of microcontroller contacts in the rational control device according to purpose is given in Table 6.1.

The power supply of the rational control device and the electric flywheels motors unit is provided by three independent stabilized power supply units of the AC/DC type. The output voltage with an amplitude of 5V of the "5V-1" power supply unit provides power to the power switching elements of the

power amplifiers. Power supply unit "5V-2" of the GPA15A-05 type forms a stabilized voltage with an amplitude of 5V for powering a microcontroller, a control unit for power amplifiers, potentiometric sensors for the angular movement of an object and tachometers.

Table 6.1

Pin of Arduino	Designation, type of signal	Appointment in the rational control device
2	PWM1	$u_{з1}(k)$ – control signal of EFM1
3	PWM2	DP_{PA1} – destabilization of parameters of PA_1
4	PWM3	$u_{з2}(t)$ – control signal of EFM2
5	PWM4	DP_{PA2} – destabilization of parameters of PA_2
6	PWM5	$u_{з3}(t)$ – control signal of ЕДМ3
7	PWM6	DP_{PA3} – destabilization of parameters of PA_3
8	PWM7	$u_{з4}(t)$ – control signal of ЕДМ4
9	PWM8	DP_{PA4} – destabilization of parameters of PA_4
10	PWM9	DP_x – destabilization of parameters of AS_x
11	PWM10	DP_y – destabilization of parameters of AS_y
12	PWM11	DP_z – destabilization of parameters of AS_z
22	HIGH/LOW	B_{PA1} – power failure of the main PA_1
23	HIGH/LOW	B_{PA2} – power failure of the main PA_2
24	HIGH/LOW	T_{PAM1} – turn on power supply of main PA_1
25	HIGH/LOW	T_{PAM2} – turn on power supply of main PA_2
26	HIGH/LOW	T_{PAR1} – turn on power supply of reserve PA_1
27	HIGH/LOW	T_{PAR2} – turn on power supply of reserve PA_2
28	HIGH/LOW	B_{PA3} – power failure of the main PA_3
29	HIGH/LOW	B_{PA4} – power failure of the main PA_4
30	HIGH/LOW	T_{PAM3} – turn on power supply of main PA_3
31	HIGH/LOW	T_{PAM4} – turn on power supply of main PA_4
32	HIGH/LOW	T_{PAR3} – turn on power supply of reserve PA_3
33	HIGH/LOW	T_{PAR4} – turn on power supply of reserve PA_3
48	HIGH/LOW	AB1 – address bus of multiplexer UTTS

Continuation of Table 6.1

Pin of Arduino	Designation, type of signal	Appointment in the rational control device
50	MISO	AB2 – address bus of multiplexer UTTS
52	SOK	U – allowing operation of multiplexer UTTS
53	SS	Output A(MUX) – angular velocity of EFM_1 (EFM_2, EFM_3, EFM_4)
A0	ADC0	$u_{PA1}(t)$ – output voltage of PA_1
A1	ADC1	$u_{PA2}(t)$ – output voltage of PA_2
A2	ADC2	$u_{PA3}(t)$ – output voltage of PA_3
A3	ADC3	$u_{PA4}(t)$ – output voltage of PA_4
A4	ADC4	u_{ASx} – output voltage of sensor AS_x
A5	ADC5	u_{ASy} – output voltage of sensor AS_y
A6	ADC6	u_{ASz} – output voltage of sensor AS_z

The power supply unit "± 12" of type FLA17A-05 forms two outputs with a common point of stabilized voltage +12V and -12V, which are used to power the operational amplifiers in the "AC-DC", "RSPS" units and only +12V to power the output circuits with an open collector of the power amplifier control unit.

Control of the output voltage of the listed power supply units by external standard means of measurement is available through the technological connector XT2.

The implementation of the control algorithms of electric flywheel motors and simulation of the destabilization of functional elements included in the block of electric motor-flywheels is explained by the detailed functional scheme of the rational control device shown in Figure 6.10.

The set of PACU and SEPA blocks in the rational control device are represented by control power amplifiers. The formation of the control voltage $u_{PA}(t)$ at the inputs of electric flywheel motors and the modeling of abnormal modes of operation is implemented by the PACU and SEPA blocks using the following control signals of the Arduino microcontroller:

1) $u_{31}(t)...u_{34}(t)$ – 8-bit width-modulated reference signals with a frequency of 1 kHz for the formation of control voltages $u_{PA1}(t)...u_{PA4}(t)$;

2) $DP_{PA1}...DP_{PA4}$ – 8-bit width-modulated signals with a frequency of 1 kHz for modeling the destabilization of power amplifier parameters;

3) $T_{PAM1}...T_{PAM4}$ – potential signals of the "Log1" or "Log0" level to turn on or off the main power amplifiers;

4) $B_{PAM1}...B_{PAM4}$ – potential signals of the "Log1" level for simulating an unauthorized power-off of the main power amplifiers;

5) $T_{PAR1}...T_{PAR4}$ – potential signals of logic "1" or logic "0" level for simulating power on or off power amplifiers.

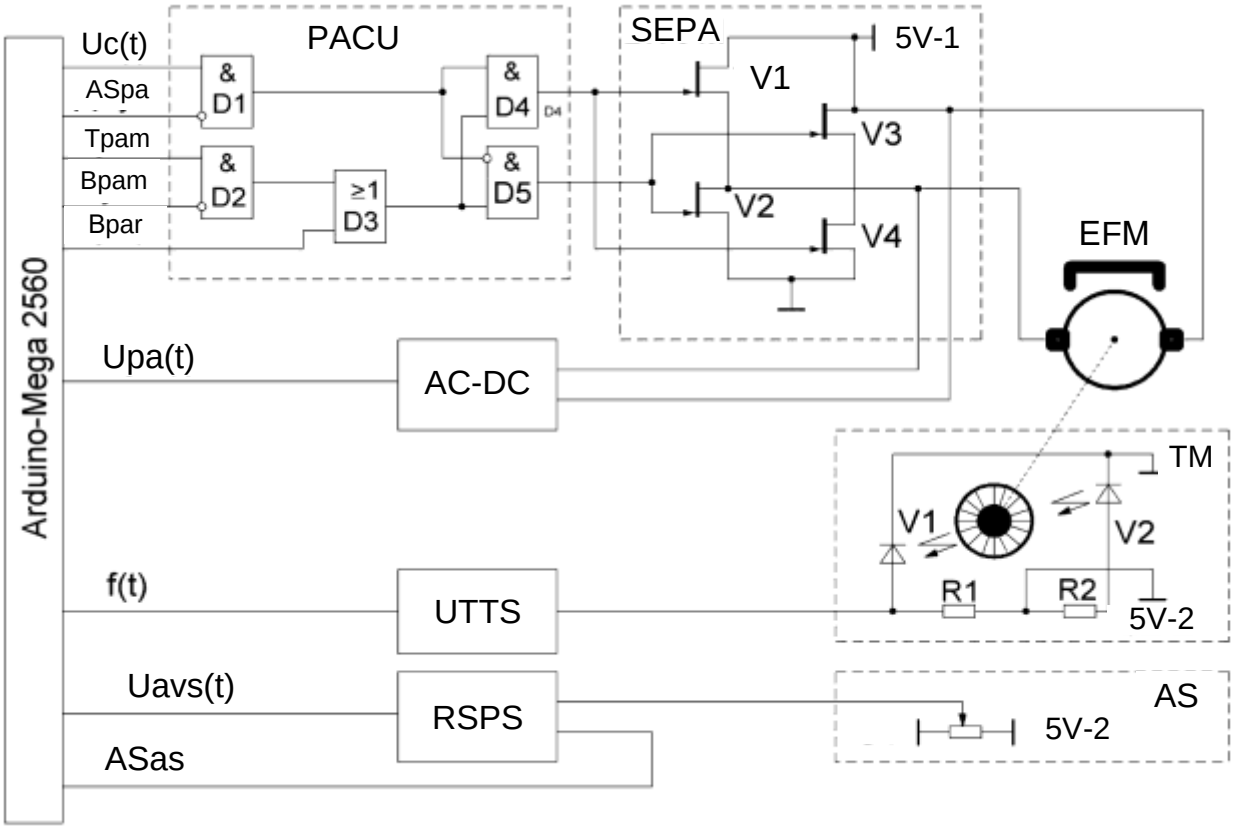

Figure 6.10 – Expanded functional scheme of one channel of the rational control device

The control of electric flywheel motors in the nominal mode of operation, according to the functional scheme (see Figure 6.10) and the cyclogram of the formation of the control voltage (Figure 6.11), is performed as follows.

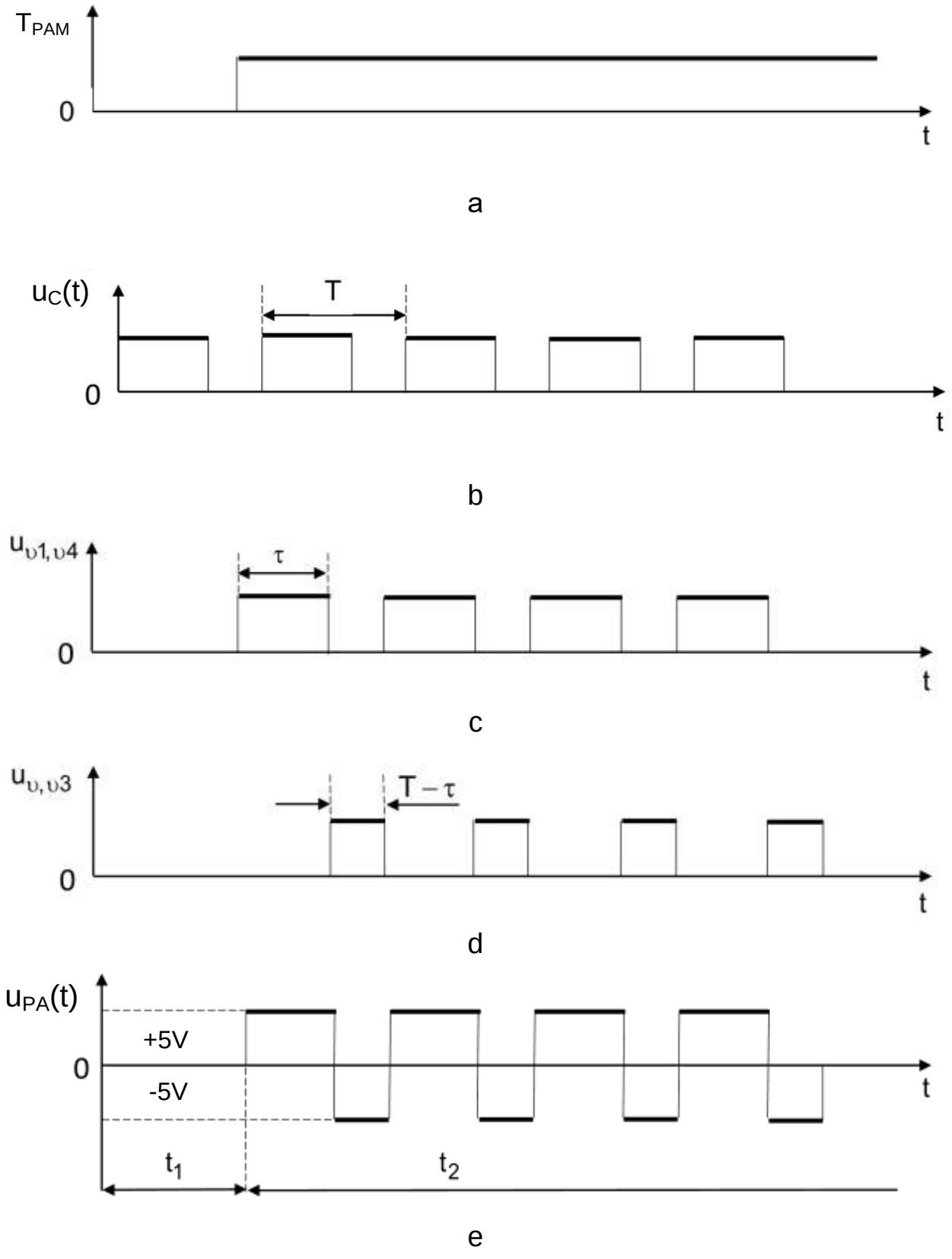

Figure 6.11 – Cyclogram of the standard control mode of electric flywheel motors

When a signal $u_3(t)$ (see Figure 6.11, b) is applied to the direct input of the logic element D1 in the form of a sequence of pulses with a duration of τ, a period of T and the presence of a potential signal T_{PAM} (see Figure 6.11, a) at the direct input of the element D2 with a level of "Log0" (switching on the power of the main power amplifier) control signals $u_{v1,v4}$ and $u_{v2,v3}$ (see Figure 6.11, c, d) do not arrive at elements V1, V4 and V2, V3 of the SEPA power switches within the time interval, and the output voltage of the power amplifier (see Figure 6.11, e) is zero.

The T_{PAM} signal of the "Log1" level simulates the power-on of the main power amplifier, as a result of which a sequence of pulses of duration $\tau = n\Delta t$, with period T, discreteness $\Delta t = T/N$, N=255 (see Figure 6.11, c) is formed at the output of element D4, in the interval , and at the output element D5 – a sequence of pulses with a duration of $T - \tau = (N - n)\Delta t$ (see Figure 6.11, d). At the same time, the output signal of element D4 with duration τ is supplied to the control inputs of switching elements V1, V4, and the output signal of element D5 with duration $(T - \tau)$ – to the control inputs of switching elements V2, V3.

With such a power amplifier control procedure, a pulse voltage $u_{PA}(t)$ (see Figure 6.11, e) of variable amplitude equal to the output voltage of the stabilized power supply "5V-1" with a "plus" sign is formed at the input of the electric motor-flywheel within the period T interval τ and "minus" in the interval $T - \tau$. The resulting value of the control voltage $u_{PA}(t)$ is determined by the following dependence on the parameters of the PWM signal $u_3(t) = \tau = n\Delta t$:

$$u_{PA}(t) = \frac{(2n - N)u_{PS}}{N};\ N = 255;\ n = \overline{1,N};\ u_{PS} = 5\ V, \qquad (6.3)$$

where u_{PS} – output voltage of the stabilized source «5V-1»;

$\frac{u_{PS}}{n}$ – conversion factor of the power amplifier;

N – the maximum value of the PWM signal code $u_G(t)$.

The parameters of the signal $u_G(t)$ specified for the formation of the required value of the output voltage of the power amplifier by the software of the Arduino microcontroller are calculated according to the formula

$$n = \frac{(u_G(t) + N)}{2}. \qquad (6.4)$$

The time interval t_2 reflects the regular mode of operation of the power amplifier.

Modeling of destabilization of the type "supply voltage break" at the input of the power amplifier is explained by the cyclogram shown in Figure 6.12.

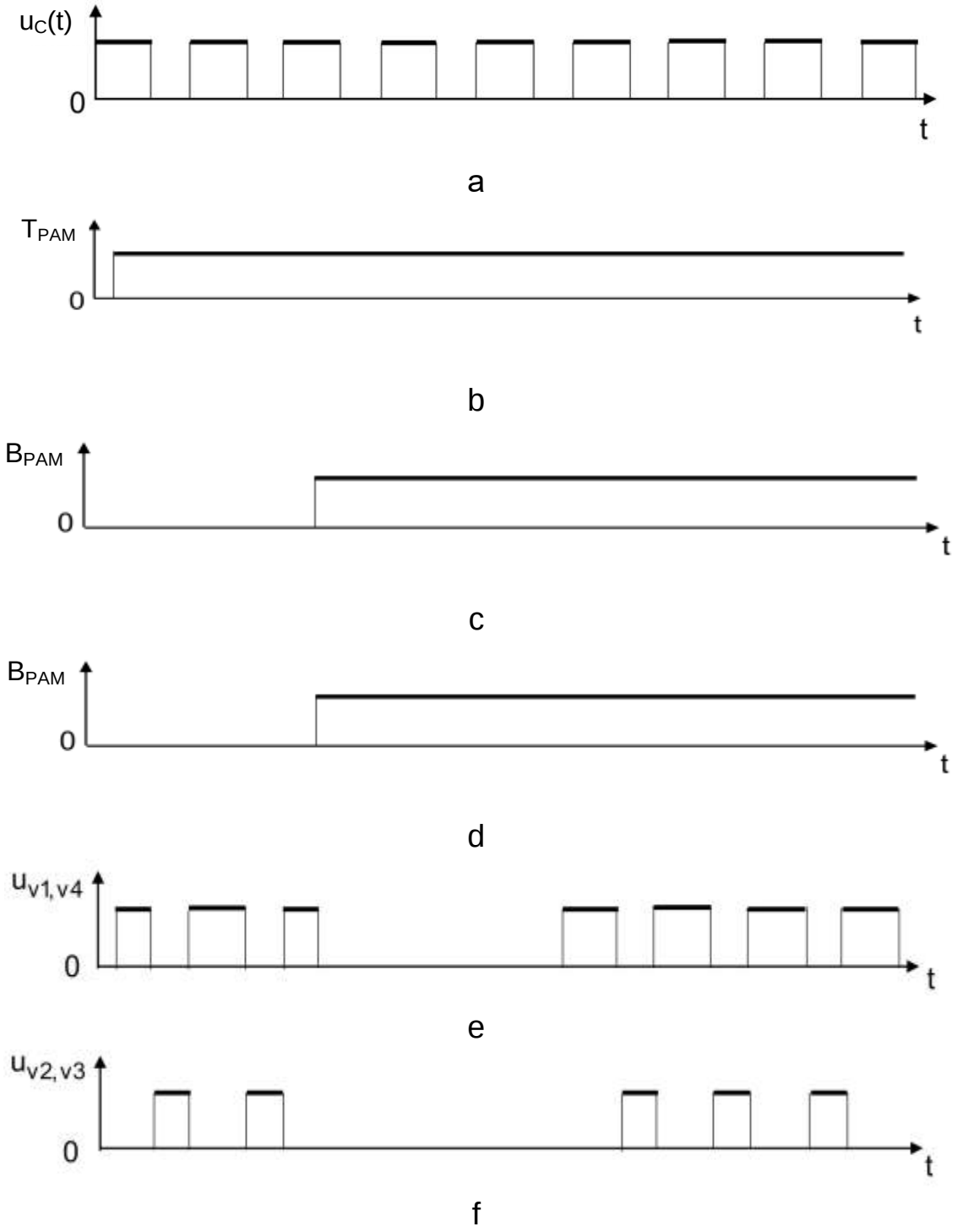

Figure 6.12 – Cyclogram of simulation of destabilization of the type "supply voltage break" at the input of the power amplifier

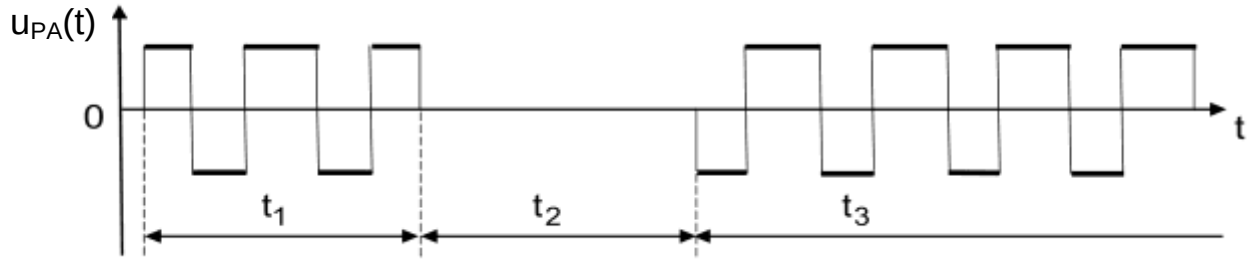

g
Figure 6.12, page 2

Imitation of the type of "break in the supply voltage" at the input of the main power amplifier is simulated by the potential signal B_{PAM} (disconnecting the main power supply), which comes from the Arduino microcontroller to the input of the SEPA.

If there is a potential T_{PAM} signal of the "Log1" level at the direct input of the element D2 and a potential B_{PAM} signal of the "Log0" level at the inverse input D2 according to the parameters of the set signal $u_G(t)$ entering the direct input of the element D1, the control signals $u_{V1,V4}$ and $u_{V2,V3}$ of the switching elements V1, V4 and V2, V3 respectively are formed by the SEPA unit.

Such a combination of control signals at the input of the SEPA ensures the formation of the output alternating sign pulse voltage $u_{PA}(t)$ of the power amplifier in the normal mode of operation, the interval t_1 in Figure 6.12.

When the level of the B_{PAM} potential signal changes from "Log0" to "Log1", the D2 element blocks the switching of the T_{PAM} command, the switching of the command to turn on the power of the main power amplifier, the control signals to the inputs of the switching elements in V1–V4 are not received, the output voltage $u_{PA}(t)$ of the power amplifier is zero. A fragment of the simulation "break of the supply voltage of the main power amplifier" is given on the time interval t_2, in Figure 6.12.

The restoration of the power amplifier's operability is carried out by the potential signal T_{PAR} (switching on the standby (reserve) power amplifier) of the "Log1" level at the input of element D3. A fragment of the simulation of the inclusion and operation of the standby power amplifier is given on the time interval t_3 in Figure 6.12.

A graphic representation of the processes of modeling the destabilization of power amplifier parameters is explained by the cyclogram shown in Figure

6.13. In the interval, the power amplifier functions in normal mode, the parameters $u_{V1,V4}$ and $u_{V2,V3}$ (Figure 6.13, d, e) of the control of the switching elements V1, V4 and V2, V3 correspond to the signal of the microcontroller, which is specified, the specified output voltage is formed by the power amplifier

$$u_{PA}(t) = \frac{(2n - N)u_{PA}}{N} \tag{6.5}$$

sign-changing amplitude (Figure 6.13, e).

The destabilization of the power amplifier parameters is modeled by the DP_{PA} signal in the form of a sequence of pulses of duration $\tau_1 = m\Delta t$ (Figure 6.13, c) with a transit period of T, which are received at the inverse input of element D1 of the SEPA unit (see Figure 6.10). At the same time, for switching elements V1, V4, the SEPA block, the duration of control signals $u_{V1,V4}$ will be equal to $\tau - \tau_1 = (n - m)\Delta t$, and for elements V2, V3, the duration of control signals $u_{V2,V3}$ will be equal to $(T - \tau + \tau_1) = (N - n + m)\Delta t$. A fragment of the time interval t_2 (Figure 6.13 a, b, c, d, e, f) reflects the destabilization mode of the power amplifier parameters.

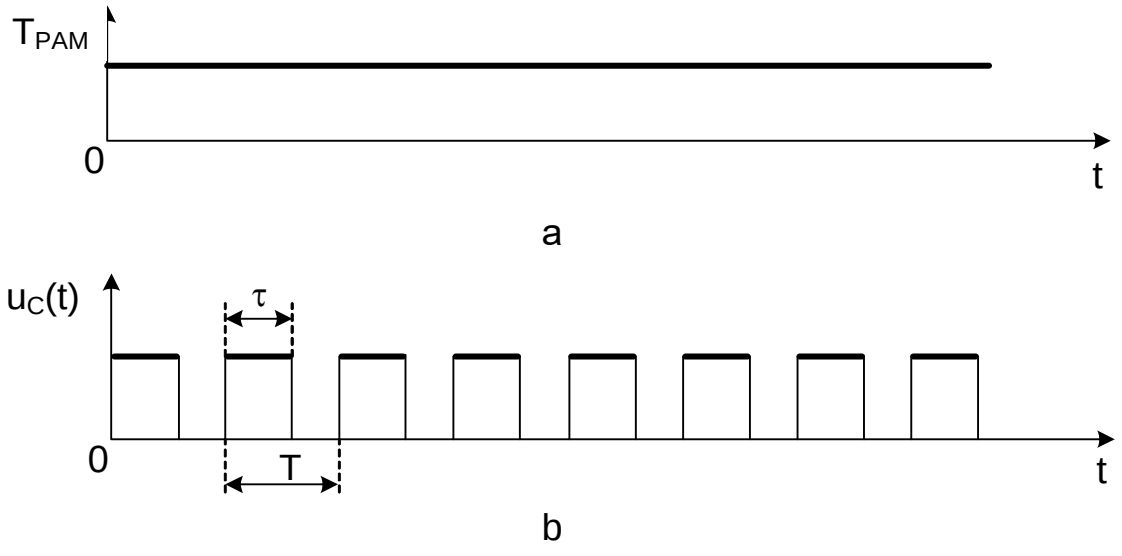

Fugure 6.13 – Cyclogram of simulation of destabilization of power amplifier parameters

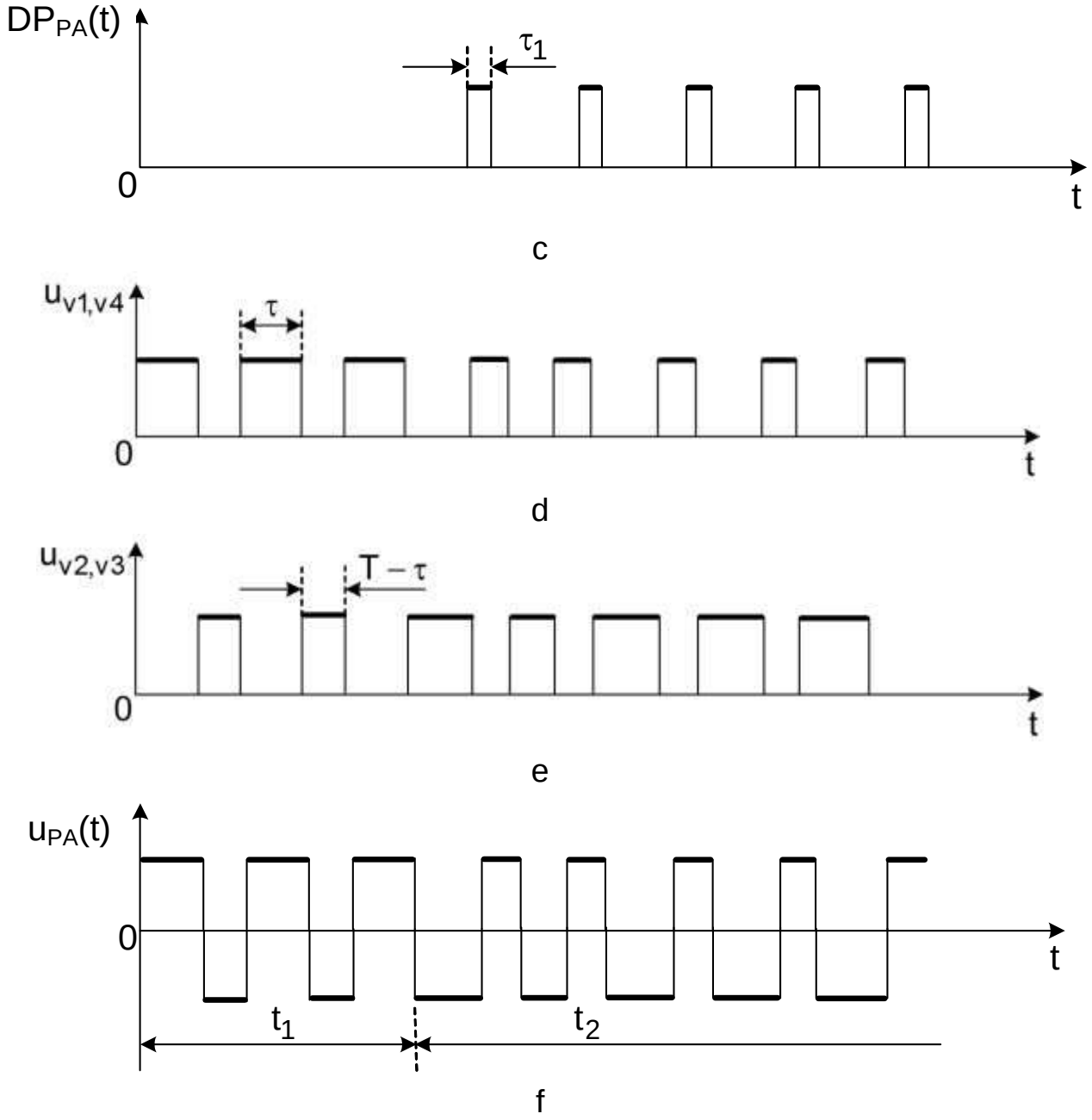

Figure 6.13, page 2

The output voltage of the power amplifier when simulating the destabilization of the conversion factor is determined by the following dependence on the parameters n and m:

$$u_{PA}(t) = \frac{\left[2(n-m)-N\right]u_{PS}}{N};\ \ n=\overline{1,N};\ \ m=\overline{1,N}. \qquad (6.6)$$

The value of the destabilized conversion factor of the power amplifier is calculated from the ratio

$$\frac{u_{PA}(t)}{\tilde{u}_{PA}(t)} = \frac{k_{PA}}{\tilde{k}_{PA}}; \quad \tilde{k}_{\Pi\Pi} = \frac{k_{PA}\left[2(n-m)-N\right]}{2n-N}, \tag{6.7}$$

where $\tilde{k}_{PA}$ – destabilized conversion factor.

The numerical value m corresponding to the given destabilization value is calculated according to the following formula:

$$m = \left[2n\left(k_{PA} - \tilde{k}_{PA}\right) + N\left(\tilde{k}_{PA} - k_{PA}\right)\right] \Big/ 2k_{PA}. \tag{6.8}$$

DP_{PA} pulse sequence, limited in duration with appropriate parameters, allows to simulate the displacement of the static characteristic of the power amplifier.

The AC-DC unit, which is part of the rational control device, is used to measure and control the output pulse alternating voltage $u_{PA}(t)$ of the power amplifiers during the operation of the flywheel electric motor unit. A fragment of the basic electrical circuit for one channel of AC-DC unit is shown in Figure 6.14.

The built-in analog-to-digital converter in the Arduino microcontroller allows you to measure only unipolar positive signals within range of (0–5)V. To measure the voltage at the outputs of the power amplifiers, in the AC-DC unit the alternating voltage with an amplitude of 10V is converted into a proportional unipolar within (0-5)V.

The circuit diagram is based on operational amplifiers, the supply voltage of which comes from a stabilized power supply unit “±12 V”.

A variable-sign pulse voltage with an amplitude from -5V to +5V is received at the input of the block. The integrator, made on the basis of the operational amplifier D1 and the RC circuit (R5, C1), converts the pulse voltage into a constant one, which varies within the same limits - from -5 to +5 V. Then, the output voltage from the integrator through the repeater D2.1 is sent to the input of the divider D2.2, which is limited in amplitude to 5 V. The operational amplifier and resistors R8, R9 shift the operating point of the element D2.4 in such a way that when changing from -5V to +5V, the voltage at the output of D2.4 changes from zero to +5V.

Experimentally obtained dependence of $u_{PA}(t)$ on the ADC code

$$u_{PA}(t) = (\text{ADC code}) \cdot 0{,}01468\,\text{B} - 7{,}45\,\text{V}. \tag{6.9}$$

The ADC code varies within the range $\overline{1{,}1024}$.

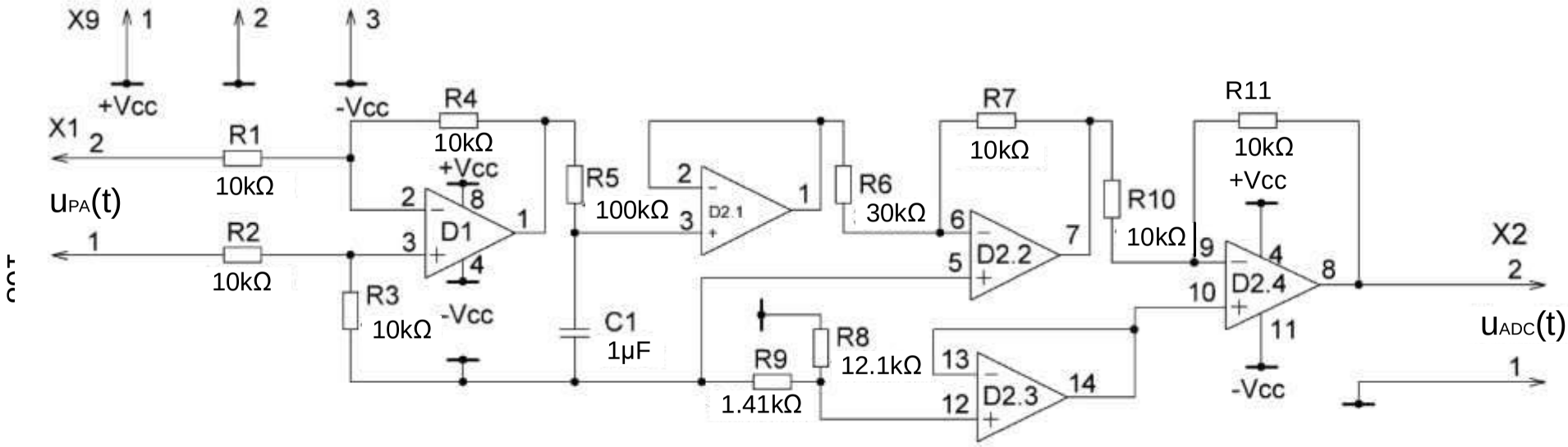

Fugure 6.14 – A fragment of the schematic diagram of the block for the conversion of pulsed alternating voltage $u_{PA}(t)$ into a unipolar voltage

The sensor for measuring the angular speed of the electric flywheel motor on the functional diagram (see Figure 6.10) is marked with the abbreviation TM. The schematic diagram of the electric sensor is shown in Figure 6.15.

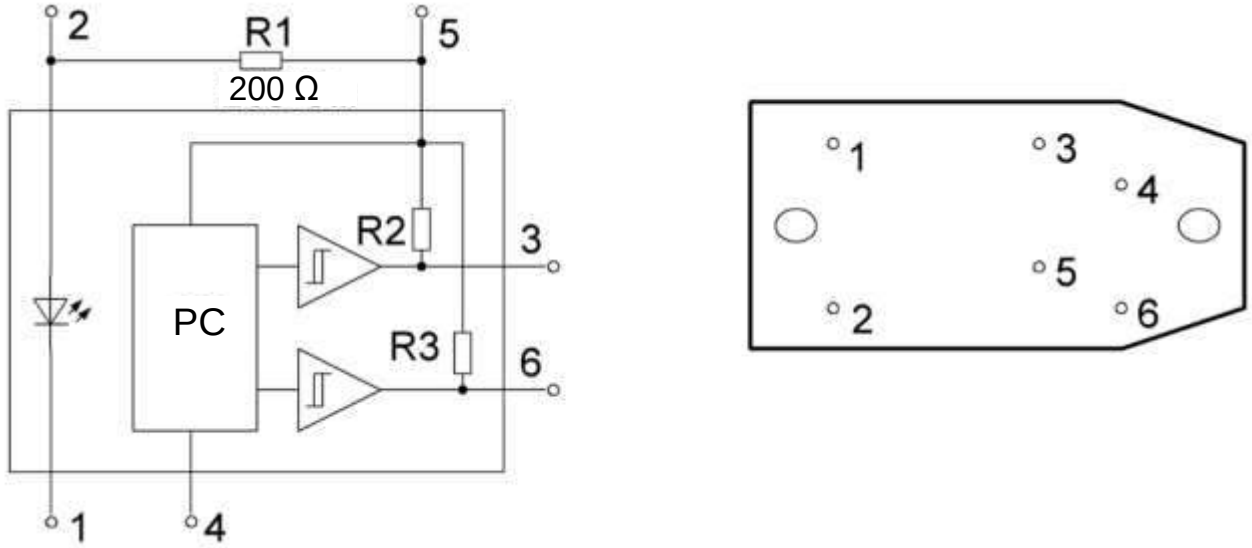

Fugure 6.15 – Schematic diagram of an infrared sensor for measuring the angular velocity of electric flywheel motors

Призначення контактів: 1 – катод; 2 – анод; 3 – вихід А; 4 – GND; 5 – Vcc; 6 – вихід В.

The supply voltage of the sensor comes from a stabilized 5V-2 power supply unit. A sequence of pulses proportional to the angular speed of the electric flywheel motor is formed at the output "A". A potential signal "Log0" or "Log1" is set at output "B" according to the direction of rotation of the electric flywheel motor.

The rational control device can simultaneously measure the angular velocity of only one electric motor. Measurement of the angular velocities of electric motors is performed sequentially as follows. At the inputs of the multiplexer installed in the UTTS block, frequency and potential signals proportional to the angular velocities and the direction of rotation of the electric motors are simultaneously received from the infrared sensors measuring the angular velocity. The selection of the measured electric motor velocity is set by the address bus S1, S2 of the multiplexer:

S1 = 0, S2 = 0 – angular velocity measurement of EFM1;

S1 = 1, S2 = 0 – angular velocity measurement of EFM 2;

S1 = 0, S2 = 1 – angular velocity measurement of EFM 3;

S1 = 1, S2 = 1 – angular velocity measurement of EFM 4.

The block for receiving signals from potentiometric sensors (RSPS) implements the functions of receiving analog signals from the angular position sensors AS_X, AS_Y, AS_Z of the gimbal frame with subsequent translation of these signals to the ADC inputs of the Arduino microcontroller. Modeling of destabilization of sensor parameters is performed by shifting their static characteristics. The RSPS unit consists of three independent channels made according to the analog adder circuit (Figure 6.16).

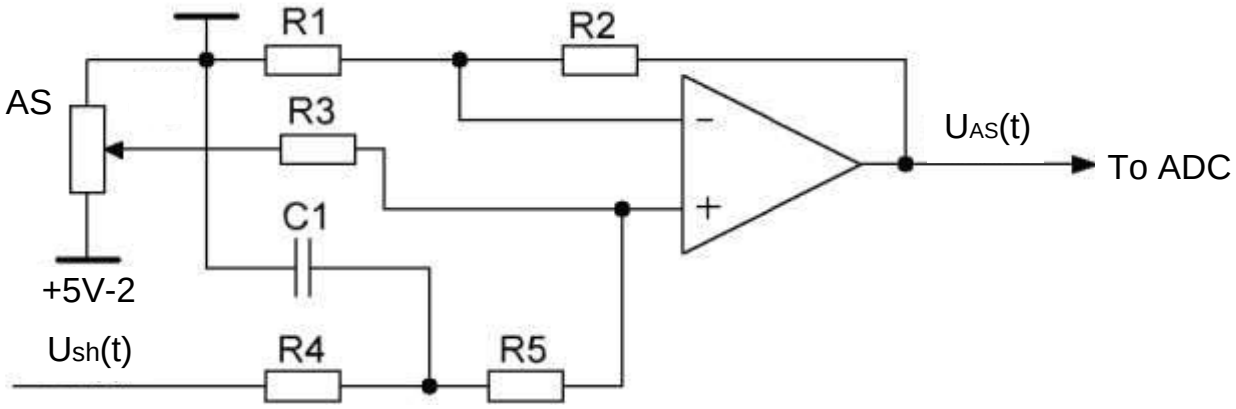

Fugure 6.16 – Basic circuit diagram of one channel of RSPS

The direct input of the operational amplifier receives voltage from the potentiometer angle sensor (AS), which corresponds to the angular position of the gimbal frame. In the absence of the $u_{sh}(t)$ signal (displacement voltage of the static characteristic), the voltage from the output of the potentiometer sensor enters the input of the ADC with a transfer coefficient equal to 1. Simulation of the destabilization of the parameters of the potentiometric sensors is implemented by applying a PWM signal to the $u_{sh}(t)$ input, which is converted to a appropriate level of voltage by the integrator (R4, C1) and determines the amount of displacement of the static characteristic.

6.4 Control of the experimental stend

The principle of control of the electric flywheel system of orientation and stabilization is based on the law of conservation of the momentum of the mechanical system, which is a certain mass of the cardan suspension and the inertial mass of the rotating flywheel. According to this law for a uniaxial flywheel system $K + H = 0$, where: $K = I\omega$ – kinetic moment of the control object; $H = I_m\omega_m$ –kinetic moment of the flywheel; I and I_m – moments of

inertia of the control object and the flywheel; ω and ω_m – angular velocities of the control object and the flywheel.

The movement of the control object under the action of the control moment created by the electric flywheel motor and in the absence of disturbing moments is described by the equation

$$I\frac{d^2\varphi}{dt^2} = -\frac{dH}{dt}. \qquad (6.10)$$

For an experimental stend with the placement of electric flywheel motors outside the regular pyramid, the control moments relative to the axes of the related coordinate system are described by the system of equations

$$M_x \sin\alpha \sin\beta \sum_{i=1}^{4}\frac{dH_i}{dt}; M_y = \sin\alpha\cos\beta\sum_{i=1}^{4}\frac{dH_i}{dt}; M_z = \cos\alpha\sum_{i=1}^{4}\frac{dH_i}{dt}. \quad (6.11)$$

The magnitudes of the control moment and angular displacement relative to a given axis are provided by the selected combination of directions of the vectors of kinetic moments.

When setting vectors of kinetic moments, as shown in Figure 6.17, the control torques created by electric flywheel motors are projected onto the axis of the associated coordinate system as follows:

$$\begin{aligned} M_x &= \sin\alpha\sin\beta\left(\dot{H}_1 + \dot{H}_2 + \dot{H}_3 + \dot{H}_4\right); \\ M_y &= \sin\alpha\cos\beta\left(-\dot{H}_1 + \dot{H}_2 - \dot{H}_3 + \dot{H}_4\right); \\ M_z &= \cos\alpha\left(-\dot{H}_1 + \dot{H}_2 + \dot{H}_3 - \dot{H}_4\right). \end{aligned} \qquad (6.12)$$

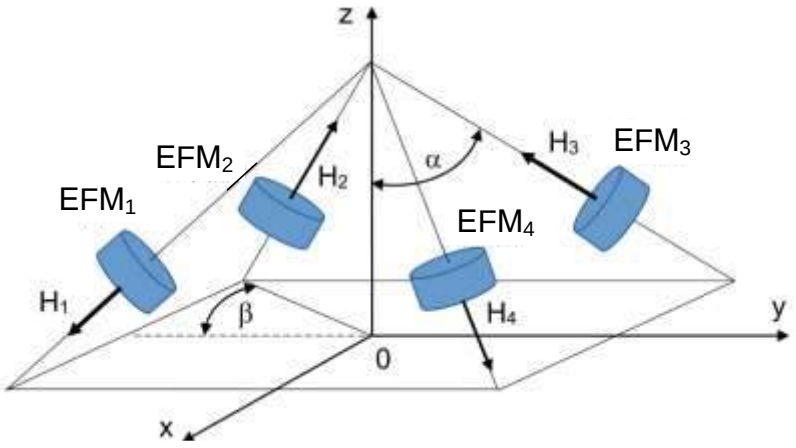

Figure 6.17 – The direction of the control moment vectors during angular movement relative to the axis Ox

When the moments are equal by module, i.e. $|\dot{H}_1| = |\dot{H}_2| = |\dot{H}_3| = |\dot{H}_4|$, the angular movement is performed only with respect to the X axis. The creation

of the necessary control moment with respect to this axis in the regular mode of operation is possible in several combinations. When the EFM_1 and EFM_2 flywheel electric motors are simultaneously activated, the control moments on the axis of the related coordinate system are projected as follows:

$$\begin{aligned} M_x &= \sin\alpha \sin\beta\left(\dot{H}_1 + \dot{H}_2\right); \\ M_y &= \sin\alpha \cos\beta\left(-\dot{H}_1 + \dot{H}_2\right) = 0; \\ M_z &= \cos\alpha\left(-\dot{H}_1 + \dot{H}_2\right) = 0. \end{aligned} \tag{6.13}$$

With the simultaneous creation of control moments by EFM_3 and EFM_4 flywheel electric motors:

$$\begin{aligned} M_x &= \sin\alpha \sin\beta\left(\dot{H}_3 + \dot{H}_4\right); \\ M_y &= \sin\alpha \cos\beta\left(-\dot{H}_3 + \dot{H}_4\right) = 0; \\ M_z &= \cos\alpha\left(\dot{H}_3 - \dot{H}_4\right) = 0. \end{aligned} \tag{6.14}$$

When all electric flywheel motors are turned on at the same time:

$$\begin{aligned} M_x &= \sin\alpha \sin\beta\left(\dot{H}_1 + \dot{H}_2 + \dot{H}_3 + \dot{H}_4\right); \\ M_y &= \sin\alpha \cos\beta\left(-\dot{H}_1 + \dot{H}_2 - \dot{H}_3 + \dot{H}_4\right) = 0; \\ M_z &= \cos\alpha\left(-\dot{H}_1 + \dot{H}_2 + \dot{H}_3 - \dot{H}_4\right) = 0. \end{aligned} \tag{6.15}$$

Projections of control moment vectors on the Oy and Oz axes when choosing combinations according to Figure 6.17 are mutually compensated.

Vectors of control moments, defined according to Figure 6.18, are projected onto the axis of the associated coordinate system as follows:

$$\begin{aligned} M_x &= \sin\alpha \sin\beta\left(-\dot{H}_1 + \dot{H}_2 - \dot{H}_3 + \dot{H}_4\right) = 0; \\ M_y &= \sin\alpha \cos\beta\left(\dot{H}_1 + \dot{H}_2 + \dot{H}_3 + \dot{H}_4\right); \\ M_z &= \cos\alpha\left(\dot{H}_1 + \dot{H}_2 - \dot{H}_3 - \dot{H}_4\right) = 0. \end{aligned} \tag{6.16}$$

Combinations of simultaneous activation of electric flywheel motors for angular movement only with respect to the Oy axis are following:

$$\begin{aligned} M_y &= \sin\alpha \cos\beta\left(\dot{H}_1 + \dot{H}_4\right); \\ M_y &= \sin\alpha \cos\beta\left(\dot{H}_2 + \dot{H}_3\right); \\ M_y &= \sin\alpha \cos\beta\left(\dot{H}_1 + \dot{H}_2 + \dot{H}_3 + \dot{H}_4\right). \end{aligned} \tag{6.17}$$

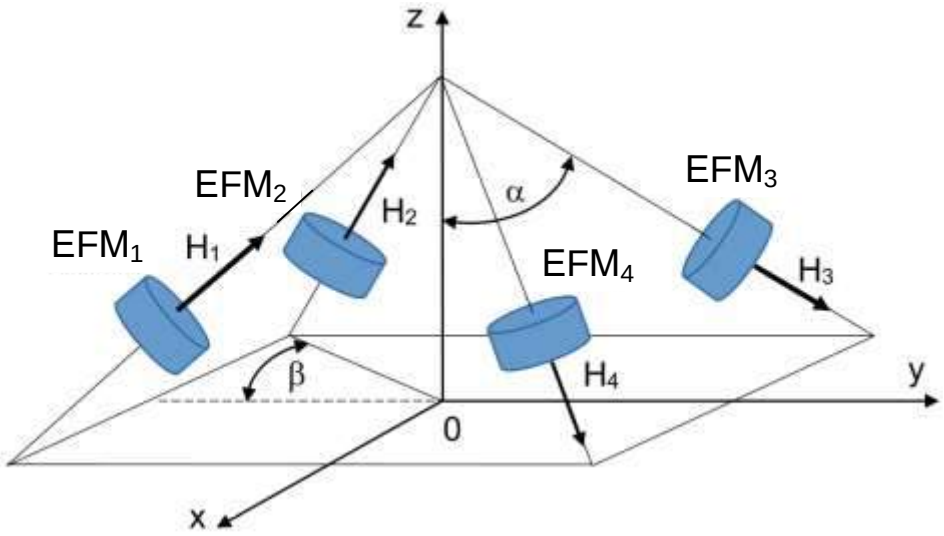

Figure 6.18 – The direction of the control moment vectors during angular movement relative to the Oy axis

Projections of the control moment vectors on the axis of the associated coordinate system, as shown in Figure 6.19, allow to perform angular movement only with respect to the Oz axis.

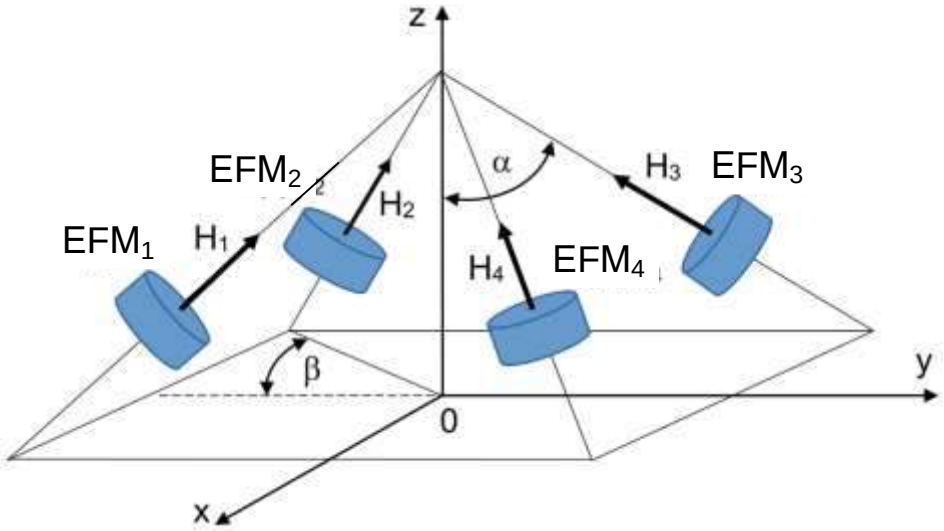

Figure 6.19 – The direction of the control moment vectors during angular movement relative to the Oz axis

According to Figure 6.19, the vectors of the control moments on the axes on the axis of the associated coordinate system are projected as follows:

$$\begin{aligned} M_x &= \sin\alpha \sin\beta\left(-\dot{H}_1 + \dot{H}_2 + \dot{H}_3 - \dot{H}_4\right); \\ M_y &= \sin\alpha \cos\beta\left(\dot{H}_1 + \dot{H}_2 - \dot{H}_3 - \dot{H}_4\right); \\ M_z &= \cos\alpha\left(\dot{H}_1 + \dot{H}_2 + \dot{H}_3 + \dot{H}_4\right). \end{aligned} \qquad (6.18)$$

In the regular mode of operation of the experimental stend, the angular movement relative to the Oz axis is provided in the following combinations of simultaneous operation of electric flywheel motors:

$$M_z = \cos\alpha\left(\dot{H}_1 + \dot{H}_3\right);$$

$$M_z = \cos\alpha\left(\dot{H}_2 + \dot{H}_4\right); \qquad (6.19)$$

$$M_z = \cos\alpha\left(\dot{H}_1 + \dot{H}_2 + \dot{H}_3 + \dot{H}_4\right).$$

With the same technical characteristics of electric flywheel motors with the same redundancy, the structure with a pyramid scheme of the placement of actuators has the following advantages:

1) the control moment relative to any of the axes of the associated coordinate system can be created by several electric flywheel motors at the same time;

2) such combinations of operation of electric flywheel motors are possible, when the braking mode can be used to reduce the kinetic moment;

3) if one or two electric motors fail, the control efficiency does not decrease, because the angular movement can be provided by at least two electric flywheel motors.

For greater functioning of the hardware and software complex, the Arduino IDE programming environment was used as part of the laptop software. The Arduino IDE provides developing of the control programs, debugging and uploading of executable code to the microcontroller of the rational control device of the electric flywheel motors unit. The programming language is C++. The Arduino IDE compiler makes it much easier to write programs for this platform.

I/O ports are used to connect any electronic components to the Arduino board. These are digital, analog or digital-analog interfaces that have their own function.

Digital pins can form and output only two values: a logical “0” (or LOW) and a logical “1” (or HIGH).

To receive or transmit signals through these ports, the program must initialize them using the function pinMode (<pin number>, <mode: INPUT/OUTPUT>), where the pin number is the pin number specified on the Arduino board. INPUT mode is required for reading data, OUTPUT is for transmission.

Analog inputs are intended for connecting analog sensors. Analog-to-digital converters built into the microcontroller are able to convert analog signals with an amplitude in the range from 0 to 5 V into a 10-bit digital code.

Digital-analog ports (or PWM – outputs with pulse-width modulation function) provide data transmission and do not require prior initialization. Such ports are marked on the board as PWM or with the sign “~” (tilde).

Each pin has an output voltage of 5 V and a maximum current load of 0.02 A.

Digital ports generate commands to turn on/off the main and backup power amplifiers, which simulates the abnormal operation modes of the power amplifiers of the "supply voltage break" type, the address selection of the measured tachometer is set, and output signals from the tachometers are received.

The analog inputs of the microcontroller in the rational control device are used to receive the measured output voltages of power amplifiers and potentiometric sensors of the angular position of electric flywheel motors unit relative to the axes of the cardan suspension frames.

Digital-analog ports form power amplifier control signals, the destabilization of power amplifier parameters and sensors of the angular position of the electric motor-flywheel unit relative to the axes of the associated coordinate system is simulated.

Downloading the executable program to the rational control device is carried out by command from the laptop. After downloading the executable program and its initialization, the rational control device works in autonomous mode, performing control functions, diagnosing the current state of the electric flywheel motor unit, restoring operability in the event of abnormal situations, and transmitting informational messages about the results of operation to the laptop via the USB channel. Visualization of information messages is formed by software on the laptop screen in the form of graphs and numerical arrays.

The experimental stend for the receach of the model unit of electric flywheel motors is essentially a modern hardware and software tool, which allows for system-level checking and testing of new ideas, principles and methods of controlling the angular position of objects with the help of kinetic moments developed by electric flywheel motors.

Chapter VII EXPERIMENTAL RESEACH OF THE MODEL UNIT OF ELECTRIC FLYWHEEL MOTORS

Interpretation of the experiment is a matter of taste.
P. L. Kapitsa (1894-1984)
- Nobel Prize laureate

An experiment is a methodical means of testing ideas and assumptions, answering questions and dispelling doubts. In order to conduct experimental studies of the model unit of electric flywheel motors, it is necessary to develop algorithmic and software support for processes of rational control of operability, as well as processes for simulating destabilizing influences. The task of experimental research is to confirm the theoretical provisions of diagnosis and restoration of performance on the example of a model unit of electric flywheel motors and to prove the practical feasibility of the principle of rational control based on diagnosis for spacecraft orientation systems.

7.1 Detection of destabilization in the model unit of electric flywheel motors

The implementation and the principle of operation of the EFM unit of pyramidal structure are presented in the chapter 6. Each of the destabilizing effects of the set D (4.1) leads to a malfunction of the EFM unit, which is an object of rational control. The operability of the rational control object depends on the operability of each of the four channels of the formation of the total vector of the kinetic moment of the EFM unit. By ensuring the operability of each channel with the help of rational management, it is possible to ensure the efficiency of the entire EFM unit. The identity of the four channels of the EFM unit allows to use the same algorithmic and software with parametric adaptation to the characteristics of each channel. This approach allows to consider the peculiarities of experimental studies on the example of one channel of rational control of the component of the kinetic moment vector under destabilizing influences [34].

The system of equations (4.3) is used as a reference model for the destabilization detection procedure in the rational control object, since the zero value of the initial conditions for the model EFM unit, and the reference model is ensured in the experimental stend. In general, the reference model is described by a finite-difference equation:

$$\hat{x}(k+1) = A\hat{x}(k) + Bu(k);$$
$$\hat{u}_S(k) = C\hat{x}(k). \tag{7.1}$$

In the EFM unit, only the angular velocity sensor – the tachometer (TM) is used. Therefore, in a specific structural form, the reference model is described by the following equation:

$$\hat{u}_{TM}(k+1) = \left(1 - \frac{T_0}{T_{EFM}}\right)\hat{u}_{TM}(k) + \frac{T_0}{T_{EFM}} k_O u_C(k), \tag{7.2}$$

where T_{EFM} – time constant of EFM;

$k_O = k_{PA} k_{EFM} k_{TM}$ – the conversion factor of the rational control object, including $\kappa_{ПП}$ – power amplifier conversion factor;

k_{EFM} – EFM conversion factor and $\kappa_{ТД}$ – conversion factor of TM;

$\hat{u}_{TM}(k)$ – estimated value of the output signal of the rational control object, i.e. the output signal of the angular velocity sensor;

$u_C(k)$ – control signal, which is applied to the rational control object;

T_0 – quantization period.

At specific values of parameters of the experimental channel, namely:

$$T_{EFM} = 1.7\,s;\ k_O = 1 \cdot 250 \frac{rad}{V\,s} \cdot 0.00396 \frac{V\,c}{rad} \approx 0.99;\ T_0 = 0.1s,$$

the reference model is described by the following equation:

$$\hat{u}_{TM}(k+1) = 0.941 u_{TM}(k) + 0.0582 u_C(k) \tag{7.3}$$

and a difference signal is

$$\Delta\hat{u}_{TM}(k+1) = \tilde{u}_{TM}(k+1) - \hat{u}_{TM}(k+1), \tag{7.4}$$

where $\tilde{u}_{TM}(k+1)$ – the output signal of the rational control object containing information about the influence of destabilizing factors.

Detection of the presence of destabilizing influences in the output signal is carried out using a two-digit predicate of the following general form:

$$Z_0 = S_2\left\{\left|\Delta\hat{u}_{TM}(k+1)\right| \geq \delta_0\right\},\ k = \overline{1,N};\ \rho_0. \tag{7.5}$$

For specific values, the predicate is described by the following equation

$$Z_0 = S_2\left\{\left|\Delta\hat{u}_{TM}(k+1)\right| \geq 0.1\right\},\ k = \overline{1,10};\ \rho_0 = 0.8. \tag{7.6}$$

The scheme of the destabilization detection algorithm in one channel of the EFM model unit is presented in Figure 7.1.

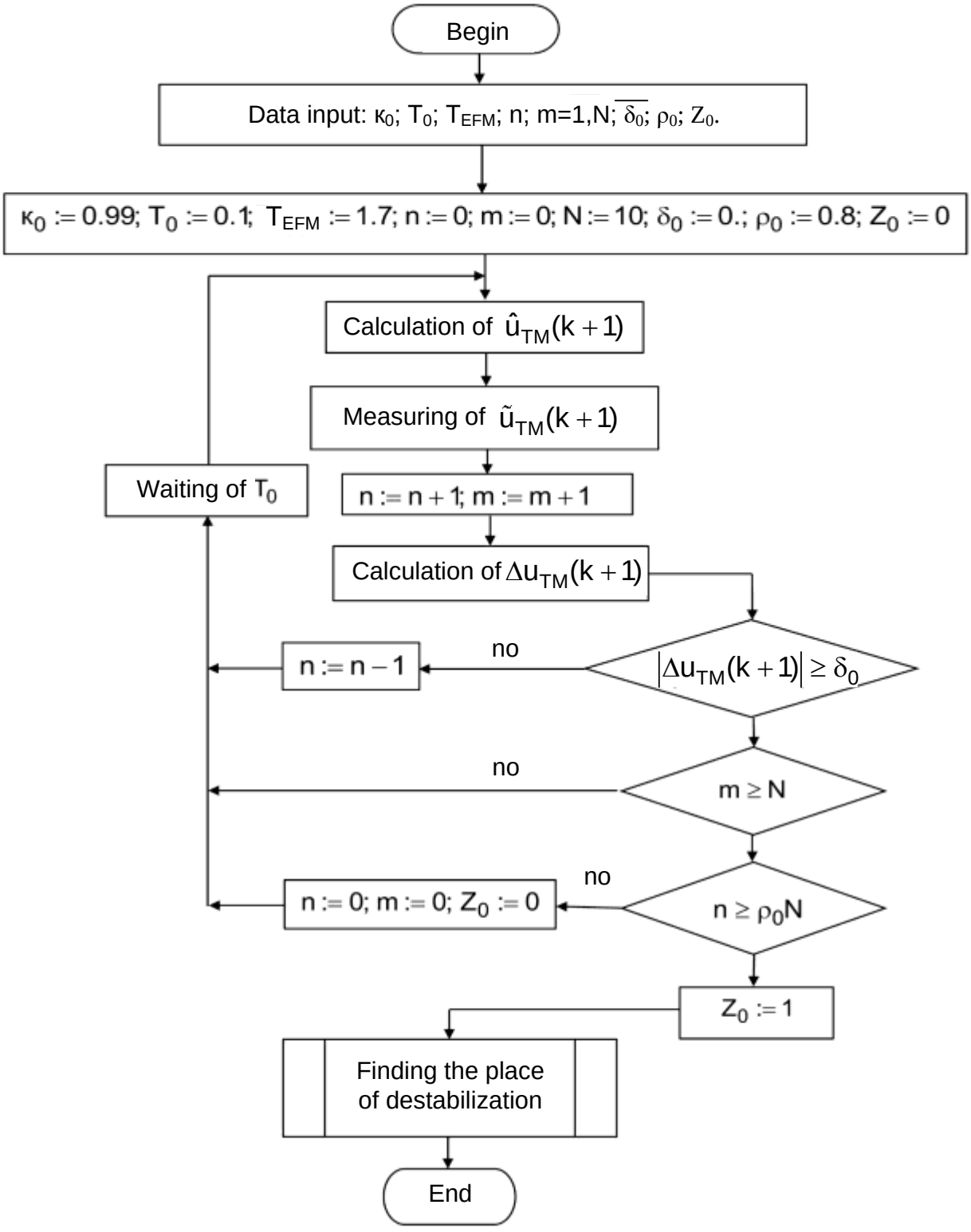

Figure 7.1 – Scheme of the destabilization detection algorithm

For the technical implementation of the destabilization detection algorithm, the database of the diagnostic block must contain numerical data:

1) $k_O = k_{PA}\, k_{EFM}\, k_{TM}$ – the product of transmission coefficients of PA, EFM and TM;

2) T_{EFM} – time constant of EFM;

3) T_0 – quantization period;

4) n – the number of measurements with a sign of destabilization at the diagnosis interval;

5) m – the number of all measurements in the diagnosis interval;

6) N – given number of measurements at the diagnosis interval;

7) δ_0 – tolerance for deviation from the norm of the output parameter of the actuator;

8) ρ – trust factor (set by the developer);

9) Z_0 – predicate of the current state of the actuator.

The software implementation of the destabilization detection algorithm is made in the Arduino IDE development environment in the C++ language. The destabilization detection program is presented in Figure 7.2.

```
float w1 = 0.0; // Angular speed of EFM rotation (rad/s)
float w1_model = 0.0; // EFM rotation frequency based on the calculation of the reference model (angular velocity)
float w1_model_m1 = 0.0; // DM rotation frequency based on the calculation of the reference model (angular velocity) - the value from the previous discretization period
float K1_T0_d_Tdm;   // Coefficients for the reference model of EFM
float T0_Tdm_Kum_Kdm;
word Takt = 0;
byte Pr_destab_UM1 = 0;  // Signs of destabilization calculated by the diagnostic algorithm
float K_um_2 = 0.02;
float K_um_2_1 = 0.02;
float U_um_2 = 0.0;    // Measurement of PA output
float U_um_2_km1 = 0.0; Prevous measurement of PA output
float U_um_2_model = 0.0;
float delta_U_um_2 = 0.0; // The difference between the reference model and measured voltage of PA
float dopusk_U_um = 0.0;
//float delta_U_um_2_measure = 0.0; // The difference between the current and previous measurement of  U_um_2;
//float delta_U_um_2_measure_km1 = 0.0; // Previous value of delta_U_um_2_measure;
//float dopusk_delta_U_um_2_measure; // Allowance for increasing (derivative) voltage of PA
```

```
      float delta_U_um_2_km1 = 0.0; // The previous value of the difference
between the reference model and measured voltage of the PA
      K1_T0_d_Tdm = 0.933;   // Coefficients for the reference model of EFM
        T0_Tdm_Kum_Kdm = 0.31;  //
        K_um_2 = 0.02;
        K_um_2_1 = 0.02;
void loop() {
      Takt = Takt + 1;
      // Measurement of the period of pulses from the encoder on EFM_x
         digitalWrite(AddrBusMX_S1, HIGH);  // Number of channel: MX-0
         digitalWrite(AddrBusMX_S2, LOW);
         digitalWrite(MX_Enable, LOW);
// The multiplexer is working - the active permission level is 0
         delay(1);
         if (Uz != 0.0) {
           Enc_T0 = pulseIn(F_AngularVel, LOW);
           Enc_T1 = pulseIn(F_AngularVel, HIGH);
           w1 = 6.28 * (20000.0 / float(Enc_T0 + Enc_T1));    }  //rad/s
         else {   Enc_T0 == 0;   Enc_T1 == 0;    w1 = 0.0;    }
         // Averaging of measurements
         SumF = SumF + w1 - Enc_Over4;
         AngVel_Aver = SumF / 4;
         Enc_Over4 = Enc_Over3;  Enc_Over3 = Enc_Over2;
         Enc_Over2 = Enc_Over1;  Enc_Over1 = w1;
         // Calculation of the DM reference model and the difference with the
physical measurement of the EFM speed and the reference model
         w1_model = ( K1_T0_d_Tdm * w1_model_m1 ) +
                           (T0_Tdm_Kum_Kdm * Uz );
         w1_model_m1 = w1_model;
         delta_w1 = abs( w1_model - AngVel_Aver ); // difference between
measured and modeled velocity
         if (w1_model == 0.0) {dopusk_w1 = 5.0;}
         else {dopusk_w1 = abs( 0.10 * w1_model );} // tolerance calculation -
10% of the reference model value
        if ( delta_w1 >= dopusk_w1 ) {
          if (CounterOfFailures < 5) {CounterOfFailures++;}
           }
         else {if (CounterOfFailures > 0) {CounterOfFailures--;}            }
```

```
 if (CounterOfFailures == 5) {Pr_destab = 1;}
else {Pr_destab = 0;}
if ((Pr_destab == 1) && (Pr_destab_m1 == 0))
   {Pr_destab_Trigger = 1;}
Pr_destab_m1 = Pr_destab;
delay(100);     }   // Discretization period
```

Figure 7.2 – Destabilization detection program

Let's consider the results of experimental studies on the detection of destabilization in the mock-up block. Figure 7.3 shows the graphs of the step-shaped reference signal that is supplied at $t = 1\,s$ and the graph of the RCO transient characteristic in the absence of destabilization.

From the graph of the transient characteristic, it follows that the duration of the RCO transient process is $t_{TP} \approx 5\,s$. The mode of operation of the RCO in this experiment is nominal, that is, the mode in which the destabilizing influence was not simulated.

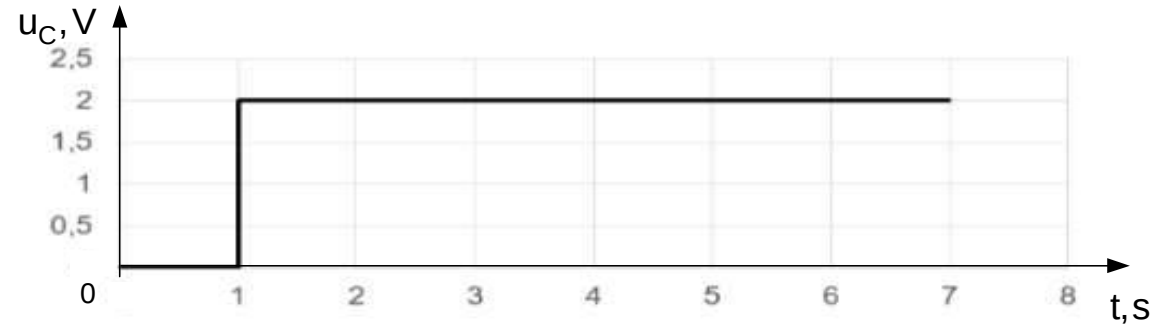

a

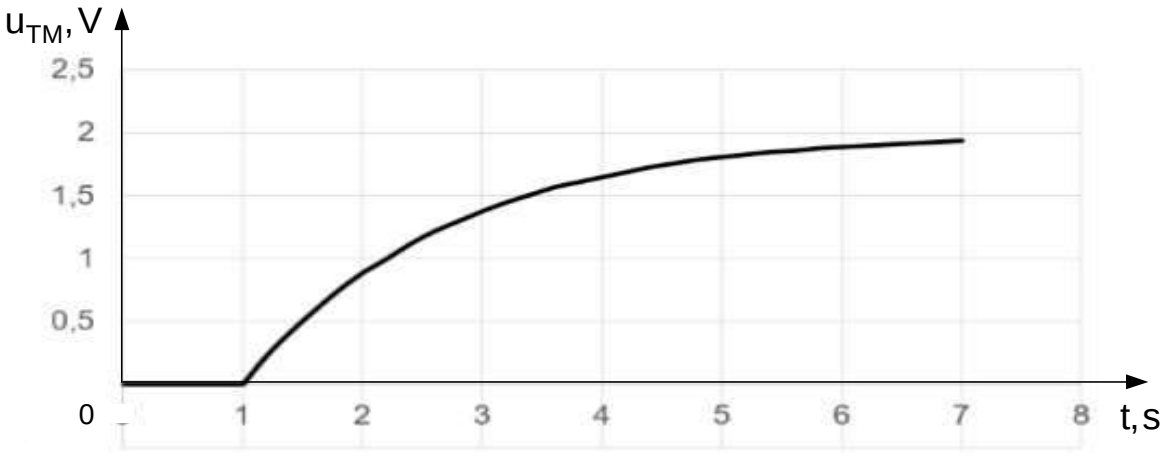

b

Figure 7.3 – Transient characteristics of the RCO for the nominal mode

When simulating the type of destabilizing effect d_{11} in the operation of the PA, which consists in reducing the amplification factor, the following results were obtained (Figure 7.4).

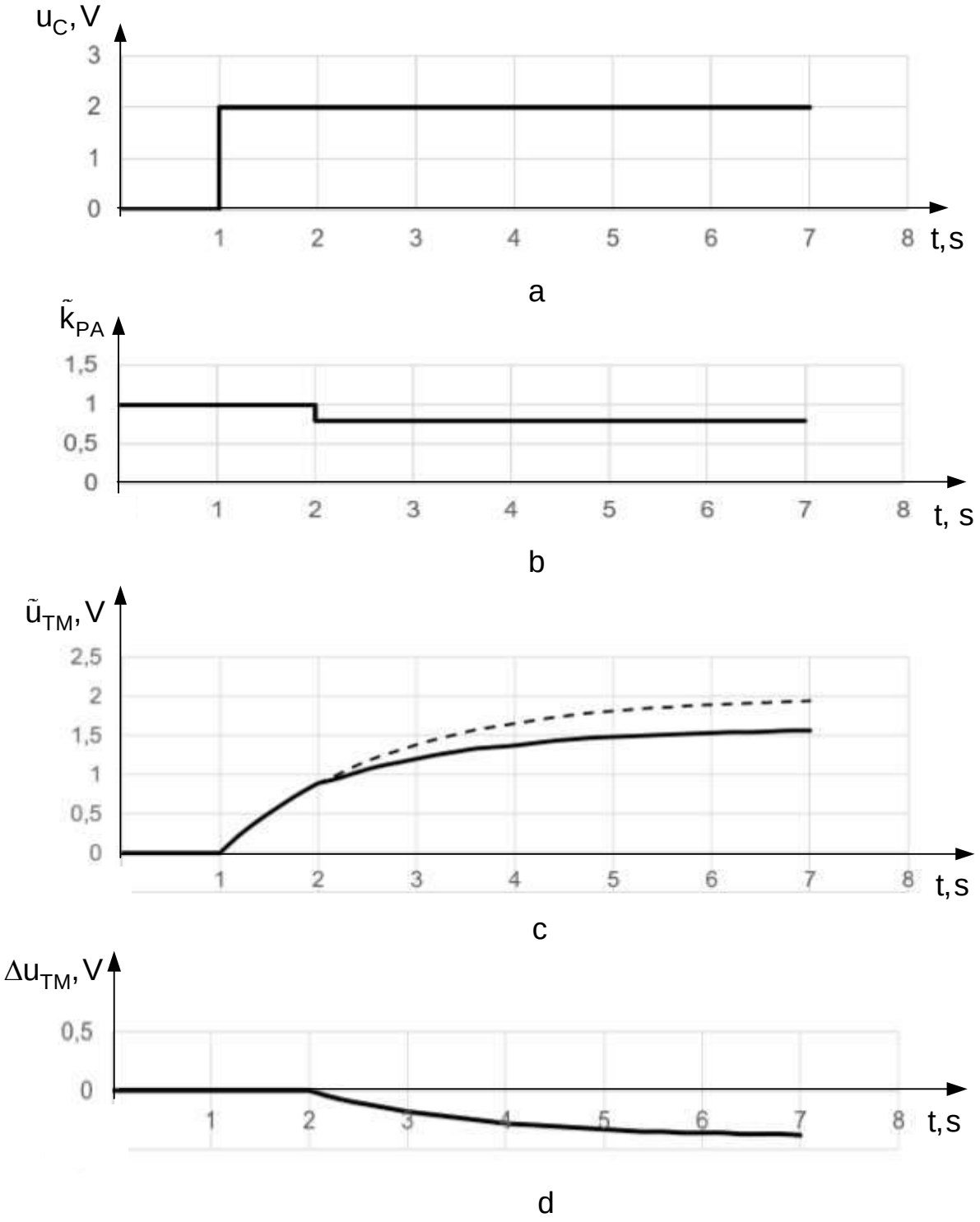

Figure 7.4 – Graphs of transient processes in RCO for the destabilization d_{11}

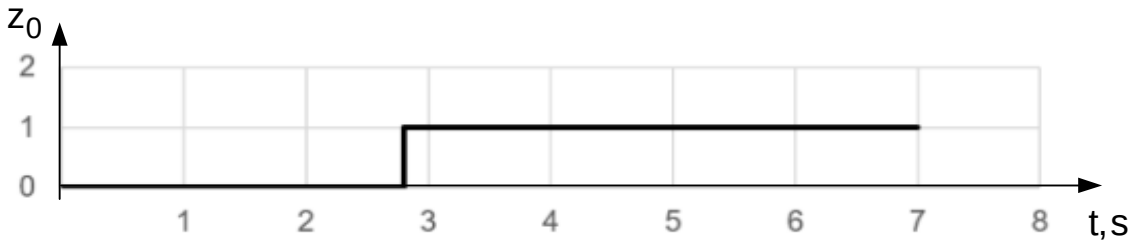

e

Figure 7.4, page 2

The graph of the desired effect of the step type, which is applied to the RCO in the first second, is presented in Figure 7.4, a. Figure 7.4, b shows the change in the PA transfer coefficient. So, up to the moment $t = 2\,s$ transfer coefficient $k_{PA} = 1$, but at the moment $t = 2\,s$ the transmission coefficient reduces at 0.2 and became $\tilde{k}_{\Pi\Pi} = 0.8$. Figure 7.4, c displays the RCO response to a step input signal and a step reduction in the PA transfer coefficient. Figure 7.4, d shows the change in the deviation of the output signal of RCO $\tilde{u}_{TM}(t)$ from the signal of the reference model $\hat{u}_{TM}(t)$ corresponding to the nominal one. Figure 7.4, e shows the graph of the predicate Z_0. Predicate value $Z_0 = 1$ apperars at the moment $t = 2.8\,s$. The duration of the period from the moment of appearance of destabilizing influence $\tilde{k}_{\Pi\Pi} = 0.8$ to the moment of detection of destabilization is $t_0 = 0.8\,s$. This is the time to detect a destabilizing influence $d_{11} = \tilde{k}_{\Pi\Pi} = 0.8$.

The obtained results of experimental studies of algorithms and programs for detection of destabilization in RCO testify to the practical possibility of quickly detecting the appearance of each influence from the set D within 1 s. It should be noted that the use of the predicate equation (7.6) allows to quickly detect both single and multiple destabilizing effects.

7.2 Search for destabilizing functional elements in the model unit

The EFM model unit uses PA, EFM and TM functional elements in each RCO channel. Each functional element can be destabilized in an experimental stend by a number of actions. So, PA can be influenced by a subset D_1:

$$D_1 = \{d_{11}, d_{12}, d_{13}, d_{14}\}, \qquad (7.7)$$

where d_{11} – reducing the gain (transfer coefficient); d_{12} – positive drift; d_{13} – negative drift; d_{14} – break of the input signal wire.

On EDM, destabilization is simulated by means of influences from a subset D_2:

$$D_2 = \{d_{21}, d_{22}, d_{23}\}, \tag{7.8}$$

where d_{21} – reducing the transfer coefficient; d_{22} – increasing the time constant; d_{23} – break in the control chain.

The efficiency of TM is destabilized by influences from a subset D_3:

$$D_3 = \{d_{31}, d_{32}, d_{33}, d_{34}\}, \tag{7.9}$$

where d_{31} – reducing the transfer coefficient; d_{32} – positive drift; d_{33} – negative drift; d_{34} – break of the output signal wire.

The search for an inoperable functional element of RCO is actually based on the detection of destabilization in its functioning. Therefore, reference models of functional elements in the form of equations describing the nominal mode of their functioning are used for detection. So, for PA as a reference model, the equation is used

$$\hat{u}_{PA}(k) = k_{PA}\, u_C(k). \tag{7.10}$$

Differential signal

$$\Delta u_{PA}(k) = \tilde{u}_{PA}(k) - \hat{u}_{PA}(k) \tag{7.11}$$

is used to form the argument of a two-valued predicate equation

$$Z_1 = S_2\left\{\left|\Delta u_{PA}(k)\right| \geq \delta_1\right\},\ k = \overline{1,N};\ \rho_1, \tag{7.12}$$

with the help of which destabilization is detected in the PA at

$$\delta_1 = 0.15,\ \rho_1 = 0.8.$$

The scheme of the algorithm for forming the values of the predicate Z_1 in one channel of the layout block is presented in Figure 7.5.

For the technical implementation of the algorithm for detecting destabilization of the power amplifier, the database of the diagnostic unit must contain numerical data:

1) k_{PA} – transfer factor of the power amplifier;
2) T_0 – quantization period;
3) n_1 – the number of measurements with an active sign of PA destabilization during the diagnosis interval;
4) m_1 – the number of all measurements in the diagnosis interval;
5) N – given number of measurements at the diagnosis interval;

6) δ_1 – tolerance for deviation from the norm of the initial parameter of the PA;

7) ρ_1 – confidence factor;

8) Z_0 – predicate of the current state of the whole EFM unit;

9) Z_1 – predicate of the current state of the power amplifier.

The software implementation of the algorithm is presented in Figure 7.6.

```
float w1 = 0.0; // Angular velocity of EFM rotation (rad/s)
float w1_model = 0.0; // EFM rotation frequency based on the calculation of the reference model (angular velocity)
float w1_model_m1 = 0.0; // EFM rotation frequency based on the reference model calculation (angular velocity) – the value from the previous discretization period
float K1_T0_d_Tdm;   // Coefficients for the reference model of the drive
float T0_Tdm_Kum_Kdm;
word Takt = 0;
byte Pr_destab_UM1 = 0;  // Signs of destabilization calculated by the diagnostic algorithm
float K_um_2 = 0.02;     float K_um_2_1 = 0.02;
float U_um_2 = 0.0;    // Measurement of PA output signal
float U_um_2_km1 = 0.0; // Measurement of PA output signal from the previous discretization period
float U_um_2_model = 0.0;
float delta_U_um_2 = 0.0; // Difference between modeled and measured
output voltage of PA
float dopusk_U_um = 0.0;
//float delta_U_um_2_measure = 0.0; // The difference between the current and previous measurement of U_um_2;
//float delta_U_um_2_measure_km1 = 0.0; // Previous value of delta_U_um_2_measure;
//float dopusk_delta_U_um_2_measure; // Allowance for increasing (derivative) output voltage of PA
float delta_U_um_2_km1 = 0.0; // The preliminary value of the difference between the model and measured output voltage of the PA
K1_T0_d_Tdm = 0.933;   // Coefficients for the reference model of the drive
 T0_Tdm_Kum_Kdm = 0.31;  //
 K_um_2 = 0.02;      K_um_2_1 = 0.02;
```

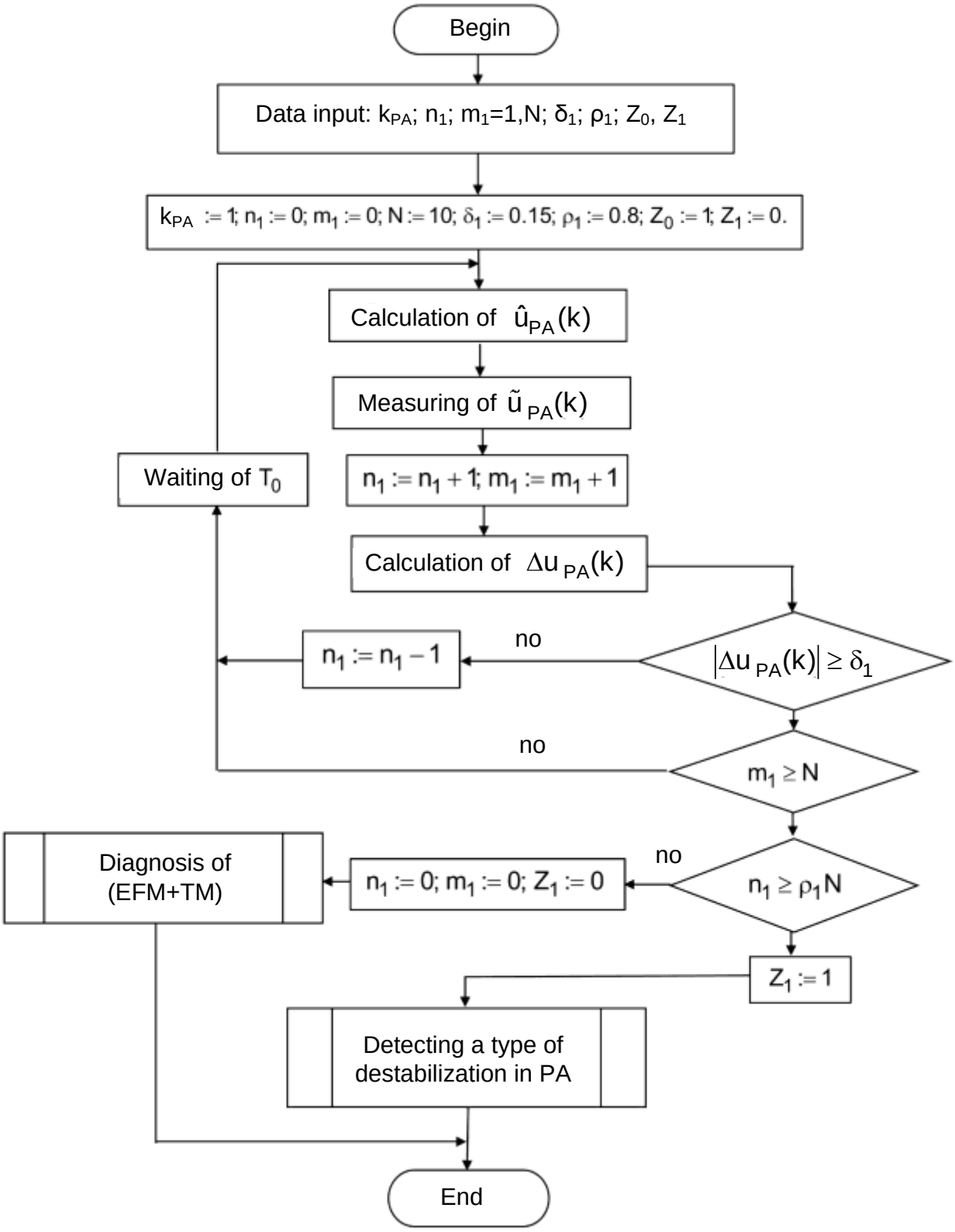

Fugure 7.5 – Scheme of the algorithm for the formation of predicate values Z_1

```
void loop() {
  Takt = Takt + 1;
  // Calculation of the reference model of the PA and the discrepancy between the physical output of the PA and the reference model
    U_um_2 = Coeff_Measure * float(analogRead(Output_UM2)) + Offset_Measure; // Measurement of PA output signal
    U_um_2_model = K_um_2 * Uz; // Calculation of PA output value according to the model
     delta_U_um_2_km1 = delta_U_um_2;
      delta_U_um_2 = abs( U_um_2_model - U_um_2 );
 if ((Pr_destab == 1) && (Pr_destab_m1 == 0)) {Pr_destab_Trigger = 1;}
    Pr_destab_m1 = Pr_destab;
 // Finding the place of failure
   if (Pr_destab_Trigger == 1) {
     Pr_destab_K_dm = 0;
     Pr_destab_PowerBreak = 0;
     Pr_destab_K_um = 0;
       if ( (delta_U_um_2 <= dopusk_U_um) )
        {
          if ((Pr_destab_K_um_Trigger == 0) && (Pr_destab_PowerBreak_Trigger == 0)) {Pr_destab_K_dm = 1;}
        }
  if ( delta_U_um_2 > dopusk_U_um ) // Destabilization of Kpa or break
{
       if ( abs(delta_U_um_2) > abs(delta_U_um_2_km1) )
         {
           if ((Pr_destab_K_um_Trigger == 0) && (Pr_destab_K_dm_Trigger == 0)) {Pr_destab_PowerBreak = 1;}
         }
      }
   // Setting triggers for signs of destabilization
  if ((Pr_destab_K_um == 1) && (Pr_destab_K_um_m1 == 0)) {Pr_destab_K_um_Trigger = 1;}
    Pr_destab_K_um_m1 = Pr_destab_K_um;
 delay(100); // Discretization period
  }
```

Figure 7.6 – Program for implementing the predicate Z_1 formation algorithm

During experimental studies of the algorithm and the program, destabilizing influences from a subset D_1 were consistently simulated. Signal graphs reflecting the process of detection of destabilization in PA are presented in Figure 7.7.

When applying a step setting signal $u_C = 2\,V$ at the moment of time $t = 1\,s$ (Figure 7.7, a) the output signal $\tilde{u}_{PA}$ maintains its nominal value until $t = 2\,s$, at this point in time, the zero drift increases by an amount $u_0 = 0{,}2\,V$ (Figure 7.7, b), u_0 вихідний the PP signal increases by an amount and becomes equal $\tilde{u}_{PA} = 2{,}2\,V$ (Figure 7.7, c). The differential signal until the moment $t = 2\,s$ is zero, and at $t = 2\,s$ increases by $\Delta u_{PA} = u_0$ (Figure 7.7, d). As a result of processing the difference signal using the predicate equation (7.12) on the time interval $t \in [2\ldots3]$ s boolean sign Z_1 gets the value «1», which indicates the inoperability of the PA.

Similar results were obtained when simulating types of destabilizing influences d_{11}, d_{13} and d_{14}.

When destabilization is detected in the (EFM+TM) subsystem, the reference model described by the equation is used:

$$\hat{u}_{TM}(k+1) = \left(1 - \frac{T_0}{T_{EFM}}\right)\hat{u}_{TM}(k) + \frac{T_0}{T_{EFM}} k_{EFM}\, k_{TM}\, u_C(k). \qquad (7.13)$$

Differential signal

$$\Delta u_{TM}(k+1) = \tilde{u}_{TM}(k+1) - \hat{u}_{TM}(k+1) \qquad (7.14)$$

contains information about destabilization in both EFM and TM.

A two-valued predicate equation is based on usage $\Delta u_{TM}(k+1)$:

$$Z_2 = S_2\left\{\left|\Delta u_{TM}(k+1)\right| \geq \delta_2\right\},\ k = \overline{1,N};\ \rho_2. \qquad (7.15)$$

When destabilization is detected in the subsystem (EFM+TM), the parameters are applied: $\delta_2 = 0{,}15$; $\rho_2 = 0{,}8$.

The scheme of the algorithm for forming predicate value of Z_2 on one channel of the model unit is presented in Figure 7.8.

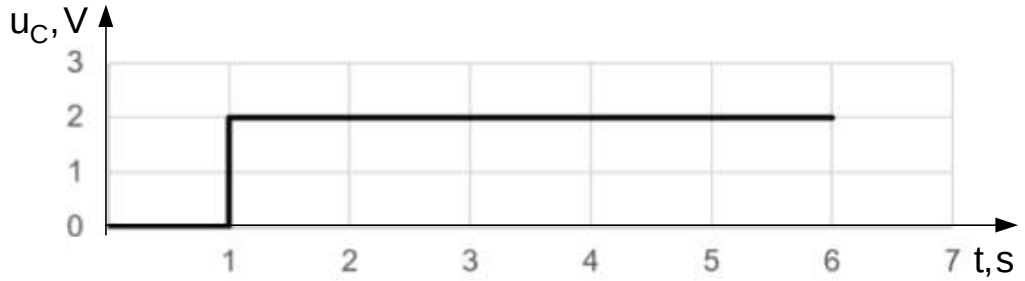

a

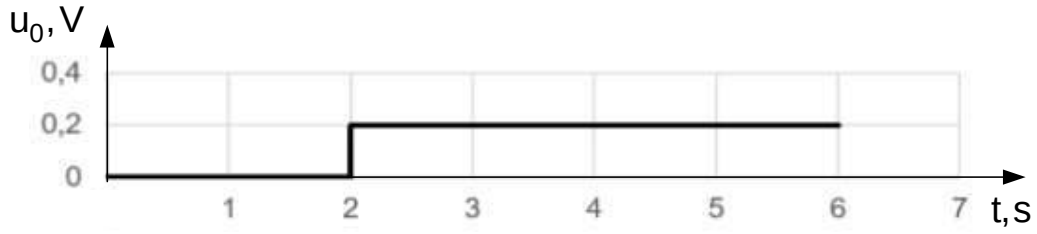

b

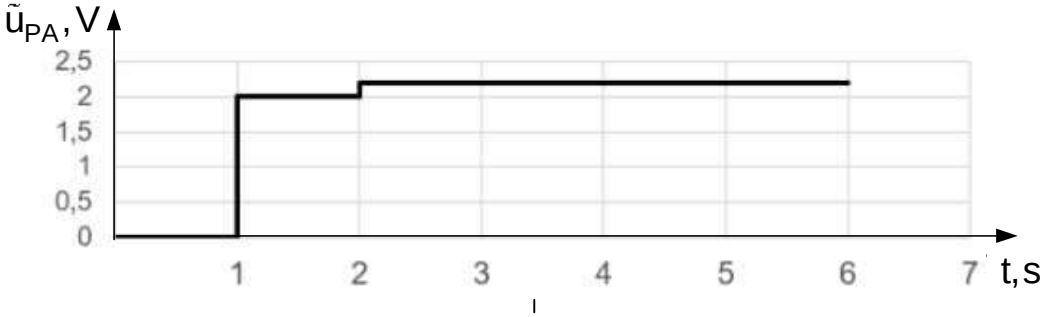

c

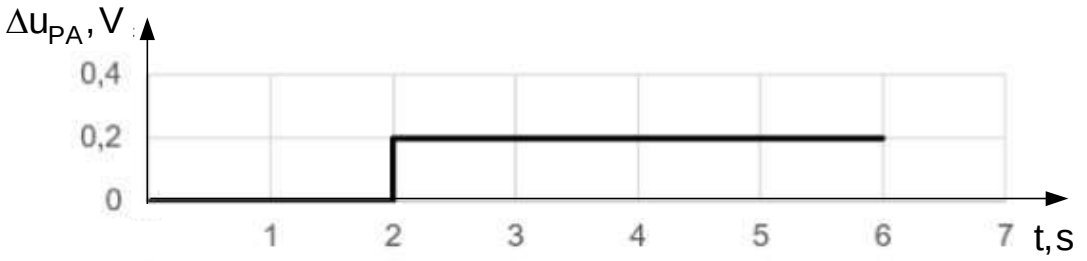

d

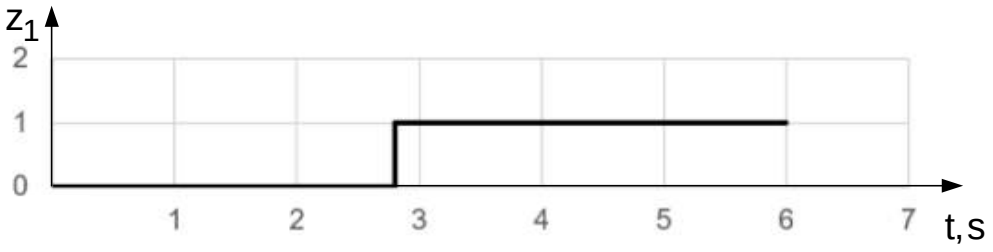

e

Figure 7.7 – Graphs of transient processes in PA with the type of destabilization d_{12}

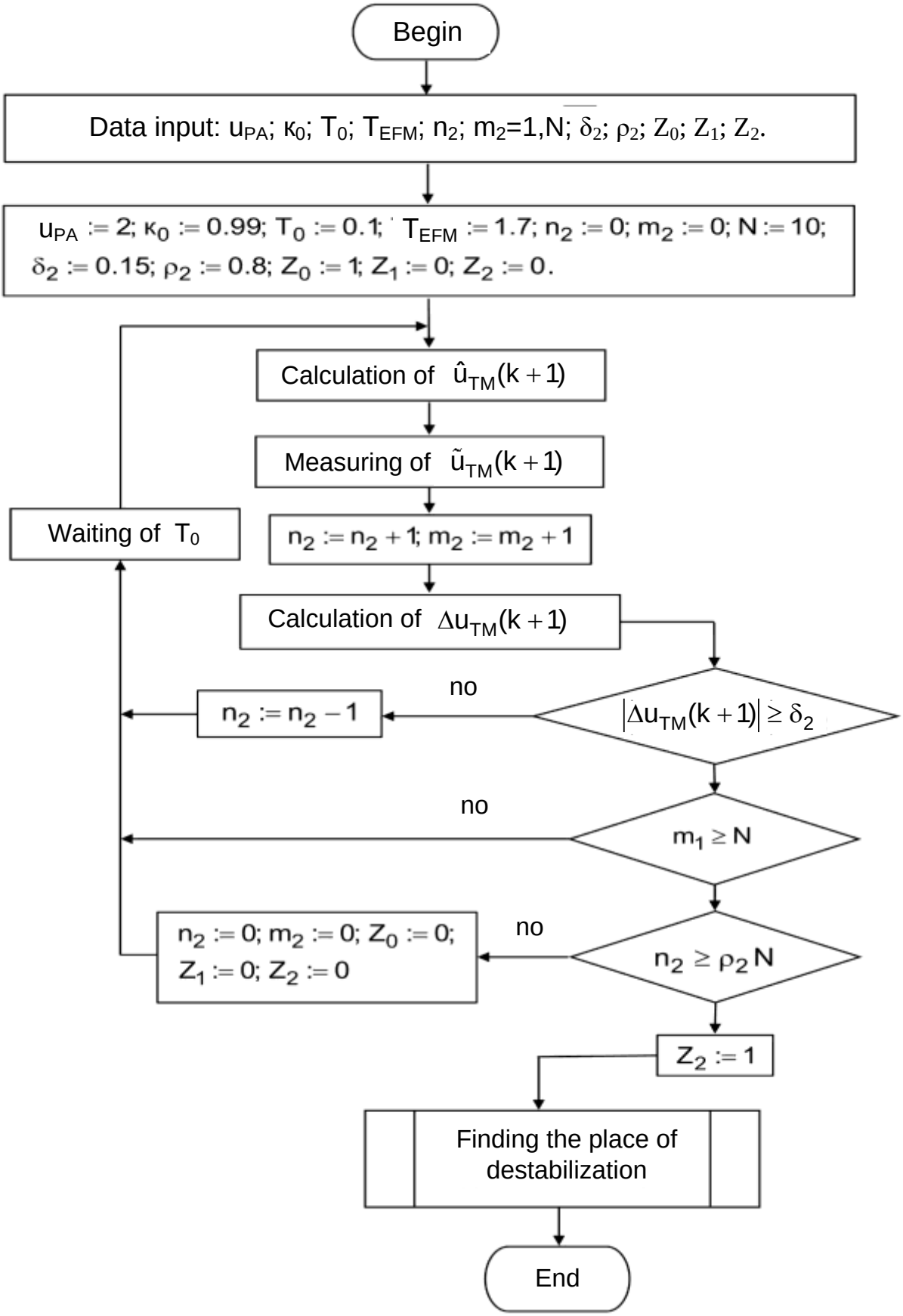

Figure 7.8 – Scheme of the algorithm for the formation of predicate value Z_2

For the technical implementation of the destabilization detection algorithm of subsystem (EFM+TM), the diagnostic block database must contain numerical data:

1) u_{PA} – напруга на виході підсилювача потужності;
2) k_0 – product of transfer coefficients of PA, EFM and TM;
3) T_0 – quantization period;
4) $T_{ЕДМ}$ – time constant of EFM;
5) n_2 – the number of measurements with signs of subsystem (EFM+TM) destabilization at the diagnostic interval;
6) m_2 – the number of all measurements in the diagnosis interval;
7) N – given number of measurements at the diagnosis interval;
8) δ_2 – tolerance for deviation from the norm of the output parameter of subsystem (EFM+TM);
9) ρ_2 – confidence factor;
10) Z_0 – predicate of the current state of the whole EFM unit;
11) Z_1 – predicate of the current state of the power amplifier;
12) Z_2 – predicate of the current state of subsystem (EFM+TM).

Let's consider the graphs of transient processes illustrating the peculiarities of the search for a destabilizing functional element in subsystem (EFM+TM). In Figure 7.9 shows graphs of signals reflecting the cyclogram of finding a destabilizing influence d_{22} – increasing the time constant.

When a specified step signal $u_C = 2\,V$ is applied to the RCO input at the moment $t = 1s$ an output step signal will also appear at the PA input $u_{PA} = 2\,V$, because $k_{PA} = 1$ (Figure 7.9, a). At the moment $t = 2\,s$ the time constant value changes from 1,7 s to 2,2 s (Figure 7.9, b). The output signal $\tilde{u}_{TM}$ reduces relative to the reference signal $\hat{u}_{TM}$ (Figure 7.9, c). Δu_{TM} The difference signal reflects this reduction (Figure 7.9, d). Processing of the difference signal Δu_{TM} using a predicate equation Z_2 (7.15) during the time interval $t \in [2…3]$ allows to get the value of a boolean attribute $Z_2 = 1$, which indicates inoperability of sumsystem (EFM+TM0.

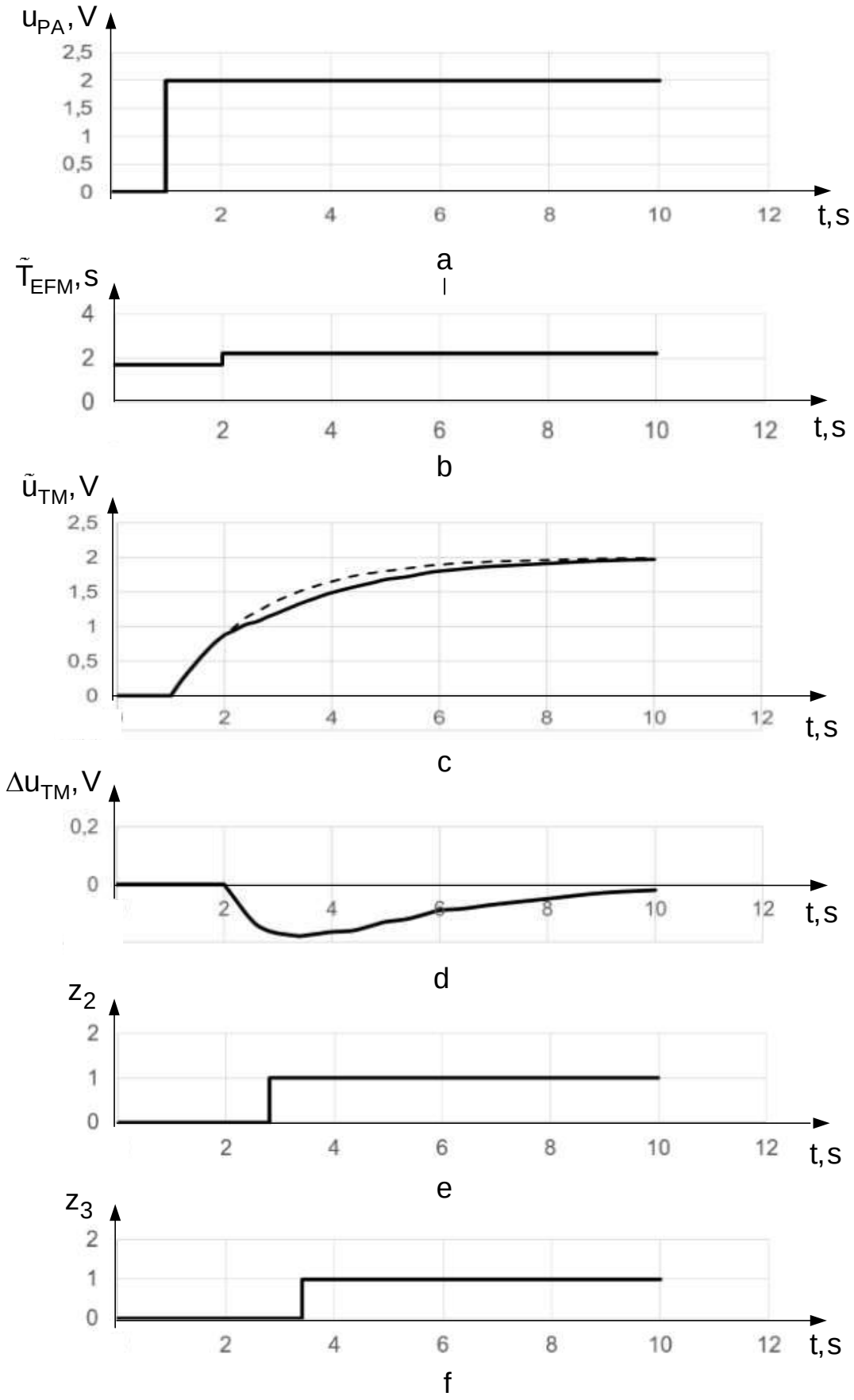

Figure 7.9 – Graphs of transient processes of subsystem (EFM+TM) in case of destabilization d_{22}

A two-valued predicate equation obtained from the corresponding diagnostic model is used to detect the destabilizing effect d_{22}:

$$Z_3 = S_2\left\{\delta_3 - \left\|\left[\Delta u_{TM}(k+2) - \Delta u_{TM}(k+1)\right]\left[u_{TM}(k) - u_{PA}(k)\right] - \right.\right.$$
$$\left.\left. - \left[\Delta u_{TM}(k+1) - \Delta u_{TM}(k)\right]\left[u_{TM}(k+1) - u_{PA}(k+1)\right]\right\|\right\};\ k = \overline{1,10};\ \rho_3. \quad (7.16)$$

When detecting d_{22}, the following parameters were used: $\delta_3 = 0{,}12$; $\rho_3 = 0{,}8$.

The scheme of the algorithm for the formation of predicate value Z_3 is presented in Figure 7.10.

For the technical implementation of the algorithm for the formation of predicate value Z_3, the database of the diagnostic block must contain numerical data:

1) u_{PA} – voltage at the output of the power amplifier;
2) k_{EFM} – conversion factor of EFM;
3) $к_{ТД}$ – conversion factor of TM;
4) T_0 – quantization period;
5) $T_{ЕДМ}$ – time constant of EFM;
6) n_3 – the number of measurements with a sign of destabilization of subsystem (EFM+TM) at the diagnosis interval;
7) m_3 – the number of all measurements in the diagnosis interval;
8) N – given number of measurements at the diagnosis interval;
9) δ_3 – tolerance for deviation from the normal value of the output parameter of subsystem (EFM+TM);
10) ρ_3 – confidence factor;
11) Z_0 – predicate of the current state of whole EFM system;
12) Z_1 – predicate of the current state of power amplifier;
13) Z_2 – predicate of the current state of subsystem (EFM+TM);
14) Z_3 – predicate of the current state of EFM.

In fig. 7.9, f shows that during the time period $t \in [2{,}6\ldots3{,}4]$ signals are processed according to the predicate equation (7.16) and when $t = 3{,}4\,s$ the Boolean sign value $Z_3 = 1$. Such a sign value means that the reason for the failure of the subsystem (EFM+TM) is a change in the inertial properties of the EDM, which are characterized by a constant time parameter T_{EFM}.

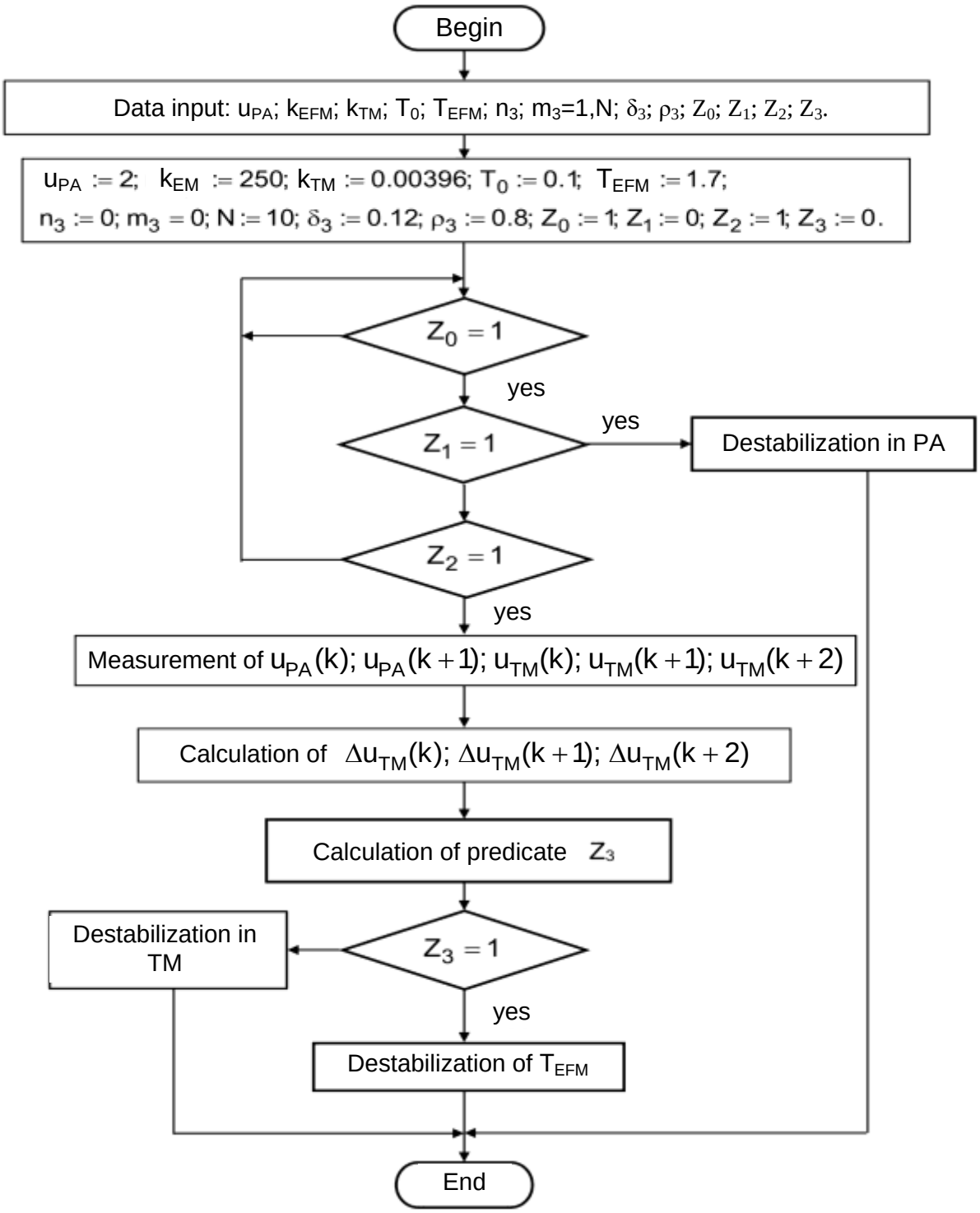

Figure 7.10 – Scheme of the algorithm for the formation of predicate value Z_3

Figure 7.11 presents graphs of characteristic signals reflecting the features of the process of searching for a destabilizing influence d_{32} – a positive drift of TM zero. At step action with PA at time $t = 1s$ with amplitude $u_{PA} = 2V$ (Figure 7.11, a) at time $t = 2s$ a jump of zero TM drift $u_0 = 0,3V$ appears (Figure 7.11, b). This will affect the change in the form of an increase

in the output signal on the transient process of the subsystem (EFM+TM) (Figure 7.11, c).

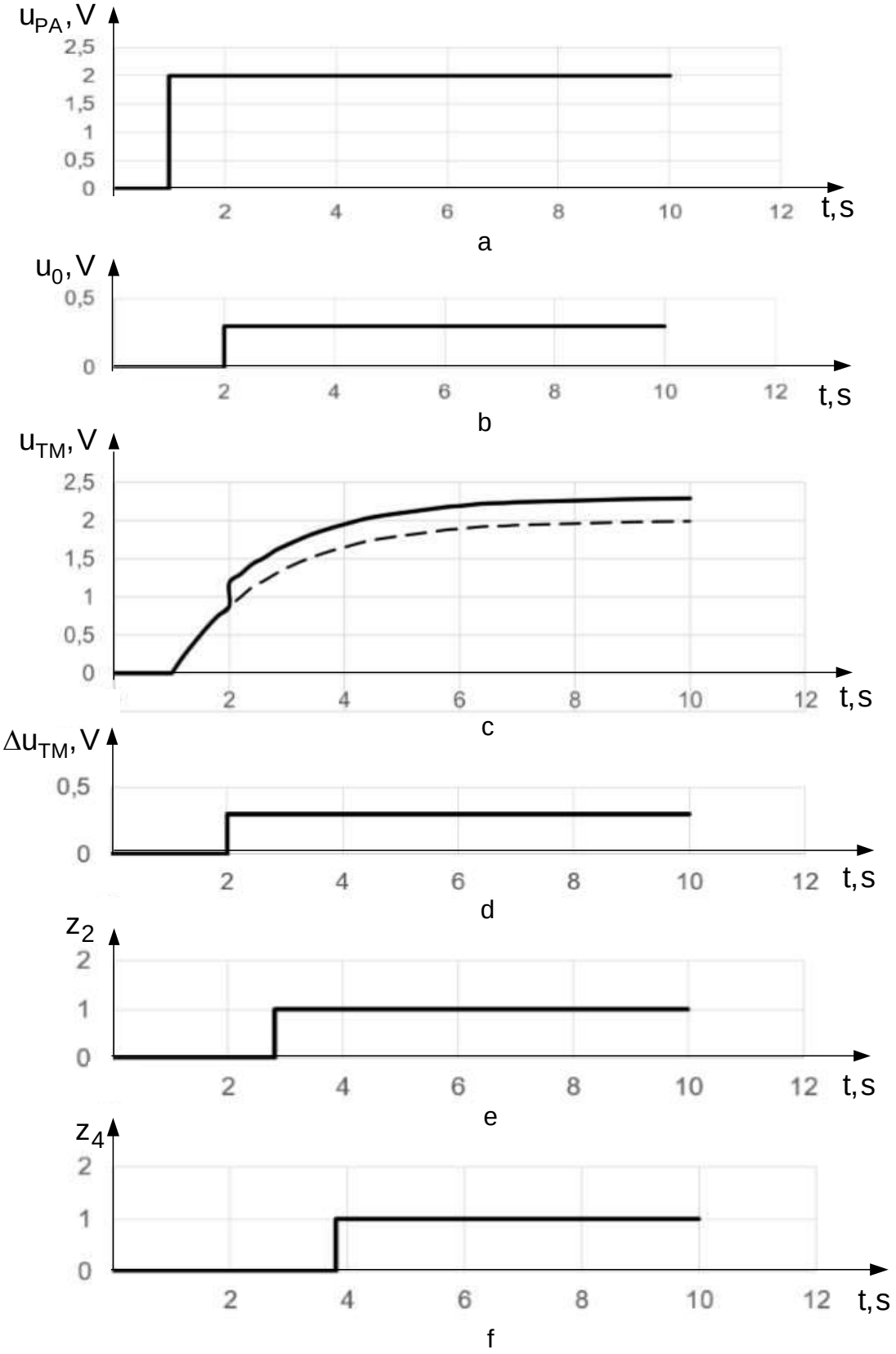

Figure 7.11 – Graphs of transient processes of subsystem (EFM+TM) in the case of destabilization d_{32}

The difference signal from the moment of time $t = 2\,s$ will increase to a constant value $\Delta u_{TM} = 0{,}3\,V$ (see Figure 7.11, d).

Δu_{TM} Next, the difference signal is processed according to the two-valued predicate equation (7.15). As a result, at the moment $\Delta t = 1{,}8\,s$ after the appearance of destabilizing influence d_{32}, the value of the Boolean sign Z_2 will indicate the appearance of destabilization in the functioning of the (EFM+TM) subsystem. The search for a destabilized functional element is carried out using a two-valued predicate equation, similar to the two-valued predicate equation (4.51), namely:

$$Z_4 = S_2\left\{\delta_4 - \left|\Delta u_{TM}(k+1) - \Delta u_{TM}(k)\right|\right\},\ k = \overline{1,N};\ \rho_4. \qquad (7.17)$$

With parameters $\delta_4 = \Delta u_{TM}$ and $\rho_4 = 0{,}8$, at the moment $t = 3{,}8\,s$, sign Z_4 acquires a single value, which indicates the presence of a destabilizing influence d_{32} that caused a malfunction of the (EFM+TM) subsystem.

In a similar way, the search for a destabilized functional element in the considered subsystem (EFM+TD) is carried out for other destabilizing influences from subsets D_2 and D_3. With destabilizing effects d_{21} – reduction of the EFM transfer coefficient and d_{31} – reduction of the TM transfer coefficient, the destabilized functional element cannot be detected. Although this is not necessary, since the only one possible means of restoring the functionality of the (EFM+TM) subsystem is signal adjustment.

7.3 Identification of destabilizing influences

After finding a destabilized functional element in the RCO, in order to obtain a complete diagnosis, it is necessary to determine the type and kind of destabilizing influences. The process of determining the type and type of destabilizing influences is essentially an identification process, as a result of which the name of the influence is established from the set $D = D_1 \cup D_2 \cup D_3$.

Let's consider instrumental means of identification to determine the type and kind of destabilizing influences in PA.

The effect of d_{11} in the EFM unit is simulated by reducing the PA gain. Therefore, the type and kind of this destabilizing influence coincide, so it is necessary to determine its type and numerical value for a complete diagnosis. A two-valued predicate equation is used to determine the kind:

$$Z_{11} = S_2\left\{\delta_{11} - \left|\Delta u_{PA}(k)u(k+1) - \Delta u_{PA}(k+1)u(k)\right|\right\},\ k = \overline{1,N};\ \rho_{11}. \quad (7.18)$$

The numerical value of the transfer factor is estimated using the arithmetic mean algorithm

$$\Delta\hat{k}_{ПП} = \frac{1}{m}\sum_{k=1}^{m}\frac{\Delta u_{PA}(k)}{u(k)}. \qquad (7.19)$$

Figure 7.12 shows graphs showing the process of obtaining a diagnosis under destabilizing influence d_{11}.

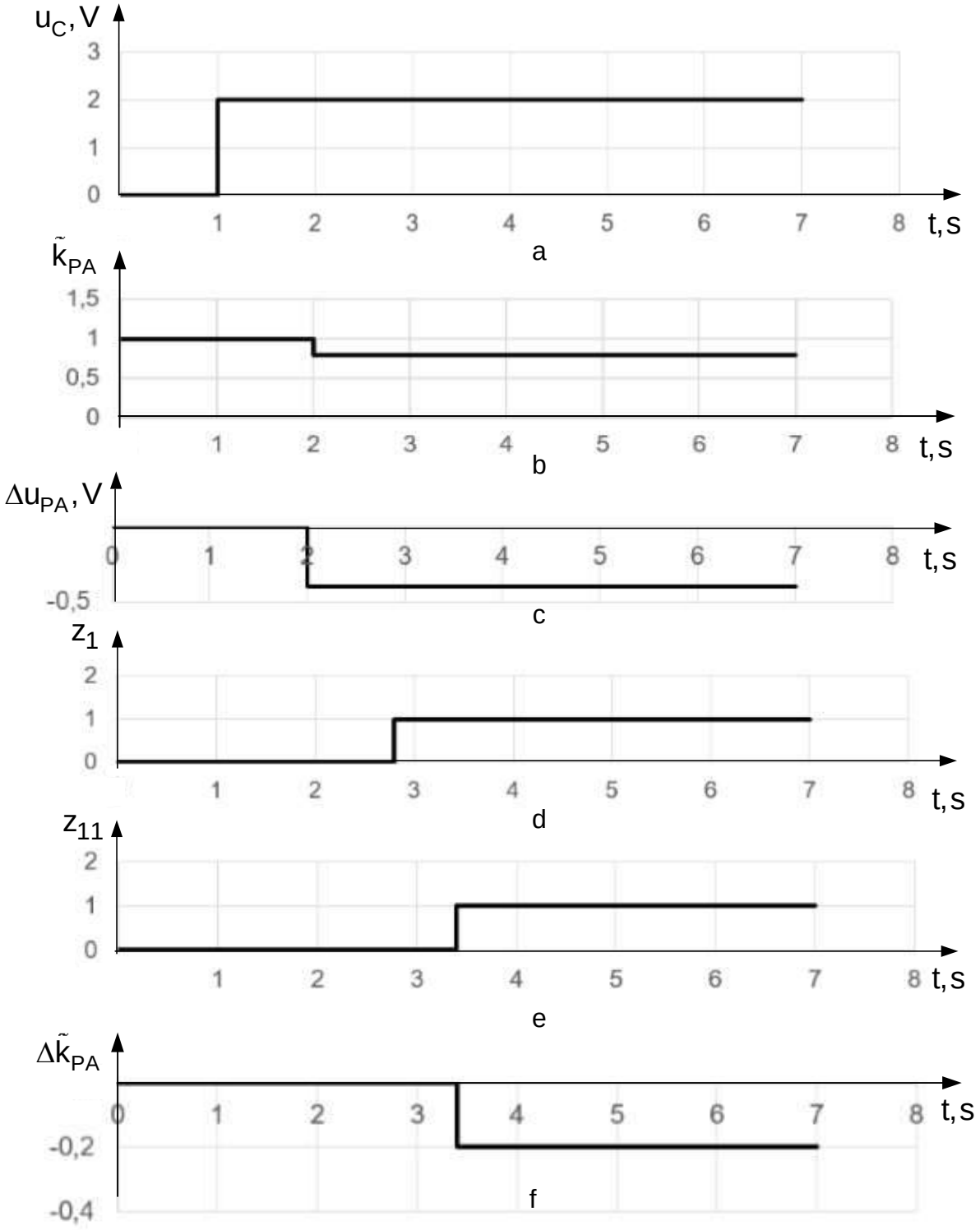

Figure 7.12 – Graphs of transient processes in PA during destabilization d_{11}

When applying to the input of the PA a step setting influence $u_C = 2\,V$ at the moment of time $t = 2\,s$, the value of the amplification factor decreases in leaps and bounds form 1 to 0,8. At this point in time, a difference signal $\Delta u_{PA} = -0,4\,V$ appears. In a moment of time $t = 2,8\,s$, a destabilizing influence is revealed. After a time interval $\Delta t = 0,8\,s$, the sign Z_{11} shows that the destabilizing action is associated with a decrease in the amplification factor. At the moment of time $t = 3,4\,s$, a numerical estimate of this decrease is obtained: $\Delta\hat{k}_{PA} = -0,5$. It took $\Delta t = 1,4\,s$ computing time to diagnose the destabilizing effect d_{11}.

B PP simulates two types of destabilizing influences: d_{12} – positive drift and d_{13} – negative drift, which are characterized by a parameter u_0. To determine the type of these influences, a two-valued predicate equation similar in structure to equation (4.30) is used, namely:

$$Z_{12} = S_2\left\{\delta_{12} - \left|\Delta u_{PA}(k+1) - \Delta u_{PA}(k)\right|\right\},\ k = \overline{1,N};\ \rho_{12}. \qquad (7.20)$$

To determine the sign of destabilizing influences, the following two-digit predicate equation is used:

$$Z_{121} = S_2\left\{\Delta u_{PA}(k) \geq \delta_{121}\right\},\ k = \overline{1,N};\ \rho_{121}. \qquad (7.21)$$

When $Z_{121} = 1$ – this means that the zero drift is positive, and when $Z_{121} = 0$ – zero drift is negative.

A complete diagnosis of destabilizing influences means obtaining a numerical estimate of the amount of drift. Therefore, to obtain a numerical estimate of the drift value, the algorithm for obtaining the root mean square value is used

$$\hat{u}_0 = \frac{1}{m}\sum_{k=1}^{m}\Delta u_{PA}(k). \qquad (7.22)$$

The graphs that consistently reveal the process of detecting the destabilizing effect of d_{13} on the performance of the PA, is shown in Figure 7.13. At the moment of time $t = 1s$, a step-specific influence $u_C = 2\,V$ is applied to the input of the PA.

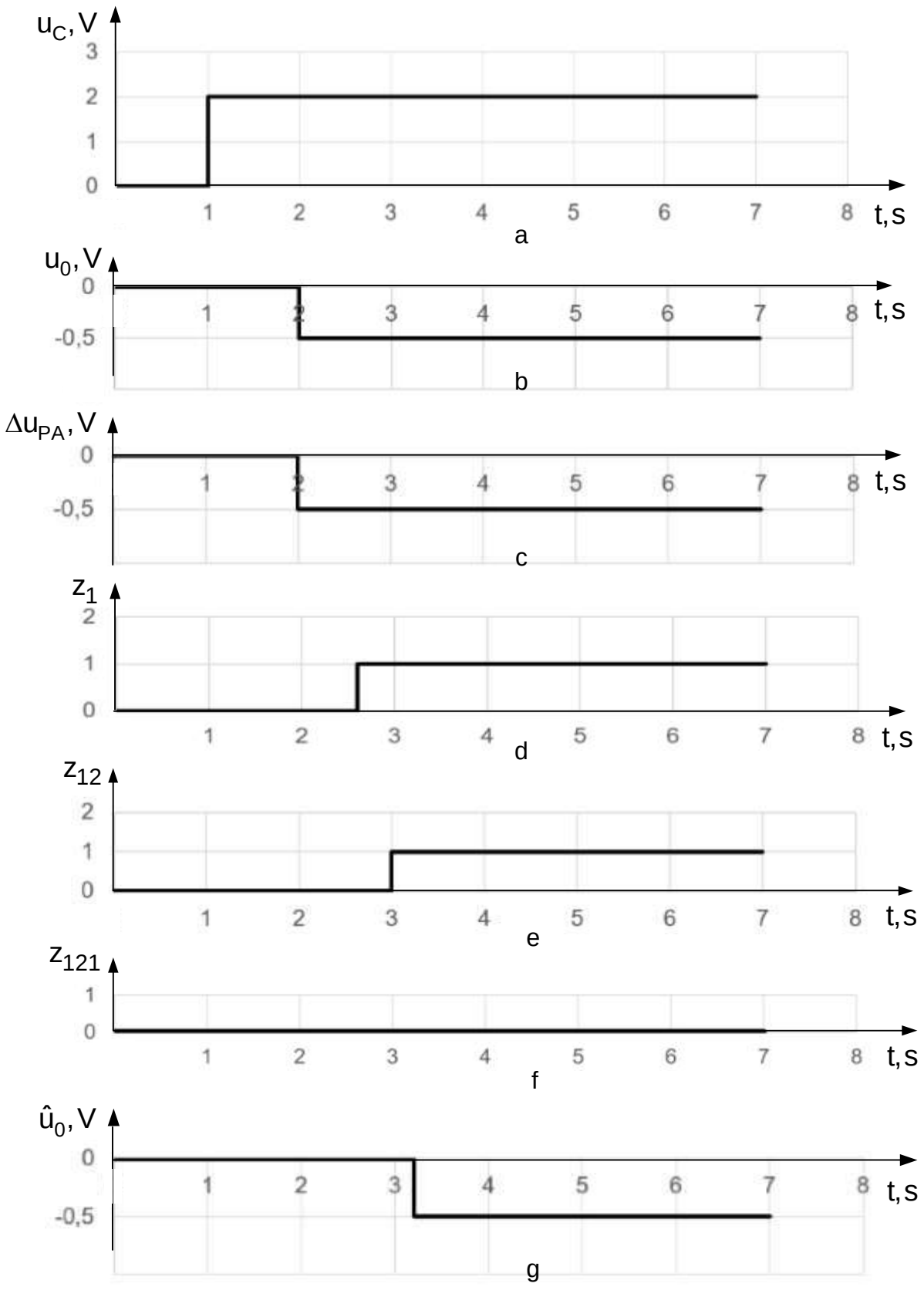

Figure 7.13 – Graphs of transient processes of PA during destabilization d_{13}

At the next moment in time $t = 2\,s$, a step-like appearance of a negative zero drift is simulated $u_0 = 0{,}5\,V$ (Figure 7.13, b). At this point in time, the difference signal changes in leaps and bounds $\Delta u_{PA} = -0{,}5\,V$ (Figure 7.13, c). With the help of Boolean sign Z_1, at the moment of time $t = 2{,}6\,s$, a malfunction in the functioning of the PA is detected (Figure 7.13, d). The Boolean sign Z_{12} at the moment of time $t = 3\,s$ acquires a single value, which indicates the presence of a zero drift (Figure 7.13, e). At the moment of time $t = 3{,}2\,s$, the value of the Boolean sign is $Z_{121} = 0$, which means the presence of a negative drift of zero (Figure 7.13, f). And by this point in time $t = 3{,}2\,s$, a numerical estimate of this drift has already been formed $\hat{u}_0 = -0{,}5$ V. Thus, from the moment $\Delta t = 1{,}2\,s$ of the appearance of a destabilizing influence to obtaining a numerical value, it was necessary to diagnose a destabilized PA.

After installing an inoperable functional element in the subsystem (EFM+TM), the kind of destabilizing influences is identified.

Destabilizing influences d_{21} – reduction of the EFM transfer coefficient and d_{31} – reduction of the TM transfer coefficient cannot be identified separately due to structural undiagnosedness [26].

However, it is not necessary to ensure the structural diagnosticity of the (EFM+TM) subsystem, because there is only one resource for parrying of d_{21} and d_{31} in the EFM miodel unit – signal adjustment. Therefore, we will consider instrumental means and graphs for determining the type and kind of destabilizing influence d_{21}. A two-valued predicate equation is used to determine the type and type of this influence:

$$Z_{21} = S_2\left\{\delta_{21} - \left|\left[\Delta u_{TM}(k+2) - \left(1 - \frac{T_0}{T_{EFM}}\right)\Delta u_{TM}(k+1)\right]u_{PA}(k) - \right.\right.$$
$$\left.\left. - \left[\Delta u_{TM}(k+1) - \left(1 - \frac{T_0}{T_{EFM}}\right)\Delta u_{TM}(k)\right]u_{PA}(k+1)\right|\right\};\ k = \overline{1,N};\ \rho_{21}. \qquad (7.23)$$

The numerical estimation of the deviation of the transfer coefficient is calculated using the formula:

$$\Delta\hat{k}_{EFM} = \frac{1}{mT_0 k_{TM}}\sum_{k=1}^{m}\frac{T_{EFM}\,\Delta u_{TM}(k+1) - (T_{EFM} - T_0)\,\Delta u_{TM}(k)}{u_{PA}(k)}. \qquad (7.24)$$

Figure 7.14 presents graphs of the processes of diagnosing the type of destabilizing influence d_{21}. The experiment was carried out with the application of a stepwise effect $u_{PA} = 2\,V$ at a moment in time $t = 1s$ (Figure 7.14, a). Until now, the reduction of the transfer coefficient was simulated: $\tilde{k}_{PA}$= 250 $\frac{rad}{Vs}$ (graph 2). Graph 1 shows the nominal value of the transfer coefficient (Figure 7.14, b). Transient characteristic 2 reflects the response of an inoperable EFM compared to an operational one, graph 1 (Figure 7.14, c). Δu_{TM} A differential signal indicates a malfunction (Figure 7.14, d). The Boolean sign Z_2 takes the value "1" at the moment of time $t = 1{,}8\,s$, which indicates the inoperability of the (EFM+TM) subsystem (Figure 7.14, e). At the moment of time $t = 2{,}4\,s$, Boolean sign $Z_{21} = 1$, which means the detecting of the cause of inoperability – k_{PA} (Figure 7.14, f).

A numerical estimate of the magnitude of the deviation of the transfer coefficient appears at the moment $t = 2{,}4\,s$. Thus, it takes $\Delta t = 1{,}4\,s$ of computing time to diagnose the deviation of the transfer coefficient.

The same diagnostic procedure is used for the kind of destabilization d_{31} – reduction of the TM transfer coefficient.

Let's consider the peculiarities of the procedure for diagnosing the kind of destabilization d_{22} – an increase in the time constant. This kind of destabilization is associated with an increase in the inertial properties of EFM.

The identification of this kind of destabilization begins with the determination of the type using a two-valued predicate equation:

$$Z_{22} = S_2\left\{\delta_{22} - \left\|\left[\Delta u_{TM}(k+2) - \left(1 - \frac{T_0}{T_{EFM}}\right)\Delta u_{TM}(k+1)\right]\times\right.\right.$$

$$\times\left[u_{TM}(k) - k_{EFM}k_{TM}u_{PA}(k)\right] - \left[\Delta u_{TM}(k+1) - \left(1 - \frac{T_0}{T_{EFM}}\right)\Delta u_{TM}(k)\right]\times$$

$$\left.\left.\times\left[u_{TM}(k+1) - k_{EFM}k_{TM}u_{PA}(k+1)\right]\right\|\right\};\ k = \overline{1,N};\ \rho_{22}. \qquad (7.25)$$

The numerical estimation of the deviation of the time constant is calculated as follows:

$$\Delta\hat{T}_{EFM} = \frac{T_{EFM}}{mT_0}\sum_{k=1}^{m}\frac{T_{EFM}\Delta u_{TM}(k+1) - (T_{EFM} - T_0)\Delta u_{TM}(k)}{u_{TM}(k) - k_{EFM}k_{TM}u_{PA}(k)}. \qquad (7.26)$$

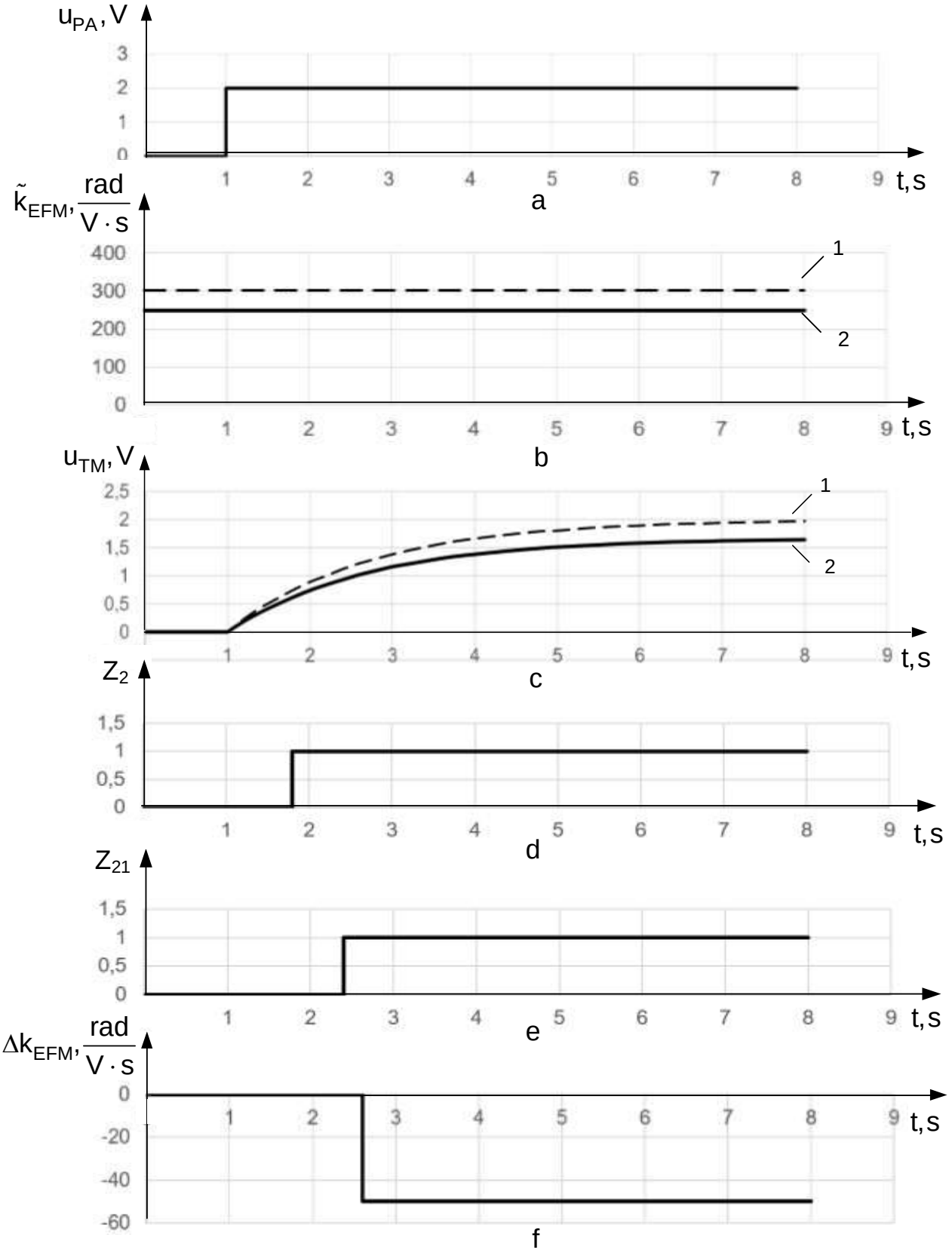

Figure 7.14 – Cyclogram of diagnosing the type of destabilization d_{21}

Figure 7.15 shows signals reflecting the process of diagnosing the type of destabilization d_{31}.

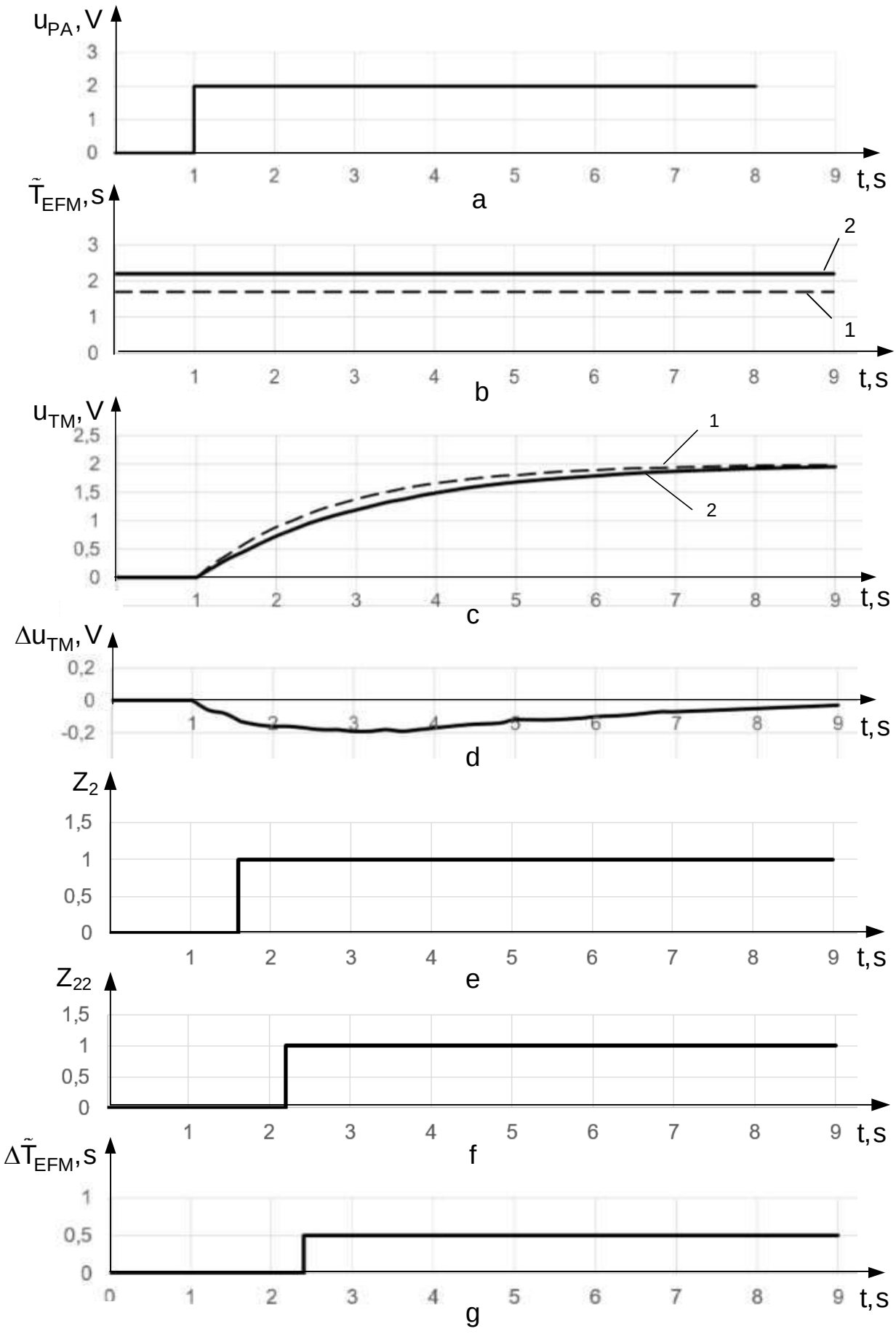

Figure 7.15 – Cyclogram of diagnosing the type of destabilization d_{31}

The experiment was carried out under test influence $u_{PA} = 2\,V$ (Figure 7.15, a) and with an increased time constant $\tilde{T}_{EFM} = 2,2\,s$ – graph 2. Graph 1 shows the nominal value (Figure 7.15, b). Delayed (graph 2) and nominal (graph 1) transient characteristics are shown in Figure 7.15, c. When a difference signal Δu_{TM} appears (Figure 7.15, d), the Boolean sign Z_1 acquires the value "1" at the moment of time $t = 1,6\,s$. The value of the Boolean sign $Z_{22} = 1$ at time $t = 2,2\,s$ indicates the found cause of EFM destabilization (Figure 7.15, e). Time interval $\Delta t = 1,2\,s$ was spent on diagnosis of destabilization d_{22}.

Let's consider how to identify the kind of destabilizing influence d_{32} for TM. Using the two-valued predicate equation (7.17), it is established, firstly, that the destabilizing influence d_{32} disrupted the performance of the TD, and secondly, that of all the destabilizing influences from the set D_3 these may be influences d_{32} and d_{33} that lead to zero drift. Thus, at $Z_4 = 1$, the type of influence is determined – it is zero drift. To determine a specific kind, it is necessary to find the sign of the drift of zero and the numerical value of its magnitude. The sign of the zero drift is set using a two-digit predicate equation:

$$Z_{41} = S_2\left\{\Delta u_{TM}(k) - \delta_{41}\right\};\ k = \overline{1,N};\ \rho_{41}. \qquad (7.27)$$

The numerical value of the zero drift value is calculated as the arithmetic mean of the discrete values of the difference signal

$$\hat{u}_0 = \frac{1}{m}\sum_{k=1}^{m}\Delta u_{TM}(k). \qquad (7.28)$$

The graphs of experimental studies of the algorithm and the program for diagnosing destabilizing influence d_{32} – positive zero drift of TM is shown in Figure 7.16. Before setting the test influence $u_{PA} = 2\,V$ the zero drift was already in the TM (Figure 7.16, b). The output signal $\Delta\tilde{u}_{TM}$ from the moment of time $t = 1\,s$ is constant and positive. The value of the Boolean sign $Z_2 = 1$ indicates the destabilization of the (EFM+TM) subsystem. As a result of finding a destabilized TM, the Boolean sign Z_4 takes on a value «1». Then, with the help of a Boolean sign, it is determined that the TM has a positive drift of zero (Figure 7.16, g) and its numerical value is $\hat{u}_0 = 0,3\,V$. Computing time $\Delta t = 1,4\,s$ was spent on diagnosing this kind of destabilizing influence, and at the same time, the accuracy of the assessment was no more than 2%.

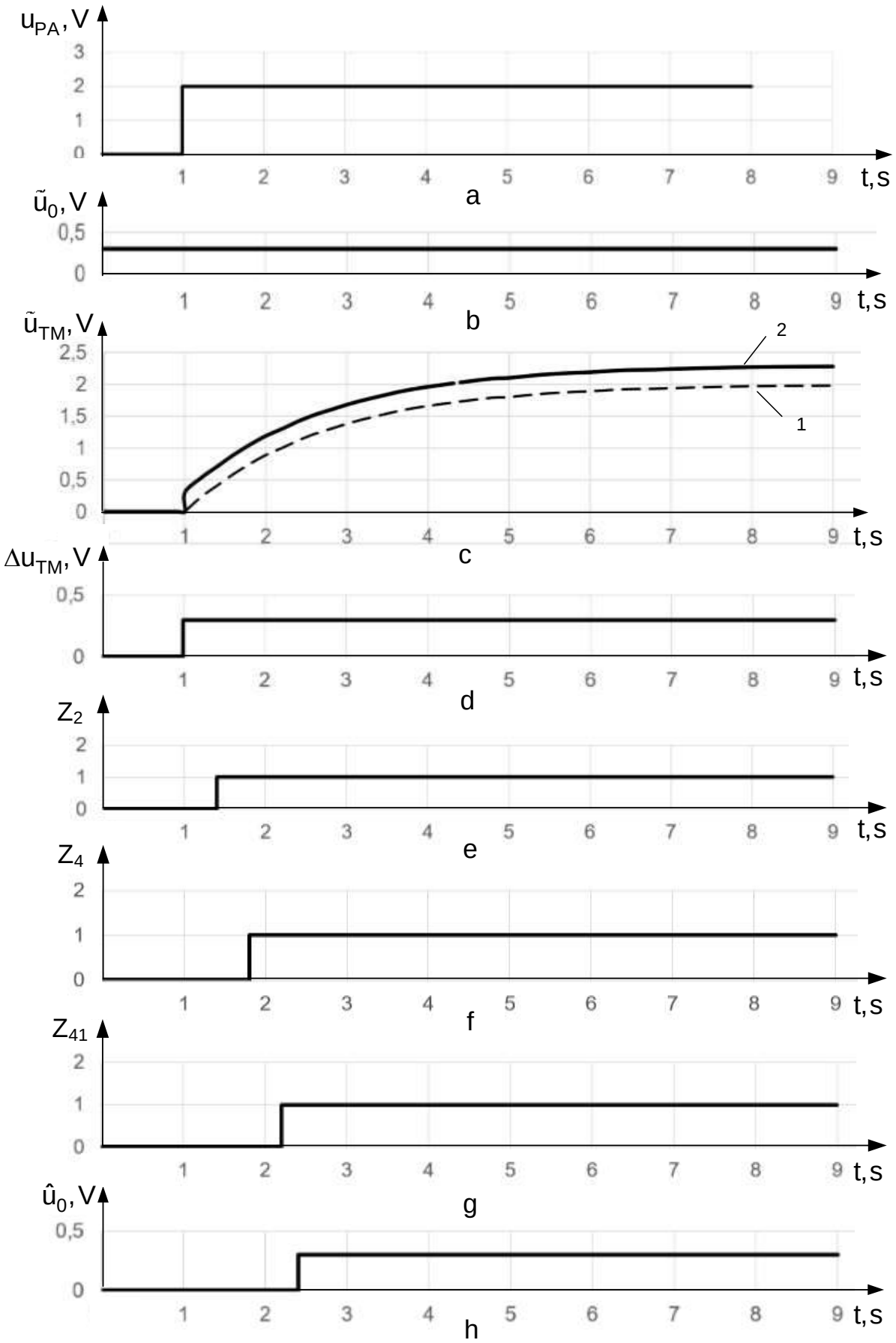

Figure 7.16 – Charts of the processes of diagnosing the kind of destabilization d_{32}

An experimental study of algorithms and programs for the identification of other unrepresented types of destabilizing influences made it possible to determine a reliable possibility of determining their type and kind during a time interval $\Delta t = 1{,}5\,s$ with an accuracy of 3%.

7.4 Restoring the performance of the model unit of electric flywheel motors

Destabilizing influences from sets D_1, D_2 and D_3 lead to disruption of RCO functioning, in other words, to disruption of its operability. In order to restore RCO performance, means of compensating the consequences of destabilizing influences, and algorithms and programs for their use are needed. In the experimental stend, the simplest option for choosing compensation means is implemented, when each type of destabilizing influence has its own means of compensation for its consequences, which ensures the restoration of RCO performance. Let's consider these tools in more detail.

Therefore, as a result of diagnosing PP, such kinds of destabilizing influences are revealed as d_{11} – reducing the transfer coefficient; d_{12} – positive drift; d_{13} – negative drift; d_{14} – break of input wire.

d_{11} In the event of a destabilizing influence, its negative effect is compensated by means of signal adjustment. At the same time, a compensating signal is added to the input control signal $u_C(k)$

$$u_K(k) = \Delta\hat{k}_{PA} u_C(k), \tag{7.29}$$

then a new control signal

$$u'_C(k) = \left(1 + \Delta\hat{k}_{PA}\right) u_C(k) \tag{7.30}$$

will ensure the operation of the RCO.

With a positive drift d_{12}, its compensation is carried out by a signal:

$$u'_C(k) = u_C(k) - \hat{u}_0. \tag{7.31}$$

With a negative drift d_{13} the control signal is shifted by the value of the estimate $\hat{u}_0$:

$$u'_C(k) = u_C(k) + \hat{u}_0. \tag{7.32}$$

With a destabilizing influence d_{14}, a complete failure of the PA is observed, and therefore the RCO is removed from the operation of the model unit by turning off the power supply and blocking its input and output signals.

The graphs of the processes of restoring the operability of the RCO under destabilizing influence d_{11} is shown in Figure 7.17.

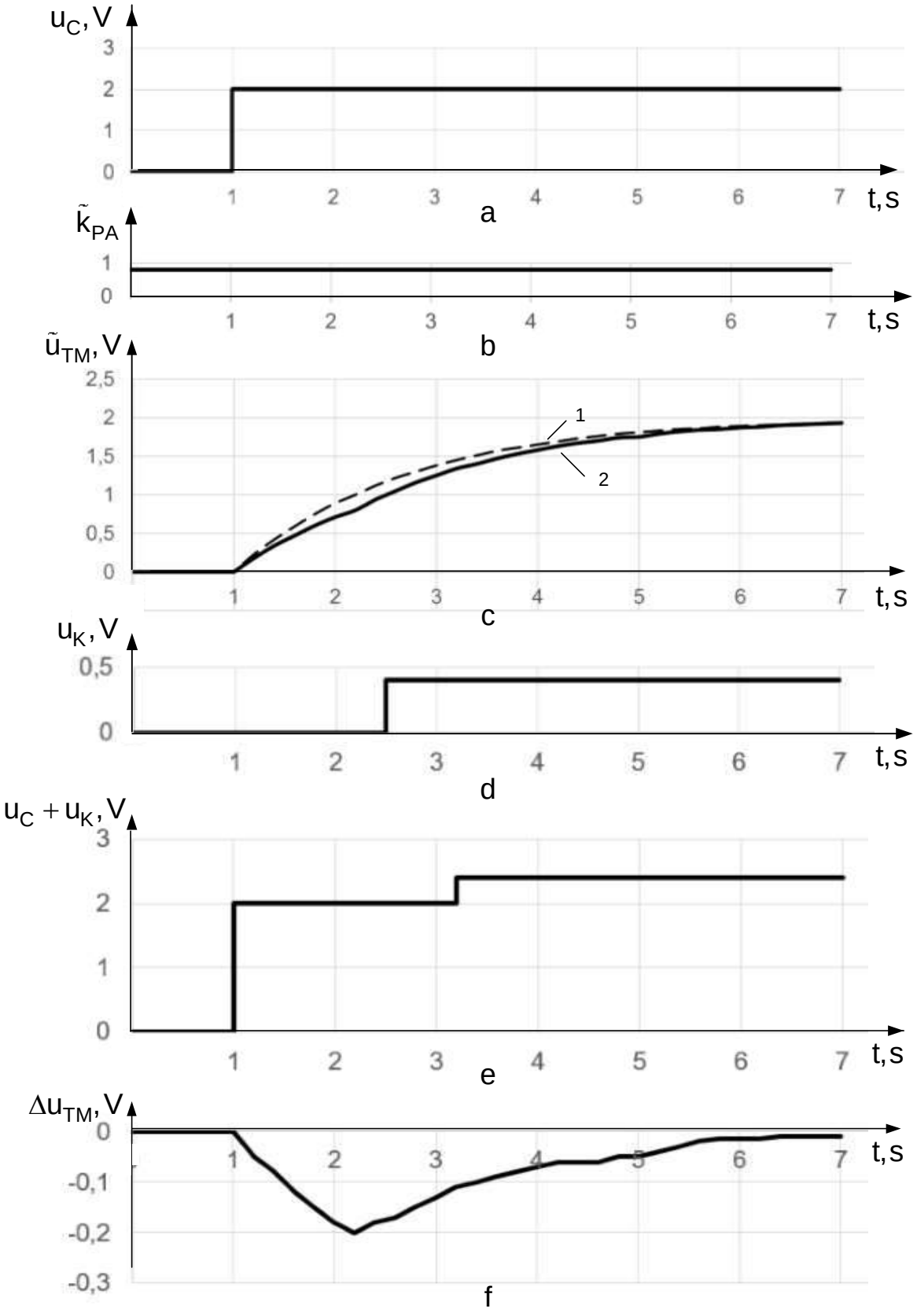

Figure 7.17 – Graphs of transient processes in the kind of destabilization d_{11}

The setting effect of the step type, which is applied to the RCO at the moment $t = 1s$, is presented in Figure 7.17, a. The destabilizing influence is introduced at the time $t = 0$ with magnitude $\tilde{k}_{PA} = 0,8$ (Figure 7.17, b). Figure 7.17, c shows two graphs of transient processes: 1 – nominal, 2 – disturbed. Before time $t = 2,5s$, diagnosis takes place, and after that – restoration of the operability. The compensatory signal appears after diagnosis (Figure 7.17, d) and the total signal of control effect is presented in Figure 7.17, d. The difference signal in the most obvious form characterizes the peculiarities of diagnosing and restoring the operability of the RCO (Figure 7.17, e). So, the diagnosis process starts from the moment $t = 1s$ of processing Δu_{TM}. The diagnosis continues until the moment $t = 2,5s$, and at the same time the quality of the operation of the EFM deteriorates, since the difference signal reflects the error of operation with respect to the nominal mode. After the moment $t = 3s$ a signal $u_K(k)$ (7.29) and a new control influence are generated (see Figure 7.17, e), which leads to a decrease, and until the moment of time $t = 4,5s$, to complete compensation of the difference signal – the error of functioning. So, the process of diagnosing and restoring the RCO's performance took $\Delta t = 3,5s$. The time of the transition process in both the nominal and destabilized modes has not changed and is $t_{PA} = 4,5s$ (see Figure 7.17, c, graph 1).

Let us consider the processes of compensating the consequences of a kind of destabilizing influence d_{12} – positive zero drift. Graphs characterizing the process of diagnosing and restoring the operability of the RCO, is shown in Figure 7.18.

A transient process begins during the application of a stepped satisfactory effect $u_C = 2V$ to the RCO (Figure 7.18, c). At the moment of time $t = 1,5s$, the zero drift increases in leaps and bounds $u_0 = 1V$ (Figure 7.18, b), which leads to the deviation of the transient process of the RCO from the nominal one (dashed curve) (Figure 7.18, c). By the moment of time $t = 3s$, the diagnosis process ends and the numerical value of the compensation voltage is formed $u_K = -0,5V$ (Figure 7.18, d). From this point in time, the controlling influence decreases in leaps and bounds (Figure 7.18, e).

The differential signal illustrates well the result of the diagnosis and recovery process (Figure 7.18, f). This graph shows that the differential signal increases during the diagnosis interval $\Delta t = 1,5s$. From the moment $t = 3s$,

the zero drift compensation process begins and the difference signal asymptotically decreases until the end of the nominal transient process of the RCO. The entire process of diagnosis and recovery did not exceed the time limit of the transition process of the RCO.

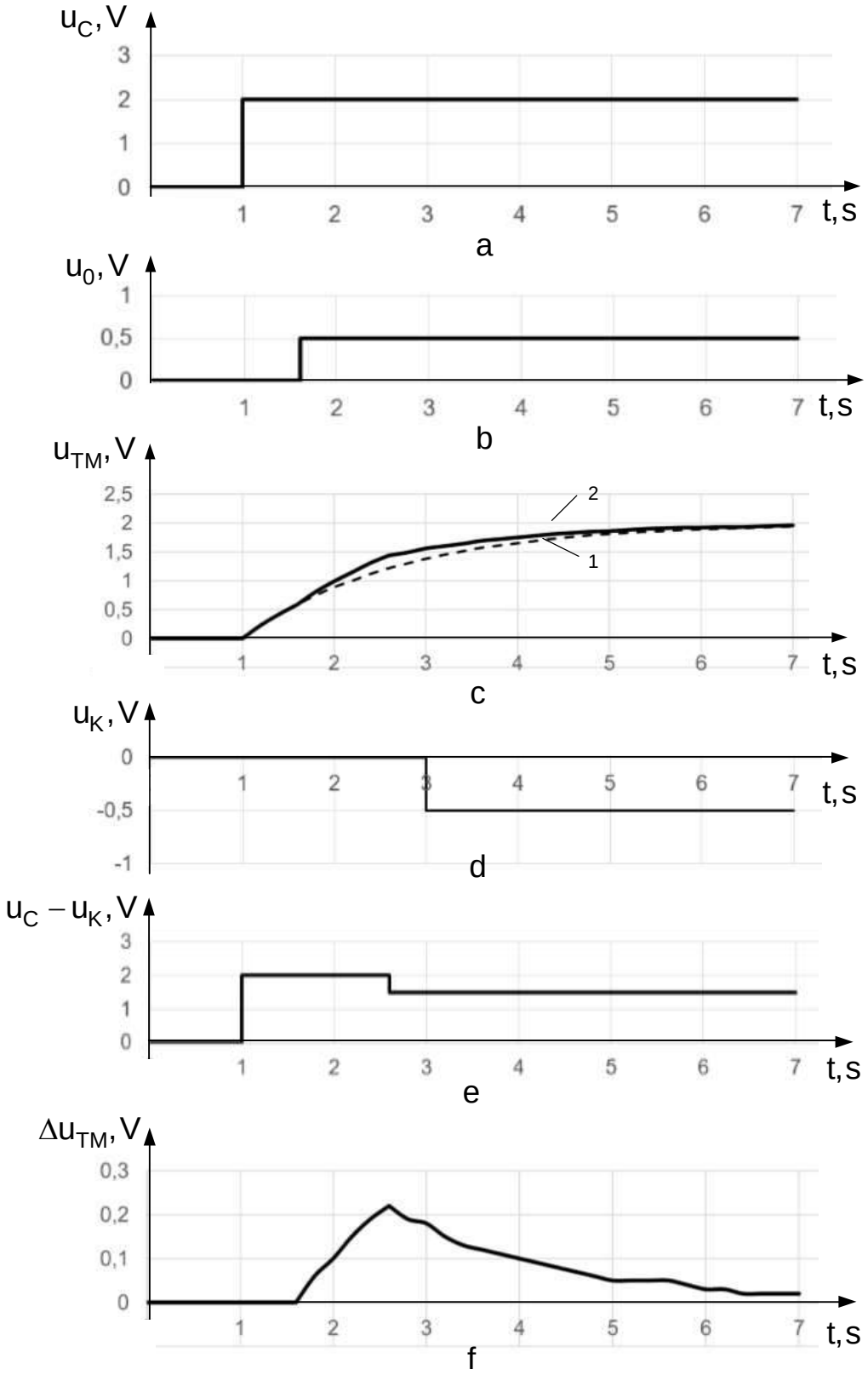

Figure 7.18 – Graphs of transient processes by kind of destabilization d_{12}

Diagnostics of the subsystem (EFM+TM) makes it possible to determine the following types of destabilizing influences: – reducing the transfer coefficient; d_{22} – increasing the time constant; d_{23} – break in the control chain; – reducing the transfer coefficient; d_{32} – positive drift; d_{33} – negative drift; d_{34} – break in output wire.

In the case of a decrease in the transfer coefficient of the EFM, restoration of its operability is possible with the help of signal adjustment, which consists in such an additional to the main control signal that the previous value of the angular velocity is restored $\omega(t)$, and hence the moment $m(t)$. The additional signal is calculated as follows:

$$u_K(k) = \Delta\hat{k}_{EFM}\, k_{TM}\, u_C(k), \tag{7.33}$$

then the adjusted control signal

$$u'_C(k) = \left(1 + \Delta\hat{k}_{EFM}\, k_{TM}\right) u_C(k). \tag{7.34}$$

Such a new control signal ensures a high-quality compensation of the destabilizing effect d_{31} and restoration of the operational efficiency of the RCO.

In case of a destabilizing effect d_{32} – an increase of the constant time to restore the operational efficiency of the RCO, the procedure of phase advance of the control signal using the following algorithm is used:

$$u'_C(k+2) = u'_C(k+1) - \left(1 - \frac{T_0}{a}\right)\left[u_C(k) - \tilde{u}_{TM}(k)\right], \tag{7.35}$$

where a – a coefficient that depends on the value of the estimate $\Delta T_{ЕДМ}$.

In the event of a break in the control circuit (kind d_{23}), the channel is completely inoperable, and therefore the procedure for removing it from the functioning process is used by turning off the power supply of all functional elements of the RCO and blocking input and output signals.

In the case of destabilization d_{31} – reduction of the transfer coefficient of TM, which cannot be distinguished from the destabilizing effect d_{21} – reduction of the transfer coefficient of EFM, a corrected control signal of the form is used to restore operational efficiency:

$$u'_C(k) = \left(1 + k_{EFM}\, \Delta\hat{k}_{TM}\right) u_C(k), \tag{7.36}$$

which ensures complete and high-quality restoration of the operability of the RCO.

If a positive drift d_{32} occurs in the operation of the TM, the output signal $\tilde{u}_{TM}(k)$ is shifted by the value of the drift estimate

$$\hat{u}_{TM}(k) = \tilde{u}_{TM}(k) - \hat{u}_0. \quad (7.37)$$

If a negative drift occurs in the TM, the output signal is restored as follows:

$$\hat{u}_{TM}(k) = \tilde{u}_{TM} + \hat{u}_0. \quad (7.38)$$

If the destabilizing influence is a break in the output of TD kind d_{34}), then one can use the estimated values of the reference model $\hat{u}_{TM}(k)$.

Let's consider how the recovery of the operational efficiency of the RCO occurs in the event of the appearance of a kind of destabilizing influence d_{22} – an increase in the constant time of EFM. Graphs of the processes taking place in the rational control system make it possible to display this more clearly (Figure 7.19).

In the course of the experiment, a stepwise effect $u_C = 2\,V$ was given at the moment of time $t = 1s$. The simulation of the jump-like increase in the EFM time constant is carried out at the moment of time $t = 1{,}5\,s$ by the value $\Delta T_{EFM} = 0{,}5\,s$ (Figure 7.19, b). Transient process in RCO is nomilnal during the interval from $t = 1s$ up to $t = 1{,}5\,s$ (Figure 7.19, c). After diagnosing the kind of destabilization, a new control influence u'_3 is formed with the help of algorithm (7.35), which exerts a forcing effect on the RCO (Figure 7.19, d). As a result, the operational efficiency of the RCO is restored (Figure 7.19, e). The difference signal makes it possible to obtain quantitative estimates of the diagnosis and recovery time $\Delta t = 1{,}5\,s + 2\,s = 3{,}5\,s$, as well as the maximum error $\Delta u_{TM} = 0{,}2\,V$ and accuracy of recovery $\Delta u_{TM}(\infty) = 0{,}1V$.

The obtained experimental data testify to the productivity of the procedures for diagnosing and restoring the operability of the ORU under such a destabilizing influence as an increase in the inertial property of the ORU.

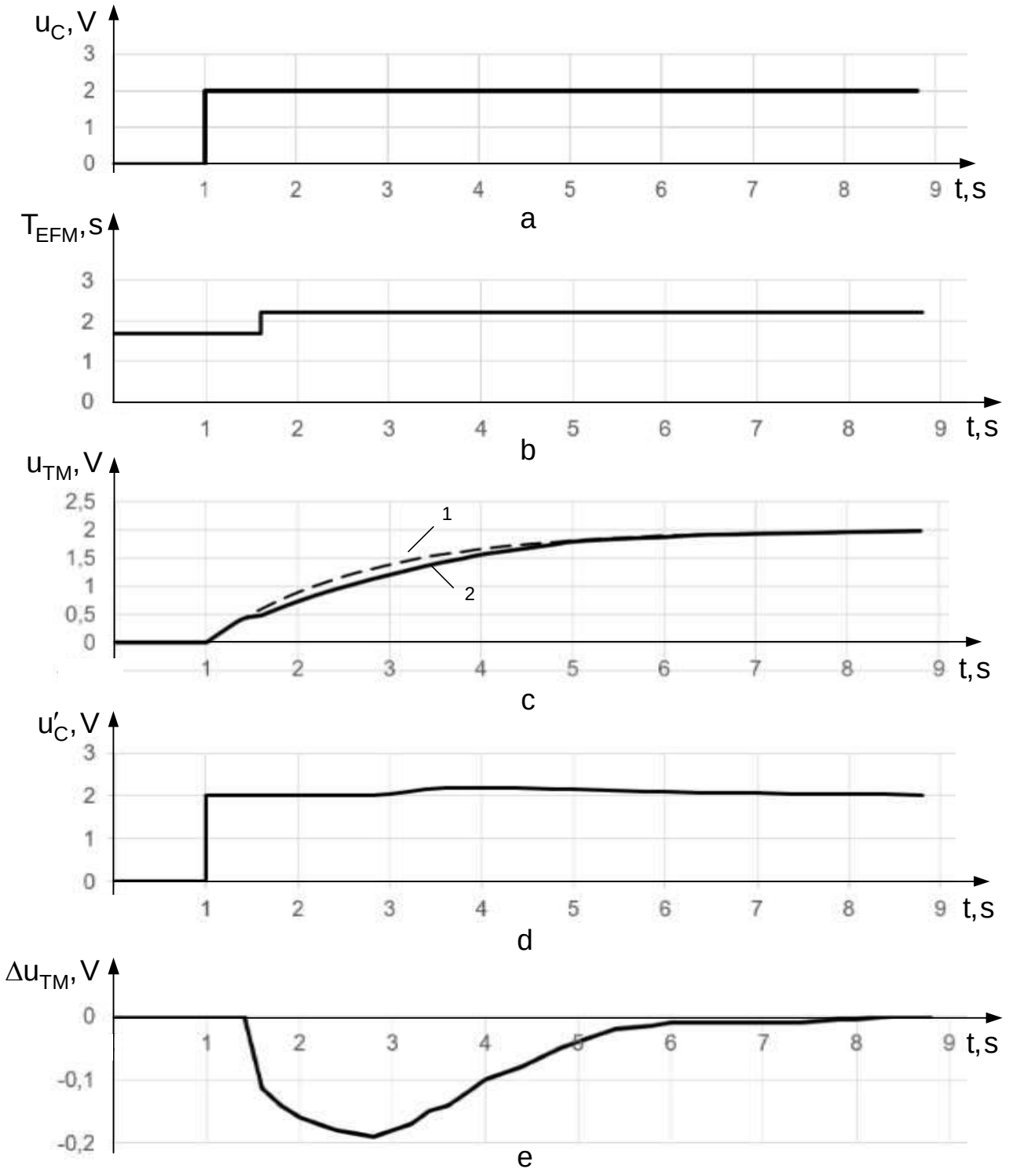

Figure 7.19 – Graphs of transient processes by kind of destabilization d_{22}

With a negative zero drift of TM – is a type of destabilizing influence d_{33}, the TM signal shifts by the amount of the drift. Transient processes caused by simulation, diagnosis, and restoration of operational efficiency of the RCO are presented in Figure 7.20.

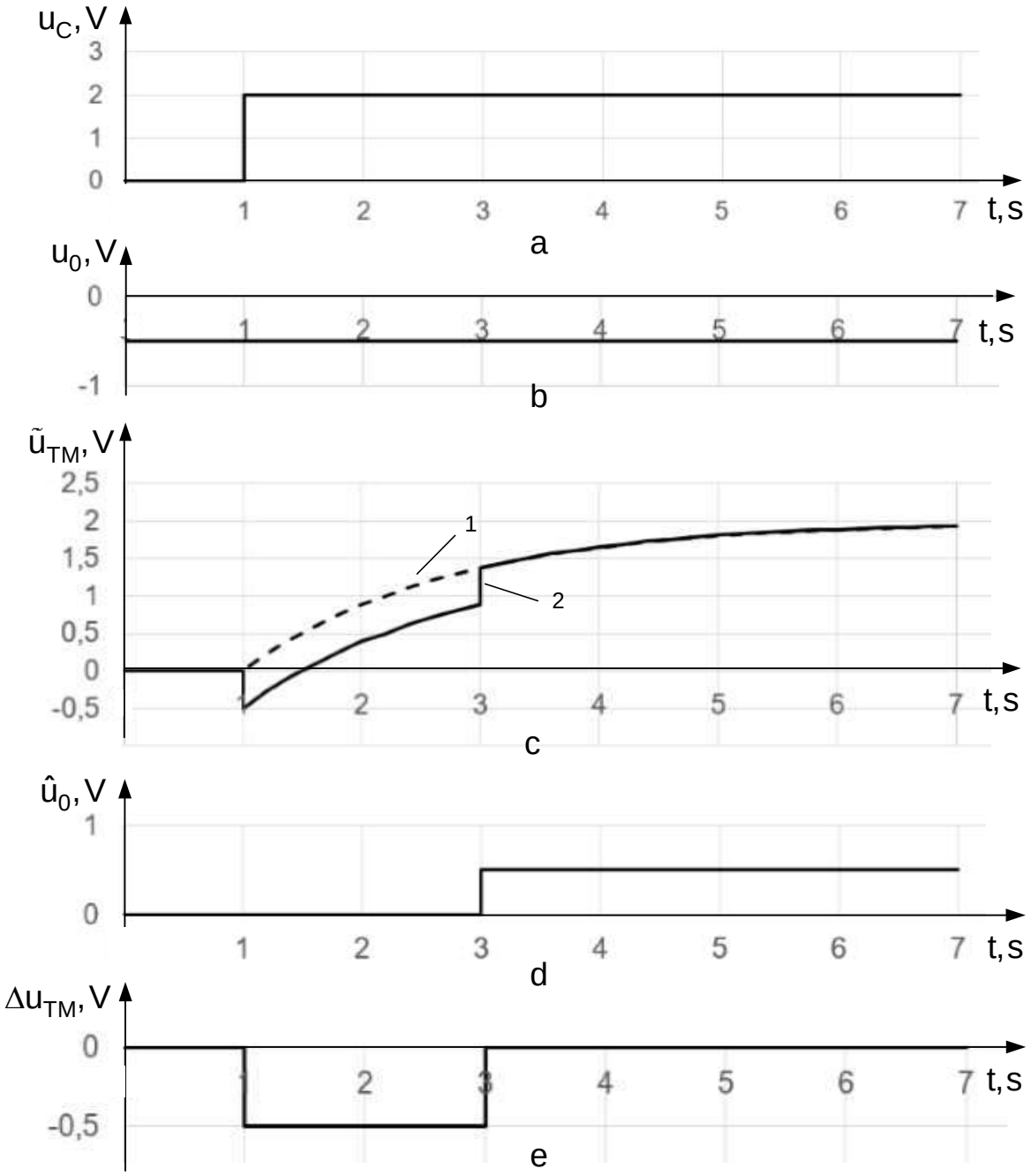

Figure 7.20 – Graphs of transient processes by kind of destabilization d_{33}

A negative drift of zero is introduced at the ьщьуте of time $t = 0$ before applying the control influence $u_0 = -0{,}5\,V$ (Figure 7.20, b). The reaction of the RCO to the step-setting influence is shifted relative to the nominal one by the amount of drift (Figure 7.20, c) to a point in time $t = 3{,}5\,s$. At the moment of time $t = 3{,}5\,s$ after diagnosis and recovery, an estimated drift $\hat{u}_0$ appears (Figure 7.20, d), which according to the algorithm (7.38) ensures the restoration of the TM output signal to the nominal one. According to the difference signal Δu_{TM}, the duration of the processes of diagnosis and

restoration of TM measurements is evident, as well as the accuracy of restoration and the nature and duration of the error in the case of an extraordinary situation associated with a negative drift of TM zero. The results of experiments with the appearance of positive drifts in the functioning of TM are similar to the considered one.

The complete failure of the TM creates a difficult abnormal situation for the RCO, associated with the lack of information about the state of the EFM. To investigate this situation, a type of destabilization d_{34} (break in the output wire of TM) was simulated in the EDM model unit. The characteristics that reflect the processes of diagnosing and restoring RCO operability in the absence of a signal from the TM, are shown in Figure 7.21.

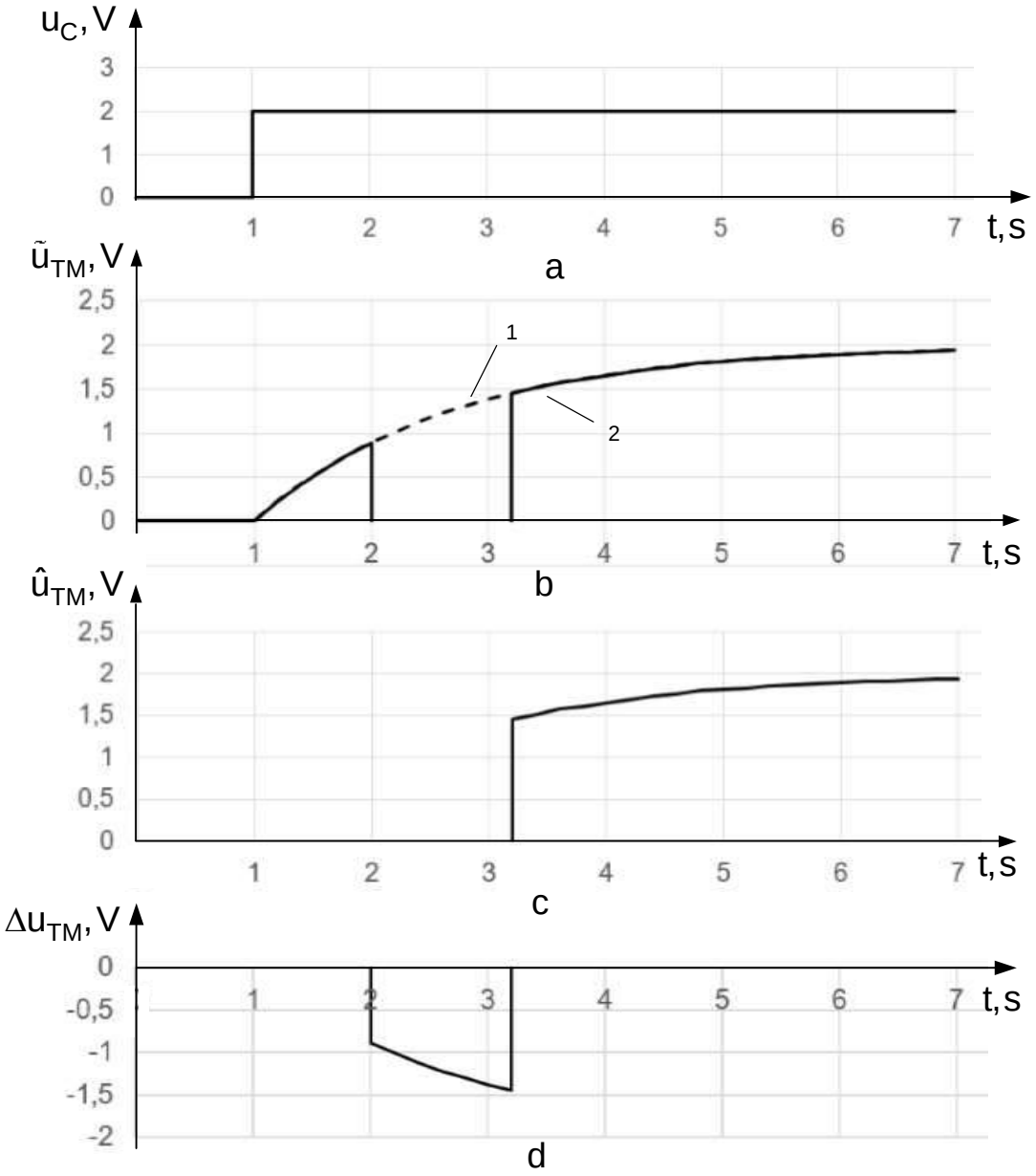

Figure 7.21 – Graphs of transient processes by kind of destabilization d_{34}

When a step control effect $u_C = 2\,V$ is presented at a moment in time $t = 1s$, a transition process begins in the RCO (Figure 7.21, b). The transitional process continues until $t = 2\,s$, because at this point in time, a break of the TM output wire is simulated. The signal from the TM disappears (see Figure 7.21, b). The absence of a signal lasts until the moment of time $t = 3{,}5\,s$. During this interval of time, diagnostics were carried out and a decision was made to resume TM measurements using the reference model. At the moment $t = 3{,}5\,s$, the data from the reference model is connected (Figure 7.21, c). As can be seen in the graph (see Figure 7.21, b). From the moment of time $t = 3{,}5\,s$, there was a restoration of TM output information, and therefore, a restoration of the operational efficiency of the RCO. The difference signal Δu_{TM} (Figure 7.21, d) makes it possible to obtain quantitative estimates of the processes of diagnosis and restoration of operability. So, computing time spent on diagnostics and recovery is $\Delta t = 1{,}5\ s$. The maximum error of RCO functioning in a abnormal situation was $\Delta u_{TMmax} = 1{,}5\ V$. The accuracy of the recovery of measurements was $\Delta u_{TM}(\infty) = 0{,}1\,V$.

Experiments with the simulation of other types of destabilization of the operation of the RCO made it possible to verify the fundamental possibility of diagnosing on a real time and restoring its operability during the transition period for the diagnosed types of destabilization of the EFM model unit.

CONCLUSION

It is not enough just to acquire knowledge: it is necessary to find its application. It is not enough to wish, it is necessary to do.

Johann Wolfgang Goethe (1749 - 1832) – one of the founders of German literature, one of the most outstanding researchers of nature of his time

The use of electric flywheel motors in systems of orientation and stabilization of space vehicles for various purposes is a trend direction in cosmonautics. The requirements of long-term space missions gives rise to the need to find new management principles that would ensure the functioning of orientation systems even in the case of unavoidable emergency situations more effectively than the used majority structures. It is obvious that the new principles should be based on the ideas and tools of adaptive control. One of the new principles of adaptive control is the principle of control by diagnosis. The implementation of this principle is connected with the use of ideas of in-depth diagnosis of the causes of abnormal situations and flexible control of excessive resources to counter them. The development of models and methods of diagnosis and restoration of operability allowed to form a new class of adaptive control systems: rational control systems.

The monograph presents the possible application of instrumental means of rational control to systems of electromechanical orientation of space vehicles.

The results of the conducted research confirmed the fundamental possibility of in-depth diagnostics of the electric flywheel motor control channel during the transition process and the possibility of flexible restoration of its operability before the end of the transition process while simulating a number of destabilizing influences.

The obtained results open the possibility to proceed to the solution of new tasks related to the formation of a complex modular structure of the software for diagnosing and restoring the operability of the entire EFM unit.

The pyramidal structure of the EFM model unit is an excessive structure, and therefore it is urgent to solve the problem of using other control channels in case of complete failure of one of them.

It also seems necessary to expand the possibilities of diagnostic procedures by using signals from sensors of the angular positions of the spacecraft. Such use will allow to expand the multitude of diagnosed destabilizing influences and increase the efficiency of obtaining a complete diagnosis.

Solving these and other problems that will inevitably arise as a result of further research and experimental work will allow the development of more efficient electromechanical actuators based on EFM for orientation systems of modern and promising spacecraft for long-term space missions.

REFERENCES

1. Rauschenbach, B. V. Control of the orientation of space apparatuses [Text] / B. V. Rauschenbach, E. N. Tokar. – M.: Science, 1974. – 600 p. (In Russian).

2. Alekseev, K. B. Control of the space apparatus [Text] / K. B. Alekseev, G. G. Bebekin; under ed. V. A. Bodner. - M.: Mashinostroenie, 1964. – 402 p. (In Russian).

3. Vasiliev, V. N. Systems of orientation of space apparatuses [Text] / V. N. Vasiliev. – M.: FSUE "NPP VNIIEM", 2009. – 310 p. (In Russian).

4. Kargu, L. I. Systems of angular stabilization of space apparatuses [Text] / L. I. Kargu. – M. : Mashinostroenie, 1973. – 176 p. (In Russian).

5. Bodner, V. A. Aircraft control systems [Text] / V. A. Bodner. - M.: Mashinostroenie, 1973. – 506 p. (In Russian).

6. Designing control systems of objects of rocket and space technique. Vol. 2. Design of spacecraft control systems and orbital station modules [Text]: textbook / Yu. S. Alekseev, E. V. Belous, G. V. Belyaev and others; pod obsch. ed. Yu. S. Alekseeva, Yu. M. Zlatkina, V. S. Kryvtsova, A. S. Kulik, V. I. Chumachenko. – Kh.: Nat. aerospace university “Kharkiv aviation Inst.”, NPP Hartron-Arkos, 2012. – 680 p. (In Russian).

7. Onboard control systems for spacecraft [Text] / A. G. Bronkin, B. G. Burdygov, S. V. Gordiyko et al. Ed. A. S. Syrova. – M .: Publishing house MAI-PRINT, 2010. – 304 p. (In Russian).

8. Iosifyan, A. G. Electromechanics in space [Text] / A. G. Iosifyan. – Series “Knowledge”, № 3, 1977. – 63 p. (In Russian).

9. Reaction wheels on the global market [Electronic resource]. – Access mode: https://blog.satsearch.co/2019-07-25-reaction-wheels-an-overview-of-attitude-control-systems-available-on-the-global-marketplace-for-space. – 15.02.2023.

10. Mathematical Encyclopedic Dictionary [Text] / Ed. Yu. V. Prokhorova. - M .: Great Russian Encyclopedia, 2003. – 845 p. (In Russian).

11. Smirnova, I. M. Regular, semi-regular and star polyhedra [Electronic resource] / I. M. Smirnova, V. A. Smirnova. – Access mode: http://emmom.ru/books/reg_pol.pdf. – 15.02.2023.

12. Sagan, K. Cosmos. Evolution of the Universe, life and civilization [Text] / K. Sagan. - St. Petersburg. : Amphora, 2008. – 370 p. (In Russian).

13. Kuhling, H. Handbook of Physics [Text] / H. Kuhling. – M. : Mir, 1982. – 520 p. (In Russian).

14. Rinard, L. A. Reaction Wheel Supplier Survey [Electronic resource]/ L. A. Rinard, E. L. Chapman, S. C. Ringler. – Access mode: https://discovery.larc.nasa.gov/PDF_FILES/ATR-2011(5389)-2_ReactionWheelSurvey.pdf. – 15.02.2023.

15. “Coupon” spacecraft [Electronic resource]. – Access mode: https://aboutspacejornal.net/2017/11/12/12. – 15.02.2023. (In Russian).

16. Tkachev, S. S. Study of controlled angular motion of vehicles with rotating elements [Electronic resource] / S. S. Tkachev. – Access mode: https:// https://keldysh.ru/council/1/tkachev-diss.pdf. – 15.02.2023. (In Russian).

17. Earth remote sensing satellite EgyptSat 1 [Electronic resource]. – Access mode: https://ecoruspace.me/EgyptSat+1.html. – 15.02.2023. (In Russian).

18. MC-2-8 satellite [Electronic resource]. – Access mode: https://yuzhmash.com/en/products/spacecraft/ms-2-8-satellite/. – 15.02.2023.

19. Melanchenko, A. G. Fault-tollerant control of an Earth observation spacecraft with redundant configuration of flywheel engines [Text] / A. G. Melanchenko // Space science and technology. – 2013. – T. 19. – № 1. – P. 28–37. (In Russian).

20. Monitor-E [Electronic resource]. – Access mode: https://innoter.com/sputniki/monitor-e/. – 15.02.2023. (In Russian).

21. Tokar, E. N. On the rational construction of systems of gyro-power stabilizers [Text] / E. N. Tokar // Space Research. – 1978. – Vol. 16, Issue 1. – P. 22–30. (In Russian).

22. Kulik, A. S. Elements of the theory of rational control of objects [Text] / A. S. Kulik – Kharkiv: National Aerospace University "KhAI", 2016. – 255 p. (In Russian).

23. Patent 116162 Ukraine, IPC G05D 1/10, G05B 13/02. System of automatic rational control [Text] / A. S. Kulik, I. A. Kulik; applicant and owner of pat. National Aerospace University "Kharkiv Aviation Institute". – No. 116162; statement 04.04.16; published 12.02.18, Bull. No. 3. (In Ukrainian).

24. Kulik, A. S. Rational control of the performance of autonomous aircraft. Part 1 [Text] / A. S. Kulik // Problems of control and informatics. – 2017. – № 3. – P. 25–38. (In Russian).

25. Kulik, A. S. Methods for modeling automatic control objects [Text]: textbook. allowance / A. S. Kulik, S. N. Pasichnik. – Kharkiv: National Aerospace University "KhAI", 2018. – 168 c.

26. Simonov, V. F. The state space method in the theory of continuous linear systems [Text]: tutorial / V. F. Simonov. – Kharkiv: Kharkiv Aviation Institute, 1983. – 122 p. (In Russian).

27. Dorf, R. Modern control systems [Text] / R. Dorf, B. Bishop. - M .: Laboratory of basic knowledge, 2002. – 832 p. (In Russian).

28. Kulik, A. S. Signal-parametric diagnostics of control systems [Text]: monograph / A. S. Kulik // State aerospace university named after N. E. Zhukovsky "KhAI" : Business Inform, 2000. – 260 p. (In Russian).

29. Siroja, I. B. Mathematical and software support of intelligent computer systems [Text]: tutorial / I. B. Siroja. – Kharkiv: Kharkiv Aviation Institute,1992. – 101 p. (In Russian).

30. Russell, S. Artificial intelligence: a modern approach [Text] / S. Russell, P. Norvig, 2nd ed. – M .: Publishing Center "Williams", 2007. – 1410 p. (In Russian).

31. Rvachev, V. L. Theory of R-functions and some of its applications [Text]: monograph / V. L. Rvachev. – K.: “Naukova dumka”. 1982. – 552 p. (In Russian).

32. Kormen, T. Algorithms: construction and analysis [Text] / T. Kormen, Ch. Leyzerson, R. Rivest. – M. : MTsNMO, 2000. – 960 p. (In Russian).

33. Rational control of objects: theory and applications [Text]: monograph / E. V. Gavrilenko [and others]; under total ed. of A. S. Kulik. – Kharkiv: National Aerospace University “Kharkiv Aviation Institute", 2018. – 308 p. (In Russian).

34. A. Kulik, K. Dergachov, V. Dzhulgakov, V. Petrenko “Intelligent Control of Electric Flywheel Motors Unit”. Published in: 2022 12th International Conference on Dependable Systems, Services and Technologies (DESSERT) Athens, Greece, 09-11 December 2022. – 6 p. // https://ieeexplore.ieee.org/document/10018730/authors#authors
DOI: 10.1109/DESSERT58054.2022.10018730

CONTENT

For notes

Наукове видання

Джулгаков Віталій Георгійович,
Дергачов Костянтин Юрійович,
Кулік Анатолій Степанович та ін.

РАЦІОНАЛЬНЕ УПРАВЛІННЯ ПРАЦЕЗДАТНІСТЮ МАКЕТНОГО БЛОКА ЕЛЕКТРОДВИГУНІВ-МАХОВИКІВ

(Англійською мовою)

Редактори: В. Джулгаков, С. Пасічник

Зв. план, 2023
Підписано до друку 30.10.2023
Формат 60x84 1/16. Папір офс. Офс. друк
Ум. друк. арк. 12,4. Обл.-вид. арк. 14. Наклад 100 пр.
Замовлення . Ціна вільна

Видавець
Національний аерокосмічний університет ім. М. Є. Жуковського
«Харківський авіаційний інститут»
61070, Харків-70, вул. Чкалова, 17
http://www.khai.edu
Видавничий центр «ХАІ»
61070, Харків-70, вул. Чкалова, 17
izdat@khai.edu

Свідоцтво про внесення суб'єкта видавничої справи
до Державного реєстру видавців, виготовлювачів і розповсюджувачів
видавничої продукції сер. ДК № 391 від 30.03.2001

Виготовлювач
Надруковано з готових оригінал-макетів у друкарні ФОП Азамаєв В. Р.
Єдиний державний реєстр юридичних осіб та фізичних осіб-підприємців.
Запис № 24800170000026884 від 25.11.1998.
Свідоцтво про внесення суб'єкта видавничої справи до Державного реєстру
видавців, виготівників і розповсюджувачів видавничої продукції.
Серія ХК № 135 від 23.02.05.
м. Харків, вул. Познанська 6, к. 84, тел. (057) 778-60-34,
e-mail:bookfabrik@mail.ua